# Hemispheric asymmetry analyses through computational neuroscience models with emphasis on EEG microstates: EEG-fMRI data integration approach

Thesis submitted by

**Ardaman Kaur**

In Partial Fulfillment of the Requirements for the Degree of

**Doctor of Philosophy**
**(Applied Physics)**

Under the Supervision of

**Dr. C Vijayakumar**
Scientist 'F'
NMR Research Centre,
INMAS, DRDO

Institute of Nuclear Medicine & Allied Sciences,
DRDO,
Lucknow Road, Timarpur,
Delhi-110054

**Dr. Rishu Chaujar**
Associate Professor,
Department of Applied Physics,
Delhi Technological University

Delhi Technological University,
Shahbad Daulatpur,
Main Bawana Road,
Delhi-110042

ARDAMAN KAUR

ORCID iD: 0000-0001-6125-6649

# ***DEDICATION***

“To the almighty God who may not give me when I ask but surely gives when I need.”

**Delhi Technological University**

**Shahbad Daulatpur, Main Bawana Road, Delhi-110042**

# CERTIFICATE

This is to certify that the thesis titled "**Hemispheric asymmetry analyses through computational neuroscience models with emphasis on EEG microstates: EEG-fMRI data integration approach"** is being submitted by **Ardaman Kaur** with registration number **2K16/PHD/AP/02** to the Delhi Technological University for the award of the Degree of Doctor of Philosophy in Applied Physics. The work embodied in this thesis is a record of bonafide research work carried out by me under the guidance of **Dr. Rishu Chaujar** and **Dr. C Vijayakumar**. It is further certified that this work is original and has not been submitted in part or fully to any other University or Institute for the award of any degree or diploma.

Ardaman Kaur
Ardaman Kaur
Candidate
Roll number:2K16/PHD/AP/02

This is to certify that the above statement made by the candidate is correct to the best of our knowledge.

7-10-20

**Dr. C Vijayakumar**
**(Joint Supervisor)**
Scientist 'F',
NMR Research Centre,
INMAS, DRDO

**Dr. Rishu Chaujar**
**(Supervisor)**
Associate Professor,
Department of Applied Physics,
Delhi Technological University

**Prof. Rinku Sharma**
**Head,**
Department of Applied Physics,
Delhi Technological University

# ACKNOWLEDGMENTS

The road taken for the completion of this dissertation was not solely traveled by me but by many individuals alongside me who contributed in one way or another for making it a smooth journey.

Firstly, I would like to extend my sincere gratitude to my mentors Dr. C Vijayakumar and Dr. Rishu Chaujar, for their valuable guidance and continuous encouragement throughout my research work. Their critical insights and vast knowledge steered me through this research. I thank them for their patience and incisive feedback that helped me improve my ideas and working methods. I am grateful for a disciplined environment that helped me grow not only as a researcher but also as an individual.

I am thankful to Prof. Rinku Sharma, Head of Department, Applied Physics, DTU, Prof. Yogesh Singh, Honorable Vice-Chancellor, DTU, Prof. S.C. Sharma, Chairman DRC, Applied Physics, DTU, Dr. Maria D'Souza, Head of Department, NMR Research Centre, INMAS, DRDO, Dr. Subash Khushu, Scientist 'G' (Retd), INMAS, DRDO, and Dr. Tarun Sekhri, Director, INMAS, DRDO for their support.

I want to extend my sincere thanks to the lab staff and technicians at INMAS, DRDO, and Department of Applied Physics, DTU. Mr. Pawan Kumar and Mrs. Prabhjot Kaur for guiding and helping me with the experimental setup for simultaneous EEG-fMRI recordings.

I want to thank my seniors Dr. Jaya Madan, Dr. Ajay Kumar, Dr. Rahul Pandey, Dr. Neha Gupta, and Dr. Mukesh Kumar, for their guidance, support, and constant insightful feedbacks.

A warm thanks to all my lab-mates who were an essential part of this journey and gave me memories I would cherish for a lifetime. Swati Agrawal, Dr. Priya Singh, Abhishek Bhardwaj, Harpreet Kaur, and Abhishek Kumar for being my friends and bringing up all the informative and stimulating conversations. Himanshu Singh and Swati Agrawal for lending their helping hand for the smooth conduct of the experiments.

I am thankful to Jasneet Singh, my dance instructor, for the exciting stress-buster dance sessions and all my friends who chose to stay.

Beyond everything, nothing can replace the love and support I received from my family. My grandparents, who always motivated me to work hard while staying on the right path. My parents, Gurmeet Singh and Davinder Kaur, for nurturing me while being my most powerful support system, and for instilling in me a positive outlook towards life. I always have looked up to my elder brother, Dr. Ripudaman Singh, and I thank him for his indispensable guidance on all my matters. I also thank my uncle, Surinder Singh, my brothers, Harshpreet Singh, Harmanpreet Singh, Japnoor Singh, and my whole family, for their support and trust in my decisions.

# ABSTRACT


## HEMISPHERIC ASYMMETRY ANALYSES THROUGH COMPUTATIONAL NEUROSCIENCE MODELS WITH EMPHASIS ON EEG MICROSTATES: EEG-fMRI DATA INTEGRATION APPROACH

It is often assumed that there is a direct correlation between the knowledge an individual possesses and that individual's actions. However, many hidden processes influence decision-making processes. Asymmetric processing of affective, cognitive, and sensory information has long been one of the fascinating properties of human brain function. Thus, understanding hemispheric asymmetry as one of those hidden processes can bridge the gap between what a person knows and what one decides to do.

One widely used technique for analysis of brain asymmetry is Electroencephalography (EEG), whose simplicity, portability, and high temporal resolution enable its usage in a relatively wide-range of real-world environments. Howbeit, it also poses a drawback of less spatial resolution as the localization of an active site is limited to several centimeters. The hemispheric difference between EEG alpha activity over the frontal regions has been termed as frontal EEG asymmetry. This phenomenon was first linked to patterns of emotion processing decades ago. functional Magnetic Resonance Imaging (fMRI) is another technique that provides a unique view of the human brain by detecting changes in blood oxygenation. It poses an advantage of high spatial resolution; however, it possesses a low temporal resolution. The hemispheric dominance in fMRI has been called the laterality index. The laterality index enables one value per subject per contrast as a descriptor for activation pattern based hemispheric dominance. Also,

simultaneous recordings and analysis of EEG-fMRI techniques, which can counteract the limitations posed by EEG-FMRI, have recently gained attention and can be gauged for effectiveness in the hemispheric asymmetry research.

The current thesis aims to corroborate the hemispheric asymmetry research by exploring the resting-state EEG/fMRI hemispheric asymmetry models after simultaneous EEG-fMRI data acquisition. These resting-state models of hemispheric asymmetry in the brain may serve as potential parameters for comprehending the human actions when engaged in any exogenously directed task. Thus, the standard resting frontal alpha EEG hemispheric asymmetry model was first examined before engagement in a Situational awareness (SA) task to vindicate the relationship between pre-task resting asymmetry and SA-task performance. SA is the knowledge of the environment, and maintenance of SA is crucial for optimal performance in the aviation and military domain. Thus, understanding the linkage of the neural mechanisms underlying the pre-task resting frontal alpha asymmetry model with subsequently performed SA-task can improve SA. For this purpose, initially, an SA-task with influence from the Stroop effect was designed and developed, and pre-task resting EEG absolute alpha power and its frontal alpha hemispheric asymmetry were assessed. This study revealed a strong association of SA-task performance measures with resting frontal alpha hemispheric asymmetry. Further, the neural mechanisms underlying pre-SA task resting absolute alpha power and its frontal asymmetry, as assessed through the EEG-informed fMRI approach, significantly influenced the SA-task's neural mechanisms.

After examining the relationship between the pre-task resting alpha EEG asymmetry model with subsequently performed SA-task, the association of this standard asymmetry model with affect and approach/withdrawal measures of an individual was gauged. The purpose of this

study was to understand the significance of real-time standalone recordings of pre-task resting alpha EEG asymmetry in terms of its connectedness with measures of positive/negative affect and approach/withdrawal behavior. Further, to strengthen the findings, the mapping between pre-task resting alpha EEG asymmetry model and fMRI through EEG-informed fMRI analysis was explored. For this purpose, initially, the robust correlation of standard resting frontal alpha asymmetry with affect and approach/withdrawal measures was carried out. Next, the neural underpinnings and Hemodynamic Lateralization Index, HLI (based on these neural underpinnings) for standard resting frontal alpha asymmetry were assessed. The results yielded no significant relationship between the standard resting frontal asymmetry and its HLI with any psychological measures.

This ambivalence on the validity of standard resting frontal alpha asymmetry in terms of its association with affect and approach/withdrawal psychological measures motivated us towards the estimation of a novel microstate-based frontal alpha asymmetry model and assessment of this model's linkage with positive/negative affect and approach/withdrawal measures. The microstates represent global electrical brain activity on the scalp that remains semi-stable for brief transient periods. The utilization of microstates was based on the evidence that supported the importance of stable EEG patterns in bringing forth the interrelation of affect and approach/withdrawal measures with resting frontal alpha asymmetry. The results revealed that the microstate-based resting frontal alpha asymmetry model correlated significantly with negative affect, and its neural underpinning's HLI significantly correlated with positive/Negative affect and approach/withdrawal measures. Thus, the novel microstate-based microstate-based resting frontal alpha asymmetry model proved efficacious in bringing forth the association with affect and approach/withdrawal measures.

In addition, to understand the role of subcortical regions, and their interaction with cortical regions in bringing forth the hemispheric asymmetries of affect and approach/withdrawal behavior, a study based on the hemispheric asymmetry model of resting fMRI graph theory functional connectivity metrics was carried out, as the viability to detect subcortical signals through EEG is still debatable. In this analysis, we report the neuroimaging finding based on Region of Interest (ROI) based analysis and graph-theory measures for global networks and sub-networks. The study revealed the involvement of emotion and memory-related subcortical-cortical interactions in positive and negative affect and basal ganglia structures in approach-withdrawal dichotomy. Further, lateralization of the strength of degree-measures of the cortical-regions vital for subcortical-cortical interaction revealed higher connectivity within the left-hemisphere for affective measures.

Thus, the current thesis demonstrates the benefit of assessing the standard resting hemispheric asymmetry model before a complex cognitive task such as SA, which holds paramount importance for the ergonomics community and for military/aviation domains. Further, the outcomes also offer an unprecedented attempt towards the development of a novel microstates-based resting hemispheric asymmetry model for bringing forth the relationship of resting EEG based asymmetry with psychological measures of affect and approach/withdrawal behavior Also, the key findings of subcortical regions and their interaction with cortical regions dominating the affect and approach/withdrawal measure can be further explored in clinical as well as task-based studies.

# LIST OF FIGURES

**Figure 1.1** Three dimensional rendered view of magnetic resonance imaging (MRI) scan depicting the left occipital lobe petalia and right frontal lobe petalia with noticeable differences in occipital (O) and frontal (F) lobes. The figure portrays the yakovlevian torque with structures surrounding the right Sylvian fissure torqued forward relative to their left counterparts. Adapted from Arthur W. Toga & Thompson (2003). ..... 2

**Figure 1.2** The figure depicts the Hemodynamic Response Function (HRF) (Adapted from Huettel et al. (2009)) ..... 8

**Figure 1.3** Diagram depicting a. the parts of neuron b. action potential, through which signals are conducted in axons and the associated membrane ionic permeabilities. At rest, membranes are permeable to $K^+$ ions, while during an action potential, the permeability towards $Na^+$ ions increases for a temporary period (Adapted from Purves et al. (2004)). ..... 12

**Figure 1.4** Schematic for data-integration of simultaneous EEG-fMRI (Modified from He & Liu (2008)) ..... 15

**Figure 1.5** Schematic for simultaneous EEG-fMRI recording hardware setup (Modified from Shah et al. (2017)). ..... 16

**Figure 2.1** Schematic illustrating the EEG preprocessing pipeline. ..... 46

**Figure 2.2** Median power spectrum (0.2 to 50 Hz) of raw artifact laden data for channels F3, F4, F7, F8, Pz, Oz, and POz (Kaur et al., 2020). ..... 50

**Figure 2.3** Median power spectrum (0.2 to 50 Hz) of final artifact removed EEG data (CSD referenced) for channels F3, F4, F7, F8, Pz, Oz, and POz (Kaur et al., 2020). ..... 51

**Figure 3.1** Schematic diagram of the methodology adopted in this study (Kaur et al., 2019). ... 61

**Figure 3.2** Schematic showing fMRI stimulus and baseline presentation paradigm for Situational awareness (SA) task (Kaur et al., 2019). ..... 64

**Figure 3.3** Schematic showing the estimation of mean hemodynamic response of each stimulus for functional connectivity analysis (Kaur et al., 2019). ..... 73

**Figure 3.4** Correlation plots between mean normalized reaction time and SA index. a. Pearson correlation b. Skipped (Pearson) correlation. Correlation plots between mean normalized reaction time and PRAFA. c. Pearson correlation d. Skipped (Pearson) correlation (Kaur et al., 2019)... 75

**Figure 3.5** Correlation plots between PRAFA and SA index and associated histograms of correlations for bootstrapped data. a. Pearson correlation b. Spearman correlation c. 20% Bend correlation d. Skipped (Pearson and Spearman) correlations (Kaur et al., 2019)..... 76
**Figure 3.6** Correlation plots between median PRAA values and SA index and histograms of correlations for bootstrapped data .a. Pearson correlation b. Spearman correlation c. 20% Bend correlation d. Skipped (Pearson and Spearman) correlations (Kaur et al., 2019)..... 77
**Figure 3.7** Neural underpinnings of Situational awareness (SA) task, as shown in (A) surface rendered view (B) slice montage view. The activations are represented at FWE corrected $p<0.05$ (Kaur et al., 2019). ..... 79
**Figure 3.8** Neural underpinnings of Pre-task resting-state alpha frontal asymmetry (PRAFA) through EEG informing SA-task based fMRI, as shown in the slice montage view. The activations are represented at uncorrected $p<0.001$(Kaur et al., 2019). ..... 80
**Figure 3.9** Neural underpinnings of Pre-task resting-state absolute alpha (PRAA) power through EEG informing SA-task based fMRI, as shown in (A) surface rendered view (B) slice montage view. The activations are represented at uncorrected $p<0.001$ (Kaur et al., 2019). ..... 82
**Figure 3.10** Schematic showing functional connectivity of neural underpinnings of SA-task with PRAA and PRAFA underpinnings. The interregional correlation was done at $r>0.5$ ($p<0.05$). The dotted arrow illustrates the functional connectivity of PRAA (frontal and temporal regions) with SA regions. The solid arrows illustrate the limbic association of PRAFA regions with SA-task regions, and the integration of dorsal/ventral pathways, memory regulation (Kaur et al., 2019). ..... 84
**Figure 4.1** Schema of the methodology adopted in this study (Kaur et al., 2020)..... 104
**Figure 4.2** Schema of the methodology adopted for proposed microstate estimation and assessment of standard and microstates based frontal alpha hemispheric asymmetry measures (Kaur et al., 2020). ..... 112
**Figure 4.3** Topographic EEG maps of spectral power density for the alpha band for a. proposed microstate based analysis and b. Standard analysis (CSD referenced). The color bar represents the log-transformed spectral power density (10*log10 (µv2/Hz)) where red represents the maximum and blue represents the minimum values (Kaur et al., 2020). ..... 123
**Figure 4.4** Correlation plots between negative affect scores and microstate based FA (F4/F3) and associated histograms of correlations for bootstrapped data. a. Pearson correlation b. 20%

Bend correlation c. Spearman correlation d. Skipped (Pearson and Spearman) correlations (Kaur et al., 2020). ..... 126
**Figure 4.5** Correlation plots between negative affect scores and microstate based FTA (F8/F7) and associated histograms of correlations for bootstrapped data. a. Pearson correlation b. 20% Bend correlation c. Spearman correlation d. Skipped (Pearson and Spearman) correlations (Kaur et al., 2020). ..... 127
**Figure 4.6** Surface rendered view of neural underpinnings of standard a. FA (channel pair F4/F3) b. FTA (channel pair F8/F7). The color bar indicates the t-values with blue being the least and red being the highest. The activations are represented at FDR corrected $p<0.05$ (Kaur et al., 2020). ..... 129
**Figure 4.7** Surface rendered view of neural underpinnings of proposed microstate based a. FA (channel pair F4/F3) b. FTA (channel pair F8/F7). The color bar indicates the t-values with blue being the least and red being the highest. The activations are represented at FDR corrected $p<0.05$ (Kaur et al., 2020). ..... 131
**Figure 4.8** Pearson correlation plots and associated histograms for bootstrapped data for correlation between a. Standard and microstate based FA (F4/F3) b. Standard and microstate based FTA (F8/F7) (Kaur et al., 2020). ..... 134
**Figure 4.9** Underlying dynamics associated with alpha asymmetry index and BOLD signal (Kaur et al., 2020). ..... 143
**Figure 5.1** Schema is indicative of the feedback loop between affective states and approach/withdrawal dichotomy. ..... 163
**Figure 5.2** Schematic of the methodology followed in the present study. ..... 165
**Figure 5.3** (a) Surface rendered view of neural substrates of PA, NA, BAS, and BIS. The color bar indicates the t-values, and the activations are represented at FDR corrected $p<0.05$ (b) The nodes and edges of PA, NA, BAS, and BIS for global graph analysis. ..... 177
**Figure 5.4** Heatmaps for the representation of the extent (no. of voxels) of neural substrates of PA, NA, BAS, and BIS measures for (a) frontal regions, (b) parietal regions, (c) temporal regions, (d) occipital regions (e) limbic regions. ..... 178
**Figure 5.5** Violin plots (kernel density plot and box plot) representing degree in the global network (N) for subcortical substrates of (a) PA (b) NA (c) BAS (d) BIS. ..... 180

**Figure 5.6** Violin plots (kernel density plot and box plot) representing betweenness centrality in the global network (N) for subcortical substrates of (a) PA (b) NA (c) BAS (d) BIS..... 181
**Figure 5.7** Sankey diagram for ROI-to-ROI connectivity analysis for PA, NA, BAS, and BIS (a) between subcortical and cortical regions (b) within subcortical regions. The width of the flow is proportional to the correlation values. ..... 184
**Figure 5.8** Sankey diagram for subcortical-cortical interaction for discrete subnetwork *(CSCN)* where the flow represents (a) the degree and (b) the betweenness centrality measures for the cortical regions of all psychological measures. ..... 186
**Figure 5.9** Violin plots (kernel density plot and box plot) representing degree in contralateral ($ConN$) and ipsilateral ($IpsN$) networks for the interaction of subcortical substrates with left and right lateralized cortical regions in (a) PA (b) NA (c) BAS (d) BIS. ..... 188
**Figure 5.10** The functional connectivity based laterality index for cortical regions vital for subcortical-cortical interaction for (a) PA (b) NA (c) BAS (d) BIS. ..... 189
**Figure 5.11** The number of active voxels based laterality index for each lobe for (a) PA (b) NA (c) BAS (d) BIS. ..... 190
**Supplementary Figure S5.1** Heatmaps for the representation of the t-values of neural substrates of PA, NA, BAS, and BIS measures for (a) frontal regions, (b) parietal regions, (c) temporal regions, (d) occipital regions, (e) limbic regions. ..... .229

# LIST OF TABLES

**Table 2.1** HAPPE preprocessing report generated for all volunteers' (N=39) EEG datasets. Independent components are abbreviated as ICs (Kaur et al., 2020)..... 48
**Table 4.1** Demographic and behavioral characteristics of study participants (N=39) (Kaur et al., 2020). ..... 106
**Table 4.2** Median and median absolute deviation of the standard and proposed microstates based frontal hemispheric asymmetry measures (Kaur et al., 2020). ..... 116
**Table 4.3** Robust correlation (Pearson, bend, spearman and skipped) of standard and proposed microstate based frontal hemispheric asymmetry measures with psychological scores (Kaur et al., 2020). ..... 125
**Table 4.4** Robust correlation (Pearson, bend, spearman, and skipped) of HLI based on standard and proposed microstate based frontal hemispheric asymmetry measures with psychological scores (Kaur et al., 2020). ..... 133
**Table 4.5** List of studies for positive/negative affect and approach/withdrawal dichotomy (Kaur et al., 2020). ..... 136
**Supplementary Table S3.1** Correlation (r) and Significance (p) values for electrodes finding strong correlation of their PRAA with behavioral SA Index (Kaur et al., 2019). .....….215
**Supplementary Table S3.2** Neural underpinnings of Situational Awareness (SA) task. The activations are represented at FWE Corrected p<0.05. The coordinates reported are in Montreal Neurological Institute (MNI) space (Kaur et al., 2019).....216
**Supplementary Table S3.3** Neural underpinnings of pre-task resting alpha frontal asymmetry (PRAFA) through EEG informing SA-task based fMRI. The activations are represented at uncorrected p<0.001. The coordinates reported are in MNI space (Kaur et al., 2019). .....218
**Supplementary Table S3.4** Neural underpinnings of pre-task resting absolute alpha (PRAA) power through EEG informing SA-task based fMRI. The activations are represented at uncorrected p<0.001. The coordinates reported are in MNI space (Kaur et al., 2019). .....219
**Supplementary Table S4.1** Neural underpinnings of standard FA (channel pair F4/F3). The activations after correction for multiple comparisons are represented at p<.05 (FDR corrected). The coordinates reported are in MNI space (Kaur et al., 2020). .....221

**Supplementary Table S4.2** Neural underpinnings of standard FTA (channel pair F8/F7). The activations after correction for multiple comparisons are represented at p<.05 (FDR corrected). The coordinates reported are in MNI space (Kaur et al., 2020). .....223
**Supplementary Table S4.3** Neural underpinnings of proposed microstate based FA (channel pair F4/F3). The activations after correction for multiple comparisons are represented at p<.05 (FDR corrected). The coordinates reported are in MNI space (Kaur et al., 2020). .....225
**Supplementary Table S4.4** Neural underpinnings of proposed microstate based FTA (channel pair F8/F7). The activations after correction for multiple comparisons are represented at p<.05 (FDR corrected). The coordinates reported are in MNI space (Kaur et al., 2020). .....227
**Supplementary Table S5.1** Neural substrates of Positive affect (PA). The activations after correction for multiple comparisons are represented at p<.05 (FDR corrected). The coordinates reported are in MNI space.....230
**Supplementary Table S5.2** Neural substrates of Negative affect (NA). The activations after correction for multiple comparisons are represented at p<.05 (FDR corrected). The coordinates reported are in MNI space.....233
**Supplementary Table S5.3** Neural substrates of Behavioral activation system (BAS). The activations after correction for multiple comparisons are represented at p<.05 (FDR corrected). The coordinates reported are in MNI space. .....237
**Supplementary Table S5.4** Neural substrates of Behavioral inhibition system (BIS). The activations after correction for multiple comparisons are represented at p<.05 (FDR corrected). The coordinates reported are in MNI space. .....240
**Supplementary Table S5.5** ROI-to-ROI correlations of subcortical with cortical regions and other subcortical areas for PA, NA, BAS, and BIS psychological measures. .....242
**Supplementary Table S5.6** Graph theory measures (degree and betweenness centrality) for the subnetwork CSCN (each cortical substrate with all subcortical neural substrates) of PA, NA, BAS, and BIS psychological measures.....245

# LIST OF APPENDICES

Appendix 1: Supplementary material for Chapter Three.....215
Appendix 2: Supplementary material for Chapter Four .....221
Appendix 3: Supplementary material for Chapter Five.....229

# LIST OF PUBLICATIONS

## ARTICLES IN INTERNATIONAL REFEREED JOURNALS (2)

1. ***Kaur, A.***, *Chaujar, R., & Chinnadurai, V. (2019).* ***Effects of Neural Mechanisms of Pretask Resting EEG Alpha Information on Situational Awareness: A Functional Connectivity Approach.*** *Human Factors.* *https://doi.org/10.1177/0018720819869129*. ***(Impact Factor: 3.165)***
2. ***Kaur, A.***, *Chinnadurai, V., & Chaujar, R. (2020).* ***Microstates-based resting frontal alpha asymmetry approach for understanding affect and approach/withdrawal behavior.*** *Scientific Reports, 10(1), 1–25.* *https://doi.org/10.1038/s41598-020-61119-7*. ***(5-year Impact Factor: 4.576)***

## ARTICLES COMMUNICATED IN INTERNATIONAL JOURNALS (1)

1. ***Kaur, A.***, *Chinnadurai, V., & Chaujar, R.* ***Distinct subcortical and cortical contributions to affect and approach/withdrawal behavior: A resting-state functional connectivity approach.*** *Manuscript communicated.*

## INTERNATIONAL CONFERENCES (6) (Not included in the thesis)

1. ***Kaur, A.***, *Chinnadurai, V., Agrawal, S., Singh, H., Khushu, S., Kumar, P., Kaur, P., Kumar, A., Chaujar, R., & Sharma., S. "****Assessment of Neural correlates of Engagement in a Situational Awareness Task using Simultaneous EEG-fMRI technique****,". International Committee on Military Medicine, pp. 216-217, November 19$^{th}$-24$^{th}$, 2017, Vigyan Bhawan, New Delhi, India.*
2. ***Kaur, A.***, *Chinnadurai, V., Agrawal, S., Singh, H., Khushu, S., Singh, A. K., Chaujar, R., & Sharma., S. C. "****Assessment of Engagement and its neurovascular correlates in a Situational Awareness Task: An EEG Informed fMRI approach****,". Brain Modes, pp. 66-67, December 11$^{th}$ -14$^{th}$, 2017, Savoy Suites, Manesar, Gurgaon, India.*
3. ***Kaur, A.***, *Chinnadurai, V., Agrawal, S., Khushu, S., Chaujar, R., & Sharma., S. "****Assessment of neural correlates of cortical communication of Alpha/Gamma bands between frontal and parietal-occipital regions in Situational Awareness task as well as in resting-state: An EEG informed fMRI approach****,". Joint Annual Meeting ISMRM-*

*ESMRMB, June 16th-21st, 2018, Paris Expo Porte de Versailles, Paris, France. http://archive.ismrm.org/2018/4514.html.*

4. ***Kaur, A.**, Chinnadurai, V., Agrawal, S., Khushu, S., Chaujar, R., & Sharma., S. "**Does Pre-task Resting state Absolute Alpha (PRAA) power and its Frontal Asymmetry Index (FAI) predict outcome of Situational Awareness task? Assessment through EEG informed fMRI approach**,". Joint Annual Meeting ISMRM-ESMRMB, June 16th-21st, 2018, Paris Expo Porte de Versailles, Paris, France.*
   *http://archive.ismrm.org/2018/4515.html.*
5. *Chinnadurai, V., Fotedar, S., Agrawal, S., **Kaur, A.**, Khushu, S., & Singh, A. " **Deep learning based Brain-computer interface system for automatic target detection using Electroencephalography data**,". International Committee on Military Medicine, pp. 47, November 19th-24th, 2017, Vigyan Bhawan, New Delhi, India.*
6. *Agrawal, S., Chinnadurai, V., **Kaur, A.**, Khushu, S., Sharma, R., & Sharma, S. "**Hemodynamic reorganization approach to estimate the functional connectivity in task based functional MRI study**,". Joint Annual Meeting ISMRM-ESMRMB, June 16th-21st, 2018, Paris Expo Porte de Versailles, Paris, France.*
   *http://archive.ismrm.org/2018/2403.html.*

# TABLE OF CONTENTS


***DEDICATION*** ..... **ii**

**CERTIFICATE** ..... **iii**

**ACKNOWLEDGMENTS** ..... **iv**

**ABSTRACT** ..... **vi**

**LIST OF FIGURES** ..... **x**

**LIST OF TABLES** ..... **xiv**

**LIST OF APPENDICES** ..... **xvi**

**LIST OF PUBLICATIONS** ..... **xvii**

**TABLE OF CONTENTS** ..... **xix**

**CHAPTER ONE: INTRODUCTION** ..... **1**

1.1 STRUCTURAL AND FUNCTIONAL ASPECTS OF HEMISPHERIC ASYMMETRY IN BRAIN ..... 1

1.2 PHYSIOLOGICAL MEASURES OF FUNCTIONAL HEMISPHERIC ASYMMETRY IN BRAIN ..... 4

1.2.1 FUNCTIONAL MAGNETIC RESONANCE IMAGING (FMRI) ..... 4

1.2.2. ELECTROENCEPHALOGRAPHY (EEG) ..... 9

1.3 RECORDING AND ANALYSIS OF SIMULTANEOUS EEG-FMRI DATA ..... 14

1.3.1 ASYMMETRIC APPROACHES ..... 16

1.3.2 SYMMETRIC APPROACHES ..... 17

1.4 IDENTIFICATION OF RESEARCH GAPS ..... 18

1.5 OBJECTIVES OF THE THESIS ..... 18

1.6 ORGANIZATION OF THE THESIS ..... 21

REFERENCES ..... 26

**CHAPTER TWO: OPTIMIZATION AND VALIDATION OF EEG PREPROCESSING PIPELINE** ..... **32**

2.1 ABSTRACT ..... 32

2.2 INTRODUCTION ..... 33

2.3 MATERIALS AND METHODS ..... 36

2.3.1 SAMPLE AND PROCEDURE ..... 36

2.3.2 DATA ACQUISITION ..... 36

2.3.3 PRELUDE TO EXISTING ARTIFACT REMOVAL TECHNIQUES ..... 37

2.3.4 OPTIMIZING EEG PREPROCESSING PIPELINE ..... 41
2.4 RESULTS AND DISCUSSION ..... 47
2.4.1 VALIDATION BY HAPPE'S PROCESSING REPORT ..... 47
2.4.2 VALIDATION VIA EEG POWER SPECTRUM ..... 49
2.5 CONCLUSION ..... 51
REFERENCES ..... 52
**CHAPTER THREE: ASSESSMENT OF LINKAGE BETWEEN RESTING ALPHA ASYMMETRY AND PERFORMANCE IN SITUATIONAL AWARENESS TASK ..... 55**
3.1 ABSTRACT ..... 55
3.2 INTRODUCTION ..... 56
3.3 MATERIALS AND METHODS ..... 60
3.3.1 SAMPLE AND PROCEDURE ..... 60
3.3.2 PARADIGM INFORMATION ..... 61
3.3.3 DATA ACQUISITION AND PRE-PROCESSING STEPS ..... 64
3.3.4 DATA ANALYSIS ..... 66
3.4 RESULTS ..... 73
3.4.1 CONFIRMATION FOR PRESENCE OF STROOP EFFECT DURING SA-TASK ..... 74
3.4.2 ASSOCIATION OF PRE-TASK RESTING INFORMATION WITH SA INDEX ..... 75
3.4.3 NEURAL UNDERPINNINGS OF SA-TASK ..... 77
3.4.4 NEURAL UNDERPINNINGS OF PRAFA AND PRAA ..... 80
3.4.5 FUNCTIONAL CONNECTIVITY ANALYSIS ..... 83
3.5 DISCUSSION ..... 85
3.5.1 VALIDATION OF PRESENCE OF STROOP EFFECT DURING SA-TASK ..... 86
3.5.2 ROLE OF PRE-TASK ABSOLUTE ALPHA INFORMATION IN SA-TASK ..... 86
3.5.3 ROLE OF PRE-TASK RESTING ALPHA FRONTAL ASYMMETRY IN SA-TASK ..... 87
3.5.4 LIMITATION OF STUDY ..... 89
3.6 CONCLUSION ..... 89
REFERENCES ..... 91
**CHAPTER FOUR: MICROSTATES-BASED RESTING FRONTAL ALPHA ASYMMETRY APPROACH FOR UNDERSTANDING AFFECT AND APPROACH/WITHDRAWAL BEHAVIOR ..... 97**
4.1 ABSTRACT ..... 97
4.2 INTRODUCTION ..... 98

4.3 MATERIALS AND METHODS ..... 103
4.3.1 SAMPLE AND PROCEDURE ..... 105
4.3.2 BEHAVIORAL MEASURES ..... 105
4.3.3 DATA ACQUISITION AND PRE-PROCESSING STEPS ..... 107
4.3.4 DATA ANALYSIS ..... 109
4.4 RESULTS ..... 121
4.4.1 ROBUST CORRELATION OF FRONTAL HEMISPHERICAL ASYMMETRY MEASURES WITH PSYCHOLOGICAL MEASURES ..... 123
4.4.2 EEG INFORMED FMRI ANALYSIS ..... 127
4.4.3 ROBUST CORRELATION OF HLI WITH PANAS, BIS/BAS MEASURES ..... 132
4.4.4 ROBUST CORRELATION AMONG FRONTAL HEMISPHERICAL ASYMMETRY MEASURES ..... 133
4.5 DISCUSSION ..... 134
4.5.1 PRELUDE TO THE PRESENT RESEARCH STUDY ..... 138
4.5.2 STANDARD ALPHA ASYMMETRY AND ITS HLI REVEAL NO CORRELATION WITH PANAS AND BIS/BAS MEASURES ..... 139
4.5.3 MICROSTATES BASED ASYMMETRY CORRELATES WITH AND DELINEATES THE NEURAL MECHANISMS OF NEGATIVE AFFECT ..... 140
4.5.4 MICROSTATE BASED ASYMMETRY REVEALS NO CORRELATION WITH BIS, POSITIVE AFFECT, AND BAS ..... 143
4.5.5 HLI OF MICROSTATES NEURAL UNDERPINNINGS REVEALS SIGNIFICANT ASSOCIATION WITH BIS, POSITIVE AFFECT, AND BAS MEASURES ..... 144
4.5.6 ABSENCE OF CORRELATION AMONG PROPOSED MICROSTATE AND STANDARD FRONTAL HEMISPHERIC ASYMMETRY MEASURES ..... 146
4.5.7 LIMITATION OF STUDY ..... 146
4.6 CONCLUSION ..... 147
REFERENCES ..... 149
**CHAPTER FIVE: THE ARCHITECTURE OF SUBCORTICAL-CORTICAL INTERACTIONS AND FUNCTIONAL ASYMMETRY DOMINATING AFFECT AND APPROACH/WITHDRAWAL BEHAVIOR: GRAPH THEORY APPROACH ..... 160**
5.1 ABSTRACT ..... 160
5.2 INTRODUCTION ..... 161
5.3 METHODS ..... 165
5.3.1 SAMPLE AND PROCEDURE ..... 165
5.3.2 BEHAVIORAL MEASURES ..... 166

5.3.3 DATA ACQUISITION AND PRE-PROCESSING STEPS ..... 166
5.3.4 DATA ANALYSIS ..... 167
5.4 RESULTS ..... 174
5.4.1 RESTING NEURAL SUBSTRATES ASSOCIATED WITH AFFECT AND APPROACH/WITHDRAWAL MEASURES ..... 174
5.4.2 FUNCTIONAL CONNECTIVITY ANALYSIS ..... 179
5.5 DISCUSSION ..... 190
5.5.1 LATERALIZATION OF CONNECTIVITY OF CORTICAL REGIONS VITAL FOR SUBCORTICAL-CORTICAL INTERACTIONS ..... 191
5.5.2 THE EMERGENCE OF THE AMYGDALA, HIPPOCAMPUS, AND PUTAMEN AS SUBCORTICAL HUBS FOR PA AND NA ..... 192
5.5.3 FRONTAL AND TEMPORAL REGIONS' ROLE IN PA AND NA ..... 193
5.5.4 THE SPECIFIC ROLE OF BASAL GANGLIA IN BAS AND BIS ..... 195
5.5.5 ROLE OF ANTERIOR CINGULATE AND ANTERIOR DIVISION OF INSULA IN BAS AND BIS ..... 196
5.5.6 POINTER FOR THE EXISTENCE OF FEEDBACK MECHANISM AMONG AFFECTIVE AND APPROACH/WITHDRAWAL STATES ..... 197
5.6 CONCLUSION ..... 198
5.7 ABBREVIATIONS ..... 199
REFERENCES ..... 201
**CHAPTER SIX: CONCLUSIONS AND RECOMMENDATIONS FOR FUTURE WORK ..... 207**
6.1 CONCLUSIONS ..... 207
6.2 RECOMMENDATIONS FOR FUTURE WORK ..... 212
REFERENCES ..... 213
**APPENDICES ..... 214**
APPENDIX 1: SUPPLEMENTARY MATERIAL FOR CHAPTER THREE ..... 215
APPENDIX 2: SUPPLEMENTARY MATERIAL FOR CHAPTER FOUR ..... 221
APPENDIX 3: SUPPLEMENTARY MATERIAL FOR CHAPTER FIVE ..... 229
REFERENCES ..... 247
**REPRINTS OF JOURNAL PUBLICATION**

# CHAPTER ONE

# INTRODUCTION

## 1.1 STRUCTURAL AND FUNCTIONAL ASPECTS OF HEMISPHERIC ASYMMETRY IN BRAIN

Hemispheric asymmetry is a paramount aspect of the organization of the human brain, and comprehending it's functional specialization is a core issue in neuroscience research (Rogers et al., 2013; A. W. Toga et al., 2009; Arthur W. Toga & Thompson, 2003). A long-established theory states that a deep grove known as the medial longitudinal fissure separates the human brain into two halves, namely the right and left hemispheres. Moreover, the corpus callosum binds the right and the left hemispheres of the brain and processes many cognitive and sensory-motor signals by integration and transferral of information from both hemispheres (Mooshagian, 2008; Roland et al., 2017). However, though almost every region in one hemisphere has an analogous area in the other, still the two brain hemispheres in humans differ in their anatomy, behavior, and function. Toga and Thomson (Arthur W. Toga & Thompson, 2003) emphasized the involvement of factors such as developmental, hereditary, pathological, evolutionary, and experiential in forming the basis for the existence of lateralization in the brain. One of the facets of macroscopic anatomical asymmetry in the human brain is the concept of Petalia, wherein a particular hemisphere protrudes in the direction of the other hemisphere. A typical observation of brain asymmetry is depicted by the left occipital lobe and the right frontal lobe petalia. Also, a notable distortion exists in the hemispheres and is known as Yakovlevian torque (see Figure 1.1) (Hugdahl, 2011). This torque, in addition to the frontal and occipital protrusions, encloses the

variability in the widths of frontal and occipital regions, with the right frontal area and left occipital region being more wider than their counterparts (Kong et al., 2018; Rentería, 2012).

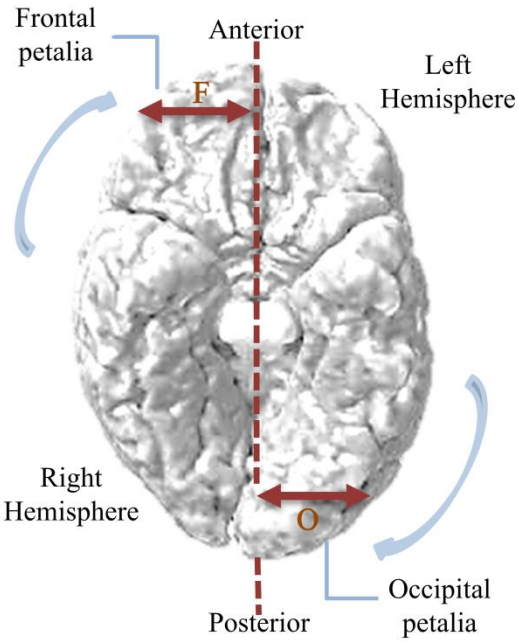


**Figure 1.1** Three dimensional rendered view of magnetic resonance imaging (MRI) scan depicting the left occipital lobe petalia and right frontal lobe petalia with noticeable differences in occipital (O) and frontal (F) lobes. The figure portrays the yakovlevian torque with structures surrounding the right Sylvian fissure torqued forward relative to their left counterparts. Adapted from Arthur W. Toga & Thompson (2003).

Further, one of the earliest observations that indicated the asymmetrical nature of the human brain were found in language-related abilities and handedness (Knecht et al., 2000; Rentería, 2012). Broca (Broca, 1861) and Wernicke (Wernicke, 1974) presented the most initial view on language lateralization in the brain. They reported that strokes and tumors in the left-hemisphere severely damaged the language-related abilities. Anterior regions of the left-hemisphere, including pars opercularis and triangularis regions of inferior frontal gyrus (also known as Broca's area), were linked to language production. In contrast, language

comprehension was found to be associated with temporal-parietal areas, including Wernicke's area (Brodmann area (BA) 21 and BA 22, BA 39 and BA 40, BA 37) (Ardila et al., 2016). Also, the structural and functional asymmetries of planum temporale (language-processing structure) and other auditory regions have been correlated to the handedness (Foundas et al., 1995).

Moreover, evidence reveals the pivotal role of hemispheric asymmetries during engagement in visual-spatial and attention tasks (Geffen et al., 1972; O'Regan & Serrien, 2018). Further, the association of hemispheric asymmetry with the performance in tasks have also been explored. Shulman et al. (2010) measured the hemispheric asymmetry during cued-target detection and peripheral cue stimulus, evoking spatial attention shifts. Their study demonstrated the right-lateralized activity in temporoparietal junction for spatial attention shifts and right-hemispheric dominance in the frontal, temporal, parietal, and temporoparietal regions during the target-detection task. Besides, few brain asymmetry models have also been linked to emotional processing (Alves et al., 2008). The first one, called the right hemisphere hypothesis, assumed the dominant functioning of the right hemisphere in emotional processing. In contrast, the second named the valence hypothesis, assumed the dominant role of the left hemisphere in positive emotions and the right hemisphere in negative ones. Both the premises have been supported to some extent by visual-field tasks evoking emotions (Canli, 1999; Wyczesany et al., 2018). Also, findings (Killgore & Yurgelun-Todd, 2007) hint the concurrent operation of both the hypotheses, suggesting these two models as disparate components of a much complex system for emotional processing.

Another studied domain is the relationship between hemispheric asymmetry and task performance. Everts et al. (2009) found the correlation of higher verbal IQ with stronger language lateralization using functional Magnetic Resonance Imaging (fMRI) modality. In yet

another task-based study (Chiarello et al., 2009), a positive relationship was observed between the degree of lateralization and an individual's reading skills. However, another study (Hirnstein et al., 2008), including a parallel performance in two cognitive tasks, showed that individuals with low lateralization perform better than more lateralized counterparts. Further, past studies (Ambrosini & Vallesi, 2015, 2016; Chen et al., 2019; Hanouneh et al., 2017) based on Electroencephalography (EEG) have also affirmed the linkage of asymmetry with performance in a task.

Thus, hemispheric asymmetry represents a fundamental feature of the human brain and plays a prominent role in emotions and cognitive functions. Further, the above-mentioned physiological measurements, namely fMRI and EEG, are frequently employed in cognitive neuroscience to understand the neural mechanisms underlying functional hemispheric asymmetry research. The subsequent section explains the physiological basis of these techniques.

## 1.2 PHYSIOLOGICAL MEASURES OF FUNCTIONAL HEMISPHERIC ASYMMETRY IN BRAIN

fMRI and EEG are the most widely employed neuroimaging techniques to gain insights into the neural mechanisms underlying the brain's hemispheric asymmetries.

### *1.2.1 FUNCTIONAL MAGNETIC RESONANCE IMAGING (fMRI)*

#### 1.2.1.1 Physiological Basis

Blood Oxygenation Level-Dependent (BOLD) fMRI measures the variation in blood oxygenation over time (Ogawa et al., 1990). fMRI is based on the principles of Magnetic Resonance Imaging (MRI) (Lauterbur, 1973; Mansfield & Grannell, 1973). MRI creates images

of biological tissues by utilizing strong magnetic fields. An MRI scanner nowadays operates with a typical field strength of 3 Tesla (T). The ground principle of MRI involves measuring signals from the tissue's hydrogen nuclei (protons), which are abundantly available in the human body. Since the proton is positively charged and also possesses a spin, it thereby induces a magnetic field and thus has a small magnetic dipole moment associated with it. However, due to the random orientation of these spin vectors, the tissue holds zero net magnetization. But, on placing this tissue in an external magnetic field, say in an MRI scanner with a static magnetic field $B_\circ$ (say $B_\circ$ =3T), the spins either align in parallel or anti-parallel direction. Besides, protons also precess around the magnetic field lines, much similar to a spinning top. Thus, the parallel alignment of these precessing protons leads to a net magnetic field in the tissue ($M$) which is longitudinal to the external magnetic field. Also, the rate of precession depends on the strength of the static external magnetic field and is mathematically expressed as the Larmor equation (Brown & Semelka, 2003), as described below (Equation 1.1).

$$\omega_\circ = \gamma B_\circ \qquad \text{Equation 1.1}$$

where $B_\circ$ is the aforementioned external field, $\omega_\circ$ is the precession frequency, and $\gamma$ is the gyromagnetic ratio whose value for protons is 42.5 MHz/T. The longitudinal magnetic field in the tissue cannot be measured directly. Hence, a Radio Frequency (RF) pulse tuned to the precession frequency of protons (Larmor frequency) in tissue is transmitted and causes two simultaneous phenomena. First, the protons gain energy and transfer to a higher energy state, and second, they exhibit in-phase precession. Thus, the longitudinal magnetization ($M_Z$) is reduced, and a transversal magnetization ($M_{XY}$) is established. Moreover, subsequently, the transversal magnetization ($M_{XY}$) reduces and longitudinal magnetization ($M_Z$) is regained as protons release the energy they gained from RF pulse. Bloch and their colleagues (F. Bloch, W.E.Hansen, 1946)

discovered this phenomenon during an experiment. They observed that a nuclear magnetic resonance (NMR) induction represents a transient phenomenon, and the signal decay occurs because of the interaction of individual spins with the environment and with each other. Thus, there exists an innate tendency not to precess indefinitely and return to the initial parallel alignment ($M_Z$). Thus, a process called 'relaxation' occurs where this spin system releases energy into the environment. Bloch (F. Bloch, W.E.Hansen,1946) presented two-time constants for relaxation namely T1 (characterized retrieval of $M_Z$) and T2 (reflected decay in $M_{XY}$). Further, it was also concluded that T1 is a result of thermal energy exchange from the spins to the surroundings and T2 of spin-spin relaxation. The equations of motion for $M$ are as described below

$$M_X = M_\circ e^{-t/T2} \sin \omega t \qquad \text{Equation 1.2}$$

$$M_Y = M_\circ e^{-t/T2} \cos \omega t \qquad \text{Equation 1.3}$$

$$M_Z = M_\circ (1 - e^{-t/T1}) \qquad \text{Equation 1.4}$$

Thus T1 is the time taken by $M_Z$ to reach 63% of $M_\circ$ and T2 is the time taken by $M_X$ and $M_Y$ to decay till 37% of $M_\circ$. The RF pulse, which results in a $90^o$ shift in the magnetization, is called a $90^o$ RF pulse. Further, on switching this RF pulse off, the transversal magnetization switches back to the longitudinal magnetization. Thus, this changing magnetic field induces an electrical signal known as free induction decay (FID) signal. The decay of this FID after the application of a $90^o$ RF pulse leads to a faster T2* decay. This decay is an amalgamation of T2 decay as well as local magnetic field inhomogeneities. These T2* effects are utilized for rapid imaging sequences, also known as T2*- weighted gradient echo sequence (Mansfield, 1977), and also are ideally suited for fMRI acquisitions.

The blood oxygenation level-dependent (BOLD) contrast process is, at present, the cornerstone of human neuroimaging (Ogawa & Lee, 1990). During an increase in neural activity in a specific brain region, the glucose requirements and, thus, the rate of flow of blood to that region increases. Thus, the firing rate of the relevant neurons affects their metabolism leading to the arrival of more oxygenated blood. The increase in the flow of oxygenated blood changes the ratio of deoxygenated hemoglobin to oxygenated hemoglobin. Deoxygenated hemoglobin is paramagnetic (4 unpaired electrons) and causes inhomogeneities in the surrounding magnetic field, causing faster dephasing of spins and thus swift decay in transverse magnetization leading to dampened T2* signal. fMRI allows the localization of the brain activity within millimeters of its origin hence results in a good spatial resolution (typically 3x3x3 $mm^3$). However, the temporal resolution is limited by the hemodynamic response time, the BOLD response that peaks 5-6 seconds after the onset of the neural stimulus and has a width of about 3 seconds. Thus, the temporal information is blurred as the hemodynamic response time is much delayed from the onset of underlying neural processes (Glover, 2011). Moreover, the the BOLD signal is modelled utilizing the hemodynamic response function (HRF) (Figure 1.2) (Logothetis & Wandell, 2004). The analysis of fMRI data depends mainly on fitting a general linear model (GLM) to the data, consisting of event timing information convolved with an HRF model. The GLM, therefore, assumes that fMRI signal varies linearly with the experimental effects at every voxel (Ã & Villringer, 2006).

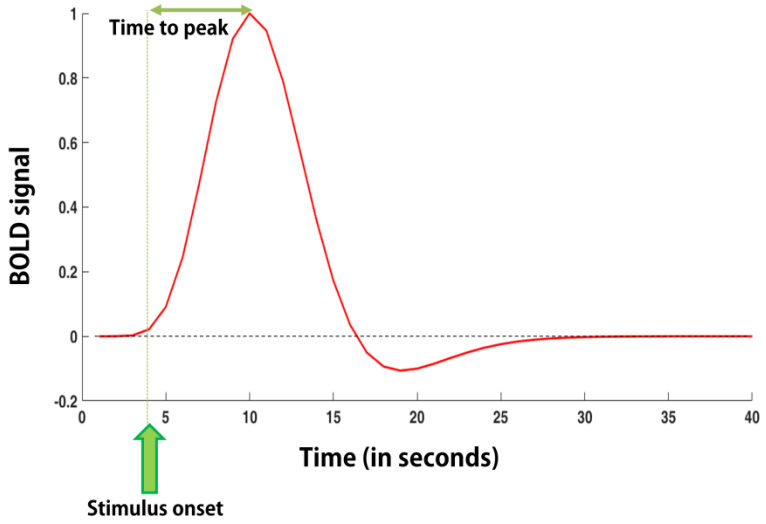


**Figure 1.2** The figure depicts the Hemodynamic Response Function (HRF) (Adapted from Huettel et al. (2009)).

### 1.2.1.2 Assessment of Hemispheric Asymmetry

Varied methods have been proposed to calculate the lateralization index based on fMRI BOLD information. The majority of such studies (Bradshaw, Thompson, et al., 2017; Karolis et al., 2019; Seghier, 2008) were task-based (language, face perception), and the asymmetry of BOLD signal strength, cluster size, and functional connectivity were utilized for hemispheric lateralization analysis. The hemispheric asymmetry linked to language processing is well-established in the fMRI side. The lateralization assessments in fMRI are conventionally estimated by comparing left and right hemispheres as given in Equation 1.5 (Bradshaw, Bishop, et al., 2017; Seghier et al., 2011).

$$LI = \frac{LH-RH}{LH+RH}$$ Equation 1.5

where LH and RH are counts of active voxels or measures of signal intensities in the left and right hemispheres, respectively.

### *1.2.2. ELECTROENCEPHALOGRAPHY (EEG)*

#### 1.2.2.1. Physiological basis

EEG is a potent technique for studying the brain's electrophysiological dynamics and linking those dynamics to various aspects such as perception, cognition, and action (Berger, 1934). EEG is a direct measure of population-level neural activity and has a high temporal resolution. However, the disadvantage is that EEG is limited to large, synchronous populations of neurons; and asynchronous activity is difficult or impossible to measure. Further, it also poses a limitation of reduced spatial resolution as the localization of an active site is limited to several centimeters. Each electrode in an EEG measures the dendritic postsynaptic potentials of neural populations in the cerebral cortex. Also, EEG substantially records the summed synchronous activity of not one, but thousands of underlying neurons as the signal reaches the electrodes after penetrating various layers of non-neural tissues, including the fluid, bones of the skull, and skin (Cohen, 2017).

Neurons are neural cells that constitute the structural and functional basis for brain function (Fratkin, 1997). These neurons form macrocircuits that involve interregional communication among a population of neurons, and microcircuits which reflect intra-regional local cell to cell interactions. The neurons, similar to other cells, consist of a cell body, called soma, which contains the nucleus and the organelles. However, neurons are specialized for

intercellular communication. The sites of interneuronal transmission in the central nervous system (CNS) are termed as synapses. The extensive branching of neurons aids electrical communication in them. Most neurons have one axon, often branched, to transmit signals to interconnected target neurons. The axon leaves the cell body from a small swelling called the axon hillock. Another salient aspect of this branching is the complex arborization of dendrites that receive synaptic inputs from other neurons (see Figure 1.3a). The typical arrangement for these communications includes axodendritic or axosomatic synapse, in which the axons of the cell of origin make their functional contact with the dendrites or cell body of the target neuron, respectively. Another less prevalent arrangement is the functional contact between adjacent cell bodies (somasomatic) and overlapping dendrites (dendrodendritic). Intrinsically neurons are not good conductors of electricity and carry a resting membrane potential (-40 to -60 mV). Stimuli cause electrical signals and, therefore, a deviation from this resting membrane potential.

Further, an axon and dendrites can found correspondence with a long electric cable that transmits voltages for certain distances. The neuron-cable theory (Byrne & Roberts, 2004) assumes that an insulating membrane surrounds dendrites and separates it from a conducting medium or extracellular space. The cable has a specific membrane capacitance ($C_M$), resistivity ($\rho_M$) and intracellular resistivity ($\rho_I$). Thus, if a membrane potential is altered at one end of the cable, the decay in voltage is exponential and is as described in the equation (Equation 1.6) below.

$$\Delta V_X = \Delta V_\circ e^{-\frac{X}{\delta}} \qquad \text{Equation 1.6}$$

where $\Delta V_X$ is the voltage change at distance x, $\Delta V_\circ$ is the imposed voltage change and $\delta$ is the 'space constant' of the cable, given by $\delta = \sqrt[2]{\frac{D}{4}\frac{\rho_M}{\rho_I}}$, where D is the diameter of the cable,

although axons are not good conductors, they send electrical signals over long distances utilizing the action potentials. Action potential carries the information along the length of axon by making the transmembrane potential positive. These electrical signals arise from ion fluxes as cell membranes are selectively permeable to different ions (potassium ions ($K^+$), chloride ions ($Cl^-$), sodium ions ($Na^+$)), and other organic anions, and also because these ions are non-uniformly distributed across the membrane (see Figure 1.3b). Further, as the action potential reaches the nerve terminal, it releases neurotransmitters, which enter the postsynaptic terminal of the adjoining neuron. The neurotransmitters cause modulation in ions permeability in the target neuron's membrane that leads to alterations in voltages and setting up of postsynaptic potentials, which represents the most prominent source of EEG signals (Buzsáki et al., 2012).

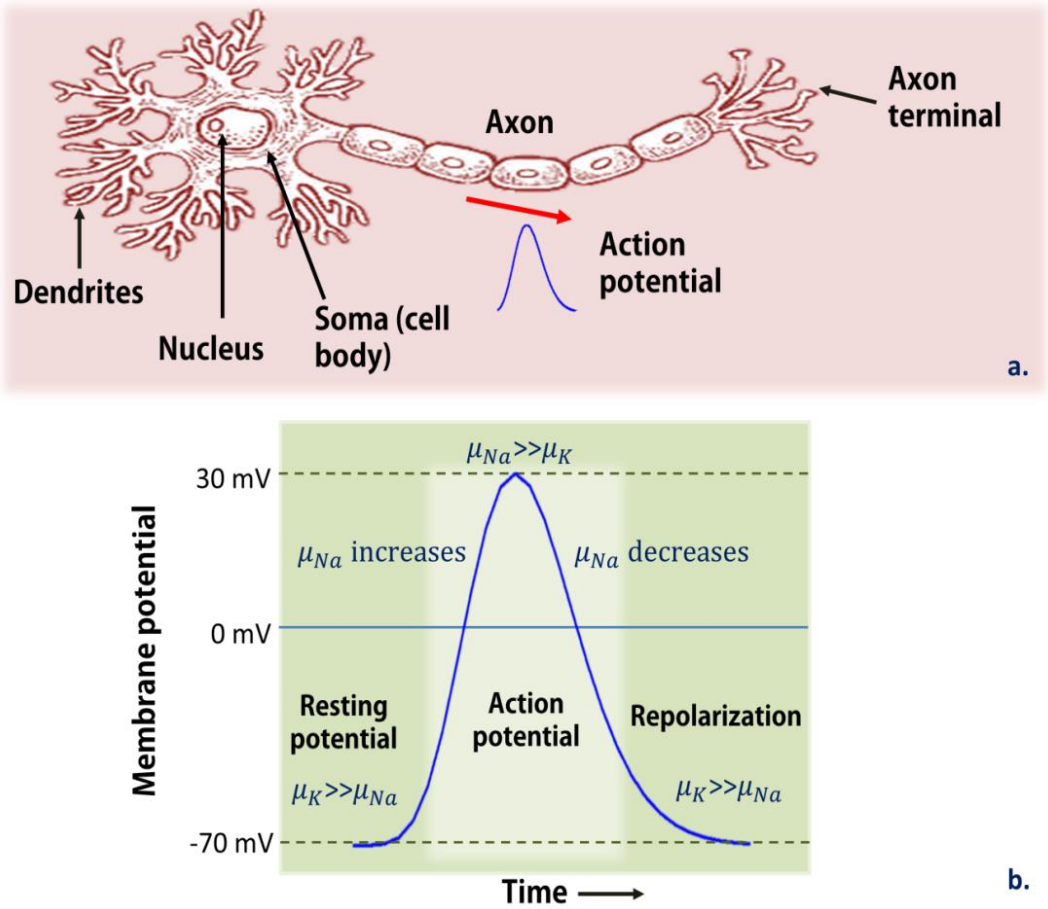


**Figure 1.3** Diagram depicting a. the parts of neuron b. action potential, through which signals are conducted in axons and the associated membrane ionic permeabilities. At rest, membranes are permeable to $K^+$ ions, while during an action potential, the permeability towards $Na^+$ ions increases for a temporary period (Adapted from Purves et al. (2004)).

### 1.2.2.2 EEG rhythms

EEG activity is categorized into specific distinctive frequencies termed as EEG rhythms. These rhythms possess intricate spatiotemporal characteristics based on amplitude, frequency, and timing and are driven by variation in the excitation of neuronal populations. Further, these variations have found tight coupling with cognitive and emotional processes. The existing EEG rhythms are delta (0-4 Hz), theta (4-8 Hz), alpha (8-12 Hz), beta (12-30 Hz), and gamma (30-70 Hz) (Buzsáki, 2009). A specific EEG rhythm worth emphasizing is the Alpha rhythm

(Barzegaran et al., 2017; Halgren et al., 2019). Modern ideas about alpha oscillations suggest their involvement in synchronizing temporal dynamics to the inhibition of neural networks. Several distinct mechanisms can serve as potential generators of alpha oscillations whose features, such as peak frequency, amplitude, and time-course can alter with the cortical region or nature of the cognitive task (Klimesch, 2012; Wolff et al., 2017).

#### 1.2.2.3 Assessment of hemispheric asymmetry

Alpha asymmetry, specifically *Frontal alpha asymmetry* (Equation 1.7) derived from absolute alpha powers, is an indirect relative frontal activity marker of asymmetry and has been widely studied in past decades as a measure to examine emotion and motivation-related trait and state differences (J. A. Coan & Allen, 2004; Davidson et al., 1990; Palmiero & Piccardi, 2017).

$$Frontal\ alpha\ asymmetry\ = \ln\left(alpha^{Right}\right) - \ln(alpha^{Left}) \qquad \text{Equation 1.7}$$

where, $alpha^{Right}$ and $alpha^{Left}$ are the standard alpha powers measured at the right and left hemispheric frontal channels for an individual's EEG data, respectively.

Frontal asymmetry has been recorded and analyzed during task engagement and resting-state conditions. One dominant view suggests that resting EEG frontal asymmetry reflects the tendencies of a person to involve in motivational (approach/withdrawal) and emotional (positive/negative) states (J. Coan, 2003; Mathersul et al., 2008). Also, during task engagement (Smith et al., 2017), the higher relative left than right frontal neural activity is known to characterize approach behavior. In contrast, withdrawal-related traits and states were linked to the greater right than left frontal neural activity. Further, other variables, such as executive functions, verbal fluency, have also been linked to frontal alpha asymmetry (Brzezicka et al., 2017; Hanouneh et al., 2017).

## 1.3 RECORDING AND ANALYSIS OF SIMULTANEOUS EEG-fMRI DATA

The complementary strengths and weaknesses of EEG and fMRI modalities have enkindled their convergence (see Figure 1.4). Thus, the simultaneous recording and analysis of noninvasive EEG and fMRI techniques have gathered considerable attention in the neuroscience community (Huster et al., 2012; Mele et al., 2019). The simultaneous recordings of EEG-fMRI were initially utilized for diagnosis and pre-surgical planning of epileptogenic EEG activity as they improved the localization of the associated neural sources (Huster et al., 2012). The analysis of the simultaneous recordings mentioned above aid in identifying the cortical region responsible for the spread of these neuronal events, which otherwise was difficult to achieve from distinct recordings. Recently, simultaneous EEG-fMRI has been recorded for spontaneous resting-state brain activity (de Munck et al., 2005; Goldman et al., 2002) as well as for stimulus-driven cognitive experiments to solve fundamental cognitive neuroscience research questions (Hoppstädter et al., 2015; Iannaccone et al., 2015). A typical experiment for simultaneous EEG-fMRI involves first, the preparation of an MR-compatible EEG cap placed on an individual's head outside the MR-scanner, and lowering the impedance of the silver electrodes for better signal quality. Next, the individual is moved to the MR-scanner with the hardware-setup, as explained in Figure 1.5. The signals are transmitted outside the MR-scanner using optical cables. An ECG lead, which serves as a temporal marker for an individual's heartbeat, is placed at its back. The onsets for fMRI volume acquisitions are also recorded by connecting the EEG recording device to the TTL output from the MR-scanner (Michel & Brandeis, 2010). Moreover, approaches that allowed direct integration of information across simultaneously recorded EEG-fMRI were needed to take full advantage of data acquired from these multimodalities. There

exist asymmetric and symmetric methods for data integration, as described in the subsequent subsection.

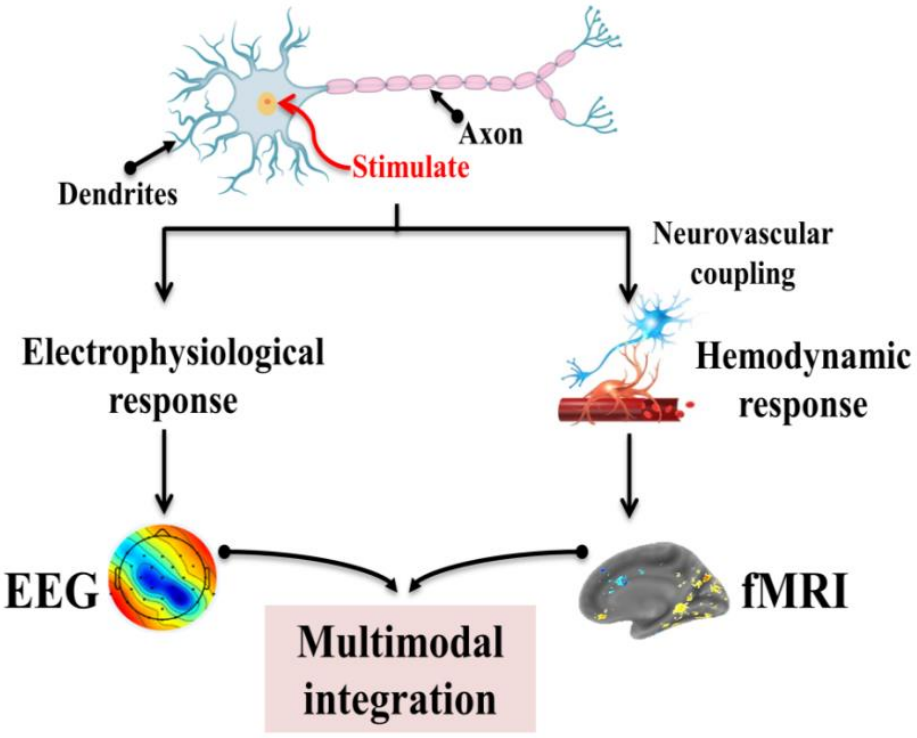


**Figure 1.4** Schematic for data-integration of simultaneous EEG-fMRI (Modified from He & Liu (2008)).

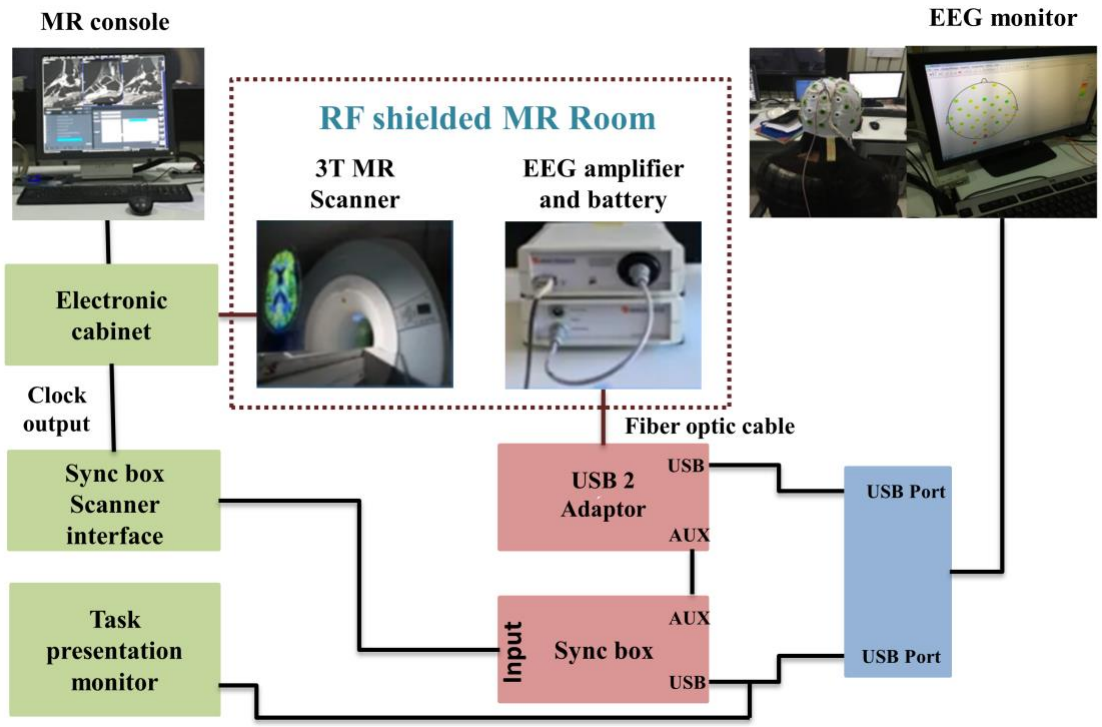


**Figure 1.5** Schematic for simultaneous EEG-fMRI recording hardware setup (Modified from Shah et al. (2017)).

### *1.3.1 ASYMMETRIC APPROACHES*

These integration approaches are characterized by a biased weighing of modalities wherein some feature of one modality guides the analysis of the other. The two main methods which exist are EEG-informed fMRI and fMRI-informed EEG approaches (Ã & Villringer, 2006).

#### 1.3.1.1 EEG informed fMRI

This technique considers associations of changes between EEG and fMRI signals over time. EEG features, such as ERP amplitudes and latencies, the power within specific EEG frequency bands, EEG synchronization, and phase coherence, are extracted from preprocessed

EEG data. Subsequently, fMRI data is preprocessed, and the derived-EEG features are utilized to modulate the modeled hemodynamic responses at the first-level parametrically. Successively, the group-level analysis is carried out for the resulting beta-estimates to divulge the significantly co-varying brain regions (Leicht et al., 2016).

#### 1.3.1.2 fMRI-informed EEG

fMRI-informed EEG exploits fMRI to guide the EEG source imaging to improve the spatial EEG inverse problem. Thus at first, a forward model is established from the previously estimated head geometry and biophysical characteristics of the brain. The forward model calculates the paths of current for a stimulated neural event. Further, utilizing the forward model, the source localization algorithms yield the most optimal collection of neural generators for a given scalp field potential. Thus, neuronal activity can possibly be approximated by distributed current sources or a limited number of single current dipoles. Finally, the statistical fMRI maps help in inferring these potential EEG generators (Wang et al., 2018).

### *1.3.2 SYMMETRIC APPROACHES*

Symmetric approaches employ forward or degenerative models to assess information jointly from both modalities. Studies under this domain have exploited independent component analysis (ICA) for integrating both the modalities. This framework correlates the trial-to-trial modulation across statistically independent maps from the fMRI (spatial ICA) and independent time courses from the EEG (temporal ICA). Thus, ICA models data as a linear combination of spatial FMRI maps and EEG time courses while maximizing independence between the maps (Wei et al., 2020).

## 1.4 IDENTIFICATION OF RESEARCH GAPS

a. The hemispheric lateralization based on EEG is linked with the preferential engagement of left, phasic, or right-lateralized sustained cognitive processes to circumvent the changing task demands. This represents yet another feature of multi-faceted hemispheric asymmetry, where it links to performance in any task engagement. However, the association of neural mechanisms of resting frontal EEG alpha asymmetry, which may affect the participation in a subsequent higher-order cognitive task such as Situational Awareness (Endsley, 1995; Sarter, 1990; Wickens, 2002), is underexplored.

b. Although the studies have proved EEG based frontal asymmetry assessment as a reliable marker of affect, approach/withdrawal behavior during emotional task-engagement, its validity in healthy individuals during resting remains ambiguous (Smith et al., 2017). Several methodological factors that may account for these conflicting results include 1) EEG-reference was chosen for the analysis, 2) across sessions stability of EEG asymmetry, 3) EEG recording length, 4) sex differences, 5) comorbid conditions and need to be further explored.

## 1.5 OBJECTIVES OF THE THESIS

***The focus of the current thesis is to examine the computational models for resting hemispheric asymmetry research utilizing the technique of simultaneous EEG-fMRI data acquisition. Exploring these resting-state EEG/fMRI hemispheric asymmetry models in the brain is vital to understand human actions when engaged in an external task. Further, the goal is to assess these resting models' potential for real-time assessment of measures of affect***

***and approach/withdrawal behavior for application in domains such as military/aviation. The precise objectives are as follows.***

a. **Employing strategies for improving the signal-to-noise ratio to alleviate the effect of MR-related and other artifacts in EEG asymmetry calculation.** This objective is carried to ensure that the asymmetry estimations are performed on an EEG data, which is devoid of Magnetic resonance (MR) gradient, cardioballistic (CB), and other conventional EEG-related artifacts. This objective involved following a specific protocol and utilizing an automated toolbox for mitigating these artifacts.

b. **Assessing the linkage between the standard resting frontal alpha EEG asymmetry model and the subsequent engagement in Situational awareness (SA) task.** This objective attempts to link the neural substrates underlying resting frontal alpha asymmetry to subsequent SA-task outcome. SA is crucial for operations in the military/aviation domain and involves the perception and comprehension of all the elements in an environment and anticipation of possible future situations. The pre-task resting frontal alpha asymmetry may index neural mechanisms that might potentiate its application as a vital parameter to be assessed before SA-task to improve SA-task's performance outcomes. The fulfillment of this objective required:

   **I.** Design and development of SA cognitive paradigm.

   **II.** Assessing EEG alpha power and its associated standard frontal hemispheric asymmetry from resting-state recordings and utilizing the robust correlation, EEG-fMRI data integration approach and functional connectivity analysis for

evaluating the effect of neural mechanisms of the resting asymmetry model on subsequent SA-task.

c. **Assessing the linkage between the standard resting frontal alpha EEG asymmetry model and positive/negative affect and approach/withdrawal behaviors.** This objective is carried to understand the relevance of real-time recordings of standard resting alpha EEG asymmetry in terms of its association with measures of affect and approach/withdrawal behavior. Further, to strengthen the findings and to potentiate the use of resting alpha EEG asymmetry for real-time assessment of affect and approach/withdrawal behavior while still restoring the related fMRI features, EEG-informed fMRI was employed. Thus, the completion of this objective included:

   **I.** Estimating the neural mechanisms and associated asymmetry in the resting functional connectivity underlying the self-reported measures of positive/negative affect and approach/withdrawal behavior.

   **II.** Assessment of standard alpha frontal asymmetry and its linkage to self-reported measures of positive/negative affect and approach/withdrawal behavior.

   **III.** Analyzing the neural mechanisms underlying these standard frontal alpha asymmetry measures utilizing the EEG-informed fMRI approach.

d. **Assessing the novel microstate-based resting frontal alpha asymmetry measures and testing its efficacy against standard frontal alpha asymmetry measures in explaining affect and approach/withdrawal behavior.** The rationale for this objective was that the

EEG patterns' stability might play a vital methodological factor in explaining the inconsistent nature of the relationship among resting frontal alpha asymmetry and affect and approach/withdrawal measures. Thus, microstates-based resting frontal alpha asymmetry was assessed as EEG microstates represent moments of quasi-stable EEG activity, and its efficacy against standard asymmetry measure was evaluated. Similar to the previous objective, EEG-informed fMRI analysis was utilized to map features of microstate-based EEG asymmetry to fMRI. The steps involved in this analysis included:

**I.** Assessment of microstate-based EEG asymmetry and its linkage to self-reported measures of positive/negative affect and approach/withdrawal behavior and to test them against the results obtained for standard resting frontal alpha EEG asymmetry.

**II.** Analyzing the neural mechanisms underlying these microstate-based frontal alpha asymmetry measures utilizing the EEG-informed fMRI approach.

**III.** Assessment of index for hemodynamic lateralization from simultaneously recorded resting-fMRI data for the neural mechanisms obtained from standard and microstate-based frontal alpha asymmetry measures and gauging their linkage to self-reported measures of affect and approach/withdrawal behavior.

## 1.6 ORGANIZATION OF THE THESIS

To accommodate all the research objectives, the thesis is organized into six chapters. The references for each chapter are listed at the end of that chapter. The elements of each chapter are as described below.

a. ***Chapter two*** comprises the methodology adopted to enhance the signal-to-noise ratio by alleviating the effects of MR gradient, CB, and other conventional EEG-related artifacts on EEG data. The chapter includes an in-depth explanation for the basis of MR gradient, CB artifacts, and the techniques at hand for alleviating these artifacts. The chapter further explains the EEG processing pipeline we adopted to remove these artifacts and validates it through a dataset utilized in the later stage of the thesis.

***b.*** The work for the completion of this thesis involved the design and development of a SA paradigm. Keeping in mind the compatibility of task performance in an MR environment, we chose to employ a modified Stroop-test to study SA. SA is knowledge about the environment and has become the focus of the ergonomics community recently and is a critical parameter for military/aviation operations (Sarter, 1990; Wickens, 2002). The work stands novel and brings clarity on the influence of neural mechanisms of pre-task resting alpha and its associated standard frontal asymmetry on subsequently performed SA-task when the Stroop effect (Jensen & Rohwer, 1966) influences the task and has been encompassed in ***Chapter three.*** It is favorable to study the effect of pre-task resting alpha and its associated frontal asymmetry on the SA-task to improve SA. For this purpose, resting pre-SA task EEG features, such as pre-task resting absolute alpha (PRAA) power and pre-task resting alpha frontal asymmetry (PRAFA) index, were assessed from eighteen healthy volunteers and their robust correlation with subsequently performed SA-task's performance measures was estimated. Further, neural underpinnings of PRAA, PRAFA in SA-task were analyzed through the EEG-informed fMRI approach, and functional connectivity analysis was performed among the neural underpinnings of

SA-task, PRAA, and PRAFA. The results actively supported the hypothesis that the resting frontal alpha asymmetry and associated neural mechanisms significantly influence the SA-task's neural mechanisms and performance measures. This work has been published (Kaur et al., 2019) in the Human Factors: The Journal of the Human Factors and Ergonomics Society.

c. After assessing the linkage among the neural mechanisms of standard resting alpha frontal asymmetry with the SA-task outcome, our goal was to test the standard alpha frontal asymmetry in terms of its linkage with psychological constructs such as affect, fatigue, personality, motivation, etc. Frontal alpha asymmetry is a reliable indicator of affect, approach/withdrawal behavior during tasks evoking emotions, and clinical populations (Reznik & Allen, 2017). However, the validity of resting frontal alpha asymmetry in healthy individuals regarding its association with affect and approach/withdrawal measures remains ambiguous. This motivated us to initially test the association of resting frontal alpha asymmetry with an individual's affect and approach/withdrawal measures.

Next, we posited that EEG information's stability may serve as an imperative parameter for bringing forth the relationship of alpha asymmetry with measures of affect and approach/withdrawal behavior. ***Chapter four*** comprises our study on the Microstates-based resting frontal alpha asymmetry approach for understanding affect and approach/withdrawal behavior, which has been published in Scientific Reports (Kaur et al., 2020). For this study, frontal alpha asymmetry based on microstates that assess quasi-stable EEG scalp topography information was evaluated and compared against standard

frontal asymmetry. Recently, in spontaneous resting EEG, it has been shown that there exist distinct periods of time exhibiting stable scalp topography, and these have been referred to as EEG microstates (Michel & Koenig, 2018). Thus, for this study, frontal alpha asymmetry based on microstates was proposed, and its effectiveness against standard frontal asymmetry was assessed. Both proposed and standard frontal alpha asymmetries were estimated from thirty-nine healthy volunteers' simultaneous EEG-fMRI recordings. Further, neural underpinnings of these asymmetry measures were determined through EEG-informed fMRI. Subsequently, the Hemodynamic Lateralization Index (HLI) of both asymmetry measures neural underpinnings was assessed. Finally, the robust correlation of both asymmetry measures and their HLI with measures of positive/negative affect and approach/withdrawal behavior was carried out. The results revealed that standard resting frontal asymmetry and its HLI yielded no significant relationship with any psychological measures. However, the microstate resting frontal asymmetry correlated significantly with negative affect, and its neural underpinning's HLI significantly correlated with positive/negative affect and approach/withdrawal measures. Thus, the results reveal that resting microstates-based frontal alpha asymmetry better assesses the neural mechanisms of affective and approach/withdrawal measures.

d. Following the analysis of association of resting standard and microstates-based frontal alpha asymmetry with affect and approach/withdrawal measures, we focussed on understanding the key role of subcortical structures, their interactions with cortical areas, and functional hemispheric asymmetry of cortical regions vital for subcortical-cortical

interactions dominating affect and approach/withdrawal behavior. This knowledge would foster the know-how on their role in subsequent task-engagement and the interlinkage among affective measures and approach/withdrawal dichotomy. This study was based solely on the hemispheric asymmetry estimation of resting fMRI graph theory functional connectivity metrics as it is difficult to adequately sense the deeper subcortical signals using conventional EEG (32-channel) (Seeber et al., 2019) and is encompassed in ***Chapter five***.

Hence, in this study, we report the neuroimaging finding based on Region of Interest (ROI) based analysis and graph-theory measures for global and subnetworks for healthy thirty-nine male volunteers. Our study revealed the association of emotion and memory-related subcortical-cortical interactions in positive and negative affect. Right, amygdala-right thalamus-frontotemporal cortical-regions emanated in positive affect, and the right putamen-left hippocampus-frontotemporal cortical-regions network stemmed for negative affect. Then, we show the involvement of basal ganglia structures in approach-withdrawal dichotomy with tight coupling of right-caudate, left-accumbens with anterior cingulate, and insular regions for withdrawal/inhibition system. Further, the distinct involvement of the insula (posterior) in affective states while insula (anterior) in approach/withdrawal systems builds-up for the existence of a feedback-loop between affective and approach/withdrawal systems. Lastly, on probing the lateralization of the strength of degree-measures of the cortical substrates vital for subcortical-cortical interaction, we found a left-hemispheric proclivity for affective measures. The key findings of this resting-study asymmetry can form the basis for studies involving task-engagement or clinical population.

e. ***Chapter six*** sums up the research and highlights the conclusions that can be drawn from the results obtained in the present thesis. This chapter also discusses some of the directions for future work that can emanate from this research.

## REFERENCES


Ã, P. R., & Villringer, A. (2006). *Simultaneous EEG – fMRI*. *30*, 823–838. https://doi.org/10.1016/j.neubiorev.2006.06.008

Alves, N. T., Fukusima, S. S., & Aznar-Casanova, J. A. (2008). Models of brain asymmetry in emotional processing. *Psychology & Neuroscience*, *1*(1), 63–66. https://doi.org/10.3922/j.psns.2008.1.010

Ambrosini, E., & Vallesi, A. (2015). Asymmetry in prefrontal resting-state EEG spectral power underlies individual differences in phasic and sustained cognitive control. *NeuroImage*. https://doi.org/10.1016/j.neuroimage.2015.09.035

Ambrosini, E., & Vallesi, A. (2016). *Domain-general Stroop Performance and Hemispheric Asymmetries : A Resting-state EEG Study*. 769–779. https://doi.org/10.1162/jocn

Ardila, A., Bernal, B., & Rosselli, M. (2016). How Localized are Language Brain Areas? A Review of Brodmann Areas Involvement in Oral Language. *Archives of Clinical Neuropsychology*, *31*(1), 112–122. https://doi.org/10.1093/arclin/acv081

Barzegaran, E., Vildavski, V. Y., & Knyazeva, M. G. (2017). Fine Structure of Posterior Alpha Rhythm in Human EEG: Frequency Components, Their Cortical Sources, and Temporal Behavior. *Scientific Reports*, *7*(1), 1–12. https://doi.org/10.1038/s41598-017-08421-z

Berger, H. (1934). Über das Elektrenkephalogramm des Menschen. *Archiv Für Psychiatrie Und Nervenkrankheiten*, *101*(1), 452–469. https://doi.org/10.1007/BF01789984

Bradshaw, A. R., Bishop, D. V. M., & Woodhead, Z. V. J. (2017). Methodological considerations in assessment of language lateralisation with fMRI: a systematic review. *PeerJ*, *5*, e3557. https://doi.org/10.7717/peerj.3557

Bradshaw, A. R., Thompson, P. A., Wilson, A. C., Bishop, D. V. M., & Woodhead, Z. V. J. (2017). Measuring language lateralisation with different language tasks: A systematic review. *PeerJ*, *2017*(10). https://doi.org/10.7717/peerj.3929

Broca, P. (1861). Remarques sur le siège de la faculté du langage articulé, suivies d'une observation d'aphémie (perte de la parole) [Remarks on the seat of the faculty of articulated language, following an observation of aphemia (loss of speech)]. *Bulletin de La Société Anatomique*, *6*, 330–357. https://doi.org/10.1111/j.1536-7150.2007.00528.x

Brown, M. A., & Semelka, R. C. (2003). *MRI Basic Principles and Applications* (3rd ed.). John Wiley & Sons, New Jersey.

Brzezicka, A., Kamiński, J., Kamińska, O. K., Wołyńczyk-Gmaj, D., & Sedek, G. (2017). Frontal EEG alpha band asymmetry as a predictor of reasoning deficiency in depressed people. *Cognition and Emotion*, *31*(5), 868–878. https://doi.org/10.1080/02699931.2016.1170669

Buzsáki, G. (2009). Rhythms of the Brain. In *Rhythms of the Brain*. https://doi.org/10.1093/acprof:oso/9780195301069.001.0001

Buzsáki, G., Anastassiou, C. A., & Koch, C. (2012). The origin of extracellular fields and currents-EEG, ECoG, LFP and spikes. *Nature Reviews Neuroscience*, *13*(6), 407–420. https://doi.org/10.1038/nrn3241

Byrne, J. M., & Roberts, J. L. (2004). From Molecules to Networks: An Introduction to Cellular and Molecular Neuroscience. In *From Molecules to Networks: An Introduction to Cellular and Molecular Neuroscience* (pp. 1–583). https://doi.org/10.1016/B978-0-12-397179-1.00010-5

Canli, T. (1999). Hemispheric asymmetry in the experience of emotion: A perspective from functional imaging. *Neuroscientist*, *5*(4), 201–207. https://doi.org/10.1177/107385849900500409

Chen, T. T., Wang, K. P., Cheng, M. Y., Chang, Y. T., Huang, C. J., & Hung, T. M. (2019). Open access impact of emotional and motivational regulation on putting performance: A frontal alpha asymmetry study. *PeerJ*, *2019*(4), 1–16. https://doi.org/10.7717/peerj.6777

Chiarello, C., Welcome, S. E., Halderman, L. K., & Leonard, C. M. (2009). Does degree of asymmetry relate to performance? An investigation of word recognition and reading in consistent and mixed handers. *Brain and Cognition*, *69*(3), 521–530. https://doi.org/10.1016/j.bandc.2008.11.002

Coan, J. (2003). *Coan JA , Allen JJB . Frontal EEG asymmetry and behavioral activation and inhibition systems . Frontal EEG asymmetry and the behavioral activation and inhibition systems*. *40*(FEBRUARY), 106–114. https://doi.org/10.1111/1469-8986.00011

Coan, J. A., & Allen, J. J. B. (2004). Frontal EEG asymmetry as a moderator and mediator of emotion. *Biological Psychology*, *67*(1–2), 7–49. https://doi.org/10.1016/j.biopsycho.2004.03.002

Cohen, M. X. (2017). Where Does EEG Come From and What Does It Mean? *Trends in Neurosciences*, *40*(4), 208–218. https://doi.org/10.1016/j.tins.2017.02.004

Davidson, R. J., Saron, C. D., Senulis, J. A., Ekman, P., & Friesen, W. V. (1990). Approach/withdrawal and cerebral asymmetry: Emotional\rexpression and brain physiology: I. *Journal of Personality and Social Psychology*, *58*(2), 330–341. https://doi.org/10.1037/0022-3514.58.2.330

de Munck, J. C., Pouwels, P. J. W., Schoonhoven, R., Van Someren, E. J. W., Hoogduin, J. M., Maurits, N. M., Gonçalves, S. I., Heethaar, R. M., Kuijer, J. P. A., & Lopes da Silva, F. H. (2005). Correlating the alpha rhythm to BOLD using simultaneous EEG/fMRI: Inter-subject variability. *NeuroImage*, *30*(1), 203–213. https://doi.org/10.1016/j.neuroimage.2005.09.062

Endsley, M. R. (1995). Toward a Theory of Situation Awareness in Dynamic Systems. *Human Factors: The Journal of the Human Factors and Ergonomics Society*, *37*(1), 32–64. https://doi.org/10.1518/001872095779049543

Everts, R., Lidzba, K., Wilke, M., Kiefer, C., Mordasini, M., Schroth, G., Perrig, W., & Steinlin, M. (2009). Strengthening of laterality of verbal and visuospatial functions during childhood and adolescence. *Human Brain Mapping*, *30*(2), 473–483. https://doi.org/10.1002/hbm.20523

F. Bloch, W.E.Hansen, M. P. (1946). Bloch_equation_Source. *Physical Review*, *70*(5), 474–485.

Foundas, A. L., Leonard, C. M., & Heilman, K. M. (1995). Morphologic Cerebral Asymmetries and Handedness: The Pars Triangularis and Planum Temporale. *Archives of Neurology*, *52*(5), 501–508. https://doi.org/10.1001/archneur.1995.00540290091023

Fratkin, J. (1997). Fundamental Neuroscience. In *Journal of Neuropathology and Experimental Neurology* (3rd ed., Vol. 56, Issue 12). https://doi.org/10.1097/00005072-199712000-00013

Geffen, G., Bradshaw, J. L., & Nettleton, N. C. (1972). Hemispheric asymmetry: Verbal and spatial encoding of visual stimuli. *Journal of Experimental Psychology*, *95*(1), 25–31. https://doi.org/10.1037/h0033265

Glover, G. H. (2011). Overview of functional magnetic resonance imaging. *Neurosurgery Clinics of North America*, *22*(2), 133–139. https://doi.org/10.1016/j.nec.2010.11.001

Goldman, R. I., Stern, J. M., Engel, J., & Cohen, M. S. (2002). Simultaneous EEG and fMRI of the alpha rhythm. *NeuroReport*, *13*(18), 2487–2492. https://doi.org/10.1097/00001756-200212200-00022

Halgren, M., Ulbert, I., Bastuji, H., Fabó, D., Eross, L., Rey, M., Devinsky, O., Doyle, W. K., Mak-McCully, R., Halgren, E., Wittner, L., Chauvel, P., Heit, G., Eskandar, E., Mandell, A., & Cash, S. S. (2019). The generation and propagation of the human alpha rhythm. *Proceedings of the National Academy of Sciences of the United States of America*, *116*(47), 23772–23782. https://doi.org/10.1073/pnas.1913092116

Hanouneh, S., Amin, H. U., Saad, N. M., & Malik, A. S. (2017). The correlation between EEG asymmetry and memory performance during semantic memory recall. *International Conference on Intelligent and Advanced Systems, ICIAS 2016*, 2–5. https://doi.org/10.1109/ICIAS.2016.7824041

He, B., & Liu, Z. (2008). Multimodal Functional Neuroimaging: Integrating Functional MRI and EEG/MEG. *IEEE Reviews in Biomedical Engineering*, *1*, 23–40. https://doi.org/10.1109/RBME.2008.2008233

Hirnstein, M., Hausmann, M., & Güntürkün, O. (2008). The evolutionary origins of functional cerebral asymmetries in humans: Does lateralization enhance parallel processing? *Behavioural Brain Research*, *187*(2), 297–303. https://doi.org/10.1016/j.bbr.2007.09.023

Hoppstädter, M., Baeuchl, C., Diener, C., Flor, H., & Meyer, P. (2015). Simultaneous EEG-fMRI reveals brain networks underlying recognition memory ERP old/new effects. *NeuroImage*, *116*, 112–122. https://doi.org/10.1016/j.neuroimage.2015.05.026

Huettel, S. A., Song, A. W., & McCarthy, G. (2009). *Functional magnetic resonance imaging*.

Hugdahl, K. (2011). Hemispheric asymmetry: Contributions from brain imaging. *Wiley Interdisciplinary Reviews: Cognitive Science*, *2*(5), 461–478. https://doi.org/10.1002/wcs.122

Huster, R. J., Debener, S., Eichele, T., & Herrmann, C. S. (2012). Methods for simultaneous EEG-fMRI: An introductory review. *Journal of Neuroscience*, *32*(18), 6053–6060. https://doi.org/10.1523/JNEUROSCI.0447-12.2012

Iannaccone, R., Hauser, T. U., Staempfli, P., Walitza, S., Brandeis, D., & Brem, S. (2015). Conflict monitoring and error processing: New insights from simultaneous EEG-fMRI. *NeuroImage*, *105*, 395–407. https://doi.org/10.1016/j.neuroimage.2014.10.028

Jensen, A. R., & Rohwer, W. D. (1966). The stroop color-word test: A review. *Acta Psychologica*, *25*(C), 36–93. https://doi.org/10.1016/0001-6918(66)90004-7

Karolis, V. R., Corbetta, M., & Thiebaut de Schotten, M. (2019). The architecture of functional lateralisation and its relationship to callosal connectivity in the human brain. *Nature Communications*, *10*(1), 1–9. https://doi.org/10.1038/s41467-019-09344-1

Kaur, A., Chaujar, R., & Chinnadurai, V. (2019). Effects of Neural Mechanisms of Pretask Resting EEG Alpha Information on Situational Awareness: A Functional Connectivity Approach. *Human Factors*. https://doi.org/10.1177/0018720819869129

Kaur, A., Chinnadurai, V., & Chaujar, R. (2020). Microstates-based resting frontal alpha asymmetry approach for understanding affect and approach/withdrawal behavior. *Scientific Reports*, *10*(1), 1–25. https://doi.org/10.1038/s41598-020-61119-7

Killgore, W. D. S., & Yurgelun-Todd, D. A. (2007). The right-hemisphere and valence hypotheses: Could they both be right (and sometimes left)? *Social Cognitive and Affective Neuroscience*, *2*(3), 240–250. https://doi.org/10.1093/scan/nsm020

Klimesch, W. (2012). Alpha-band oscillations, attention, and controlled access to stored information. *Trends in Cognitive Sciences*, *16*(12), 606–617. https://doi.org/10.1016/j.tics.2012.10.007

Knecht, S., Dräger, B., Deppe, M., Bobe, L., Lohmann, H., Flöel, A., Ringelstein, E. B., & Henningsen, H. (2000). Handedness and hemispheric language dominance in healthy humans. *Brain*, *123*(12), 2512–2518. https://doi.org/10.1093/brain/123.12.2512

Kong, X. Z., Mathias, S. R., Guadalupe, T., Abé, C., Agartz, I., Akudjedu, T. N., Aleman, A., Alhusaini, S., Allen, N. B., Ames, D., Andreassen, O. A., Vasquez, A. A., Armstrong, N. J., Bergo, F., Bastin, M. E., Batalla, A., Bauer, J., Baune, B. T., Baur-Streubel, R., … Orhan, F. (2018). Mapping cortical brain asymmetry in 17,141 healthy individuals worldwide via the ENIGMA consortium. *Proceedings of the National Academy of Sciences of the United States of America*, *115*(22), E5154–E5163. https://doi.org/10.1073/pnas.1718418115

Lauterbur, P. C. (1973). Image Formation by Induced Local Interactions: Examples Employing Nuclear Magnetic Resonance. *Nature*, *242*, 190–191. https://doi.org/10.1038/246421a0

Leicht, G., Vauth, S., Polomac, N., Andreou, C., Rauh, J., Mußmann, M., Karow, A., & Mulert, C. (2016). EEG-Informed fMRI Reveals a Disturbed Gamma-Band-Specific Network in Subjects at High Risk for Psychosis. *Schizophrenia Bulletin*, *42*(1), 239–249. https://doi.org/10.1093/schbul/sbv092

Logothetis, N. K., & Wandell, B. A. (2004). Interpreting the BOLD signal. *Annual Review of Physiology*, *66*, 735–769. https://doi.org/10.1146/annurev.physiol.66.082602.092845

Mansfield, P. (1977). Multi-planar image formation using NMR spin echoes. *Journal of Physics C: Solid State Physics*, *10*(3). https://doi.org/10.1088/0022-3719/10/3/004

Mansfield, P., & Grannell, P. K. (1973). NMR "diffraction" in solids? *Journal of Physics C: Solid State Physics*, *6*(6:), L422–L425.

Mathersul, D., Williams, L. M., Hopkinson, P. J., & Kemp, A. H. (2008). Investigating Models of Affect: Relationships Among EEG Alpha Asymmetry, Depression, and Anxiety. *Emotion*, *8*(4), 560–572. https://doi.org/10.1037/a0012811

Mele, G., Cavaliere, C., Alfano, V., Orsini, M., Salvatore, M., & Aiello, M. (2019). Simultaneous EEG-fMRI for functional neurological assessment. *Frontiers in Neurology*, *10*(JUL).

https://doi.org/10.3389/fneur.2019.00848

Michel, C. M., & Brandeis, D. (2010). *Simultaneous EEG and fMRI : Recording, Analysis, and Application* (Vol. 9780195372). https://doi.org/10.1093/acprof:oso/9780195372731.003.0001

Michel, C. M., & Koenig, T. (2018). EEG microstates as a tool for studying the temporal dynamics of whole-brain neuronal networks: A review. *NeuroImage*, *180*, 577–593. https://doi.org/10.1016/j.neuroimage.2017.11.062

Mooshagian, E. (2008). Anatomy of the corpus callosum reveals its function. *Journal of Neuroscience*, *28*(7), 1535–1536. https://doi.org/10.1523/JNEUROSCI.5426-07.2008

O'Regan, L., & Serrien, D. J. (2018). Individual Differences and Hemispheric Asymmetries for Language and Spatial Attention. *Frontiers in Human Neuroscience*, *12*(October), 1–13. https://doi.org/10.3389/fnhum.2018.00380

Ogawa, S., & Lee, T. -M. (1990). Magnetic resonance imaging of blood vessels at high fields: In vivo and in vitro measurements and image simulation. *Magnetic Resonance in Medicine*, *16*(1), 9–18. https://doi.org/10.1002/mrm.1910160103

Ogawa, S., Lee, T. -M, Nayak, A. S., & Glynn, P. (1990). Oxygenation-sensitive contrast in magnetic resonance image of rodent brain at high magnetic fields. *Magnetic Resonance in Medicine*, *14*(1), 68–78. https://doi.org/10.1002/mrm.1910140108

Palmiero, M., & Piccardi, L. (2017). Frontal EEG Asymmetry of Mood: A Mini-Review. *Frontiers in Behavioral Neuroscience*, *11*(November), 1–8. https://doi.org/10.3389/fnbeh.2017.00224

Purves, D., Augustine, G. J., Fitzpatrick, D., Hall, W. C., LaMantia, A.-S., McNamara, J. O., & Williams, S. M. (2004). *Neuroscience* (3rd ed.). Sinauer Associates, Inc.

Rentería, M. E. (2012). Cerebral asymmetry: A quantitative, multifactorial, and plastic brain phenotype. *Twin Research and Human Genetics*, *15*(3), 401–413. https://doi.org/10.1017/thg.2012.13

Reznik, S. J., & Allen, J. J. B. (2017). Frontal asymmetry as a mediator and moderator of emotion: An updated review. *Psychophysiology*, *January*. https://doi.org/10.1111/psyp.12965

Rogers, L. J., Vallortigara, G., & Andrew, R. J. (2013). Divided Brains. In *Divided Brains*. https://doi.org/10.1017/cbo9780511793899

Roland, J. L., Snyder, A. Z., Hacker, C. D., Mitra, A., Shimony, J. S., Limbrick, D. D., Raichle, M. E., Smyth, M. D., & Leuthardt, E. C. (2017). On the role of the corpus callosum in interhemispheric functional connectivity in humans. *Proceedings of the National Academy of Sciences of the United States of America*, *114*(50), 13278–13283. https://doi.org/10.1073/pnas.1707050114

Sarter, N. B. (1990). Situation awareness. A critical but ill-defined phenomenon. *Proceedings of the Human Factors Society*, 23.

Seeber, M., Cantonas, L. M., Hoevels, M., Sesia, T., Visser-Vandewalle, V., & Michel, C. M. (2019). Subcortical electrophysiological activity is detectable with high-density EEG source imaging. *Nature Communications*, *10*(1), 1–7. https://doi.org/10.1038/s41467-019-08725-w

Seghier, M. L. (2008). Laterality index in functional MRI: methodological issues. *Magnetic Resonance Imaging*, *26*(5), 594–601. https://doi.org/10.1016/j.mri.2007.10.010

Seghier, M. L., Kherif, F., Josse, G., & Price, C. J. (2011). Regional and hemispheric determinants of language laterality: Implications for preoperative fMRI. *Human Brain Mapping*, *32*(10), 1602–1614. https://doi.org/10.1002/hbm.21130

Shah, N. J., Arrubla, J., Rajkumar, R., Farrher, E., Mauler, J., Kops, E. R., Tellmann, L., Scheins, J., Boers, F., Dammers, J., Sripad, P., Lerche, C., Langen, K. J., Herzog, H., & Neuner, I. (2017). Multimodal Fingerprints of Resting State Networks as assessed by Simultaneous Trimodal MR-PET-EEG Imaging. *Scientific Reports*, *7*(1), 1–13. https://doi.org/10.1038/s41598-017-05484-w

Shulman, G. L., Pope, D. L. W., Astafiev, S. V., McAvoy, M. P., Snyder, A. Z., & Corbetta, M. (2010). Right hemisphere dominance during spatial selective attention and target detection occurs outside the dorsal frontoparietal network. *Journal of Neuroscience*, *30*(10), 3640–3651. https://doi.org/10.1523/JNEUROSCI.4085-09.2010

Smith, E. E., Reznik, S. J., Stewart, J. L., & Allen, J. J. B. (2017). Assessing and conceptualizing frontal EEG asymmetry: An updated primer on recording, processing, analyzing, and interpreting frontal alpha asymmetry. *International Journal of Psychophysiology*, *111*, 98–114. https://doi.org/10.1016/j.ijpsycho.2016.11.005

Toga, A. W., Narr, K. L., Thompson, P. M., & Luders, E. (2009). Brain asymmetry: Evolution. *Encyclopedia of Neuroscience*, 303–311. https://doi.org/10.1016/B978-008045046-9.00936-0

Toga, Arthur W., & Thompson, P. M. (2003). Mapping brain asymmetry. *Nature Reviews Neuroscience*, *4*(1), 37–48. https://doi.org/10.1038/nrn1009

Wang, H., Lei, X., Zhan, Z., Yao, L., & Wu, X. (2018). A new fMRI informed mixed-norm constrained algorithm for EEG source localization. *IEEE Access*, *6*(c), 8258–8269. https://doi.org/10.1109/ACCESS.2018.2792442

Wei, H., Jafarian, A., Zeidman, P., Litvak, V., Razi, A., Hu, D., & Friston, K. J. (2020). Bayesian fusion and multimodal DCM for EEG and fMRI. *NeuroImage*, *211*(February), 116595. https://doi.org/10.1016/j.neuroimage.2020.116595

Wernicke, C. (1974). Der Aphasische Symptomencomplex; Eine Psychologische Studie Auf Anatomischer Basis. In *Springer Verlag*.

Wickens, C. D. (2002). Situation awareness and workload in aviation. *Current Directions in Psychological Science*, *11*(4), 128–133. https://doi.org/10.1111/1467-8721.00184

Wolff, N., Zink, N., Stock, A. K., & Beste, C. (2017). On the relevance of the alpha frequency oscillation's small-world network architecture for cognitive flexibility. *Scientific Reports*, *7*(1), 1–12. https://doi.org/10.1038/s41598-017-14490-x

Wyczesany, M., Capotosto, P., Zappasodi, F., & Prete, G. (2018). Hemispheric asymmetries and emotions: Evidence from effective connectivity. *Neuropsychologia*, *121*, 98–105. https://doi.org/10.1016/j.neuropsychologia.2018.10.007

# CHAPTER TWO

# OPTIMIZATION AND VALIDATION OF EEG PREPROCESSING PIPELINE

## 2.1 ABSTRACT

The simultaneous recording of electroencephalogram (EEG) and functional magnetic resonance imaging (fMRI) lays out several benefits for specific neuroscience researches. However, the potential advantages come at the expense of the unavoidable existence of artifacts, which contaminate the EEG signals in the magnetic resonance (MR) environment. Thus, to obtain an acceptable EEG data quality in simultaneous EEG-fMRI recordings, it is imperative to ensure the mitigation of these artifacts. The MR gradient artifact and the cardioballistic (CB) artifact represent the two significant sources of EEG artifacts. The rapid switching of gradients during MR acquisition induces an electromotive force on the EEG electrodes, giving rise to MR gradient artifact. At the same time, local changes in the field generated by cerebral blood flow and variations in heartbeat cause CB artifact. The present chapter examines in-detail the significant types of artifacts present in the simultaneously recorded EEG data. It also presents different techniques available for alleviating these artifacts. Further, the chapter discusses the EEG preprocessing pipeline followed in the current thesis work. We utilized the template-based method of Brain vision analyzer software for MR gradient artifact correction and FMRIB plug-in of EEGLAB for CB artifact correction. Further, we employed the functionalities of the Harvard automated processing pipeline for electroencephalography (HAPPE) toolbox in a supervised manner to mitigate conventional EEG-related artifacts such as ocular and muscle artifacts.

Lastly, the validation of the EEG preprocessing pipeline based on a dataset of thirty-nine volunteers has also been presented.

## 2.2 INTRODUCTION

Simultaneous EEG-fMRI acquisitions in clinical and cognitive neurosciences have gained significant attention recently (He & Liu, 2008; Murta et al., 2015; Rosa et al., 2010). The simultaneous recordings of EEG-fMRI were, in the first instance were utilized to delineate epileptic networks in patients undergoing pre-surgical planning (Huster et al., 2012; Murta et al., 2012). Thus, the analysis of simultaneous recordings helps identify regions responsible for the spread of these neuronal events. However, the compromised EEG data quality is a significant downside of the simultaneous EEG-fMRI recording procedure. A standard view on the EEG data quality acquired inside the MR machine suggests that losses are inevitable and hence must be condoned. Thus, to fully utilize the EEG information recorded inside the scanner, the artifacts reduction techniques should be optimally followed.

The two principal sources of artifacts in EEG recorded inside an MRI machine, are first the artifacts introduced by sequentially switching of gradients in the MRI imaging process (MR gradient artifact), which results in the superimposition of EEG data with large amplitudes (order of mV) (Allen et al., 2000). And second is the CB artifact (Allen et al., 1998), which involves the interplay between the static external magnetic field ($B_\circ$) and the cardiovascular system. The cardiovascular artifact is synchronous to simultaneously recorded cardiac rhythm or Electrocardiogram (ECG) signal. ECG signal is recorded by placing an electrode, referenced against the specified EEG reference, at the lower back. This placement scheme corroborates enlarged R peaks and reduces the effect of movement and respiratory artifacts on the ECG

channel. However, the ECG signal is affected by the magnetic field with a substantial deflection detected between onset and offset of S wave and T wave, respectively, with sign dependent on the polarity of the static magnetic field ($B_\circ$).

The underlying cause of CB artifact is the electromagnetism induced by the movement of electrically conductive material in the static external magnetic field ($B_\circ$). Precisely, this induced electromagnetism is caused due to the cardiac activity (deceleration/acceleration of heartbeat), which mainly gives rise to axial head rotation. Besides, the blood movement underneath the EEG electrodes can also cause steady motion in the EEG electrodes. Further, the acceleration of this electrically conductive blood can contribute to CB artifacts by giving rise to Hall voltage (proportional to ($B_\circ$)). A visual comparison of simultaneously recorded EEG and ECG signals revealed an approximate delay of 200 ms between the R peak of ECG wave and EEG artifact spike, concluding the interference from a volunteer's cardiovascular parameters, including heart rate. Moreover, analysis of CB artifact's spectral features based on their Global Field Power (GFP), which measures the standard deviation across all channels, revealed that the head sphere's total spatial topography indeed designates the pulse artifact. Secondly, these topographies constituted rotational, moving, and polarity inverting characteristics (Mulert & Lemieux, 2010; Ullsperger & Debener, 2010).

The other primary source of EEG artifact, as mentioned above, arises due to the utilization of Echo-Planar Imaging (EPI), which involves rapidly changing magnetic field gradients for fMRI acquisition and is called the MR gradient artifact. Yet another MR imaging-related artifact is the Radio Frequency (RF) artifact. RF artifact is mitigated by utilizing low-pass filtering as it contains higher frequency components than the actual EEG signal. Also, the gradient switching's periodic nature makes the MR gradient artifact correction less complicated

than CB artifact correction. Typically, the electrodes and its leads in the EEG system are made from electrically conducting Ag/AgCl material for recording electrical EEG signals. Hence, the strong RF emission during scans and static, changing magnetic fields (gradient switching) results in the induction of currents in these electrodes and its leads as per Faraday's law. Thus, the EEG signal is superimposed with the artifacts in the form of potentials resulting from this induced current, and there exists a substantial overlap between the power spectrum of EEG and image acquisition artifact. In particular, the artifact wave period matches the time between the consecutive RF pulses, which is known as the time to repeat (TR). Further, the slices acquired within this TR at slice repetition time ($TR_{Slice}$) are recorded as signal peaks in the scalp potential. The recorded EEG is thus influenced by the gradient artifact, which repeats itself at the harmonics of the inverse of the slice repetition time ($1/TR_{Slice}$). For, e.g., we can observe the gradient artifact peaks for an acquisition involving TR=2 sec and the number of slices acquired within this TR to be 30 at frequencies 15,30,45…Hz (harmonics of $\frac{1}{2/30}$) (Masterton et al., 2007; Mulert & Lemieux, 2010; Ullsperger & Debener, 2010).

Usually, in a 3T MRI during the EPI sequence, the CB artifact is about 200 µV, and the MR gradient artifact is about 3 mV. Howbeit, the brain rhythms like alpha (8-12 Hz) range between 50-100 µV, while the visual event-related potentials (ERP's) lie within 4-10 µV (Lee et al., 2020). Hence, since CB and MR gradient artifact amplitudes exceed that of the actual EEG signal, efficient methods should be adopted to alleviate their effect. This chapter examines the methods available for mitigating the effects of the aforementioned MR gradient artifact and CB artifact. Further, the chapter outlines the specific pipeline adopted and brings forth the supervised employment of functionalities of the Harvard Automated Processing Pipeline for Electroencephalography (HAPPE) toolbox (Gabard-Durnam et al., 2018) adopted for ensuring

the removal of other conventional EEG artifacts (ocular, muscle-related artifacts). Finally, the chapter highlights the steps taken for validating the removal of MR, CB, and other EEG-related artifacts and highlights the results obtained for EEG artifact removal in concurrently recorded resting EEG-fMRI dataset of 39 healthy male volunteers, which were a part of a study included in Chapter four of this thesis.

## 2.3 MATERIALS AND METHODS

### *2.3.1 SAMPLE AND PROCEDURE*

This chapter presents the implementation of the EEG artifact removal pipeline on 39 healthy male volunteers (age range 18-24 years, Mean=19.57; Standard Deviation (SD)=1.28). All participants provided written and informed consent, and the experiment was conducted as per The Code of Ethics of the World Medical Association (Declaration of Helsinki). All measurements were also approved by the Institute of Nuclear Medicine and Allied Sciences (INMAS) institutional ethical committee (Number: ECR/824/Inst/DL/2016). All subjects were right-handed volunteers recruited among university students and underwent six-minute eyes closed simultaneous recording of resting-state EEG-fMRI data.

### *2.3.2 DATA ACQUISITION*

Continuous EEG data were acquired simultaneously $T2^*$ acquisition (T2* EPI sequence: TR 2000 ms, TE 30 ms, FA $90^o$, 30 slices with thickness 5mm and distance factor 0%, FoV 240 mm with voxel size 3.8X3.8X5.0 mm) for the resting-state eyes-closed condition using a 32-channel MR-compatible brain vision cap. The electrodes were placed according to the international 10-20 system with a separate electrode called the reference electrode, placed

between Fz and Cz electrodes, that provided the reference for recording the data. The impedance level for each electrode was kept less than 5 KΩ. The recorded EEG signal was digitized and transmitted with a 5000 Hz sampling frequency. The acquisition of EEG signals was accomplished using Brain vision recorder software (Brain Products GmbH, Gilching, Germany). ECG signal was also recorded by placing an ECG electrode at the volunteer's back.

### *2.3.3 PRELUDE TO EXISTING ARTIFACT REMOVAL TECHNIQUES*

#### 2.3.3.1 TECHNIQUES FOR REMOVAL OF CB ARTIFACT

One of the frequently used CB artifact removal methods is based on the Average Artifact Subtraction (AAS) algorithm (Allen et al., 1998, 2000). The AAS method's prerequisite is the detection of the cardiac cycle's onsets, which are derived from the simultaneously recorded ECG signals. Next, for each EEG channel, an artifact template is constructed separately by utilizing these onsets as time-locking events, and subsequently, averaging EEG over a pre-defined epoch is performed. This resultant artifact template over substantial trials averages out the EEG signal and represents the CB artifact. Finally, to remove the CB artifact, this template is subtracted from the entire EEG data. Further, the CB template construction and artifact correction is performed for each channel separately as the amplitudes of CB artifact differ in electrodes due to various factors, including the variability in their positions/orientations w.r.t gradients. Nevertheless, the AAS algorithm suffers from multiple drawbacks based on accurate detection of cardiac cycle onset, temporal stability of artifact, absence of concurrence between the cardiac rhythm and the event of activity, and the selection of the length of the template (Laufs et al., 2008).

Accurately marking the cardiac cycle onset improves the CB correction (Allen et al., 1998). However, it is hard to identify the onsets precisely as the MR gradient and CB artifact contaminate the ECG channel. Software packages like Brain vision analyzer (Brain Products GmbH, Gilching, Germany) align the markers by taking the jitter information into account and thus minimize the overall jitter before the actual correction process. Moreover, the variation in the R-R interval makes the selection of the length of the template tricky. Brain vision analyzer software (Brain Products GmbH, Gilching, Germany) employs the building of a template such that it incorporates the CB artifact for all R-R intervals existing in the present moving-average window. This template is employed to each QRS interval based on the R-R period, which circumvents the effect of template length issues on pulse artifact correction procedure (Ellingson et al., 2004).

To overcome the temporal-stability drawback, Niazy and colleagues (Niazy et al., 2005) suggested building the artifact template utilizing the channel-based temporal principal component analysis (PCA). The temporal-stability assumption states that within a chosen moving-average, the CB contribution to the EEG channel changes slowly over time and is similar to adjacent cardiac cycles. Hence, the assumption that one template is sufficient for each CB epoch may not always be correct. The technique employed by Niazy et al. (2005) does not assume these local similarities in CB artifacts. Their method is called an Optimal basis set (OBS) wherein among the principal temporal components, the first few are considered to represent various CB artifact templates, and their joint utilization subside the CB artifact in the EEG data. This tool is available as an FMRIB plug-in for the EEGLAB environment provided by the University of Oxford Centre for Functional MRI of the Brain (FMRIB).

Another spatial patterns based approach can be used to alleviate the CB artifacts from the EEG data. This approach's advantage is that it doesn't necessarily require the pre-knowledge of onsets of each cardiac cycle. The two subcomponents on which spatial topography based methods rely are Independent Component Analysis (ICA) and PCA (Srivastava et al., 2005). These subcomponents assume that the actual EEG activity is independent (physiologically) from the CB artifact, and thus a limited number of components would adequately represent the CB artifact activity. Bénar et al. (2003) visually identified these CB artifacts by inspecting the similarity between the concurrently recorded ECG signal and the components' time courses. The remaining components, when back-projected, resulted in the mitigation of the CB artifacts. However, the spatial pattern approaches' effectiveness as compared to template-based methods at 3T fields is still debatable. Nonetheless, the application of ICA with template-based techniques may prove productive in the future.

#### 2.3.3.2 TECHNIQUES FOR REMOVAL OF MR GRADIENT ARTIFACT

The MR gradient artifact correction also extensively utilizes the template-based method mentioned above to detect and remove MR gradient artifacts (Allen et al., 2000). First and foremost, similar to the CB artifact correction, the EEG intervals contaminated by the gradient artifact are selected. The efficacy of the artifact removal technique primarily depends on the precision of the artifact intervals' selection. Brain vision analyzer (Brain Products GmbH, Gilching, Germany) software supports two methods for detecting artifacts. First is the simple gradient method, wherein for selected channels, the sum of the gradients of the curves between subsequent data are estimated and marked with 'Scan Start' marker on exceeding a particular threshold. Second is the gradient method with Template drift detection (TDD). TDD automatically assesses the drifts and shifts in the individual artifact intervals. TDD's working

principle is based on significant narrow maxima created by the interference caused by the changing magnetic field gradients. TDD performs the interpolation of the data around the peaks and estimates the temporal drifts accurately. Besides, it also builds an internal table containing information about the position of peaks. Thus, comparing this attribute for a particular artifact interval with the other intervals gives the measurement of displacement in data points in that interval. The position of the 'Scan Start marker' is thus optimized based on the drifts, which compensate for the displacement caused by the repeated drifts (Mulert & Lemieux, 2010).

Further, following the detection of scanned intervals, different methods are available for template averages assessment and subsequent subtraction for mitigation of MR gradient artifact in Brain Vision Analyzer software based on a. sliding average calculation for a definite number of intervals, b. selecting pre-defined scanned intervals for average and including other intervals, if correlation exceeds a specific value (default is 0.975), c. utilizing all scanned intervals for averaging and template calculation. Moreover, to remove any residual frequencies present in the EEG data post the template subtraction process, the filtering process is performed on the data. Niazy et al. (Niazy et al., 2003, 2005) further established the fMRI artifact template removal (FASTR), a plug-in for EEGLAB wherein a distinct artifact template is formed to reduce the fluctuations due to the temporal variations in the MR gradient artifact. Thus, a combination of moving average template with the basis functions derived from temporal PCA on residual artifacts is performed. Additionally, they employed the OBS method, as mentioned earlier, for alleviating the remaining artifacts.

#### 2.3.3.3 REMOVAL OF CONVENTIONAL EEG ARTIFACTS

In addition to CB and MR gradient artifacts, the EEG signal is also contaminated by electrical line interference, electrode displacement, and volunteer-induced ocular and muscle movements. A series of steps, including filtering, removing the artifacts, and re-referencing EEG signals, are typically performed to address the conventional EEG artifacts. For this purpose, the Harvard Automated Preprocessing Pipeline (HAPPE) toolbox (Gabard-Durnam et al., 2018) provides an automated approach to removing these typical EEG artifacts. HAPPE is freely available MATLAB based software that can be operated in a semi-automated or fully-automated mode and further utilizes the functionalities of EEGLAB.

### *2.3.4 OPTIMIZING EEG PREPROCESSING PIPELINE*

This thesis carefully followed the preprocessing procedures to alleviate the MR gradient, CB, and other conventional EEG artifacts. The steps followed (see Figure 2.1) are discussed below and have also been published as Supplementary material in Kaur, Chinnadurai, & Chaujar (2020).

a. **Employing Average Artifact Subtraction (AAS) based MR gradient artifact removal algorithm in the brain vision analyzer**

To mitigate gradient artifact and remove any residuals, we used the AAS (Allen et al., 2000; Ritter et al., 2010) method of the Brain vision analyzer (Brain Products GmbH, Gilching, Germany). As discussed in previous sections, the AAS algorithm operates primarily by creating a template of MR scanner artifacts in EEG data whose quality majorly depends on the artifact intervals' precise localization. We used the fMRI volume markers (labeled as ‘TR’) for forming the MR gradient template. These markers

accurately identify each MR acquisition's starting point and are regularly spaced, thus helping build a better MR gradient template. Further, the MR scanner and amplifier were synchronized with each other via Brain Vision Sync Box; therefore, the template drift detection and compensation were not implemented. The subsequent correction was performed by utilizing the sliding average calculation with the default number of intervals for sliding average as an averaging method. This step yielded gradient artifact removed data with no residuals at harmonics of the MRI slice/volume excitation frequency, i.e., 15, 30, 45 Hz, and so on.

b. **Trimming of MR uncorrected EEG data before Cardio Ballistic (CB) correction:**

There exist 6 seconds of data before the start of the first fMRI block acquisition (identified by the first TR marker) wherein pulse sequence prepares itself. Since the MR gradient correction starts from the first TR marker, the gradient effect is retained on these 6 seconds prior data for ECG and EEG electrodes. This can lead to reduced quality of CB artifact cleaning. Hence, we subjected only the data of the fMRI volumes to the CB artifact removal and removed these 6 seconds prior data. Subsequently, the CB artifact removal was performed in the FMRIB plug-in of EEGLAB provided by the University of Oxford Centre for Functional MRI of the Brain (FMRIB). The method detects combined adaptive thresholding and the Teager energy operator, followed by a correction algorithm for detecting the ECG data's QRS peaks (Christov, 2004; Kim et al., 2004). This algorithm delivers an average specificity and sensitivity of 99% in aligning the events and correcting false negatives and positives. Next, the OBS method is exploited for the

removal of the CB artifact. Hence, this step of the trimming prior EEG data before CB rectification has yielded a good quality of CB artifact removed data.

c. **Supervised utilization of functionalities of Harvard Automated Processing Pipeline for Electroencephalography (HAPPE):**

For alleviating conventional EEG artifacts from the MR gradient and CB artifact rectified datasets and ensuring better data quality, we also employed the HAPPE toolbox. The steps selected from the functionalities of the HAPPE toolbox are described below.

**I.** All EEG channels with MR gradient and CB artifact rectified data were filtered with 0.1 Hz (high pass) and 70 Hz (low pass) filtering process.

**II.** The Cleanline plug-in of EEGLAB was utilized next to remove the electrical (line) noise. Cleanline (Mullen, 2012) uses the multi-taper regression approach to eliminate the electrical line noise without compromising the EEG signal.

**III.** The average log power across all channels was assessed, and their normed joint probability was estimated. The channels having a joint probability of more than three standard deviations are identified as contaminated channels and are removed from further processing.

**IV.** Next, Wavelet enhanced Independent Component Analysis (W-ICA) approach was used before conventional ICA, where artifact components are rejected. The W-ICA approach removes muscle, ocular artifacts, and signal discontinuities while retaining the entire length of the data, thus improving the decomposition of subsequently performed ICA.

The first step in W-ICA involves performing extended infomax ICA on the EEG signal and then subjecting the derived components' time series to wavelet transformation, which

generates the coefficients using Coiflets (level 5) wavelet to expound the EEG signal (Castellanos & Makarov, 2006). The coefficients are subsequently subjected to thresholding (Donoho, 1995; Donoho & Johnstone, 1994) and are determined using the following equation

$$Threshold = \frac{median(abs(d))}{0.6745} * \sqrt{2\log(n)} \qquad \text{Equation 2.1}$$

where n is the length of ICA components, and d is the set of coefficients. Thus, the component time-series with large amplitudes fail to survive the thresholding and constitute an artifact time series. Therefore, to remove these artifacts, they are subtracted from the original time series. Thus, within component artifact is removed at this step; however, no ICA component is rejected.

**V.** After W-ICA, HAPPE implements an extended infomax ICA algorithm again. Subsequently, at this stage, the components are rejected using an automated component rejection algorithm called the Multiple Artifact Rejection Algorithm (MARA) (Winkler et al., 2011). MARA is a machine-learning algorithm that evaluates six features on each component and then allocates each component with a probability, which defines the percentage of artifact contamination in a specific component. Further, HAPPE rejects any component having this probability measure more than 0.5. The six features are as follows.

i. Mean local skewness:= This feature identifies blinks or loose contact of an electrode by measuring local skewness, where larger skewness values point out the probable artifact.

ii. Log alpha power:= This feature works by classifying the components with robust alpha band powers as non-artifact components.

iii. Lambda:= Lambda feature encapsulates the deviation observed in the power spectrum of a component from 1/f distribution and mainly identifies the muscle-related artifacts.

iv. Fit error:= It is the mean squared error estimated among the component's distribution and f distribution, specifically in 8-15 Hz.

v. The range within the pattern:= It defines the (log) difference between a component's highest and lowest activation magnitudes. The larger range within the pattern represents an artifact component.

vi. Current density norm:= Here, a cerebral-based activity model is used to source-model the components, and due to their complex source models, artifact components contain high current density norm.

The statistics of the components retained after ICA are included in the generation of data quality metrics.

**VI.** Finally, any channels removed in the previous analysis were subjected to spherical interpolation, and a complete channel set is created.

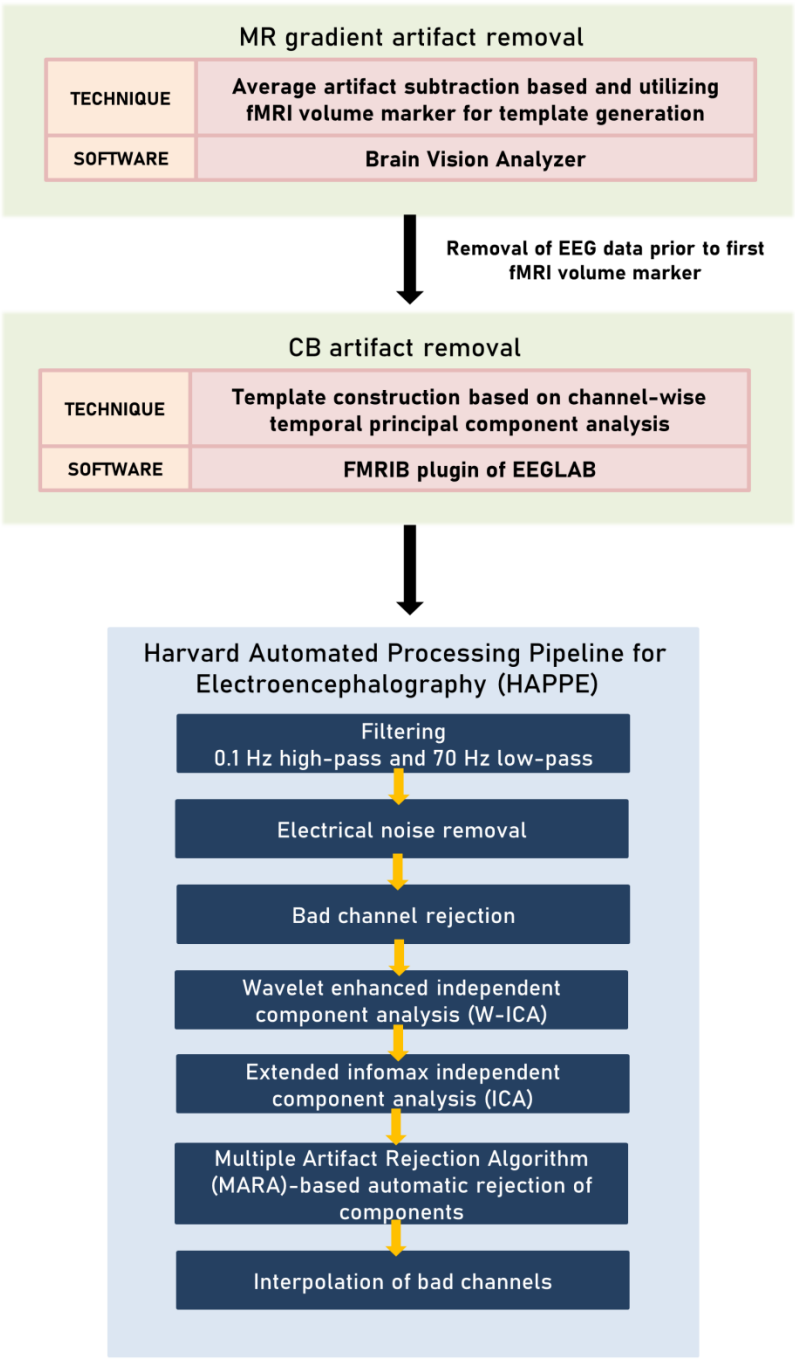


**Figure 2.1** Schematic illustrating the EEG preprocessing pipeline.

## 2.4 RESULTS AND DISCUSSION

This chapter introduced the severe artifacts present in EEG data, which is recorded simultaneously with fMRI. Further, we presented the various techniques available to mitigate these artifacts, and finally, we furnished the optimized pipeline followed for the alleviation of these artifacts. This section presents the validation for the EEG preprocessing pipeline explained in the previous section by applying this pipeline on the dataset of 39 healthy male volunteers.

### *2.4.1 VALIDATION BY HAPPE'S PROCESSING REPORT*

HAPPE generated a report table accommodating the data metrics and descriptive statistics for all 39 volunteers. The performance of the EEG preprocessing pipeline was gauged effectively using these metrics. Table 2.1 shows the HAPPE processing obtained for these 39 volunteers and highlights the following points.

a. An average of 95% of the selected 31 channels (excluding ECG) were marked as good channels and were used for subsequent processing.
b. The interpolated (bad channels) covered the central region electrodes, namely Fz and Cz.
c. On average, 11% of the independent components were rejected for a sample of 39 volunteers per file during HAPPE. Further, 96% of the EEG variance per file was retained on average, signifying acceptable data loss after the MARA component rejection step.
d. Additionally, the mean and median artifact probabilities of components that were retained after MARA-based component rejection on average were only 0.1 and 0.06, respectively. Since no individual files volunteer files crossed the threshold of 0.25 in mean and median artifact probabilities, hence all of them were considered for further analysis.

**Table 2.1** HAPPE preprocessing report generated for all volunteers' (N=39) EEG datasets. Independent components are abbreviated as ICs (Kaur et al., 2020).

| Volunteers' File Number | Volunteers' File Length In Secs | Number Of Channels User Selected (excluding ECG) | Number of Segments Post Segment Rejection | Number Of Good Channels Selected (excluding ECG) | Percent Of Good Channel Selected (excluding ECG) | Interpolated Channel IDs | Number Of ICs Rejected | Percent Of ICs Rejected | Percent Variance Kept Of Post Waveleted Data | Median Artifact Probability Of Kept ICs | Mean Artifact Probability Of Kept ICs | Range Artifact Probability Of Kept ICs | Min Artifact Probability Of Kept ICs | Max Artifact Probability Of Kept ICs |
|---|---|---|---|---|---|---|---|---|---|---|---|---|---|---|
| Volunteer_1 | 410.0 | 31 | 1 | 31 | 96.875 | - | 2 | 6.5 | 96.4 | 0.02 | 0.07 | 0.47 | 0.00185 | 0.47 |
| Volunteer_2 | 410.0 | 31 | 1 | 29 | 90.625 | Cz FC1 | 6 | 20.7 | 89.1 | 0.04 | 0.09 | 0.41 | 0.00258 | 0.42 |
| Volunteer_3 | 410.0 | 31 | 1 | 31 | 96.875 | - | 5 | 16.1 | 93.3 | 0.14 | 0.16 | 0.43 | 0.00033 | 0.43 |
| Volunteer_4 | 410.0 | 31 | 1 | 29 | 90.625 | Cz FC2 | 5 | 17.2 | 96.3 | 0.08 | 0.12 | 0.38 | 0.00026 | 0.38 |
| Volunteer_5 | 410.0 | 31 | 1 | 31 | 96.875 | - | 2 | 6.5 | 98.2 | 0.06 | 0.10 | 0.27 | 0.00024 | 0.27 |
| Volunteer_6 | 410.0 | 31 | 1 | 31 | 96.875 | - | 0 | 0.0 | 100.0 | 0.03 | 0.07 | 0.43 | 0.00019 | 0.43 |
| Volunteer_7 | 410.0 | 31 | 1 | 31 | 96.875 | - | 2 | 6.5 | 97.9 | 0.03 | 0.09 | 0.43 | 0.00026 | 0.43 |
| Volunteer_8 | 410.0 | 31 | 1 | 31 | 96.875 | - | 3 | 9.7 | 96.7 | 0.05 | 0.12 | 0.49 | 0.00014 | 0.49 |
| Volunteer_9 | 410.0 | 31 | 1 | 31 | 96.875 | - | 2 | 6.5 | 96.8 | 0.02 | 0.10 | 0.47 | 0.00088 | 0.47 |
| Volunteer_10 | 410.0 | 31 | 1 | 31 | 96.875 | - | 3 | 9.7 | 97.8 | 0.03 | 0.05 | 0.24 | 0.00102 | 0.25 |
| Volunteer_11 | 410.0 | 31 | 1 | 30 | 93.75 | Cz | 4 | 13.3 | 96.3 | 0.14 | 0.13 | 0.42 | 0.00161 | 0.42 |
| Volunteer_12 | 410.0 | 31 | 1 | 30 | 93.75 | Cz | 2 | 6.7 | 99.0 | 0.04 | 0.11 | 0.49 | 0.00055 | 0.49 |
| Volunteer_13 | 410.0 | 31 | 1 | 31 | 96.875 | - | 3 | 9.7 | 96.6 | 0.08 | 0.12 | 0.38 | 0.00031 | 0.38 |
| Volunteer_14 | 410.0 | 31 | 1 | 31 | 96.875 | - | 2 | 6.5 | 98.4 | 0.02 | 0.07 | 0.50 | 0.00029 | 0.50 |
| Volunteer_15 | 410.0 | 31 | 1 | 29 | 90.625 | FC1 Fz | 0 | 0.0 | 100.0 | 0.02 | 0.05 | 0.34 | 0.00015 | 0.34 |
| Volunteer_16 | 410.0 | 31 | 1 | 30 | 93.75 | Cz | 5 | 16.7 | 95.1 | 0.09 | 0.10 | 0.42 | 0.00027 | 0.42 |
| Volunteer_17 | 410.0 | 31 | 1 | 31 | 96.875 | - | 3 | 9.7 | 97.1 | 0.04 | 0.06 | 0.37 | 0.00076 | 0.37 |
| Volunteer_18 | 410.0 | 31 | 1 | 30 | 93.75 | Cz | 3 | 10.0 | 93.2 | 0.03 | 0.05 | 0.21 | 0.00067 | 0.21 |
| Volunteer_19 | 410.0 | 31 | 1 | 31 | 96.875 | - | 1 | 3.2 | 99.6 | 0.02 | 0.07 | 0.43 | 0.00037 | 0.43 |
| Volunteer_20 | 410.0 | 31 | 1 | 30 | 93.75 | Fz | 0 | 0.0 | 100.0 | 0.04 | 0.07 | 0.31 | 0.00054 | 0.31 |
| Volunteer_21 | 410.0 | 31 | 1 | 31 | 96.875 | - | 8 | 25.8 | 92.6 | 0.19 | 0.19 | 0.47 | 0.00149 | 0.48 |
| Volunteer_22 | 410.0 | 31 | 1 | 31 | 96.875 | - | 5 | 16.1 | 92.6 | 0.16 | 0.17 | 0.44 | 0.00648 | 0.44 |
| Volunteer_23 | 410.0 | 31 | 1 | 29 | 90.625 | Fz TP9 | 2 | 6.9 | 99.0 | 0.04 | 0.08 | 0.48 | 0.00010 | 0.48 |
| Volunteer_24 | 410.0 | 31 | 1 | 30 | 93.75 | Cz | 2 | 6.7 | 99.2 | 0.03 | 0.07 | 0.31 | 0.00002 | 0.31 |
| Volunteer_25 | 410.0 | 31 | 1 | 30 | 93.75 | TP9 | 12 | 40.0 | 72.4 | 0.11 | 0.15 | 0.49 | 0.00137 | 0.49 |
| Volunteer_26 | 410.0 | 31 | 1 | 31 | 96.875 | - | 2 | 6.5 | 98.2 | 0.05 | 0.12 | 0.48 | 0.00051 | 0.48 |
| Volunteer_27 | 410.0 | 31 | 1 | 31 | 96.875 | - | 2 | 6.5 | 99.3 | 0.02 | 0.04 | 0.21 | 0.00008 | 0.21 |

| | | | | | | | | | | | | | | |
|---|---|---|---|---|---|---|---|---|---|---|---|---|---|---|
| Volunteer_28 | 410.0 | 31 | 1 | 30 | 93.75 | Fz | 2 | 6.7 | 98.4 | 0.02 | 0.06 | 0.30 | 0.00016 | 0.30 |
| Volunteer_29 | 410.0 | 31 | 1 | 31 | 96.875 | - | 0 | 0.0 | 100.0 | 0.01 | 0.06 | 0.36 | 0.00010 | 0.36 |
| Volunteer_30 | 410.0 | 31 | 1 | 31 | 96.875 | - | 0 | 0.0 | 100.0 | 0.01 | 0.03 | 0.19 | 0.00003 | 0.19 |
| Volunteer_31 | 410.0 | 31 | 1 | 31 | 96.875 | - | 7 | 22.6 | 92.5 | 0.07 | 0.12 | 0.48 | 0.00029 | 0.48 |
| Volunteer_32 | 410.0 | 31 | 1 | 31 | 96.875 | - | 3 | 9.7 | 97.2 | 0.09 | 0.14 | 0.49 | 0.00097 | 0.49 |
| Volunteer_33 | 410.0 | 31 | 1 | 31 | 96.875 | - | 6 | 19.4 | 87.7 | 0.06 | 0.13 | 0.47 | 0.00351 | 0.48 |
| Volunteer_34 | 410.0 | 31 | 1 | 30 | 93.75 | Cz | 5 | 16.7 | 93.5 | 0.08 | 0.13 | 0.40 | 0.00216 | 0.41 |
| Volunteer_35 | 410.0 | 31 | 1 | 30 | 93.75 | Cz | 7 | 23.3 | 90.5 | 0.10 | 0.18 | 0.47 | 0.00147 | 0.47 |
| Volunteer_36 | 410.0 | 31 | 1 | 30 | 93.75 | Fz | 1 | 3.3 | 99.8 | 0.04 | 0.10 | 0.40 | 0.00030 | 0.40 |
| Volunteer_37 | 410.0 | 31 | 1 | 31 | 96.875 | - | 4 | 12.9 | 96.3 | 0.05 | 0.10 | 0.41 | 0.00022 | 0.41 |
| Volunteer_38 | 410.0 | 31 | 1 | 30 | 93.75 | Cz | 6 | 20.0 | 84.1 | 0.06 | 0.15 | 0.48 | 0.00049 | 0.48 |
| Volunteer_39 | 410.0 | 31 | 1 | 31 | 96.875 | - | 2 | 6.5 | 99.2 | 0.02 | 0.09 | 0.43 | 0.00036 | 0.43 |

### *2.4.2 VALIDATION VIA EEG POWER SPECTRUM*

The data quality was further validated by subjecting the 39 EEG data files to power spectrum assessment. Figure 2.2 shows the median power spectrum plots of raw EEG data for the range of 0.2 to 50 Hz. The figure depicts the MR gradient artifact peaks at 15, 30, 45 Hz, and so on (i.e., multiples of no. of slices/TR) for channels F3, F4, F7, F8, Pz, Oz, and POz. Next, we subjected the final artifact removed EEG data to Current Source Density (CSD) referencing (Kayser, 2009; Kayser & Tenke, 2015) and subsequently to the estimation of the power spectrum between 0.2 Hz to 50 Hz frequency range. The median power spectrum plots of the final artifact removed EEG data for channels F3, F4, F7, F8, Pz, Oz, and POz is shown in Figure 2.3. The observations following Figure 2.3 are as mentioned below.

a. The MR gradient artifact peaks observed at the 15, 30, 45 Hz (i.e., multiples of no. of slices/TR) range in raw data have been cleaned appropriately in the final processed data.
b. The median spectral power of artifact removed EEG data reveals parietal and occipital alpha and beta bands.

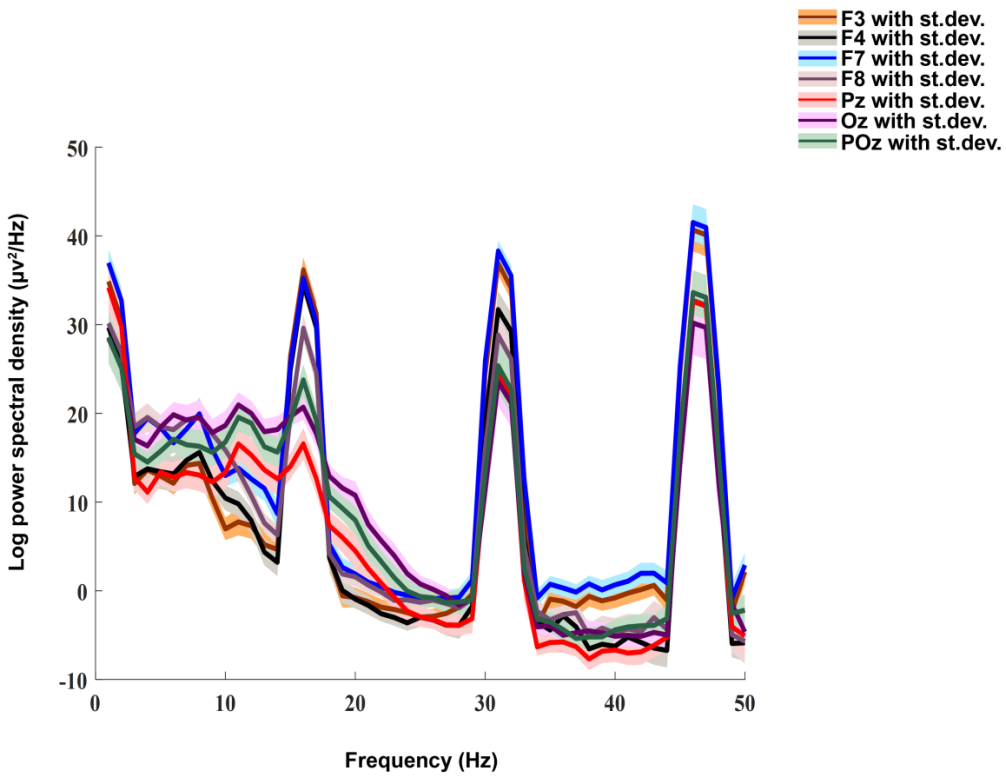


**Figure 2.2** Median power spectrum (0.2 to 50 Hz) of raw artifact laden data for channels F3, F4, F7, F8, Pz, Oz, and POz (Kaur et al., 2020).

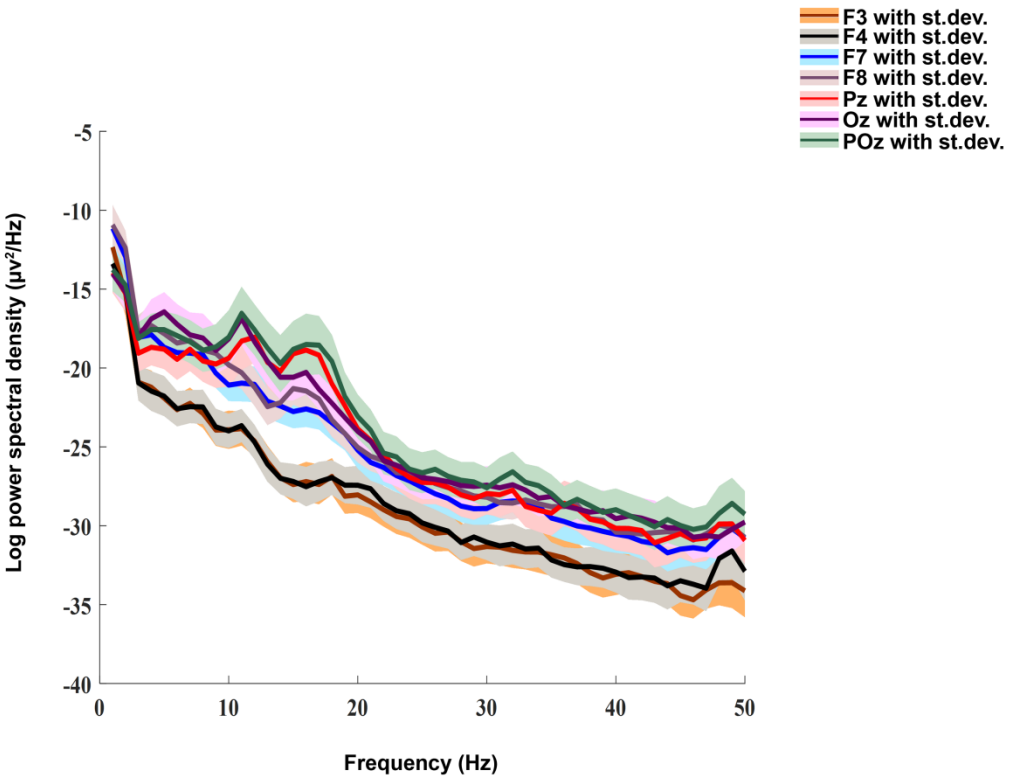


**Figure 2.3** Median power spectrum (0.2 to 50 Hz) of final artifact removed EEG data (CSD referenced) for channels F3, F4, F7, F8, Pz, Oz, and POz (Kaur et al., 2020).

## 2.5 CONCLUSION

In this chapter, the primary artifacts present in the EEG data simultaneously recorded with fMRI, i.e., MR gradient, CB artifacts in addition to conventional EEG artifacts, have been discussed in detail. Further, the various techniques available for mitigating these artifacts have been conferred. Next, the steps we adopted to optimize the EEG preprocessing pipeline with their rationale have been presented. Subsequently, the EEG preprocessing pipeline's validation was carried out to ensure that the EEG asymmetry estimations are devoid of the various sources

of EEG artifacts. The validation was first carried out based on the HAPPE toolbox's processing report, which presented statistics of metrics such as percentages of channels selected as good channels, percentages of independent components rejected, the mean and median artifact probabilities of independent components, etc. Next, the median spectral power of raw and artifact removed data were plotted and compared. The results revealed that the final artifact removed data was suitably cleaned for the various artifact sources and exhibited acceptable data loss. Further, the subsequent chapters cover the exploration of resting EEG/fMRI hemispheric asymmetry models for application in military/aviation domains.

## REFERENCES


Allen, P. J., Josephs, O., & Turner, R. (2000). A method for removing imaging artifact from continuous EEG recorded during functional MRI. In *NeuroImage* (Vol. 12, Issue 2, pp. 230–239). https://doi.org/10.1006/nimg.2000.0599

Allen, P. J., Polizzi, G., Krakow, K., Fish, D. R., & Lemieux, L. (1998). Identification of EEG events in the MR scanner: The problem of pulse artifact and a method for its subtraction. *NeuroImage*, *8*(3), 229–239. https://doi.org/10.1006/nimg.1998.0361

Bénar, C. G., Aghakhani, Y., Wang, Y., Izenberg, A., Al-Asmi, A., Dubeau, F., & Gotman, J. (2003). Quality of EEG in simultaneous EEG-fMRI for epilepsy. *Clinical Neurophysiology*, *114*(3), 569–580. https://doi.org/10.1016/S1388-2457(02)00383-8

Castellanos, N. P., & Makarov, V. A. (2006). Recovering EEG brain signals: Artifact suppression with wavelet enhanced independent component analysis. *Journal of Neuroscience Methods*, *158*(2), 300–312. https://doi.org/10.1016/j.jneumeth.2006.05.033

Christov, I. I. (2004). Real time electrocardiogram QRS detection using combined adaptive threshold. *BioMedical Engineering Online*, *3*, 1–9. https://doi.org/10.1186/1475-925X-3-28

Donoho, D. L. (1995). De-Noising by Soft-Thresholding. *IEEE TRANSACTIONS ON INFORMATION THEORY*, *41*(3).

Donoho, D. L., & Johnstone, J. M. (1994). Ideal spatial adaptation by wavelet shrinkage. *Biometrika*, *81*(3), 425–455. https://doi.org/10.1093/biomet/81.3.425

Ellingson, M. L., Liebenthal, E., Spanaki, M. V., Prieto, T. E., Binder, J. R., & Ropella, K. M. (2004). Ballistocardiogram artifact reduction in the simultaneous acquisition of auditory ERPS and fMRI. *NeuroImage*, *22*(4), 1534–1542. https://doi.org/10.1016/j.neuroimage.2004.03.033

Gabard-Durnam, L. J., Leal, A. S. M., Wilkinson, C. L., & Levin, A. R. (2018). The harvard automated processing pipeline for electroencephalography (HAPPE): Standardized processing software for

developmental and high-artifact data. *Frontiers in Neuroscience*, *12*(February), 1–24. https://doi.org/10.3389/fnins.2018.00097

He, B., & Liu, Z. (2008). Multimodal Functional Neuroimaging: Integrating Functional MRI and EEG/MEG. *IEEE Reviews in Biomedical Engineering*, *1*, 23–40. https://doi.org/10.1109/RBME.2008.2008233

Huster, R. J., Debener, S., Eichele, T., & Herrmann, C. S. (2012). Methods for simultaneous EEG-fMRI: An introductory review. *Journal of Neuroscience*, *32*(18), 6053–6060. https://doi.org/10.1523/JNEUROSCI.0447-12.2012

Kaur, A., Chinnadurai, V., & Chaujar, R. (2020). Microstates-based resting frontal alpha asymmetry approach for understanding affect and approach/withdrawal behavior. *Scientific Reports*, *10*(1), 1–25. https://doi.org/10.1038/s41598-020-61119-7

Kayser, J. (2009). Current source density (CSD) interpolation using spherical splines - CSD Toolbox (Version 1.1). *New York State Psychiatric Institute: Division of Cognitive Neuroscience*. http://psychophysiology.cpmc.columbia.edu/Software/CSDtoolbox

Kayser, J., & Tenke, C. E. (2015). On the benefits of using surface Laplacian (Current Source Density) methodology in electrophysiology. *Internation Journal of Psychophysiology*, *97*(3), 171–173.

Kim, K. H., Yoon, H. W., & Park, H. W. (2004). Improved ballistocardiac artifact removal from the electroencephalogram recorded in fMRI. *Journal of Neuroscience Methods*, *135*(1–2), 193–203. https://doi.org/10.1016/j.jneumeth.2003.12.016

Laufs, H., Daunizeau, J., Carmichael, D. W., & Kleinschmidt, A. (2008). Recent advances in recording electrophysiological data simultaneously with magnetic resonance imaging. *NeuroImage*, *40*(2), 515–528. https://doi.org/10.1016/j.neuroimage.2007.11.039

Lee, H. J., Huang, S. Y., Kuo, W. J., Graham, S. J., Chu, Y. H., Stenroos, M., & Lin, F. H. (2020). Concurrent electrophysiological and hemodynamic measurements of evoked neural oscillations in human visual cortex using sparsely interleaved fast fMRI and EEG. *NeuroImage*, *217*(May), 116910. https://doi.org/10.1016/j.neuroimage.2020.116910

Masterton, R. A. J., Abbott, D. F., Fleming, S. W., & Jackson, G. D. (2007). Measurement and reduction of motion and ballistocardiogram artefacts from simultaneous EEG and fMRI recordings. *NeuroImage*, *37*(1), 202–211. https://doi.org/10.1016/j.neuroimage.2007.02.060

Mulert, C., & Lemieux, L. (2010). *EEG - FMRI Physiological Basis, Technique, and Applications*. Springer Berlin Heidelberg.

Mullen, T. (2012). *CleanLine EEGLAB Plugin. San Diego, CA: Neuroimaging Informatics Toolsand Resources Clearinghouse (NITRC).*

Murta, T., Leal, A., Garrido, M. I., & Figueiredo, P. (2012). Dynamic Causal Modelling of epileptic seizure propagation pathways: A combined EEG-fMRI study. *NeuroImage*, *62*(3), 1634–1642. https://doi.org/10.1016/j.neuroimage.2012.05.053

Murta, T., Leite, M., Carmichael, D. W., Figueiredo, P., & Lemieux, L. (2015). Electrophysiological correlates of the BOLD signal for EEG-informed fMRI. *Human Brain Mapping*, *36*(1), 391–414. https://doi.org/10.1002/hbm.22623

Niazy, R. K., Beckmann, C. F., Iannetti, G. D., Brady, J. M., & Smith, S. M. (2005). Removal of FMRI

environment artifacts from EEG data using optimal basis sets. *NeuroImage*, *28*(3), 720–737. https://doi.org/10.1016/j.neuroimage.2005.06.067

Niazy, R. K., Iannetti, G., Beckmann, C. F., Brady, M., & Smith, S. M. (2003). Improved FMRI artifact reduction from simultaneously acquired EEG data using slice dependant template matching. *Imaging*, *44*(1999), 2003–2003.

Ritter, P., Becker, R., Freyer, F., & Villringer, A. (2010). EEG quality: The image acquisition artefact. *EEG - FMRI: Physiological Basis, Technique, and Applications*, 153–171. https://doi.org/10.1007/978-3-540-87919-0_9

Rosa, M. J., Daunizeau, J., & Friston, K. J. (2010). EEG-fMRI integration: A critical review of biophysical modeling and data analysis approaches. *Journal of Integrative Neuroscience*, *9*(4), 453–476. https://doi.org/10.1142/S0219635210002512

Srivastava, G., Crottaz-Herbette, S., Lau, K. M., Glover, G. H., & Menon, V. (2005). ICA-based procedures for removing ballistocardiogram artifacts from EEG data acquired in the MRI scanner. *NeuroImage*, *24*(1), 50–60. https://doi.org/10.1016/j.neuroimage.2004.09.041

Ullsperger, M., & Debener, S. (2010). *Simultaneous EEG and FMRI Recording, Analysis, and Application*. Oxford University Press.

Winkler, I., Haufe, S., & Tangermann, M. (2011). Automatic Classification of Artifactual ICA-Components for Artifact Removal in EEG Signals. *Behavioral and Brain Functions*, *7*, 1–15. https://doi.org/10.1186/1744-9081-7-30

# CHAPTER THREE

# ASSESSMENT OF LINKAGE BETWEEN RESTING ALPHA ASYMMETRY AND PERFORMANCE IN SITUATIONAL AWARENESS TASK

This chapter is a marginally modified version of the research article published as Kaur, A., Chaujar, R., & Chinnadurai, V. (2019). Effects of Neural Mechanisms of Pretask Resting EEG Alpha Information on Situational Awareness: A Functional Connectivity Approach. *Human Factors*. https://doi.org/10.1177/0018720819869129.

## 3.1 ABSTRACT

In this study, the influence of pre-task resting neural mechanisms of resting alpha and its corresponding frontal asymmetry model on Situational Awareness (SA) task is studied. Pre-task EEG information and the Stroop effect are known to influence task engagement independently. However, the influence of neural mechanisms of pre-task resting absolute alpha (PRAA) and pre-task resting alpha frontal asymmetry (PRAFA) on the SA-task, which is undergoing the Stroop effect, is still not understood. The study involved pre-task resting EEG measurements from 18 healthy individuals, followed by fMRI acquisition during the SA-task. To understand the effect of pre-task alpha information and Stroop effect on SA, a robust correlation between mean reaction time, SA-index, PRAA, and PRAFA was assessed. Further, neural underpinnings of PRAA, PRAFA in SA-task, and functional connectivity were analyzed through the EEG-informed fMRI approach. Significant robust correlation of reaction time was observed with SA-index (Pearson: r=0.50, pcorr=0.05) and PRAFA (Pearson: r=0.63; pcorr= 0.01) respectively.

Similarly, SA-index significantly correlated with PRAFA (Pearson: r=0.56, pcorr=0.01; Spearman: r=0.61, pcorr=0.007), and PRAA (Pearson: r=0.59, pcorr=0.005; Spearman: r=0.59, pcorr=0.002). The neural-underpinnings of the SA-task revealed regions involved in visual-processing and higher-order cognition. PRAA was primarily underpinned at frontal-temporal areas and functionally connected to SA-task regions of the emotional regulation. PRAFA has correlated with limbic and parietal-regions, which are involved in integrating visual, emotion, and memory information of the SA-task. The results suggest a strong association of reaction time with SA-task and PRAFA and strongly support the hypothesis that PRAFA, PRAA, and associated neural mechanisms significantly influence the SA-task outcome. Since SA is vital to operate complex systems, thus, it is beneficial to study the effect of pre-task resting information on the SA-task to improve SA.

## 3.2 INTRODUCTION

Neuro ergonomics, the field which investigates the behavioral aspects of the human brain by integrating knowledge from both neuroscience and neuroimaging with ergonomics, has evolved immensely in the last decade (Gramann et al., 2017; Hancock & Szalma, 2003; Mehta et al., 2013; Sestito et al., 2018). This interdisciplinary approach would be beneficial in comprehending human abilities for augmenting their interaction with various environments.

Situational awareness (SA), which is knowledge about the environment, is one of the constructs that has become the focus of the ergonomics community recently (Endsley, 1995b; Endsley et al., 2016). It begins with the perception of the elements in the environment (Level-1), comprehension of their meaning (Level-2), and ends at decision-making (Level-3) (Endsley, 1995b; Endsley et al., 2016). Maintenance of SA is essential for optimum performance in the

military, aviation domain. However, many physiological and psychological factors can cause a loss of SA (Endsley et al., 2015; Klamklay, 2002). These factors include attention, long-term and working memory, automaticity, and experience of an individual. Previous research majorly examined the association of the factors mentioned above with the loss of SA individually, since it is difficult to test the SA model as a whole (Endsley, 2015).

The maintenance of SA primarily depends on the individual's ability to allocate cognitive resources to perform specific functions by filtering out functions-irrelevant stimuli. This cognitive process is better studied through the Stroop effect, which involves performing a less automated task (e.g., recognizing the ink color) while inhibiting the interference arising from a more automated task (e.g., reading the word). Past research (Jensen & Rohwer, 1966; Kang et al., 2013; Scarpina & Tagini, 2017) reported the Stroop test application in measuring cognitive functions such as attention, processing speed, cognitive flexibility, and working memory. Specifically, in their study, Klamklay (2002) reported a high positive correlation of performance and SA with Stroop color and word test. Despite these works, many questions are still needed to be addressed for a better understanding of the maintenance of SA. They are, 1) Does SA gets influenced by the Stroop effect during the SA-task? 2) What are the neural mechanisms of SA when it is influenced by the Stroop effect? 3) What are the pre-task factors that can affect the neural mechanisms in SA? Understanding these aspects requires an in-depth analysis of multimodal information acquired from an individual while performing the SA-task influenced by the Stroop effect.

Cognitive neuroscience employs divergent assessment techniques such as functional magnetic resonance imaging (fMRI), electroencephalography (EEG), functional near infra-red spectroscopy (fNIRS), and positron emission tomography (PET) to study the functional

dynamics of the brain during task engagement. Hence, the appropriate use of these techniques will facilitate us in understanding neural mechanisms underlying the Stroop effect on SA and ways to ameliorate it under various environments. Catherwood et al. (2014) employed EEG for mapping brain activity and suggested an early coactivity in high order and perception areas during the loss of SA. The aforementioned study investigated the association of loss of SA with concurrent activity in high-level cognitive regions and those for perceptual (visual) processing through EEG source analysis. Although this study revealed valuable neural insights of SA, it did not address the association of pre-task resting information with the behavioral outcome of the subsequently performed SA-task.

Pre-task resting-state information refers to non-random and intricate patterns of inherent activity occurring while the brain is not involved in a task (Raichle & Snyder, 2007). Electroencephalography (EEG) signatures acquired during pre-task resting state have been known as a contributor to the outcome of subsequently performed cognitive tasks. In particular, frontal alpha asymmetry and peak alpha oscillations (8–12 Hz) have been investigated extensively in the past decades (Ambrosini & Vallesi, 2015; Grandy et al., 2013) as a measure to examine emotion-related (J. Davidson, 1992; Richard J Davidson, 2010; Tomarken et al., 1992) and motivation-related state and trait-related changes (R J Davidson et al., 1990; Tomarken et al., 1990). J. Coan (2003) postulated the frontal asymmetry's approach-withdrawal model, wherein an increase in relative left-frontal activity indicates a tendency to engage or approach a stimulus. In contrast, a decrease in relative left-frontal activity suggests increased withdrawal and reduced approach motivation. Frontal hemispheric asymmetry has also been conceptualized and, to some extent, proved to be a moderator and mediator of emotion (James A. Coan & Allen, 2004; Gable

et al., 2017; Reznik & Allen, 2017). A study by Balconi et al. (2017) elucidated the predictive effect of resting-state activity and approach/withdrawal dichotomy.

Further, the absolute power of alpha oscillations from which frontal asymmetry is derived has also been linked to reflect performance in various cognitive functions (Angelakis et al., 2004), including attention, arousal, working memory, long-term memory, and reading. There is a shred of clear evidence that alpha and beta bands of resting EEG predict individual differences in attentional blink magnitudes (MacLean et al., 2012; Shapiro et al., 2017). López Zunini et al. (2013) explored the mutual relationship between cognitive states and resting-state alpha powers by showing that alpha band resting-state activity before a verbal recognition task can predict accuracy during the task.

However, no published works provide a better understanding of the association of pre-task resting EEG alpha and the associated asymmetry with the performance of subsequently performed SA-task when the Stroop effect influences the task. Also, there is no clarity in understanding the influence of neural mechanisms of pre-task resting alpha information and associated functional connectivity on subsequently performed SA-task.

Hence, in the present work, the association of pre-task resting EEG alpha and the associated asymmetry on the subsequently performed SA-task has been investigated. In particular, the SA-task is designed to have more influence from the Stroop effect; hence, the ability of pre-task resting information in assessing the behavioral outcome of SA in those conditions can be studied. To confirm the presence of the Stroop effect during the SA-task, the robust correlation of the reaction time, which assesses the Stroop effect with the SA index of the individual during the same task, is carried out. Then, as this study primarily aims to understand the effect of pre-task alpha information on an individual's SA, the pre-task information is

correlated with the SA index and further subjected to the EEG-informed fMRI analysis for understanding its neural mechanisms. Integration of EEG and fMRI through the EEG-informed fMRI approach has emerged to balance their complementary temporal and spatial resolutions (Abreu et al., 2018; Huster et al., 2012; Murta et al., 2014; Zwaag, 2013). This technique enables us to assess regions that correspond to the task engagement (neural underpinnings of the SA-task) as well as the regions whose neural activity is manifested as cortical EEG power (neural underpinnings of EEG powers). Subsequently, to understand the modulation of neural underpinnings of SA-task by neural mechanisms underlying pre-task resting alpha information, functional connectivity among neural underpinnings of SA-task, pre-task alpha power, and its associated hemispheric asymmetry was estimated and analyzed.

## 3.3 MATERIALS AND METHODS

The schematic diagram of the methodology adopted in this study is illustrated in Figure 3.1.

### *3.3.1 SAMPLE AND PROCEDURE*

Pre-task resting-state EEG and task-fMRI studies were performed on eighteen healthy volunteers (12 males, 6 females, Mean age= 24 years, Standard deviation (S.D.)= 3 years). All volunteers completed informed consent procedures approved by the local institutional review board. This research complied with the American Psychological Association Code of Ethics.

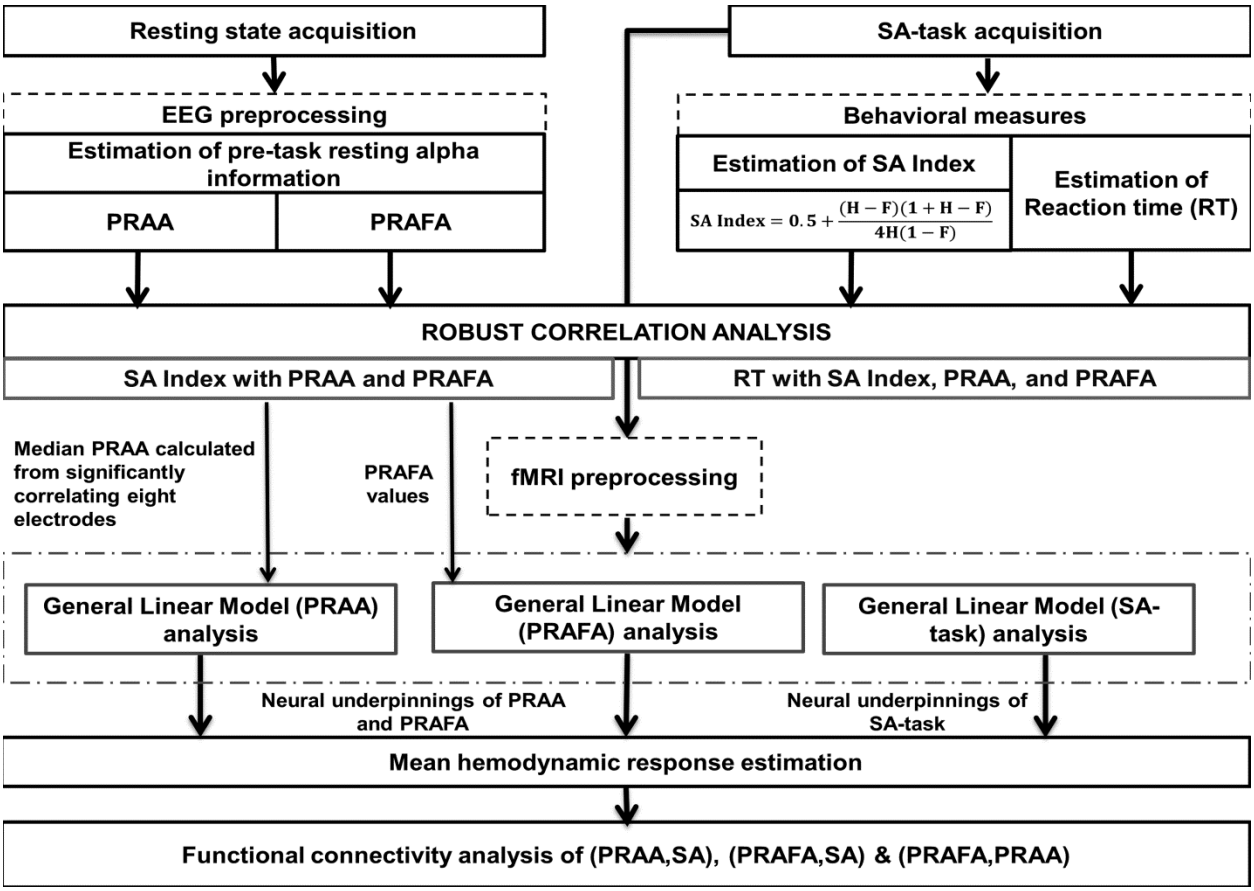


**Figure 3.1** Schematic diagram of the methodology adopted in this study (Kaur et al., 2019).

### *3.3.2 PARADIGM INFORMATION*

Catherwood et al. (2014) employed an abstract task and a real-world urban threat detection task to assess the loss of SA by measuring EEG information for the same. Their study concluded the rapid and early coactivity of visual and higher-order regions for both abstract and more real-world content. Keeping in mind the compatibility of task performance in an MR environment, we chose to employ a modified Stroop-test to study situational awareness. Stroop-colour and word test is a neuropsychological test used to assess the ability to inhibit cognitive interference that occurs when the processing of a specific stimulus feature impedes the

simultaneous processing of a second stimulus attribute. Scarpina et al. (2017) also report the application of the Stroop test in measuring cognitive functions such as attention, processing speed, cognitive flexibility, and working memory. Similar to the study by Catherwood et al. (2014), in our study, the "situation" is defined in terms of target information within a visual field. The essential requirements resemble many real-world situations requiring perceptual and cognitive processing to identify a target item.

The choice of the Stroop test was made as it requires any volunteer to perform a less automated task while inhibiting the interference arising from a more automated task. This holds parallel to the concept of SA, wherein identifying which elements the operator needs to perceive and understand is an important parameter that facilitates the decision-making process. We modified the basic Stroop test by inserting questions about the presence of an object in the previous environment at random intervals, which is in-line with Endsley's original task where random questions are asked to the volunteer about the driving simulation. Hence, in our paradigm, volunteers were exposed to a paradigm wherein each slide, they had to perceive the question being displayed, comprehend its meaning, and answer from a given set of four choices. Each stimulus slide lasted for 4.5 seconds on the screen and was followed by a baseline slide for 3 seconds. The baseline slide is the fixation block of the paradigm where no specific task was carried out by the volunteers except viewing standard blank slide with a cross. In the paradigm, 20 stimulus slides were made where the volunteer had to observe and orient the true sense of Stroop color and word test question. Moreover, in five stimulus slides, the volunteer was randomly asked about the presence of an object in the previous environment. Level 1 SA (perception) in our paradigm was achieved by the visual perception of the questions being placed. Volunteers slowly transited to Level 2 SA (comprehension) while understanding the

meaning of the question being asked. E.g., one of the slides asked the volunteer to observe the color of text, where the text was ‘Eight’ written in green color, as shown in Figure 3.2. Thus, the volunteer had to observe all the choices, including a green-colored object and the number eight, and make a final choice by pressing a button on the same slide. At random times during the task, the volunteers were inquired about the particular features in the previous environment with a question such as; did you notice this object in the previous environment? (see Figure 3.2). These questions were modified and drafted to go in sync with the Endsley’s original task (Endsley, 1995a). These questions mainly triggered the bottom-top process where the volunteer had to shift the attention to another additional goal, which was to focus on other elements in the environment. Further, volunteers were not trained for the occurrence of these random questions before the experiment.

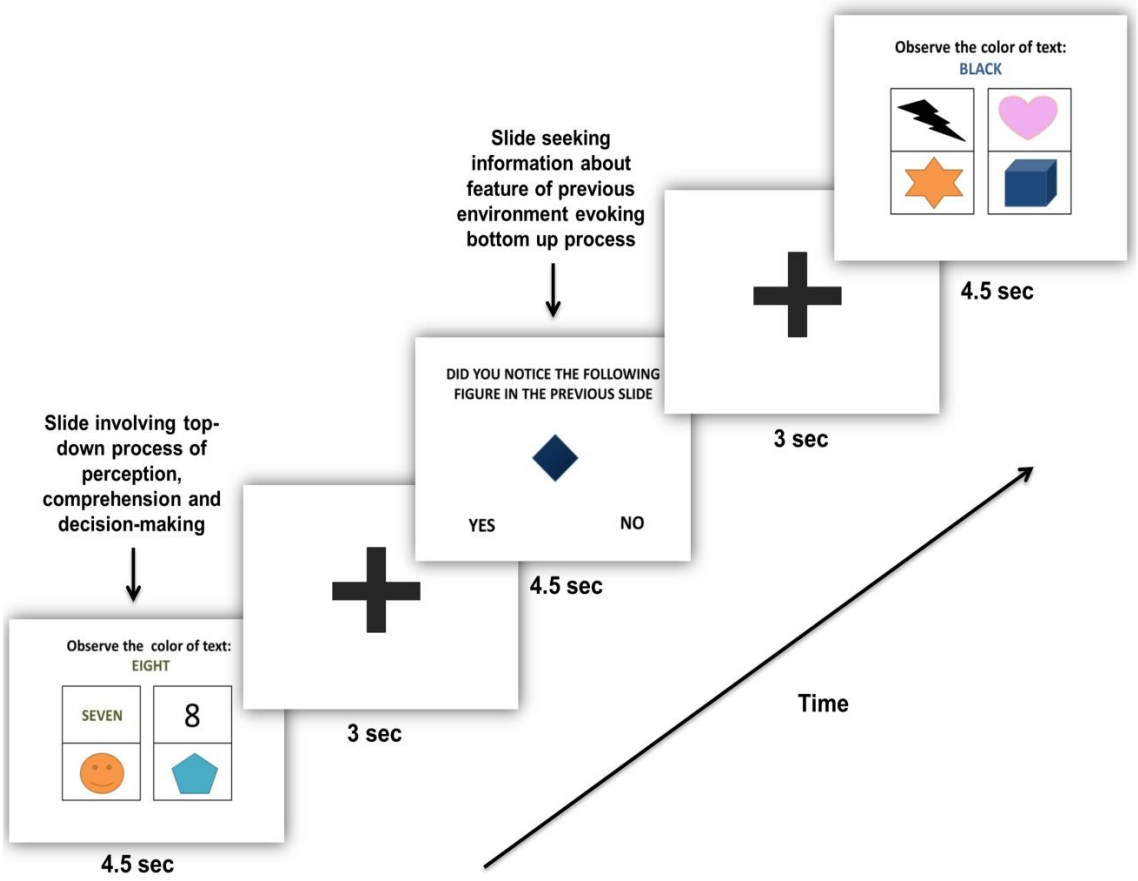


**Figure 3.2** Schematic showing fMRI stimulus and baseline presentation paradigm for Situational awareness (SA) task (Kaur et al., 2019).

### *3.3.3 DATA ACQUISITION AND PRE-PROCESSING STEPS*

#### 3.3.3.1 Pre-task resting EEG data acquisition and pre-processing

Pre-task resting-state EEG data were acquired using MRI compatible Brain-Amp EEG amplifier and electrode cap with 31 Ag/AgCl electrodes positioned according to the 10/20 system and 1 ECG channel. The reference electrode was placed between Fz and Cz electrodes. Raw EEG data were sampled at 5 kHz using brain vision recorder (Brain Products GmbH,

Gilching, Germany), and impedances of electrodes were kept below 10 kΩ. We recorded resting-EEG on all volunteers while they were at rest in the MRI room. Resting-state EEG recording lasted for 6 minutes and included the eyes-closed condition. The eyes closed condition was chosen, as alpha rhythm, which is the EEG correlate of relaxed wakefulness, is best obtained while the eyes are closed. Further, functional connectivity in the alpha band decreases in the eyes-open condition compared to the eyes-closed condition (Barry & De Blasio, 2017; Gómez-Ramírez et al., 2017).

The acquired EEG data were corrected for gradient and cardio-ballistic artifacts using Brain vision analyzer's (BVA) algorithms (Brain Products GmbH, Gilching, Germany), and ocular artifacts were removed using the ICA approach in BVA. Then, the alpha band's power spectral densities (8-12 Hz) of every channel were computed for the entire duration of resting acquisition using Welch's overlapped segment averaging estimator. The spectral densities of alpha-band power were then log-transformed for further analysis.

#### 3.3.3.2 fMRI data acquisition and pre-processing

Functional and anatomical MR imaging was performed in a 3T MR Siemens scanner. During the SA-task, fMRI scanning was carried out with a T2* weighted EPI sequence, and 247 functional blocks were acquired. The other acquisition parameters were set as number of slices=36, slice thickness = 3 mm, TR = 3000ms, flip angle = 90°, TE = 36ms, Field of View (FOV) = 230X230. The whole-brain anatomical scan was also acquired using a T1-weighted sequence with the parameters TR = 1900ms, flip angle = 9°, TE = 2.49ms, FOV=256X256. The acquired fMRI data were pre-processed, co-registered, normalized to Montreal Neurological

Institute (MNI) template, and smoothed using a Gaussian kernel (6mm full-width half-maximum) in SPM12 (https://www.fil.ion.ucl.ac.uk/spm/).

### *3.3.4 DATA ANALYSIS*

#### 3.3.4.1 Estimation of the SA index as a behavioral measure of task

Quantification of SA in previous literature has been done using Quantitative Assessment of Situational Awareness (QASA) (Edgar et al., 2018; Nikolla et al., 2018; Stanislaw & Todorov, 1999). QASA involves the collection and analysis of volunteers' responses to true/false statements using signal detection theory metrics. As this study aims to understand the Stroop effect on SA-task, we required to keep more than one task-irrelevant option along with the correct answer in the slides in order to bring more Stroop effect during task engagement. Hence, each slide had one correct answer (signal) and three wrong answers (noise). We have calculated Hits (H) as a ratio between the number of correct answers selected by the individual and the total number of correct answers. In order to calculate False Alarm (F), we have grouped all three task-irrelevant answers in the slide as one false category. Hence, if the individual selects any task-irrelevant stimuli as an answer, it is considered a single false category. Thus, a false alarm is estimated as the ratio between the number of task-irrelevant stimuli identified as correct and the total number of false. The purpose of doing this was to ensure that the volunteer uses his/her cognitive resources in observing all the options in addition to the hit. This assessment of true/false from volunteers' answers for the adaptation of signal detection theory metrics, and eventual quantification of SA allowed us to assess the Stroop effect during the task engagement. The additional slides that enquired about the presence of a particular object in the previous environment evoked yes-no responses from the volunteers. These yes-no responses on signal

trials (when an object was present in the previous environment) and noise trials (when an object was absent in the previous environment) were also added to the proportion of hits (correct identification) and false alarms (incorrect identification). Hence, using the estimated H and F, SA Index was derived as

$$SA\ Index = 0.5 + \frac{(H - F)(1 + H - F)}{4H(1 - F)} \quad \text{Equation 3.1}$$

Ben-david et al. (2012) have also employed a similar concept of signal detection theory (SDT) for analysis of emotional Stroop color and word task where the percentage of correct identification of color provided the rate of hits (H). In a complementary fashion, the percentage of incorrect identifications of color as word provided the rate of false alarms (F).

Subsequently, the behavioral score of SA-task of each volunteer was combined in a vector form ($SA_{all}$) as

$$SA_{all} = \{SAIndex_i | i = 1\ toN\} \quad \text{Equation 3.2}$$

where N is the total number of volunteers who participated in the study, these estimations were implemented via programming in Matlab 2013b.

#### 3.3.4.2 Estimation of reaction time to corroborate Stroop effect on SA-task

Reaction time was estimated specifically for slides involving the Stroop effect to validate its presence in SA-task. Mean reaction time was calculated for every volunteer and combined in a vector form ($RT_{all}$) as

$$RT_{all} = \{RTIndex_i | i = 1\ toN\} \quad \text{Equation 3.3}$$

where N is the number of volunteers who participated in the study; subsequently, the robust correlation between response time, SA index, and pre-task alpha information was assessed.

#### 3.3.4.3 Estimation of pre-task resting alpha information

As mentioned in earlier sections, this study focuses on understanding the role of the pre-task EEG alpha signatures in the outcome of the subsequently performed SA-task. Hence, in this study, the pre-task resting alpha information was assessed by measuring pre-task resting absolute alpha (PRAA) power and its associated hemispherical asymmetry through pre-task resting alpha frontal asymmetry (PRAFA) index. The methods of estimating these two indices are explained below.

At first, the average PRAA values of every channel of each volunteer was estimated and organized as

$$PRAA_{all} = \left\{ PRAA_{i,j} \middle| \begin{matrix} i = 1\ toN \\ j = 1\ toM \end{matrix} \right\} \quad \text{Equation 3.4}$$

N and M are the total number of volunteers who participated in the study and the total EEG channels, respectively. Each row in the matrix $PRAA_{all}$ contains details about the PRAA of every channel of a particular volunteer.

Further, PRAFA was calculated through the PRAFA index based on differences of absolute alpha values measured from frontal hemispheres (Ellis et al., 2017; Smith et al., 2017) as given in Equation 3.5

$$PRAFA_{all} = \{PRAFA_i | i = 1\ toN\} \quad \text{Equation 3.5}$$

where N is the number of volunteers and $PRAFA_i$ is the PRAFA of the i$^{th}$ volunteer, which is estimated as $\log(\propto_{Right}) - \log(\propto_{Left})$. The $\propto_{Right}$ is the median of absolute alpha values of F4, F8 channels and $\propto_{Left}$ was estimated by computing the median of absolute alpha values of F3, F7 channels for every volunteer. These channels were chosen because hemispheric asymmetry has been linked to mid-frontal (F3, F4) and lateral frontal (F7, F8) sites (Coan &Allen, 2003; Harmon-jones, Gable, &Peterson, 2010; Wheeler, Davidson, &Tomarken, 1993).

The PRAFA is an ideal index to assess neural mechanisms associated with the hemispherical asymmetry. Higher scores on the PRAFA index indicate relatively higher alpha power and lower inhibition in the right frontal hemisphere than the left hemisphere. Many researchers (Klimesch, 2012; Sadaghiani & Kleinschmidt, 2016; Uusberg et al., 2013) have observed that neural activity as reflected by blood oxygenated level dependent (BOLD) signal, correlates negatively with alpha power. This implies that a higher PRAFA index is suggestive of higher neural activity in the left frontal hemisphere and vice versa. Numerous studies (Balconi et al., 2014; De Pascalis et al., 2013; Ferreira et al., 2006; Harmon-Jones et al., 2010; Jones et al., 2009; Mennella et al., 2017; Papousek et al., 2014; Schneider et al., 2016) reflect the association of greater left frontal activity with a general motivational or approach system, and the higher right frontal activity with avoidance or withdrawal system.

#### 3.3.4.4 Robust correlations among reaction time, SA index, and pre-task resting information

Robust correlations were implemented in the Robust correlation Matlab toolbox (Pernet et al., 2013). This method protects against bivariate or univariate outliers. Pearson, Spearman, Bend and Skipped correlation coefficients and their bootstrapped confidence intervals were

computed. Further, both p-values and confidence intervals were Bonferroni corrected for multiple comparisons.

To substantiate the influence of the Stroop effect on SA, the robust correlation of reaction times pertaining to slides evoking the Stroop effect was estimated with the SA index as well as PRAA and PRAFA. Thus, $RT_{all}$ was correlated with $SA_{all}$ vector, $PRAA_{all}$, and $PRAFA_{all}$. Further, to explore the role of pre-task resting information in the behavioral outcome of the subsequently performed SA-task, the robust correlation of SA index with PRAA and PRAFA was carried out. Each row of $PRAA_{all}$ was thus correlated with the $SA_{all}$ vector to assess the most informative EEG channels, which are associated with the behavioral outcome of subsequently performed task. Eight EEG channels (fp2, poz, c4, pz, p7, cp1, o1, oz) were significantly correlated with the SA index. Hence, their median was computed for the purpose of passing it as a covariate in the EEG-informed fMRI model to estimate the neural underpinnings of PRAA. Similarly, $PRAFA_{all}$ was also subjected to the robust correlation analysis with the $SA_{all}$ index. The median value of the PRAFA was then used as a covariate in the EEG-informed fMRI model to assess the neural underpinnings of PRAFA.

#### 3.3.4.5 Estimation of neural underpinnings of SA-task, PRAFA, and PRAA

The assessment of the SA-task's neural underpinnings reveals the brain regions involved during the task. This has been estimated by the general linear model approach using the statistical parametric model (SPM 12). In this model, at the first level of analysis, t-contrast was specified for testing the SA-task effect (active-baseline), where active comprised all the stimuli, and statistical parametric maps were constructed for canonical HRF and its temporal and dispersion derivatives. These contrast images of each subject were then passed onto second-level

group analyses. Similarly, the neural underpinnings of PRAFA and PRAA were assessed through the EEG-informed fMRI approach. Both PRAFA and PRAA were subjected as a global covariate at the second-level to two independent EEG-informed fMRI models. The results of the second-level analysis of the neural underpinnings of the SA-task, as well as PRAFA and PRAA, were subjected to the one-way analysis of variance (ANOVA) statistical method. The F-contrast was computed, and significant activations for the SA-task and PRAFA and PRAA were analyzed at FWE corrected $p<0.05$ significance.

#### 3.3.4.6 Functional connectivity analysis

This study aims to understand the modulation of SA-task's neural underpinnings by neural mechanisms of pre-task resting alpha information. Therefore, functional connectivity analysis was carried out to understand the interaction between SA-task's neural underpinnings with PRAA and PRAFA. It is estimated by assessing the mutual correlations of the mean hemodynamic response of different neural underpinnings pertaining to the SA stimuli. Specifically, the functional connectivity (FC) between $x^{th}$ neural underpinning of PRAA (PRAA(x)) and $y^{th}$ neural underpinning of SA (SA(y) is estimated as

$$FC[PRAA(x), SA(y)] = Corr(mHR_{PRAA}(x), mHR_{SA}(y)) \quad \text{Equation 3.6}$$

Similarly, functional connectivity (FC) between PRAFA and SA neural underpinnings is estimated as

$$FC[PRAFA(z), SA(y)] = Corr(mHR_{PRAFA}(z), mHR_{SA}(y)) \quad \text{Equation 3.7}$$

Additionally, the functional connectivity (FC) between $x^{th}$ neural underpinning of PRAA (PRAA(x)) and $z^{th}$ neural underpinning of PRAFA (PRAFA(z)) is further estimated as

$$FC[PRAA(x), PRAFA(z)] = Corr(mHR_{PRAA}(x), mHR_{PRAFA}(z)) \quad \text{Equation 3.8}$$

where $mHR_{PRAA}(x), mHR_{PRAFA}(z)\ and\ mHR_{SA}(y)$ are the mean hemodynamic responses of the x[th], z[th,] and y[th] neural underpinnings of PRAA, PRAFA, and SA, respectively pertaining to the SA-task stimuli. The mean hemodynamic responses of every neural underpinning pertaining to PRAA, PRAFA, and SA are estimated by forming a vector whose elements are the average hemodynamic response of all the voxels of that specific neural underpinning corresponding to a particular SA stimuli block (Figure 3.3). For example, the mean hemodynamic response of x[th] neural underpinning of PRAA, $mHR_{PRAA}(x)$ is estimated as

$$mHR_{PRAA}(x) = \left\{ \left| Avg\left(mHR^{i}_{PRAA} | \ i = 1{:}\,Nx\right) \right|_{BI}; BI = 1{:}\,N_{SABlocks} \right\} \quad \text{Equation 3.9}$$

where $Nx$ is the total number of voxels in the x[th] underpinning of PRAA, $N_{SABlocks}$ is the total number of SA-task stimuli blocks, which in our experiment is 25, and *BI* is the block index. The mean hemodynamic response of every voxel pertaining to each stimulus was carried out by measuring time to peak (TTP) and width (W) of hemodynamic response function (HRF) for each stimulus (Lindquist et al., 2009). The TTP and W of each task stimulus were observed to be having mean values of 3.78 seconds and 1.9 seconds, respectively. This suggests that the hemodynamic response of the task stimuli was very well contained inside the block time of 4.5 seconds during the task. The correlation threshold for the correlation among the neural underpinnings of SA, PRAA, and PRAFA was set more than 0.5, and t-test ($p<0.05$) for group analysis was performed for the in-depth understanding of the association between underpinnings of PRAA and SA, PRAFA and SA and PRAFA and PRAA.

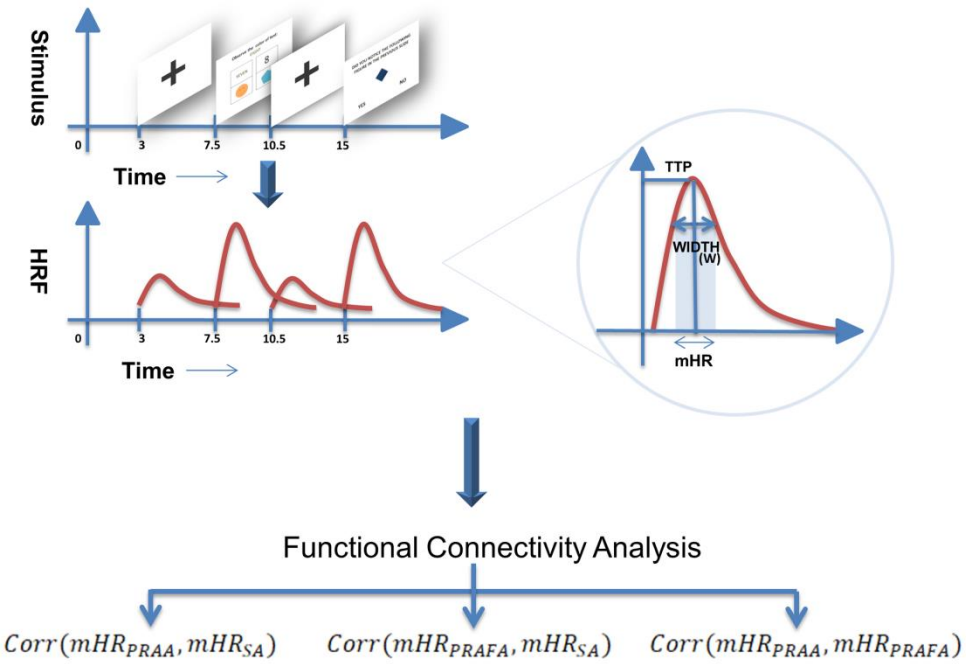


**Figure 3.3** Schematic showing the estimation of mean hemodynamic response of each stimulus for functional connectivity analysis (Kaur et al., 2019).

## 3.4 RESULTS

As mentioned in the earlier sections, this study aims to understand the influence of neural mechanisms of pre-task resting information on SA. Particularly, the SA-task is designed to have more influence from the Stroop effect; wherefore, the ability of pre-task resting information in assessing the behavioral outcome of SA in those conditions can be studied. Additionally, this study validated the existence of the Stroop effect in SA-task by correlating the reaction time, which assesses the Stroop effect with the SA index as well as pre-task resting parameters. The

study also focuses on bringing better clarity of interactions between neural mechanisms associated with SA-task and pre-task resting information through functional connectivity analysis. The pre-task resting information has been assessed by estimating both PRAA and PRAFA. The following sections present the results of this study in detail.

### *3.4.1 CONFIRMATION FOR PRESENCE OF STROOP EFFECT DURING SA-TASK*

The results of robust correlations revealed significant association among the reaction time of the stimuli evoking the Stroop effect in SA-task with a SA index. Strong and significant Pearson and Pearson skipped correlation was observed between reaction time and SA index measures (Figure 3.4a: Pearson r=0.51, 95% CI= [0.07; 0.84], $p_{corr}$=0.05; Figure 3.4b: Pearson skipped $r_{skipped}$=0.51, 95% CI= [0.06; 0.83]). Bend, Spearman, and Spearman skipped correlations revealed insignificant p-values for this analysis.

Similarly, reaction time revealed significant positive Pearson and Pearson skipped correlations with PRAFA (Figure 3.4c: Pearson r=0.63, 95% CI= [0.16; 0.87], $p_{corr}$=0.011; Figure 3.4d: Pearson skipped $r_{skipped}$=0.44, 95% CI= [0.03; 0.75]). However, insignificant p-values were revealed for Bend, Spearman, and Spearman skipped correlations. Further, no significant correlations were observed between reaction time and PRAA. Hence, these results validate the presence of the Stroop effect in the SA-task.

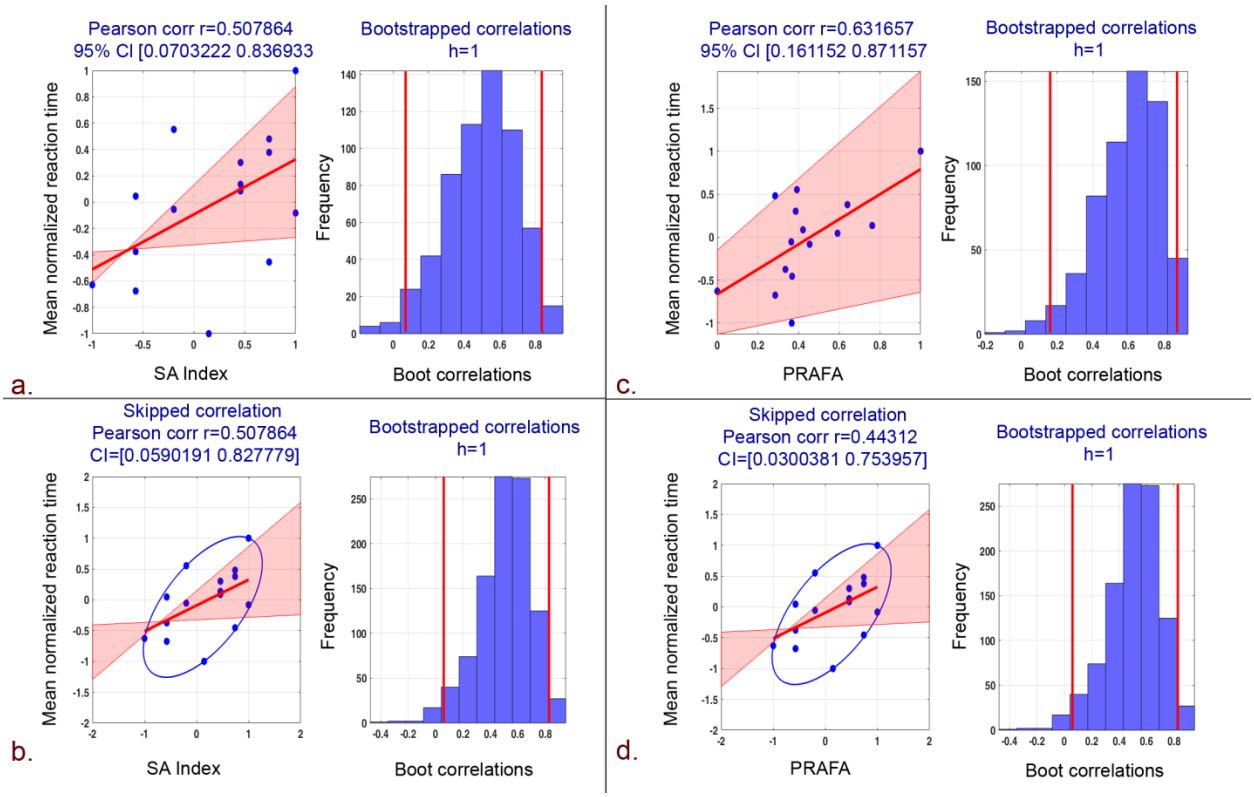


**Figure 3.4** Correlation plots between mean normalized reaction time and SA index. a. Pearson correlation b. Skipped (Pearson) correlation. Correlation plots between mean normalized reaction time and PRAFA. c. Pearson correlation d. Skipped (Pearson) correlation (Kaur et al., 2019).

### *3.4.2 ASSOCIATION OF PRE-TASK RESTING INFORMATION WITH SA INDEX*

The results of robust correlations revealed significant role of pre-task resting measures with behavioral performance in SA-task. In particular, robust correlation analysis revealed a strong and significant correlation between PRAFA and SA index measures (Figure 3.5a: Pearson r=0.56, 95% CI= [0.15; 0.79], $p_{corr}$=0.01; Figure 3.5b: Spearman r=0.61, 95% CI= [0.12; 0.90], $p_{corr}$=0.007). Skipped (Pearson and Spearman) and bend correlations among PRAFA values and SA index measures also yielded stronger correlations (Figure 3.5c: Bend correlation coefficient =0.51, 95% CI= [0.09; 0.88], $p_{corr}$=0.03; Figure 3.5d: Pearson $r_{skipped}$=0.56, 95% CI= [0.16; 0.79]; Spearman $r_{skipped}$=0.61, 95% CI= [0.12; 0.91]).

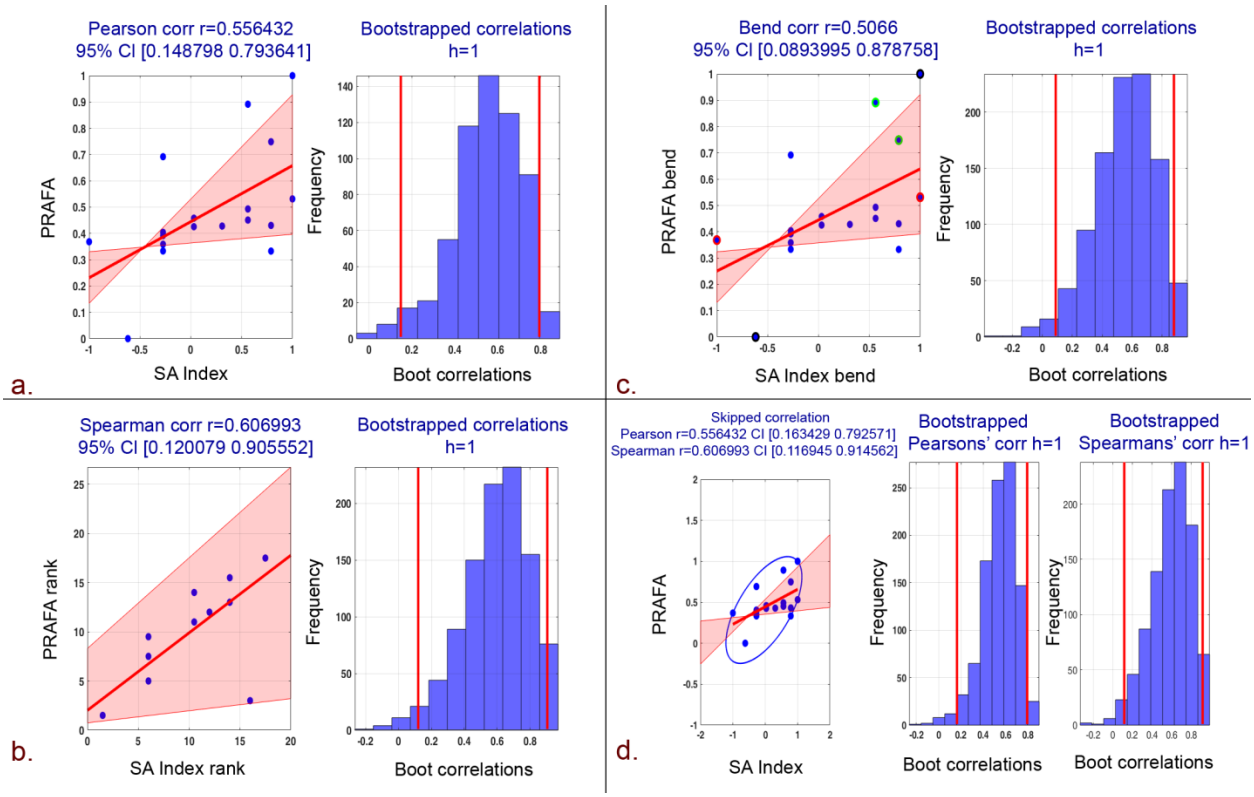


**Figure 3.5** Correlation plots between PRAFA and SA index and associated histograms of correlations for bootstrapped data. a. Pearson correlation b. Spearman correlation c. 20% Bend correlation d. Skipped (Pearson and Spearman) correlations (Kaur et al., 2019).

Similarly, PRAA was strongly correlating with the SA index across eight electrodes. The correlation coefficients of all these channels, as well as the respective significance levels, have been tabulated in Supplementary Table S3.1 (see Appendix 1). Median of PRAA of these strongly correlating eight electrodes have also revealed a significant positive correlation with behavioral SA index (Figure 3.6a: Pearson r=0.59, 95% CI= [0.23; 0.88], $p_{corr}$=0.005; Figure 3.6b: Spearman r=0.59, 95% CI= [0.09; 0.89], $p_{corr}$=0.002). Skipped (Pearson and Spearman) and bend correlations among median of PRAA values and SA index measures also yielded significant correlations (Figure 3.6c: Bend correlation coefficient =0.62, 95% CI= [0.18; 0.89], $p_{corr}$=0.004; Figure 3.6d: Pearson $r_{skipped}$=0.76, 95% CI= [0.55; 0.91]; Spearman $r_{skipped}$=0.79,

95% CI= [0.51; 0.92]). Hence, these results reveal the significant association between pre-task resting measures and behavioral performance of the subsequently performed SA-task.

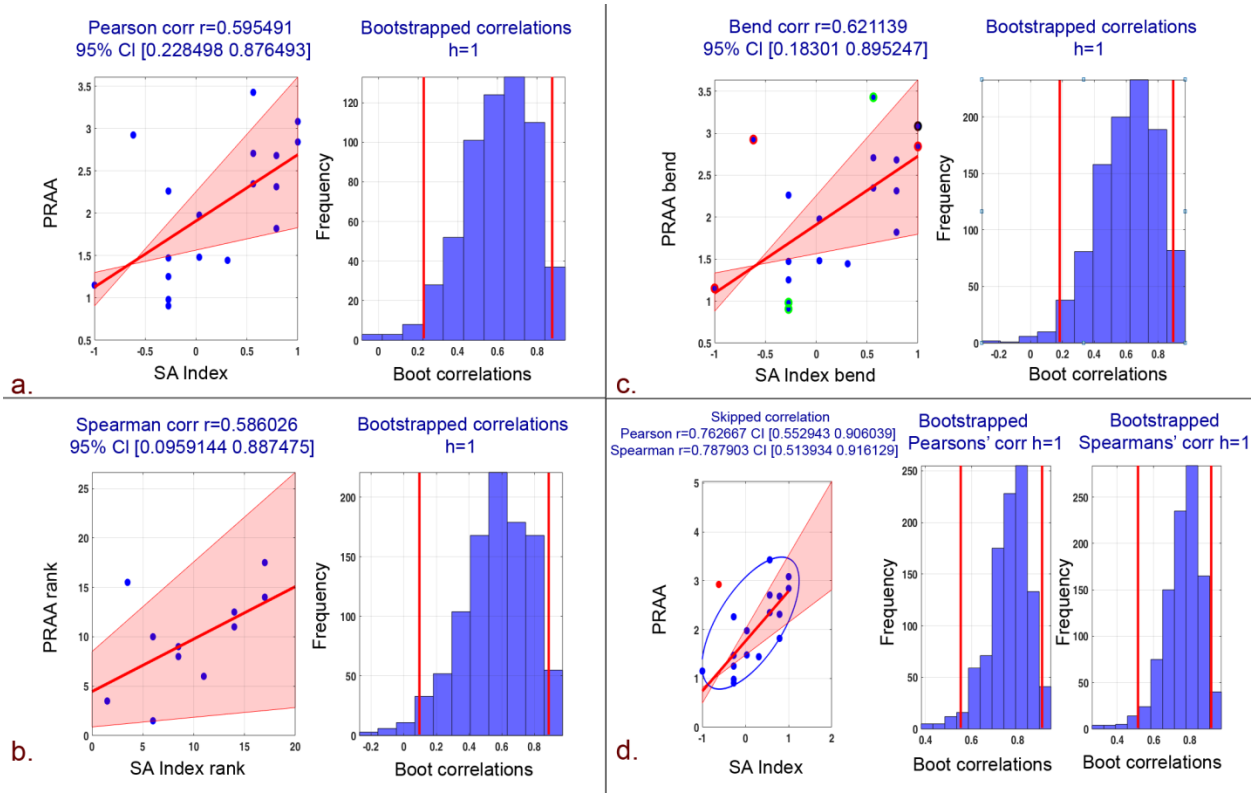


**Figure 3.6** Correlation plots between median PRAA values and SA index and histograms of correlations for bootstrapped data .a. Pearson correlation b. Spearman correlation c. 20% Bend correlation d. Skipped (Pearson and Spearman) correlations (Kaur et al., 2019).

### *3.4.3 NEURAL UNDERPINNINGS OF SA-TASK*

Figure 3.7 shows the neural underpinnings of SA-task (FWE corrected $p<.05$), and regions are tabulated in Supplementary Table S3.2 (see Appendix 1). The significant activations during the SA-task relative to the baseline were analyzed using the categorical approach. The baseline is the neural activity observed during the paradigm fixation block where no specific task was carried out except viewing standard blank slide with a cross. The group analysis of the GLM

model showed significant neural activations in primary and high-level visual processing areas, including the lateral occipital cortex (inferior and superior division), occipital fusiform gyrus, and temporal-occipital fusiform gyrus. Also, significant involvement of the frontal lobe (Inferior, middle, and superior frontal gyrus) was observed as the neural underpinning of the SA-task. The presence of activity in the visual cortex and occipital-temporal regions justified the attainment of level 1 (perception) of SA, where primary and high-level visual processing regions are involved. The significant activations in motor areas, precuneous, Inferior, middle, and superior frontal gyrus, posterior cingulate gyrus elucidate their role in high order cognition required to form level 2 (comprehension) and level 3 (decision-making) of SA.

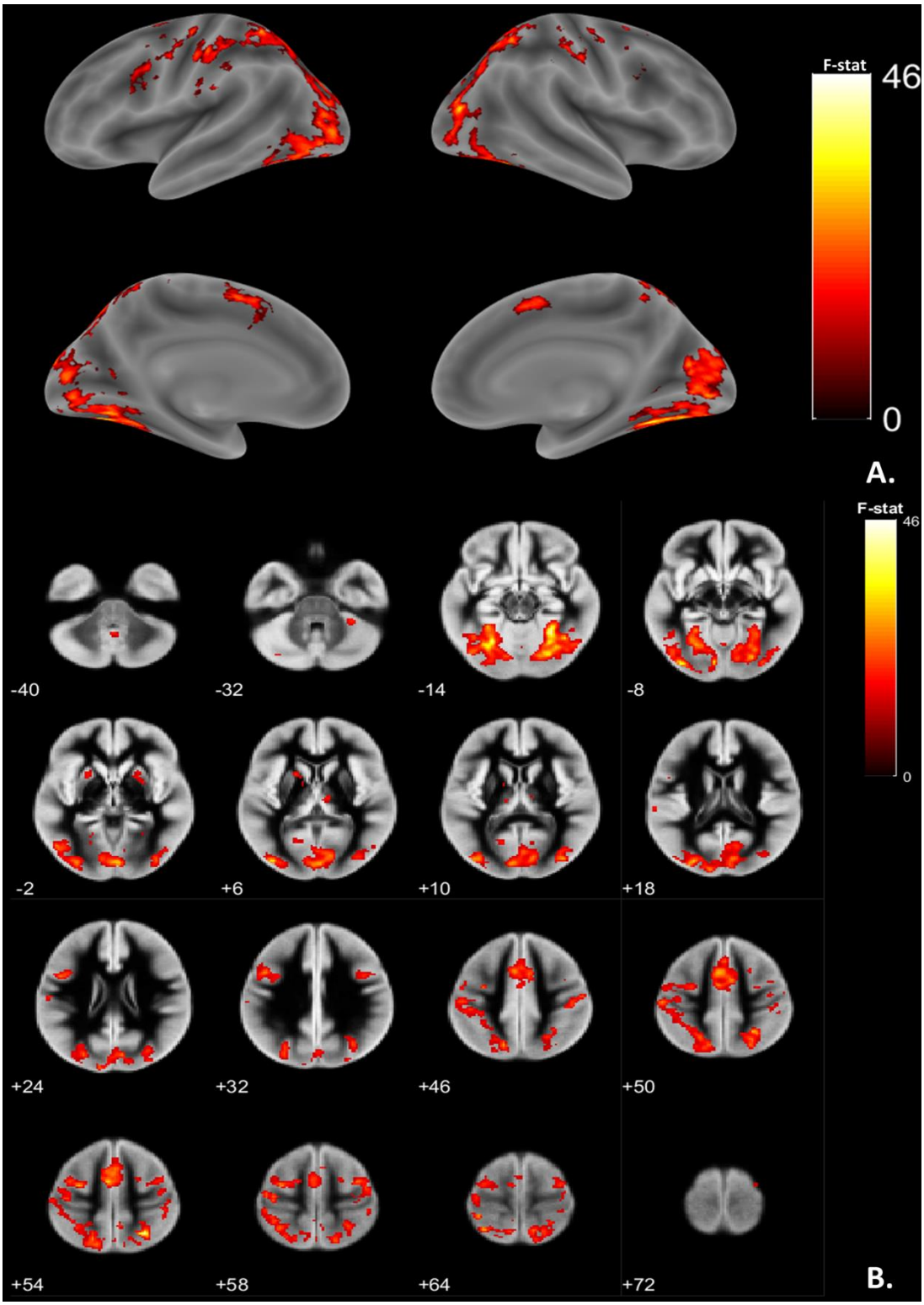


**Figure 3.7** Neural underpinnings of Situational awareness (SA) task, as shown in (A) surface rendered view (B) slice montage view. The activations are represented at FWE corrected $p<0.05$ (Kaur et al., 2019).

### *3.4.4 NEURAL UNDERPINNINGS OF PRAFA AND PRAA*

Reznik & Allen (2017) explored the frontal hemispherical differences of alpha as a predictor, moderator, and mediator of emotional regulation. However, it is still unclear which brain regions, in particular, are involved in mediating the emotional regulation during the SA-task. Thus, in order to decipher these neural underpinnings during the SA-task, PRAFA was passed as a global covariate in an independent EEG-informed fMRI model. Figure 3.8 shows the neural underpinning of PRAFA as assessed by this EEG-informed fMRI model, and details of the regions are tabulated in Supplementary Table S3.3 (see Appendix 1). The significant activations were observed in the parahippocampal gyrus, precuneous cortex, insular cortex, and parietal operculum cortex all at uncorrected p<.001.

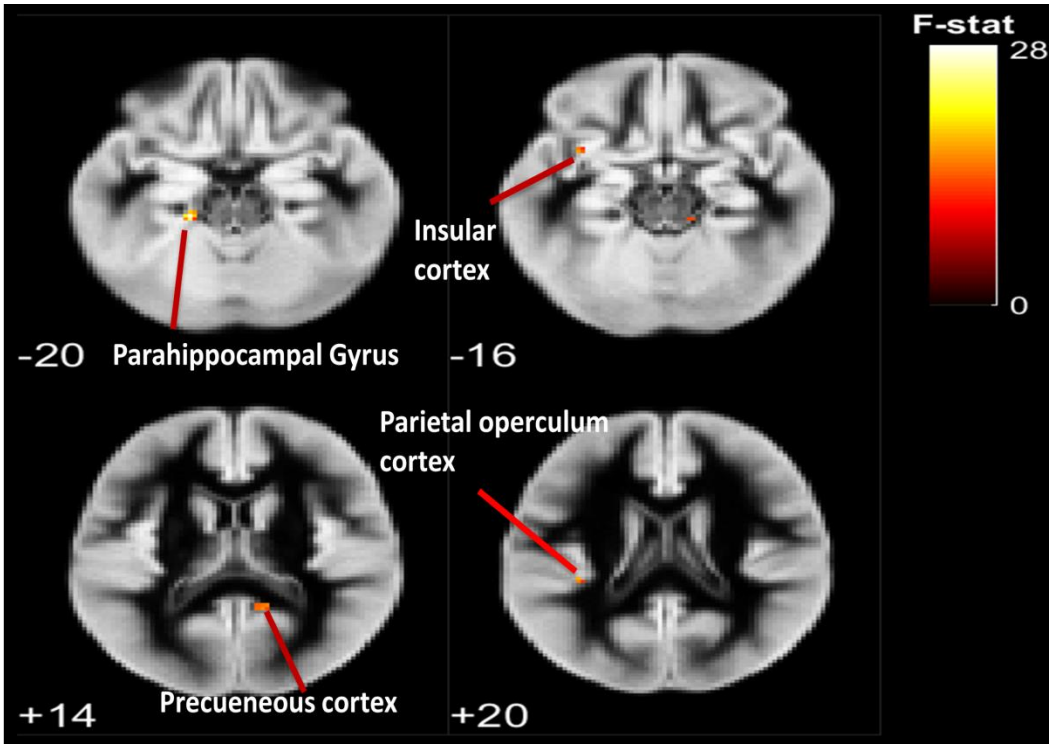


**Figure 3.8** Neural underpinnings of Pre-task resting-state alpha frontal asymmetry (PRAFA) through EEG informing SA-task based fMRI, as shown in the slice montage view. The activations are represented at uncorrected p<0.001(Kaur et al., 2019).

Similarly, the neural underpinnings of PRAA, as assessed by the independent EEG-informed fMRI analysis, are shown in Figure 3.9, and the regions are tabulated in Supplementary Table S3.4 (see Appendix 1). The neural underpinnings of PRAA revealed significant activations in both the frontal and temporal cortex at uncorrected $p<.001$. In particular, the frontal pole, middle frontal gyrus, superior frontal gyrus, inferior frontal gyrus has shown stronger activation in the frontal cortex. In addition, the right hippocampus, precuneous cortex, cingulate gyrus, thalamus, inferior temporal gyrus, and middle temporal gyrus have also shown significant involvement. These regions are well known for their role in the individual's emotional stability (Kassam et al., 2011; Kohn et al., 2014). Further, the PRAA has also revealed a correlation with neural activity in visual and attention regions such as an occipital pole, lateral occipital cortex, and temporal fusiform cortex.

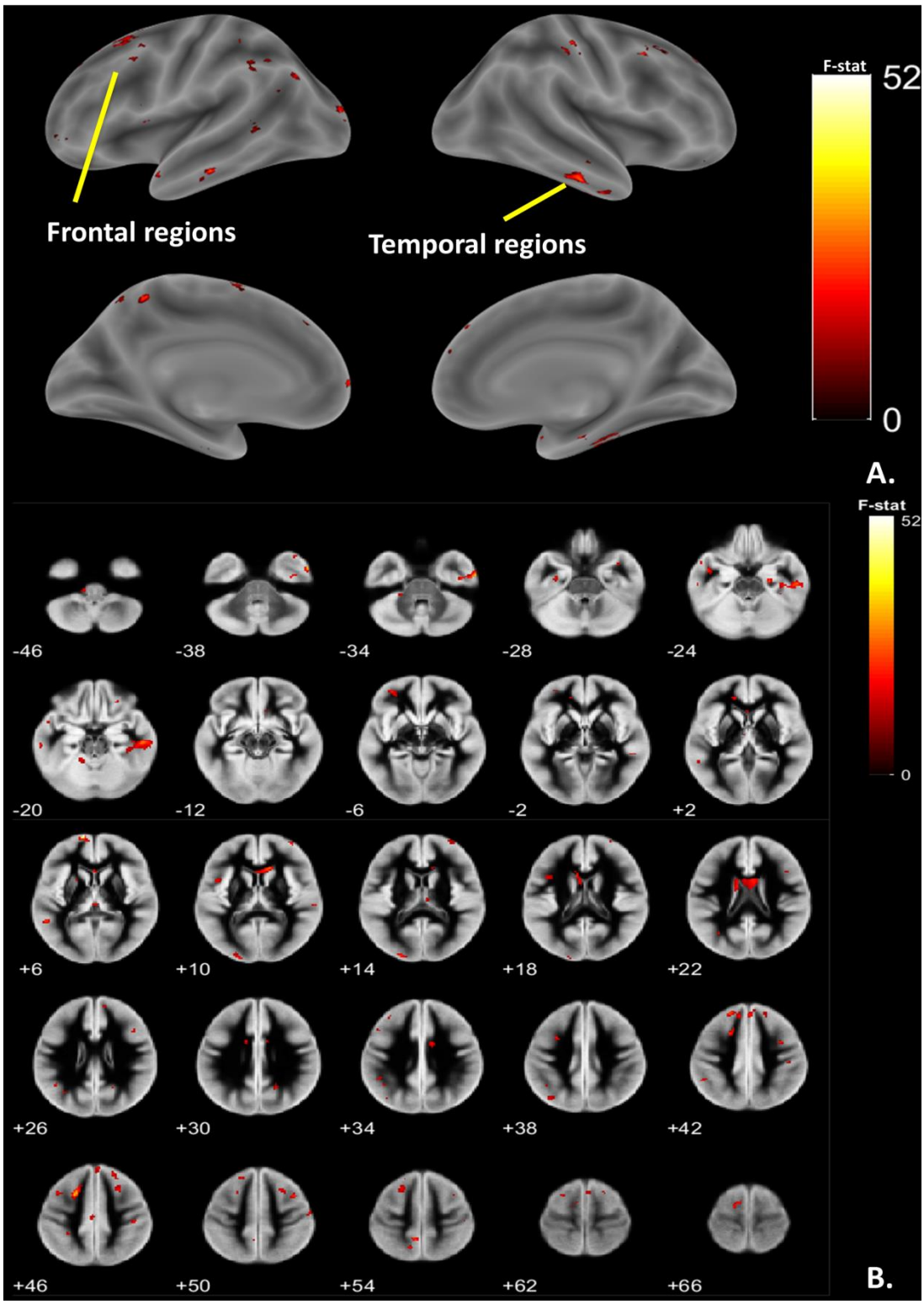


**Figure 3.9** Neural underpinnings of Pre-task resting-state absolute alpha (PRAA) power through EEG informing SA-task based fMRI, as shown in (A) surface rendered view (B) slice montage view. The activations are represented at uncorrected $p<0.001$ (Kaur et al., 2019).

### *3.4.5 FUNCTIONAL CONNECTIVITY ANALYSIS*

The functional connectivity between the neural underpinnings of PRAFA and neural underpinnings of PRAA has revealed strong mutual interaction across those regions. Similarly, the functional connectivity approach brought a better understanding of changes in neural mechanisms of SA-tasks by pre-task resting information.

#### 3.4.5.1 Connectivity between PRAA and SA neural underpinnings

Figure 3.10 shows strong interactions of the frontal (frontal pole, middle frontal gyrus, superior frontal gyrus) and temporal (middle temporal gyrus, temporal pole) underpinnings of PRAA with the neural underpinning of SA-task such as the inferior frontal gyrus, middle frontal gyrus, precentral gyrus, motor cortex, occipital lobe regions (occipital fusiform gyrus, lateral occipital cortex) and parietal regions (precuneous cortex, postcentral gyrus). Further, the subcortical underpinning of SA-task in left putamen specifically connected to the frontal and temporal pole underpinnings of PRAA.

#### 3.4.5.2 Connectivity between PRAFA and SA neural underpinnings

The connectivity results revealed strong interactions of the insula (PRAFA neural underpinning) with postcentral gyrus and left putamen of the SA-task (see Figure 3.10). The parietal operculum cortex of PRAFA neural underpinning significantly correlated with many neural underpinnings of SA-task such as the lateral occipital cortex, occipital fusiform gyrus, postcentral gyrus, precuneous cortex, regions. Another neural underpinning of PRAFA, the precuneous cortex correlated with the intracalcarine cortex, juxtapositional lobule cortex, lateral occipital cortex, middle frontal gyrus, occipital fusiform gyrus, postcentral gyrus, precentral

gyrus, precuneous cortex, right thalamus areas of SA-task. On the other hand, the Parahippocampal gyrus showed no correlation with SA clusters.

### 3.4.5.3 Connectivity between PRAFA and PRAA neural underpinnings

Figure 3.10 shows the connectivity within the neural underpinnings of PRAFA and PRAA. The connectivity results ($r>0.5$; $p<0.05$) revealed a significant correlation of the insula, parietal operculum cortex, and precuneous cortex (neural underpinnings of PRAFA) with frontal-temporal underpinnings of PRAA. Parahippocampal gyrus (neural underpinning of PRAFA) correlated explicitly with the temporal pole underpinning of PRAA.

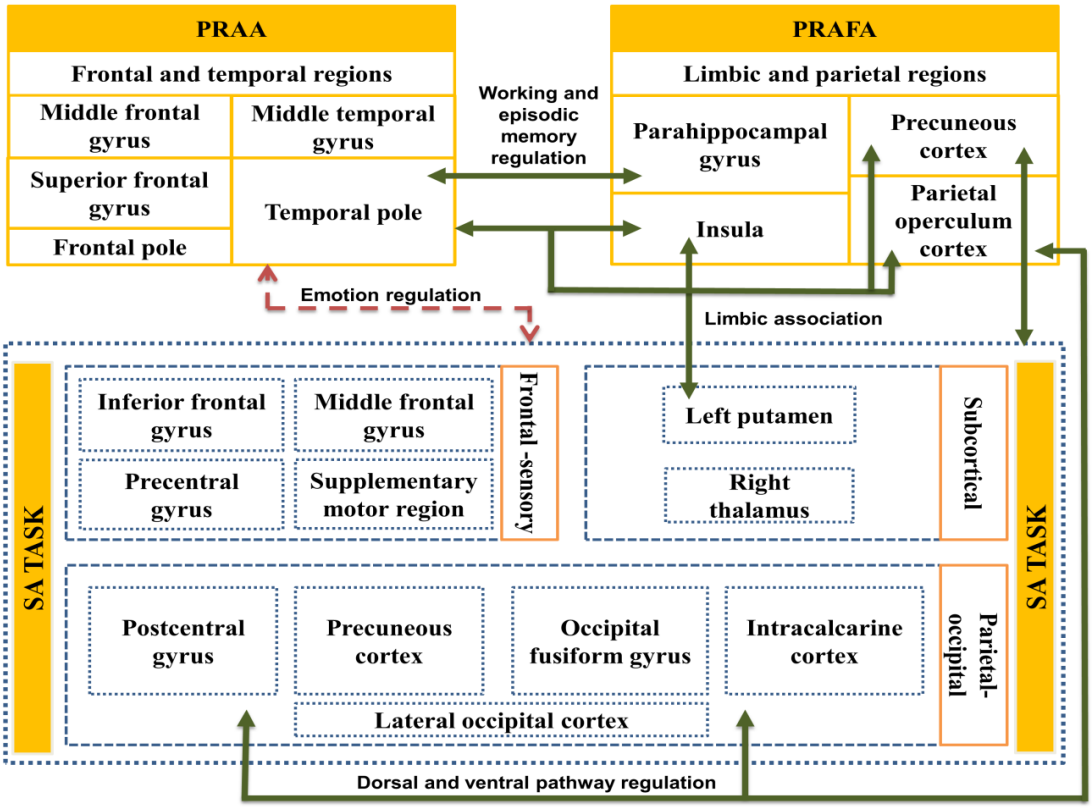


**Figure 3.10** Schematic showing functional connectivity of neural underpinnings of SA-task with PRAA and PRAFA underpinnings. The interregional correlation was done at $r>0.5$ ($p<0.05$). The dotted arrow illustrates the functional connectivity of PRAA (frontal and temporal regions) with SA regions. The solid arrows illustrate the limbic association of PRAFA regions with SA-task regions, and the integration of dorsal/ventral pathways, memory regulation (Kaur et al., 2019).

## 3.5 DISCUSSION

Our study aims to explore the influence of pre-task resting alpha information such as PRAFA and PRAA on SA. In particular, the SA-task is designed to have more influence from the Stroop effect; hence, the ability of pre-task resting information in assessing the behavioral outcome of SA in those conditions can be studied. The study extends to explore the neural underpinnings of the task, pre-task resting information and revealed through functional connectivity analysis that neural underpinnings of PRAFA and PRAA significantly interact with the neural underpinnings of SA-task and influence the behavioral outcome of SA.

SA generally possesses alternation between top-down and bottom-up processes. Top-down processing is a goal-driven process where attention is directed in accordance with active goals. On the contrary, bottom-up is a data-driven process wherein perceived cues from the environment activate new goals. In this study, the neural underpinnings of the SA-task revealed significant engagement of the visual cortex and occipital-temporal regions. The strong involvement of these regions pertaining to the memory (temporal regions) and visual processing justifies the hypothesis of Catherwood et al. (2014) that rapid memory operation is engaged during the reversal of bottom-up cognitive operations in SA. Similarly, the strong arousal was observed in sensory, precuneous, frontal gyrus, posterior cingulate gyrus during the SA-task. These regions have also been observed by Catherwood et al. (2014) and have been linked with cognition under uncertainty. Hence, the present study provides neuroimaging validation of regions associated with SA-task engagement, as observed in the aforementioned study.

### *3.5.1 VALIDATION OF PRESENCE OF STROOP EFFECT DURING SA-TASK*

In this study, the increase in reaction time during the Stroop effect in SA-task correlated positively with the SA index. This goes in line with the previous studies where delayed reaction times were observed when the font color and the word were different compared to when they were the same (Klamklay, 2002; Repov, 2004). This happens during the Stroop effect as the processing of a color impedes the simultaneous processing of a second stimulus attribute (word). Thus, our results show that the more the reaction time in the Stroop effect, the better is the performance in the task. Further, the Stroop effect's reaction time also correlated positively with the pre-task EEG alpha parameter PRAFA.

### *3.5.2 ROLE OF PRE-TASK ABSOLUTE ALPHA INFORMATION IN SA-TASK*

The changes in alpha EEG oscillation are known to be a marker of inhibition caused by neural activity. The neural underpinning, as assessed by functional imaging, facilitates to pinpoint the involvement of cognitive trait and state of the individual in the modulations of alpha oscillations. In this study, changes observed in pre-task absolute alpha information have been revealed to be significantly modulating neural mechanisms associated with subsequently performed SA-task. This is evident through a higher positive, robust correlation observed between the SA index and PRAA of eight channels (mainly posterior).

The neural underpinnings of PRAA observed in this study were primarily from frontal, temporal, and few parietal regions. Figure 3.10 clearly illustrates the strong functional connectivity between frontal-temporal regions of PRAA with neural underpinnings of the SA-task. Although the temporal lobe is the hub of memory management, the functional connectivity between frontal and temporal lobes has also been studied (Kennis et al., 2013; Lacruz et al.,

2007; Pfeifer et al., 2016) for their association with emotional regulation and arousal of affect. This clearly explains the effect of PRAA on SA-task as there is a demand for rapid memory management for the purpose of comprehension and understanding of environments. Further, the neural underpinnings of PRAA observed in the parietal regions such as angular gyrus, precuneous have been well studied as main areas involved in the mentalization process ( Frith & Frith, 2006). This is one of the core cognitive resources recruited during the comprehension stage of the SA-task.

### *3.5.3 ROLE OF PRE-TASK RESTING ALPHA FRONTAL ASYMMETRY IN SA-TASK*

The hemispheric asymmetry and lateralization of arousal of task-related neural activity are strongly connected with modulation of many cognitive state and trait behaviors, particularly approach/withdrawal behavior (Alves & Fukusima, n.d.; J. Davidson, 1992; Spielberg et al., 2010). The EEG alpha asymmetry is one of the validated information which estimates the hemispherical asymmetry and associated cognitive state and trait behavior modulations. In this study, the high positive, robust correlation of PRAFA with SA index indicates the possible role of pre-task cognitive state/ trait behavior as assessed by EEG asymmetry in the SA-task engagement. This further supports the suggestion of Catherwood et al. (2014) that the asymmetry of brain processes is linked with neural mechanisms of SA.

Further, neural underpinnings of PRAFA revealed areas of the limbic lobe (insular cortex and parahippocampal gyrus) and parietal cortex (precuneous and parietal operculum cortex). During situational awareness task, the perception and attention resources play a vital role in the task's behavioral outcome (Thilakarathne, 2015). The limbic region has direct access to perceptual information prior to sensory cortical systems and also modulates innate behaviors,

including motivation and avoidance behaviors (Nishijo et al., 2018). In particular, the insula in the limbic lobe plays a critical role in integrating bottom-up interceptive prediction error signals with top-down predictions from high-level cortical areas (Gu et al., 2013; Klein et al., 2013; Lu et al., 2016).

Similarly, the role of working and episodic memory in situational awareness task is nicely explained by the neural underpinning of PRAFA and their functional connectivity with neural underpinnings of SA-task (Figure 3.10). During SA-task, the individual perceives the environment and encodes the situational information as episodic and working memory (Gutzwiller & Clegg, 2013; Heenan et al., 2014; Johannsdottir & Herdman, 2005). Any decay of this encoded information in episodic and working memory leads to loss of SA, which pauses the individual to reassess the situations again (Gartenberg et al., 2013). This is known as the resumption lag. The neural underpinnings of PRAFA (parahippocampal gyrus and posterior parietal cortex) are involved in the regulation and maintenance of these episodic (Behrendt, 2013) and working memory (Schon et al., 2015). The Situations are assessed by the individual by integrating informational and spatial content of objects in the situations and associated emotional and spatiotemporally information (Behrendt, 2013). Posterior parietal regions, which are part of the dorsal visual stream, communicate spatial environmental information through the parahippocampal cortex. The integration of objects and contextual emotional information (Aminoff et al., 2013) with the parahippocampal cortex are derived from the ventral visual stream (neural underpinning of SA-task) and insula. Thus, it is evidently clear that the neural underpinning of PRAFA controls key regions pertaining to understanding the situations during the SA-task. Further, a parietal association of PRAFA is also supported by many research work

wherein precuneous forms a central hub for the link between the frontal and parietal regions (Bullmore & Sporns, 2009; Gong et al., 2009; Iturria-Medina et al., 2008).

### *3.5.4 LIMITATION OF STUDY*

In this study, SA-task is designed to have more influence from the Stroop effect; hence, the ability of pre-task resting information in assessing the behavioral outcome of SA in those conditions can be studied. The robust correlation of the reaction time with the SA index of the individual has validated the presence of the Stroop effect during the SA-task. However, the possibility of association of pre-task resting information with other cognitive traits and states such as fatigue, mental workload (Borghini et al., 2014) cannot be ignored. Hence, more elaborate research could be carried out in the future to reveal the role of specific cognitive/affective traits and states independently in the behavioral outcome and neural mechanisms of SA-tasks.

## 3.6 CONCLUSION

SA is a complex cognitive task, and the present study explored the association of the neural mechanisms associated with pre-task resting alpha information (PRAA and PRAFA) on SA. SA-task is designed to have more influence from Stroop effect and the ability of pre-task resting information in assessing SA in those conditions has been studied. The positive correlation of reaction time with the SA index, as well as PRAFA, validates the presence of the Stroop effect in the SA-task. A robust positive correlation of behavioral outcome of SA-task with PRAA and PRAFA suggests that the variability in an individual's PRAFA and PRAA are vital parameters to be observed prior to SA-task. The present findings are also part of the first efforts in

understanding the SA-task's neural underpinnings using functional imaging. Further, the role of PRAA and PRAFA on the SA-task has been reinforced by assessing the functional connectivity of SA-task neural underpinnings with PRAA and PRAFA underpinnings. The connectivity results revealed a strong connection of the neural underpinnings of PRAA and PRAFA, which are associated with cognitive and affective state/trait factors, with visual, memory, and high-order cognition regions involved in SA-task. In particular, the connectivity of pre-task alpha asymmetry with the SA-task's neural underpinnings reveals the modulation of integration of perceived contextual information, emotion, and retrieval of memory associated with the situational awareness by the pre-task trait/state information. Our results are encouraging and could be employed in operations that involve maintenance of good situational awareness, wherein neural mechanisms associated with pre-task resting alpha, and corresponding frontal asymmetry model could be utilized as a reliable predictor of an individual's performance in those operations.

Further, to unveil the association of the discussed pre-task resting frontal alpha asymmetry model with constructs of affect and approach/withdrawal behavior, a study covered in the next chapter was carried out. The affect and approach/withdrawal behavior measures have been linked to the frontal alpha asymmetry model during task engagement, evoking emotion, and the clinical population. However, their association during the resting-state is still debatable. Hence, the subsequent chapter visits the relationship of affect and approach/withdrawal dichotomy with the standard resting frontal alpha asymmetry model. Further, it introduces a novel resting microstates-based frontal alpha asymmetry model as a more reliable indicator of neural mechanisms underlying affect and approach/withdrawal measures.

## REFERENCES


Abreu, R., Leal, A., & Figueiredo, P. (2018). *EEG-Informed fMRI : A Review of Data Analysis Methods*. *12*(February), 1–23. https://doi.org/10.3389/fnhum.2018.00029

Alves, N. T., & Fukusima, S. S. (n.d.). *Laterality : Asymmetries of Body , Brain and Cognition Patterns of brain asymmetry in the perception of positive and negative facial expressions*. *February 2015*, 37–41. https://doi.org/10.1080/13576500802362927

Ambrosini, E., & Vallesi, A. (2015). Asymmetry in prefrontal resting-state EEG spectral power underlies individual differences in phasic and sustained cognitive control. *NeuroImage*. https://doi.org/10.1016/j.neuroimage.2015.09.035

Aminoff, E. M., Kveraga, K., & Bar, M. (2013). The role of the parahippocampal cortex in cognition. *Trends in Cognitive Sciences*, *17*(8), 379–390. https://doi.org/10.1016/j.tics.2013.06.009

Angelakis, E., Lubar, J. F., Stathopoulou, S., & Kounios, J. (2004). Peak alpha frequency: An electroencephalographic measure of cognitive preparedness. *Clinical Neurophysiology*, *115*(4), 887–897. https://doi.org/10.1016/j.clinph.2003.11.034

Balconi, M., Finocchiaro, R., & Canavesio, Y. (2014). Reward-system effect (BAS rating), left hemispheric "unbalance" (alpha band oscillations) and decisional impairments in drug addiction. *Addictive Behaviors*, *39*(6), 1026–1032. https://doi.org/10.1016/j.addbeh.2014.02.007

Balconi, M., Vanutelli, M. E., & Grippa, E. (2017). Resting state and personality component (BIS/BAS) predict the brain activity (EEG and fNIRS measure) in response to emotional cues. *Brain and Behavior*, *7*(5), 1–15. https://doi.org/10.1002/brb3.686

Barry, R. J., & De Blasio, F. M. (2017). EEG differences between eyes-closed and eyes-open resting remain in healthy ageing. *Biological Psychology*, *129*(April), 293–304. https://doi.org/10.1016/j.biopsycho.2017.09.010

Behrendt, R. (2013). *Conscious experience and episodic memory : hippocampus at the crossroads*. *4*(May), 1–14. https://doi.org/10.3389/fpsyg.2013.00304

Ben-david, B. M., Chajut, E., & Algom, D. (2012). *The Pale Shades of Emotion : A Signal Detection Theory Analysis of the Emotional Stroop Task*. *3*(7), 537–541.

Borghini, G., Astolfi, L., Vecchiato, G., Mattia, D., & Babiloni, F. (2014). Neuroscience and Biobehavioral Reviews Measuring neurophysiological signals in aircraft pilots and car drivers for the assessment of mental workload , fatigue and drowsiness. *Neuroscience and Biobehavioral Reviews*, *44*, 58–75. https://doi.org/10.1016/j.neubiorev.2012.10.003

Bullmore, E., & Sporns, O. (2009). Complex brain networks: Graph theoretical analysis of structural and functional systems. *Nature Reviews Neuroscience*, *10*(3), 186–198. https://doi.org/10.1038/nrn2575

Catherwood, D., Edgar, G. K., Nikolla, D., Alford, C., Brookes, D., Baker, S., & White, S. (2014). Mapping brain activity during loss of situation awareness: An EEG investigation of a basis for top-down influence on perception. *Human Factors*, *56*(8), 1428–1452. https://doi.org/10.1177/0018720814537070

Coan, J. (2003). *Coan JA , Allen JJB . Frontal EEG asymmetry and behavioral activation and inhibition systems . Frontal EEG asymmetry and the behavioral activation and inhibition systems*.

*40*(FEBRUARY), 106–114. https://doi.org/10.1111/1469-8986.00011

Coan, J A, & Allen, J. J. B. (2003). Frontal EEG asymmetry and the behavioral activation and inhibition systems. *Psychophysiology*, *40*(1), 106–114. https://doi.org/10.1111/1469-8986.00011

Coan, James A., & Allen, J. J. B. (2004). Frontal EEG asymmetry as a moderator and mediator of emotion. *Biological Psychology*, *67*(1–2), 7–49. https://doi.org/10.1016/j.biopsycho.2004.03.002

Davidson, J. (1992). *Anterior cerebral asymmetry and the nature of emotion*. *151*, 125–151.

Davidson, R J, Saron, C. D., Senulis, J. A., Ekman, P., & Friesen, W. V. (1990). Approach/withdrawal and cerebral asymmetry: Emotional\rexpression and brain physiology: I. *Journal of Personality and Social Psychology*, *58*(2), 330–341. https://doi.org/10.1037/0022-3514.58.2.330

Davidson, Richard J. (2010). Symposium on Emotion Hemispheric Substrates. *Psychological Science*, *3*(1), 39–43.

De Pascalis, V., Cozzuto, G., Caprara, G. V., & Alessandri, G. (2013). Relations among EEG-alpha asymmetry, BIS/BAS, and dispositional optimism. *Biological Psychology*, *94*(1), 198–209. https://doi.org/10.1016/j.biopsycho.2013.05.016

Edgar, G. K., Catherwood, D., Baker, S., Sallis, G., Bertels, M., Edgar, H. E., Nikolla, D., Buckle, S., Goodwin, C., & Whelan, A. (2018). Quantitative Analysis of Situation Awareness (QASA): modelling and measuring situation awareness using signal detection theory. *Ergonomics*, *61*(6), 762–777. https://doi.org/10.1080/00140139.2017.1420238

Ellis, A. J., Kinzel, C., Salgari, G. C., & Loo, S. K. (2017). Frontal alpha asymmetry predicts inhibitory processing in youth with attention deficit/hyperactivity disorder. *Neuropsychologia*, *102*, 45–51. https://doi.org/10.1016/j.neuropsychologia.2017.06.003

Endsley, M. R. (1995a). Measurement of Situation Awareness in Dynamic Systems. *Human Factors: The Journal of the Human Factors and Ergonomics Society*, *37*(1), 65–84. https://doi.org/10.1518/001872095779049499

Endsley, M. R. (1995b). Toward a Theory of Situation Awareness in Dynamic Systems. *Human Factors: The Journal of the Human Factors and Ergonomics Society*, *37*(1), 32–64. https://doi.org/10.1518/001872095779049543

Endsley, M. R. (2015). Situation awareness misconceptions and misunderstandings. *Journal of Cognitive Engineering and Decision Making*, *9*(1), 4–32. https://doi.org/10.1177/1555343415572631

Endsley, M. R., Bolstad, C. A., & Carolina, N. (2015). *Individual Differences in Pilot Situation Awareness Individual Differences in Pilot Situation Awareness*. *8414*(November), 37–41. https://doi.org/10.1207/s15327108ijap0403

Endsley, M. R., Bolté, B., & Jones, D. G. (2016). *Designing for Situation Awareness: An Approach to User-Centeres Design*.

Ferreira, C., Deslandes, A., Moraes, H., Cagy, M., Basile, L. F., Piedade, R., & Ribeiro, P. (2006). The relation between EEG prefrontal asymmetry and subjective feelings of mood following 24 hours of sleep deprivation. *Arquivos de Neuro-Psiquiatria*, *64*(2 B), 382–387. https://doi.org/10.1590/S0004-282X2006000300006

Frith, C. D., & Frith, U. (2006). *The Neural Basis of Mentalizing Minireview*. 531–534.

https://doi.org/10.1016/j.neuron.2006.05.001

Gable, P. A., Neal, L. B., & Threadgill, A. H. (2017). Regulatory behavior and frontal activity: Considering the role of revised-BIS in relative right frontal asymmetry. *Psychophysiology*, *March 2016*, 1–18. https://doi.org/10.1111/psyp.12910

Gartenberg, D., Breslow, L., Mccurry, J. M., Exelis, I. T. T., & Trafton, J. G. (2013). *Situation Awareness Recovery*. https://doi.org/10.1177/0018720813506223

Gómez-Ramírez, J., Freedman, S., Mateos, D., Pérez Velázquez, J. L., & Valiante, T. (2017). Exploring the alpha desynchronization hypothesis in resting state networks with intracranial electroencephalography and wiring cost estimates. *Scientific Reports*, *7*(1), 1–11. https://doi.org/10.1038/s41598-017-15659-0

Gong, G., He, Y., Concha, L., Lebel, C., Gross, D. W., Evans, A. C., & Beaulieu, C. (2009). Mapping anatomical connectivity patterns of human cerebral cortex using in vivo diffusion tensor imaging tractography. *Cerebral Cortex*, *19*(3), 524–536. https://doi.org/10.1093/cercor/bhn102

Gramann, K., Fairclough, S. H., Zander, T. O., & Ayaz, H. (2017). *Editorial : Trends in Neuroergonomics*. *11*(April), 11–14. https://doi.org/10.3389/fnhum.2017.00165

Grandy, T. H., Werkle-bergner, M., Chicherio, C., & Schmiedek, F. (2013). *Peak individual alpha frequency qualifies as a stable neurophysiological trait marker in healthy younger and older adults*. *50*, 570–582. https://doi.org/10.1111/psyp.12043

Gu, X., Hof, P. R., Friston, K. J., & Fan, J. (2013). Anterior insular cortex and emotional awareness. *Journal of Comparative Neurology*, *521*(15), 3371–3388. https://doi.org/10.1002/cne.23368

Gutzwiller, R. S., & Clegg, B. A. (2013). The role of working memory in levels of situation awareness. *Journal of Cognitive Engineering and Decision Making*, *7*(2), 141–154. https://doi.org/10.1177/1555343412451749

Hancock, P. A., & Szalma, J. L. (2003). *The future of neuroergonomics*. *44*, 238–249. https://doi.org/10.1080/1463922021000020927

Harmon-Jones, E., Gable, P. A., & Peterson, C. K. (2010). The role of asymmetric frontal cortical activity in emotion-related phenomena: A review and update. *Biological Psychology*, *84*(3), 451–462. https://doi.org/10.1016/j.biopsycho.2009.08.010

Heenan, A., Herdman, C. M., Brown, M. S., & Robert, N. (2014). *Effects of Conversation on Situation Awareness and Working Memory in Simulated Driving*. https://doi.org/10.1177/0018720813519265

Huster, R. J., Debener, S., Eichele, T., & Herrmann, C. S. (2012). Methods for simultaneous EEG-fMRI: An introductory review. *Journal of Neuroscience*, *32*(18), 6053–6060. https://doi.org/10.1523/JNEUROSCI.0447-12.2012

Iturria-Medina, Y., Sotero, R. C., Canales-Rodríguez, E. J., Alemán-Gómez, Y., & Melie-García, L. (2008). Studying the human brain anatomical network via diffusion-weighted MRI and Graph Theory. *NeuroImage*, *40*(3), 1064–1076. https://doi.org/10.1016/j.neuroimage.2007.10.060

Jensen, A. R., & Rohwer, W. D. (1966). The stroop color-word test: A review. *Acta Psychologica*, *25*(C), 36–93. https://doi.org/10.1016/0001-6918(66)90004-7

Johannsdottir, K. R., & Herdman, C. M. (2005). *The Role of Working Memory in Supporting Drivers '*

*Situation Awareness for Surrounding Traffic*. https://doi.org/10.1177/0018720810385427.Copyright

Jones, N. A., Field, T., & Almeida, A. (2009). Right frontal EEG asymmetry and behavioral inhibition in infants of depressed mothers. *Infant Behavior and Development*, *32*(3), 298–304. https://doi.org/10.1016/j.infbeh.2009.04.004

Kang, C., Lee, G. J., Yi, D., Mcpherson, S., Rogers, S., Tingus, K., & D, P. H. L. P. (2013). *Normative data for healthy older adults and an abbreviated version of the Stroop test*. *June*, 37–41.

Kassam, K. S., Markey, A. R., Cherkassky, V. L., Loewenstein, G., & Just, M. A. (2011). *Identifying Emotions on the Basis of Neural Activation*.

Kaur, A., Chaujar, R., & Chinnadurai, V. (2019). Effects of Neural Mechanisms of Pretask Resting EEG Alpha Information on Situational Awareness: A Functional Connectivity Approach. *Human Factors*. https://doi.org/10.1177/0018720819869129

Kennis, M., Rademaker, A. R., & Geuze, E. (2013). Neuroscience and Biobehavioral Reviews Neural correlates of personality : An integrative review. *Neuroscience and Biobehavioral Reviews*, *37*(1), 73–95. https://doi.org/10.1016/j.neubiorev.2012.10.012

Klamklay, J. (2002). *Individual differences and situation awareness*. Retrospective Theses and Dissertations. 1004. https://lib.dr.iastate.edu/rtd/1004

Klein, T. A., Ullsperger, M., & Danielmeier, C. (2013). Error awareness and the insula: links to neurological and psychiatric diseases. *Frontiers in Human Neuroscience*, *7*(February), 1–14. https://doi.org/10.3389/fnhum.2013.00014

Klimesch, W. (2012). Alpha-band oscillations, attention, and controlled access to stored information. *Trends in Cognitive Sciences*, *16*(12), 606–617. https://doi.org/10.1016/j.tics.2012.10.007

Kohn, N., Falkenberg, I., Kellermann, T., Eickhoff, S. B., Gur, R. C., & Habel, U. (2014). *Neural correlates of effective and ineffective mood induction*. 864–872. https://doi.org/10.1093/scan/nst055

Lacruz, M. E., García Seoane, J. J., Valentin, A., Selway, R., & Alarcón, G. (2007). Frontal and temporal functional connections of the living human brain. *European Journal of Neuroscience*, *26*(5), 1357–1370. https://doi.org/10.1111/j.1460-9568.2007.05730.x

Lindquist, M. A., Meng, J., Atlas, L. Y., & Wager, T. D. (2009). NeuroImage Modeling the hemodynamic response function in fMRI : Ef fi ciency , bias and mis-modeling. *NeuroImage*, *45*(1), S187–S198. https://doi.org/10.1016/j.neuroimage.2008.10.065

López Zunini, R. A., Thivierge, J. P., Kousaie, S., Sheppard, C., & Taler, V. (2013). Alterations in Resting-State Activity Relate to Performance in a Verbal Recognition Task. *PLoS ONE*, *8*(6), 1–8. https://doi.org/10.1371/journal.pone.0065608

Lu, C., Yang, T., Zhao, H., Zhang, M., Meng, F., Fu, H., Xie, Y., & Xu, H. (2016). Insular Cortex is Critical for the Perception, Modulation, and Chronification of Pain. *Neuroscience Bulletin*, *32*(2), 191–201. https://doi.org/10.1007/s12264-016-0016-y

MacLean, M. H., Arnell, K. M., & Cote, K. A. (2012). Resting EEG in alpha and beta bands predicts individual differences in attentional blink magnitude. *Brain and Cognition*, *78*(3), 218–229. https://doi.org/10.1016/j.bandc.2011.12.010

Mehta, R. K., Parasuraman, R., Mckinley, A., & Neuroscience, A. (2013). *Neuroergonomics : a review of*

*applications to physical and cognitive work*. *7*(December), 1–10. https://doi.org/10.3389/fnhum.2013.00889

Mennella, R., Patron, E., & Palomba, D. (2017). Frontal alpha asymmetry neurofeedback for the reduction of negative affect and anxiety. *Behaviour Research and Therapy*, *92*, 32–40. https://doi.org/10.1016/j.brat.2017.02.002

Murta, T., Leite, M., & Carmichael, D. W. (2014). *Electrophysiological Correlates of the BOLD Signal for EEG-Informed fMRI*. *00*. https://doi.org/10.1002/hbm.22623

Nikolla, D., Edgar, G., Catherwood, D., & Matthews, T. (2018). Can bottom-up processes of attention be a source of 'interference' in situations where top-down control of attention is crucial? *British Journal of Psychology*, *109*(1), 85–98. https://doi.org/10.1111/bjop.12251

Nishijo, H., Rafal, R., & Tamietto, M. (2018). *Editorial : Limbic-Brainstem Roles in Perception , Cognition , Emotion , and Behavior*. *12*(June), 10–12. https://doi.org/10.3389/fnins.2018.00395

Papousek, I., Weiss, E. M., Schulter, G., Fink, A., Reiser, E. M., & Lackner, H. K. (2014). Prefrontal EEG alpha asymmetry changes while observing disaster happening to other people: Cardiac correlates and prediction of emotional impact. *Biological Psychology*, *103*, 184–194. https://doi.org/10.1016/j.biopsycho.2014.09.001

Pernet, C. R., Wilcox, R., & Rousselet, G. A. (2013). *Robust correlation analyses : false positive and power validation using a new open source Matlab toolbox*. *3*(January), 1–18. https://doi.org/10.3389/fpsyg.2012.00606

Pfeifer, J. H., Masten, C. L., Borofsky, L. A., Dapretto, M., Fuligni, A. J., Lieberman, M. D., Pfeifer, J. H., Masten, C. L., Borofsky, L. A., Dapretto, M., Fuligni, A. J., & Lieberman, M. D. (2016). *Neural Correlates of Direct and Reflected Self-Appraisals in Adolescents and Adults : When Social Perspective-Taking Informs Self-Perception Published by : Wiley on behalf of the Society for Research in Child Development Stable URL : http://www.jstor.org/*. *80*(4), 1016–1038.

Raichle, M. E., & Snyder, A. Z. (2007). *A default mode of brain function : A brief history of an evolving idea*. *2*, 1083–1090. https://doi.org/10.1016/j.neuroimage.2007.02.041

Repov, G. (2004). The mode of response and the Stroop effect : A reaction time analysis Naèin odgovarjanja in Stroopov uèinek : analiza reakcijskih èasov. *Horizons*, *114*, 105–114.

Reznik, S. J., & Allen, J. J. B. (2017). Frontal asymmetry as a mediator and moderator of emotion: An updated review. *Psychophysiology*, *January*. https://doi.org/10.1111/psyp.12965

Sadaghiani, S., & Kleinschmidt, A. (2016). Brain Networks and α-Oscillations: Structural and Functional Foundations of Cognitive Control. *Trends in Cognitive Sciences*, *20*(11), 805–817. https://doi.org/10.1016/j.tics.2016.09.004

Scarpina, F., & Tagini, S. (2017). *The Stroop Color and Word Test*. *8*(April), 1–8. https://doi.org/10.3389/fpsyg.2017.00557

Schneider, M., Chau, L., Mohamadpour, M., Stephens, N., Arya, K., & Grant, A. (2016). EEG asymmetry and BIS/BAS among healthy adolescents. *Biological Psychology*, *120*, 142–148. https://doi.org/10.1016/j.biopsycho.2016.09.004

Schon, K., Newmark, R. E., Ross, R. S., & Stern, C. E. (2015). *A Working Memory Buffer in Parahippocampal Regions : Evidence from a Load Effect during the Delay Period*. 1–10.

https://doi.org/10.1093/cercor/bhv013

Sestito, M., Harel, A., Nador, J., & Flach, J. (2018). *Investigating Neural Sensorimotor Mechanisms Underlying Flight Expertise in Pilots : Preliminary Data From an EEG Study*. *12*(December), 1–13. https://doi.org/10.3389/fnhum.2018.00489

Shapiro, K. L., Hanslmayr, S., Enns, J. T., & Lleras, A. (2017). Alpha, beta: The rhythm of the attentional blink. *Psychonomic Bulletin and Review*, 1–8. https://doi.org/10.3758/s13423-017-1257-0

Smith, E. E., Reznik, S. J., Stewart, J. L., & Allen, J. J. B. (2017). Assessing and conceptualizing frontal EEG asymmetry: An updated primer on recording, processing, analyzing, and interpreting frontal alpha asymmetry. *International Journal of Psychophysiology*, *111*, 98–114. https://doi.org/10.1016/j.ijpsycho.2016.11.005

Spielberg, J. M., Stewart, J. L., Levin, R. L., & Miller, G. A. (2010). *NIH Public Access*. *2*(1), 1–16. https://doi.org/10.1111/j.1751-9004.2007.00064.x.Prefrontal

Stanislaw, H., & Todorov, N. (1999). Calculation of signal detection theory measures. *Behavior Research Methods, Instruments, and Computers*, *31*(1), 137–149. https://doi.org/10.3758/BF03207704

Thilakarathne, D. J. (2015). Modelling of situation awareness with perception , attention , and prior and retrospective awareness q. *Biologically Inspired Cognitive Architectures*, *12*, 77–104. https://doi.org/10.1016/j.bica.2015.04.010

Tomarken, A. J., Davidson, R. J., & Henriques, J. B. (1990). Resting frontal brain asymmetry predicts affective responses to films. *Journal of Personality and Social Psychology*, *59*(4), 791–801. https://doi.org/10.1037/0022-3514.59.4.791

Tomarken, A. J., Davidson, R. J., Wheeler, R. E., & Kinney, L. (1992). Psychometric Properties of Resting Anterior EEG Asymmetry: Temporal Stability and Internal Consistency. In *Psychophysiology* (Vol. 29, Issue 5, pp. 576–592). https://doi.org/10.1111/j.1469-8986.1992.tb02034.x

Uusberg, A., Uibo, H., Kreegipuu, K., & Allik, J. (2013). EEG alpha and cortical inhibition in affective attention. *International Journal of Psychophysiology*, *89*(1), 26–36. https://doi.org/10.1016/j.ijpsycho.2013.04.020

Wheeler, R. E., Davidson, R. J., & Tomarken, A. J. (1993). Frontal brain asymmetry and emotional reactivity: A biological substrate of affective style. In *Psychophysiology* (Vol. 30, Issue 1, pp. 82–89). https://doi.org/10.1111/j.1469-8986.1993.tb03207.x

Zwaag, W. Van Der. (2013). SC. *NeuroImage*. https://doi.org/10.1016/j.neuroimage.2013.05.114

# CHAPTER FOUR

# MICROSTATES-BASED RESTING FRONTAL ALPHA ASYMMETRY APPROACH FOR UNDERSTANDING AFFECT AND APPROACH/WITHDRAWAL BEHAVIOR

This chapter is a marginally modified version of the research article published as Kaur, A., Chinnadurai, V., & Chaujar, R. (2020). Microstates-based resting frontal alpha asymmetry approach for understanding affect and approach/withdrawal behavior. *Scientific Reports*, 10(1), 1–25. https://doi.org/10.1038/s41598-020-61119-7

## 4.1 ABSTRACT

The role of resting frontal alpha-asymmetry in explaining neural mechanisms of affect and approach/withdrawal behavior is still debatable. The present study explores the ability of the quasi-stable resting EEG asymmetry information and the associated neurovascular synchronization/desynchronization in bringing more insight into the understanding of neural-mechanisms of affect and approach/withdrawal behavior. For this purpose, a novel frontal alpha-asymmetry based on microstates, that assess quasi-stable EEG scalp topography information, is proposed and compared against standard frontal-asymmetry. Both proposed and standard frontal alpha-asymmetries were estimated from thirty-nine healthy volunteers resting-EEG simultaneously acquired with resting-fMRI. Further, neurovascular mechanisms of these asymmetry measures were estimated through EEG-informed fMRI. Subsequently, the Hemodynamic Lateralization Index (HLI) of the neural-underpinnings of both asymmetry measures was assessed. Finally, the robust correlation of both asymmetry-measures and their

HLI's with PANAS, BIS/BAS was carried out. The standard resting frontal-asymmetry and its HLI yielded no significant correlation with any psychological-measures. However, the microstate resting frontal-asymmetry correlated significantly with negative affect, and its neural underpinning's HLI significantly correlated with Positive/Negative affect and BIS/BAS measures. Finally, alpha-BOLD desynchronization was observed in neural underpinning, whose HLI correlated significantly with negative affect and BIS. Hence, the proposed resting microstate-frontal asymmetry better assesses the neural-mechanisms of affect, approach/withdrawal behavior.

## 4.2 INTRODUCTION

Understanding the neural mechanisms associated with functional hemispheric asymmetry of affect, approach/withdrawal measures is a core focus in neuroscience. Numerous studies revealed an association of functional hemispheric asymmetry with positive/negative affect and approach/withdrawal dichotomy. This linkage was initially observed in many studies where left hemispheric lesion affected the perception of positive emotions whilst damage to the right hemisphere impaired the perception of negative emotions (Aben et al., 2017; Killgore & Yurgelun-Todd, 2007; Nijboer & Jellema, 2012). Subsequently, there was a surge in elucidating the role of frontal hemispheric asymmetry based on the alpha signature of electroencephalography (EEG) in manifesting the individual differences in affect and approach/withdrawal measures (J. J. B. Allen et al., 2018; Hewig, 2018; Palmiero & Piccardi, 2017). Davidson and colleagues (R. J. Davidson et al., 1993; R J Davidson et al., 1990; Richard J. Davidson, 2004), in their studies, suggested the lateralization of the prefrontal cortex (PFC) with respect to positive/motivational valence. Thus, the right PFC was observed to be linked with

avoidance/negative emotion and left PFC with approach/positive emotion. Nevertheless, Carver & Harmon-Jones (2009) showed the association of the left hemisphere with negative emotion anger and thus proposed to eliminate the differentiation of positive and negative valence from the affective model. Subsequently, a larger number of studies concentrated on EEG frontal asymmetry through the induction of emotional/motivational states or tasks to understand the neural mechanisms associated with the evoked approach/withdrawal behavior (Andreas & Hewig, 2017; Balconi et al., 2017; Eftekhari et al., 2017; Fedorowicz, 2012; Gollan et al., 2014; Jacob et al., 2017; Rey et al., 2014; Studer et al., 2013) and other specific tasks (Kelley & Schmeichel, 2014). This has led to ample literature which examined alterations in frontal EEG asymmetry in clinical and healthy populations (Adolph & Margraf, 2017; Brzezicka et al., 2017; Flasbeck et al., 2017; Frenkel et al., 2017; Greimel et al., 2018; Lachman et al., 2016; Conny W.E.M. Quaedflieg et al., 2015; Stewart & Allen, 2018; van der Vinne et al., 2017).

Although the aforementioned studies have proved EEG based frontal asymmetry assessment as a reliable indicator of affect, approach/withdrawal behavior during emotional tasks, it's validity in healthy individuals during resting still remains ambiguous. In one large resting EEG study, Tomarken and colleagues ( a J. Tomarken et al., 1992; A. J. Tomarken et al., 1992) revealed a significant negative correlation of resting Frontal asymmetry (FA; channel pair: F4, F3) with negative affect and positive correlation of resting Anterior Temporal Asymmetry (ATA; channel pair: T4, T3) with positive affect for female subjects. Jacobs & Snyder (1996), in their study, revealed the negative correlation of resting Frontal Temporal Asymmetry (FTA; channel pair: F8, F7) with negative affect in men, further Hall & Petruzello (1999) showed that resting FA positively predicted the positive affect of both sexes. Pertaining to approach and withdrawal measures, studies by Harmon-Jones & Allen (1997) and De Pascalis et al. (2013)

reported a significant positive correlation of approach measure, Behavioral Activation System (BAS) with resting FA. The aforementioned studies are in sync with the hypothesis that positive affect correlates positively with alpha asymmetry ($\ln(alpha^{Right}) - \ln(alpha^{Left})$) and links to the left hemisphere, howbeit negative affect correlates negatively with the same and associates with the right hemisphere. Conversely, in another study (Sutton & Davidson, 1997), absolutely no significant relationship was observed between resting FA and measures of positive and negative valence for both sexes. Similarly, Schneider et al. (2016) observed an absence of correlation between resting alpha FA and measures of approach/withdrawal behavior. In contradiction to the above hypothesis, Hagemann et al. (1998) showed that subjects exhibiting greater relative left-hemispheric resting cortical activation at the anterior temporal site reported more intense NA in response to negative stimuli. Further, in the same line of research (Hagemann et al., 1999), it was found that subjects scoring high on NA demonstrated greater relative left-sided resting cortical activation at the anterior temporal region than subjects scoring low on NA.

Most findings of the aforementioned literature are based on two fundamental assumptions. Firstly, the above studies assume the acquired EEG to possess only stable cognitive information. Hence, these studies correlate the single session EEG information directly with affect and approach/ withdrawal measures. However, many studies ( a J. Tomarken et al., 1992; Wheeler et al., 1993) revealed that the stable EEG patterns across previous sessions showed the interrelation of affect and approach/ withdrawal measures with frontal alpha asymmetry. This brings the importance of assessing the stable EEG patterns and information from single session recordings as unstable EEG information may be influenced by interference from many cognitive factors. Recent EEG studies of wakeful rest have shown that global

electrical brain activity on the scalp remains semi-stable for transient periods (Khanna, 2016; Michel & Koenig, 2018).In specifics, there exists a finite number of scalp potential topographies in spontaneous resting EEG activity that remains stable for a definite time before rapidly shifting to a different topography that once again attains a stable state. These distinct epochs of topographic stability have been referred to as 'EEG microstates'. Lehmann et al. (1998) substantiated that EEG microstates represent blocks of consciousness, and these microstates are modulated by the content of the thoughts. Additionally, Milz et al. (2017) postulated the role of intracranial sources in the alpha band in predominantly determining these EEG microstate topographies. Further, Shafi et al. (2017), in their study, highlighted the role of microstates in individual variability of human fluid intelligence and in response to cognitive training. Howbeit, there is no study to date that has explored the quasi-stable state as assessed by EEG microstates for understanding frontal hemispheric asymmetry. Also, their ability over standard EEG frontal asymmetry in explaining affect and approach/withdrawal dichotomy is still unmapped.

The second important assumption is that EEG alpha power is inversely (Fink et al., 2005; Lenartowicz et al., 2016; Wright et al., 2015) related to neural activation. Hence, an increase in the left hemisphere's neural activation is linked to increased frontal asymmetry scores. This enables us in concluding that the positive correlation of affect and approach/withdrawal measures with frontal asymmetry score $(\ln(\alpha lpha^{Right}) - \ln(\alpha lpha^{Left}))$ is the resultant of left hemispherical neuronal activity and vice versa. However, recently, many neuro-vascular studies (Arakaki et al., 2018; Benedek et al., 2011; Klimesch et al., 1999; Palva & Palva, 2011) have observed alpha-BOLD synchronization wherein the alpha power correlates positively with neural activation during task engagement. Hence, there is a need to fully understand the neurovascular coupling and neural underpinning associated with frontal EEG asymmetry (J. J. B.

Allen et al., 2018) and how alpha-BOLD synchronization or desynchronization during resting-state associates with affect and approach/withdrawal behavior. Few researchers brought better understanding by studying the role of hemispheric asymmetry in affect, approach/avoidance behavior through functional MR imaging. Rohr et al. (2013) concluded that the affective elements in the underlying organization of emotion are predominantly associated with the network of right-hemispheric regions. K. A. Lindquist et al. (2016) proposed that the implementation of valence depends on a set of valence-general limbic and paralimbic brain regions. Though the above studies gave significant insights, the congruence between resting-EEG frontal alpha asymmetry and resting-fMRI is still uncharted. This is vital for a better understanding of neuro-vascular aspects of resting frontal asymmetry and their association with affect and approach/withdrawal behavior.

Hence, the present study proposes an EEG microstate based approach for assessment of quasi-stable frontal hemispherical asymmetry measures of resting-state affect and approach/withdrawal behavior. It further aims to compare the performance of microstate based frontal hemispheric asymmetry against the standard resting EEG frontal asymmetry measures. For this purpose, resting EEG was acquired from a sample of 39 healthy male subjects. This multichannel resting-EEG signal from all subjects was parsed into a limited number of distinct quasi-stable microstates. These microstates were back-fitted to each subject's EEG data to obtain microstate time-series data specific to each subject. The microstate time-series was further filtered at alpha frequency band and EEG microstate based frontal asymmetry measures were derived from channel pairs F4/F3 (FA) and F8/F7 (FTA). Further, the robust correlation of both standard and EEG microstate based frontal hemispheric asymmetry with positive/negative affect (PANAS) and approach (BAS)/withdrawal (BIS) behavior was carried out.

Moreover, the study focuses on bringing a better understanding of neural mechanisms associated with functional hemispheric asymmetry of affect and approach/ withdrawal behavior during resting-state. For this purpose, standard and microstates based resting EEG frontal asymmetries were subjected to the EEG informed fMRI approach, and the associated neural underpinning of both EEG frontal asymmetries were independently estimated. Thereafter, the hemodynamic lateralization index (HLI) based on the amplitude of hemodynamic response function (HRF) of regions part of the neural underpinning of both EEG frontal asymmetries were assessed. Further, the estimated HLI was subjected to a robust correlation with resting-state affect and approach/ withdrawal psychological scores. Finally, the results were analyzed to understand the ability of proposed EEG microstate estimates in revealing neural-vascular insights of association of functional hemispherical asymmetry with resting-state affect and approach/ withdrawal behavior.

## 4.3 MATERIALS AND METHODS

Figure 4.1 depicts the schema of the methodology adopted in this study.

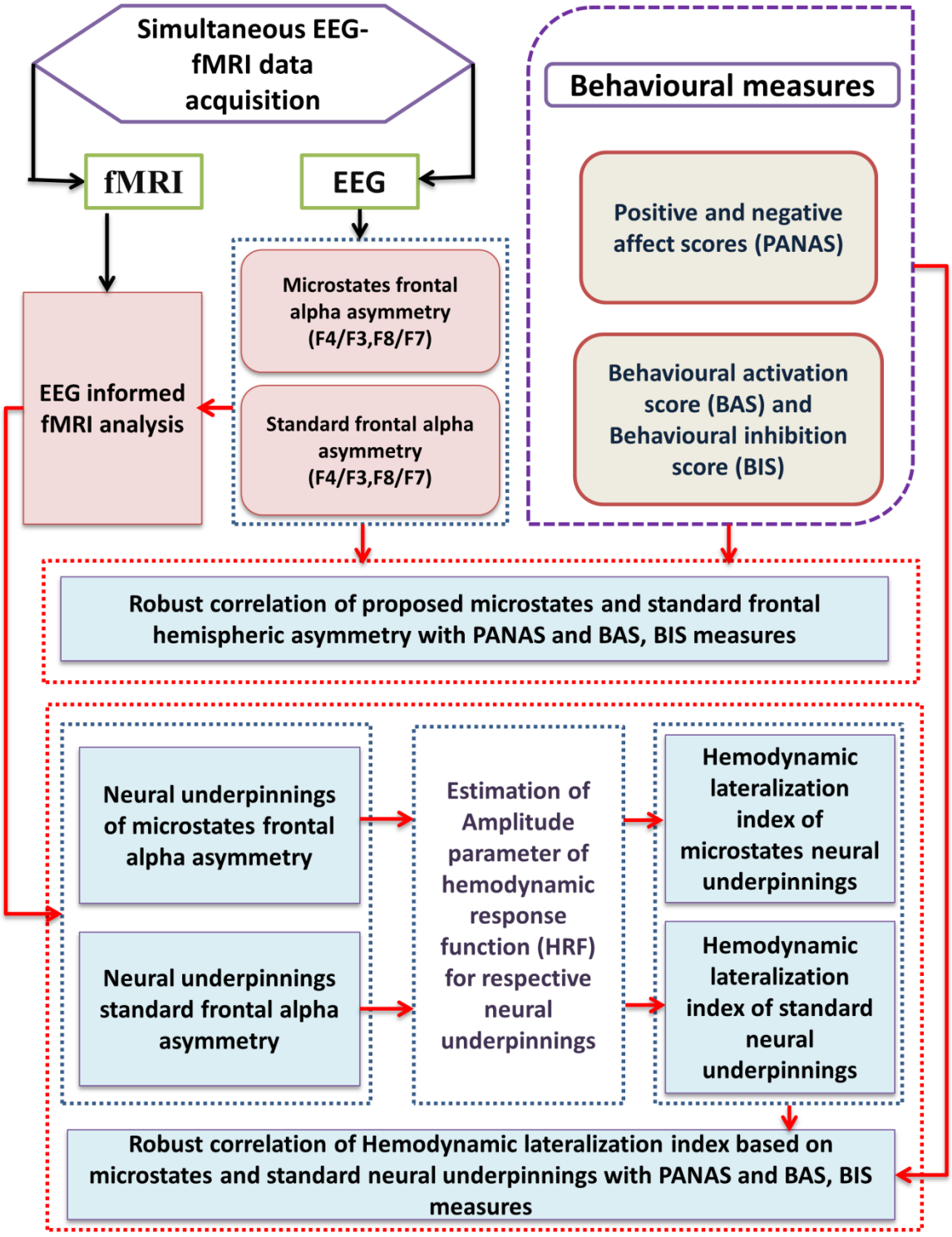


**Figure 4.1** Schema of the methodology adopted in this study (Kaur et al., 2020).

### *4.3.1 SAMPLE AND PROCEDURE*

Thirty-nine healthy participants (all males; age range 18-24 M=19.57; SD=1.28) took part in this study after providing a written and informed consent to the protocol. The experiment has been carried out in accordance with The Code of Ethics of the World Medical Association (Declaration of Helsinki), and all measurements were also approved by the Institute of Nuclear Medicine and Allied Sciences (INMAS) institutional ethical committee (Number: ECR/824/Inst/DL/2016). All subjects were volunteers recruited among university students and were right-handed. Subjects completed a personality questionnaire for positive affect and negative affect and Behavioral inhibition system (BIS)/ Behavioral approach system (BAS). The questionnaires were in the English language, and all the volunteers were fluent in the English language. The resting-state fMRI and EEG data analyzed in this paper were collected after the subject completed the psychological questionnaires. The simultaneous EEG-fMRI resting-state recording lasted for 6 minutes with eyes closed condition.

### *4.3.2 BEHAVIORAL MEASURES*

To assess the dispositional affect and approach/withdrawal parameters in resting state, PANAS scores and BIS/BAS measures were evaluated for each individual. We also estimated the Profile of mood states using POMS scores for prior exclusion criteria. Table 4.1 presents descriptive characteristics for the study participants with the mean and standard deviation values.

#### 4.3.2.1 Positive and Negative Affect

Positive and negative affect scores were evaluated for each volunteer. Positive and Negative Affect Schedule (PANAS) consists of mood scales devised to assess affect at the present moment (Watson & Clark, 1988). These scales are highly uncorrelated, stable over time,

and consistent, and both scales demonstrate good discriminant and convergent validity (John & Julie, 2004; Tuccitto et al., 2010). Positive and negative affect scores showed good internal consistency in our study (Cronbach's alphas= 0.89; 0.91).

#### 4.3.2.2 Behavioral approach system (BAS)/ Behavioral inhibition system (BIS)

BIS and BAS scores were calculated for each subject (Cooper et al., 2007) and evaluation included 24 items (20 score-items and four fillers, each measured on a four-point Likert scale), and two total scores for BIS (range = 7–28; 7 items) and BAS (range = 13–52; 13 items). In our study, BIS and BAS scales showed good internal consistency (Cronbach's alphas= 0.93; 0.92).

#### 4.3.2.3 POMS (Profile of mood states)

Volunteers were also asked to fill in forms for the POMS (Renger, 1993). It measures six different dimensions of mood swings, namely Tension or Anxiety, Vigor or Activity, Anger or Hostility, Depression or Dejection, Fatigue or Inertia, Confusion, or Bewilderment. These scores formed the basis for exclusion criteria. All selected volunteer returned self-report scores for all the modes within a relatively normal range.

**Table 4.1** Demographic and behavioral characteristics of study participants (N=39) (Kaur et al., 2020).

| Variable | Mean (M) | Std. Dev (SD) |
|---|---|---|
| Age | 19.57 | 1.28 |
| Positive Affect scores | 39.66 | 5.66 |
| Negative Affect scores | 14.64 | 4.29 |
| BAS scores | 23.42 | 3.5 |
| BIS scores | 15.28 | 2.7 |

### *4.3.3 DATA ACQUISITION AND PRE-PROCESSING STEPS*

MRI data was acquired in a Siemens 3T scanner. After acquiring a high-resolution T1-weighted anatomic rapid gradient-echo image (T1 MPRAGE sequence TR 1900ms, TE 2.49ms, FA $9^{o}$, 160 slices with slice thickness 0.9 mm and distance factor of 50%, FoV 240 mm with voxel size 0.9X0.9X0.9 mm), we acquired 205 T2*-weighted EPI images for resting-state eyes-closed condition (T2* EPI sequence: TR 2000ms, TE 30ms, FA $90^{o}$, 30 slices with thickness 5mm and distance factor 0%, FoV 240 mm with voxel size 3.8X3.8X5.0 mm). Continuous EEG data were acquired simultaneously during resting state T2* acquisition using a 32-channel MR-compatible brain vision cap. The electrodes were placed according to the international 10-20 system with a separate electrode called the Reference electrode, placed between Fz and Cz electrodes, that provided the reference for recording the data. Electrocardiogram (ECG) was also recorded. The impedance level for each electrode was kept less than 5 KΩ. The recorded EEG signal was digitized and transmitted with a 5000 Hz sampling frequency. The acquisition of EEG signals was accomplished using Brain vision analyzer software. These steps were also briefly discussed in Chapter two.

The fMRI data pre-processing for 205 resting-state volumes was done using the default pre-processing pipeline for volume-based analysis in CONN software. The pre-processing procedure included the realignment and unwarping of the T2*-weighted image with the mean functional image for motion correction followed by the translation of center to (0, 0, 0) coordinates and slice time correction of functional data. Functional outlier detection (ART-based identification of outlier scans for scrubbing) was performed, followed by segmentation and direct normalization to MNI space. Next, functional smoothening with a Gaussian Kernel with

FWHM of 6 mm was carried out. Further, translation of structural center to (0, 0, 0) and simultaneous structural segmentation and normalization were performed.

EEG data were corrected for gradient artifact using the Brain vision analyzer's (Ritter et al., 2007, 2010)average artifact subtraction algorithm (AAS) (P. J. Allen et al., 1998, 2000). A template from MR scanner artifacts was created by averaging the MR scanner artifacts over fixed intervals which were accurately specified by utilizing the fMRI volume markers (labeled as 'TR'). Subsequently, this average was subtracted from the EEG data. Further, the gradient artifact removed data accommodated six seconds of data prior to the start of the first fMRI block acquisition (identified by the first TR marker). These six seconds is the time the fMRI pulse sequence prepares itself before acquiring the first fMRI block. This prior time interval accommodated gradient-contaminated ECG; hence we truncated these 6 seconds prior data and subjected only the data pertaining to the fMRI volumes to the subsequent cardio ballistic (CB) artifact removal. The CB artifact removal was performed in the FMRIB plugin. The method detects the QRS peaks in the ECG data using combined adaptive thresholding (Niazy et al., 2005) and the Teager energy operator (Christov, 2004), followed by a correction algorithm. Further, the removal of the CB artifact is performed based on the Optimal Basis Set (OBS) method (Kim et al., 2004).

In addition, we also employed the HAPPE toolbox (Gabard-Durnam et al., 2018) for further ensuring the quality of conventional EEG artifact removal from the scanner and CB artifact corrected datasets. The following steps utilizing the HAPPE toolbox were adopted. First, the scanner and CB artifact removed data were subjected to the filtering process with 0.1 Hz high pass and 70 Hz low pass filtering, and all the EEG channels were selected for further analysis. This was followed by the removal of the electrical (line) noise using the Cleanline plugin

(Mullen, 2012) of EEGLAB. The functionality of HAPPE was utilized next to identify and remove the contaminated channels. HAPPE identifies the contaminated channels by evaluating the normed joint probability of average log power across all the channels and rejecting the channels whose joint probability is more than three standard deviations. Wavelet enhanced ICA (W-ICA) approach was implemented to correct for EEG artifact while retaining the entire length of the data file. The W-ICA approach removes ocular and muscle-related artifacts and improves the decomposition of later performed ICA, which eventually rejects artifact components. Next, independent components (ICs) with the extended infomax independent component analysis (ICA) were computed, and the MARA plugin (Winkler et al., 2011, 2014) of EEGLAB was employed for automatic component rejection. MARA evaluates each component on six features and eventually assigns a probability of artifact contamination to that component. Further, HAPPE's pipeline automatically rejected any components with artifact probabilities higher than 0.5. Subsequently, segmentation of data based on the markers, rejection of segments, and interpolation of removed channels were carried out. Finally, the processing report about the quality of data was generated. The EEG pre-processing procedures in this study have also been explained in detail in Chapter two.

### *4.3.4 DATA ANALYSIS*

#### 4.3.4.1 Assessment of frontal hemispherical asymmetry measures

The main objective of the study was to understand the neural mechanisms associated with the affect, approach/withdrawal behavior, as explained by the hemispherical asymmetry measures. For this purpose, the present study proposes an EEG microstate based frontal hemispheric assessment approach and aims to compare its advantage over the standard EEG

frontal asymmetry approach. The following subsections explain the methods for estimating the proposed EEG microstate based frontal hemispheric asymmetry as well as the standard frontal EEG asymmetry.

#### *4.3.4.1.1 EEG microstates based estimation of hemispheric asymmetry*

Many recent studies (Michel & Koenig, 2018; Pessoa, 2014; Sigman & Dehaene, 2008) have indicated that individual brain mechanisms involve extensive parallel processing in distributed brain networks. These distributed brain networks are observed as the scalp field potential in EEG, and the state of global neural activity is measured as a topographical map at that moment of time. The changes in this topography reflect variations in the global coordination of neural activity over time. EEG microstates were proposed to represent changes in behavior, thoughts, and emotions and can be classified into a few topographies, which have explained 90% of continuous EEG variance. Microstate analysis considers millisecond time range signals from all electrodes to create a global picture of a functional state during that interval.

The schema of the methodology adopted for microstate estimation is explained in Figure 4.2. The aim of a microstate analysis is first to segment EEG maps into microstate prototypes and second to re-express the spatial-temporal characteristics of the EEG time-series through these microstate prototypes.

In this study, let X be the time series EEG information that was acquired from the volunteers. At first, the EEG data X has been pre-processed for removing the artifacts and was referenced to the average referencing. Then, it was subjected to the estimation of Global field power (GFP). GFP is the measure of global brain response to an event and is represented as

$$\text{GFP} = \sqrt{\left(\sum_{i=1}^{C}(X_i(t) - X_{mean}(t))^2\right)/C} \qquad \text{Equation 4.1}$$

where $X_i$ is the measured potential at the i[th] electrode at a given time-point t, $X_{mean}$is the mean value of all $X_i$'s and C represents the total number of channels. GFP, therefore, represents the standard deviation of the electrode values and indicates, on average, how strong potential is being recorded across the electrode montage (Murray et al., 2008). For each volunteer, a selection of data points for the further processing has been carried out by filtering estimated GFPs based on minimum peak distance of 20 milliseconds and the threshold amplitude of one standard deviation of estimated GFP. Then, the filtered EEG data points of every individual are concatenated to form the GFP datasets for further clustering process as follows

$$\chi = \{x_{GFP}{}^1, x_{GFP}{}^2, \ldots\ldots\ldots x_{GFP}{}^S\} \qquad \text{Equation 4.2}$$

where $\chi$ is of the concatenated GFP dataset and $x_{GFP}{}^i$ are selected data points based on the GFP criteria of the i[th] volunteer, and S is the total number of volunteers. In this study, thirty-nine volunteers dataset has been subjected to analysis.

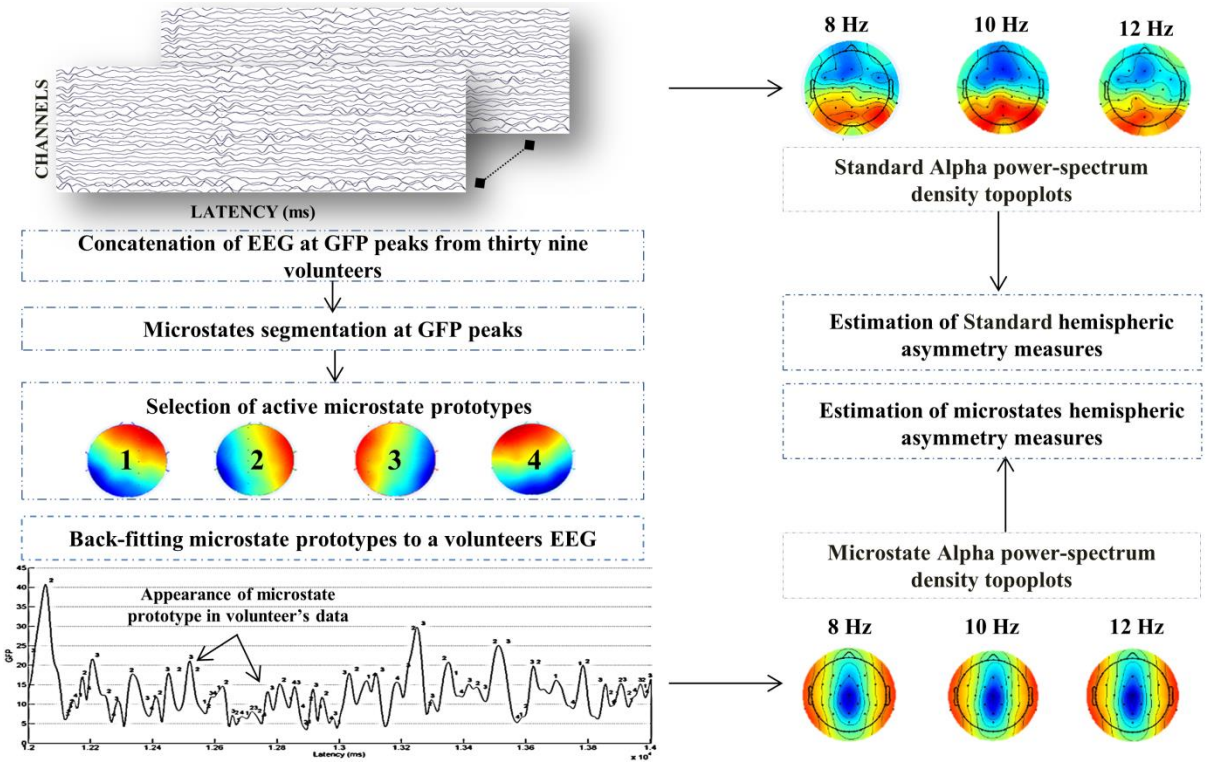


**Figure 4.2** Schema of the methodology adopted for proposed microstate estimation and assessment of standard and microstates based frontal alpha hemispheric asymmetry measures (Kaur et al., 2020).

Further, concatenated GFP dataset $\chi$ was subjected to the clustering process through the modified K-means clustering algorithm (Poulsen et al., 2018). The modified K-means clustering algorithm requires the initialization of both number (K) of microstate prototype vectors and their components values (Kretowski, 2019). Thus, the clustering algorithm was randomly initialized with a set of microstate prototype vectors as the center of initial clusters as follows

$$Z = \{z_i | \; i = 1 \; to \; K\} \qquad \text{Equation 4.3}$$

where K is the total number of microstate prototype vectors (cluster center). In this study, the K is initialized with 8. The clustering algorithm was allowed to iterate and minimize the orthogonal euclidean distance between the data points in $\chi$ as given below.

$$\tau_n = arg\min_k\{D_{kn}^2\} \quad \text{Equation 4.4}$$

$$D_{kn}^2 = \chi_n^T.\chi_n - (\chi_n^T.z_k)^2 \quad \text{Equation 4.5}$$

where $\tau_n$ represents the microstate label for n$^{th}$ sample, $\chi_n$ represents the n$^{th}$ time sample of the concatenated dataset, $z_k$ represents the prototypical map for the k$^{th}$ microstate cluster and $D_{kn}$ represents the distance between $\chi_n$ and microstate $k$ for the n$^{th}$ time sample. Thus, this clustering algorithm allocates each EEG sample to the cluster whose prototype it is most comparable to and then re-estimates microstate prototypes by averaging newly assigned samples (Poulsen et al., 2018). The maximal iterations were set to 1000, and the threshold for convergence was 1e$^{-6}$ for analysis in this study.

Subsequently, a review of goodness of fit and selection of active microstates is carried out based on global explained variance (GEV) and cross-validation (CV) criterion. It evaluates how well microstate segmentation explains the EEG data, which has been used to estimate the prototypes. Therefore, GEV measures how similar the EEG sample and the microstate prototype are; and is calculated as follows.

$$GEV_n = \frac{\left(Corr\left(\chi_n, z_{\tau_n}\right).x_{GFP_n}\right)^2}{\sum_{n'}^{N} {x_{GFP}}_{n'}^2} \quad \text{Equation 4.6}$$

where $\chi_n$represents the n$^{th}$ time sample of the concatenated dataset, $z_{\tau_n}$ $(\tau_n = k)$ is the prototypical map the k$^{th}$ microstate cluster and $x_{GFP_n}$ represents the n$^{th}$ time sample of the GFP data, and N represents the total time samples in concatenated dataset $\chi$. GEV is thus the measure of correlation among the EEG dataset and associated microstate prototype weighted by the EEG dataset's fraction of the total squared GFP (Poulsen et al., 2018). After that, to calculate the GEV

for a given cluster, the GEV of its members is summed. Subsequently, CV, which is a measure related to the residual noise, $\in$ is estimated as

$$CV = \sigma^2 . \left( \frac{C-1}{C-K-1} \right) \quad \text{Equation 4.7}$$

$$\sigma^2 = \frac{\sum_n^N \chi_n^T . \chi_n - (\chi_n^T . z_k)^2}{N(C-1)} \quad \text{Equation 4.8}$$

where $\sigma^2$ is the variance of the residual noise, C is the total number of EEG channels, N represents the number of time samples in concatenated dataset $\chi$, and K is the total number of clusters. The aim is to obtain a low value of CV. The active microstate prototypes obtained in this study are consistent with the normative EEG microstate classes identified by many studies (Al Zoubi et al., 2019; Brodbeck et al., 2012; Khanna, 2016; Michel & Koenig, 2018; Musso et al., 2010; Van De Ville et al., 2010).

Following the selection of an active number of microstate prototypes, the EEG of each volunteer is re-expressed as a sequence of microstate classes by back-fitting these active microstate prototypes on each volunteer's EEG data. Back fitting implies assigning microstate labels to the EEG dataset based on the dataset's topographic similarity with the microstate prototype. The estimated re-expressed back fitted dataset is represented as follows.

$$X_{re-expressed} = \{\mu_n |\ where\ \mu_n \in Z_{k'}\} \quad \text{Equation 4.9}$$

$$\text{where } \mu_n = arg\min(GMD_n)$$

The global map dissimilarity (GMD) index measures the topographical similarity between each microstate prototype vector with the EEG sample vector. The GMD is calculated as

$$GMD_n = \frac{\left\| \frac{X_n}{X_{GFP_n}} - \frac{z_{k'}}{z_{GFP_{k'}}} \right\|}{\sqrt{C}} \qquad \text{Equation 4.10}$$

where $X_n$represents the n[th] time sample of the pre-processed dataset, $z_{k'}$ represents the prototypical map for the k[th] microstate cluster. In an ideal condition, if the microstate prototype vector and the EEG sample vector of interest are having the same topographic distribution, then the GMD index will be zero. In case if both the vectors are topographically opposite, then the GMD index would be positively higher. Hence, in this study, instead of the thresholding the GMD index, the microstate prototype vector, which yields a significantly less GMD index, is chosen as the label for that particular EEG sample vector. Finally, microstates statistics using labels obtained from back-fitted prototypes were calculated.

Subsequently, the microstate prototype vector's amplitude associated with each label in microstate re-expressed EEG data of every individual is subjected to the alpha band power (8 – 12 Hz) estimation. The estimated alpha power map of the microstate re-expressed EEG data was used to estimate EEG microstate based frontal hemispheric asymmetry as follows.

$$Asymmetry_{MS} = \ln\left(\alpha\left(X_{re-expressed}{}^{Right}\right)\right) - \ln\left(\alpha\left(X_{re-expressed}{}^{Left}\right)\right) \qquad \text{Equation 4.11}$$

$\alpha\left(X_{re-expressed}{}^{Right}\right)$ and $\alpha\left(X_{re-expressed}{}^{Left}\right)$ are the alpha powers measured at the right and left hemispheric channel of microstate re-expressed EEG data, respectively.

#### *4.3.4.1.2 Standard EEG estimation of hemispheric asymmetry*

In order to estimate standard frontal asymmetry, the preprocessed EEG data is first re-referenced to CSD reference using the CSD toolbox (Kayser & Tenke, 2006a, 2006b). Recent work suggests that the CSD transformation reduces the influence of non-frontal sources to

frontal asymmetry and may provide a better index of individual differences in frontal asymmetry (Smith et al., 2017). Subsequently, the power spectral density (PSD) of alpha frequency (8-12 Hz) was extracted. The estimated alpha power map EEG data was used to calculate standard EEG frontal hemispheric asymmetry as follows.

$$Asymmetry_{\ Standard} = \ln\left(\alpha(X)^{Right}\right) - \ln(\alpha(X)^{Left}) \qquad \text{Equation 4.12}$$

$\alpha(X)^{Right}$ and $\alpha(X)^{Left}$ are the standard alpha powers measured at the right and left hemispheric channels of individual EEG data, respectively.

Table 4.2 presents the median and median absolute deviation values for EEG asymmetries for mid-frontal and lateral-frontal sites.

**Table 4.2** Median and median absolute deviation of the standard and proposed microstates based frontal hemispheric asymmetry measures (Kaur et al., 2020).

| **Variable** | **Channel pair F4/F3 (FA)** | | **Channel pair F8/F7 (FTA)** | |
|---|---|---|---|---|
| | Median | Median Absolute Deviation | Median | Median Absolute Deviation |
| Standard hemispheric asymmetry[a] | 0.0347 | 0.3509 | -0.052 | 0.3655 |
| Microstates based hemispheric asymmetry[a] | -0.2324 | 0.1427 | 0.0256 | 0.0896 |

[a]The difference between log-transformed alpha values from one right-hemispheric electrode to the corresponding electrodes on the left.

#### 4.3.4.2 Robust correlation of frontal hemispherical asymmetry measures with psychological measures

Further, estimated EEG microstate and standard frontal hemispherical asymmetries are correlated with PANAS and BAS, BIS measures. These robust correlations were carried out for hemispherical measures that are estimated for both channel pairs F4/F3 i.e. Frontal Asymmetry (FA) and F8/F7, i.e., Frontal Temporal Asymmetry (FTA) independently. The rationale for choosing these channels was based on the linkage of hemispheric asymmetry to mid-frontal (F3, F4) and lateral frontal (F7, F8) sites (J. Coan, 2003; Harmon-Jones et al., 2010; Wheeler et al., 1993). Robust correlations were implemented in the Robust correlation Matlab toolbox (Pernet et al., 2013). This method detects and protects against any bivariate or univariate outliers. Pearson, Bend, and Spearman correlation coefficients, as well as bootstrapped confidence intervals, were computed to evaluate each correlation. Both p-values and confidence intervals were Bonferroni corrected for multiple comparisons.

#### 4.3.4.3 Assessment of neural mechanisms associated with functional hemispheric asymmetry measures

One of the focuses of the current study is to understand the neural mechanisms associated with proposed and standard functional hemispheric asymmetry measures in explaining the affect and approach/ withdrawal behavior during resting state. For this purpose, both proposed and standard hemispheric asymmetry measures were subjected to the EEG informed fMRI, and their neural underpinnings were estimated. Subsequently, the lateralization index based on differences in the amplitude of hemodynamic response of neural underpinnings of both hemispheric asymmetry measures was assessed. Finally, the estimated lateralization index was

correlated with PANAS and BAS, BIS psychological measures to understand the ability of both hemispheric asymmetry measures in explaining affect and approach/ withdrawal behavior during resting state. The following sub-sections explain these operations in detail.

#### *4.3.4.3.1 EEG informed fMRI analysis*

Estimation of neural underpinnings of proposed microstate based EEG asymmetry and standard asymmetry was carried out as follows. At first, the estimated alpha powers for frontal channels F3, F4 F7, and F8 were downsampled to match the acquisition blocks of fMRI (TR: 2 seconds). This was carried out by taking the median of the alpha powers for these specific channels corresponding to each fMRI scan time, which is 2 seconds. The onset time of EEG and fMRI acquisition were also matched. This yielded one EEG alpha power corresponding to each fMRI scan, respectively. Thereafter, microstate based and standard FA and FTA were estimated. The first-level analysis in the present study was performed in SPM12. Different design matrices were obtained each for microstate based and standard asymmetry respectively for each subject wherein microstate based and standard FA and FTA parametrically modulated the fMRI regressors in EEG informed fMRI analysis (Abreu et al., 2018; Laufs et al., 2003; Murta et al., 2014; Pisauro et al., 2017; Sclocco et al., 2014).

The first-level analysis in our study was performed in SPM12, and the time series of fMRI regressors and parametric modulators were convolved with canonical HRF and with its time and dispersion derivatives. Further, at first-level, an F-contrast was defined for parametric modulators subsuming both non-derivative (canonical HRF) and derivative terms (time and dispersion derivatives) for microstate based FA, standard FA, microstate based FTA, and standard FTA models.

Subsequently, for the second level of analysis, the first-level contrast images, along with the dispersion and temporal derivatives, were subjected to the extraction of amplitude measures from the basis sets (Calhoun et al., 2004; Gawlowska et al., 2018; Kok et al., 2016; M. A. Lindquist & Wager, 2007; Wymbs et al., 2012). The robust regression toolbox (Wager et al., 2005) was used to conduct group-level random-effects analysis. The robust regression toolbox uses iteratively re-weighted least squares (IRLS), which detects influential extreme outliers. Thus, the IRLS analysis reduces the likelihood of false-positive and negative findings with no reduction in power and minimizes the effect of extreme outliers (Fritsch et al., 2015). The IRLS has proved beneficial with small samples (n = 10), and the benefits tend to increase with larger sample sizes (n = 40). Further, IRLS controls false-positive rates at an appropriate level when no true effects are present. The contrast image for amplitude summary measure was then subjected for the whole brain analysis corrected with voxel-wise False Discovery Rate (FDR) thresholded at $q < .05$. This yielded the underpinning of both microstate based FA and FTA and standard FA and FTA.

#### *4.3.4.3.2 Estimation of Hemodynamic lateralization index and its robust correlation with psychological measures*

The lateralization index measures the hemispherical dominance within the large-scale brain network that integrates the neural underpinnings associated with resting affect and approach/withdrawal behavior. The neural activity associated with each hemisphere's neural underpinnings causes differential electrical potential on the cortical surface of the respective hemisphere. This is measured as the EEG asymmetry index, as explained in the earlier sections. In the mean-time, these differential neural activities of each hemisphere generate a feed-forward signal, which results in differential hemodynamic response at the location of neural activity.

Measurement of these hemodynamic hemispherical differences facilitates a better understanding of hemispherical dominance within the large scale brain interactions. Diverse methods have been proposed to calculate the hemodynamic lateralization index on the basis of fMRI BOLD information. As most of these studies involved task engagement, the hemispherical difference of cluster size and BOLD signal strength (Bradshaw et al., 2017; Branco et al., 2006; Jansen et al., 2006; Jones et al., 2011; Seghier, 2008) were normally used to estimate the HLI.

The main motivation behind this estimation is to understand whether hemodynamic asymmetry reveals more insight into understanding the neurovascular mechanisms of the affect and approach /withdrawal behavior. For this purpose, initially, we estimated the hemodynamic response function metric that is hemodynamic response function amplitude (HRF_Amp) at every voxel by independently subjecting the pre-processed resting fMRI data to blind deconvolution method as proposed by Wu et al. (2015). The estimation of HRF was carried out independently by assuming acquired fMRI BOLD signal $y(t)$ as the convolution of neural states $n(t)$ with $HRF(t)$. This is represented as

$$y(t) = conv\big(n(t), HRF(t)\big) + \in (t) \qquad \text{Equation 4.13}$$

where $\in (t)$ is the noise in the measurement. Further, $n(t)$ is substituted by a hypothetical neural activation model as follows.

$$\hat{n}(t) = \sum_{\tau=0}^{\infty} \delta(t-\tau) \qquad \text{Equation 4.14}$$

where $\delta(t-\tau)$ is the delta function. This allows fitting $HRF(t)$according to $\hat{n}(t)$ using a canonical HRF and two derivatives (temporal and dispersion derivatives). This model is subjected to a blind deconvolution approach for retrieving the hemodynamic response function

$(HRF(t))$ of every voxel. Once $HRF(t)$ is obtained, an approximation of $\tilde{n}(t)$ can be calculated using the inverse Fourier transform (deconvolution). Then, $HRF(t)$ was utilized to estimate the HLI for the neural underpinnings of both microstate based FA and FTA and standard FA and FTA, all considered together. Hence, the cluster results of EEG informed fMRI were used only for the selection of regions for estimating HLI as follows.

$$HLI(n) = \ HRF_{Amp}{}_n^R - HRF_{Amp}{}_n^L \qquad \text{Equation 4.15}$$

where $HRF\_Amp_n^R$ and $HRF\_Amp_n^L$ are the median amplitude of hemodynamic response function of the $n^{th}$ neural underpinnings in the right and left hemispheres, respectively. The median of estimated HLI of neural underpinnings of proposed microstate based EEG asymmetry and the standard EEG asymmetry measures were finally subjected to the robust correlations with PANAS and BIS/BAS measures.

## 4.4 RESULTS

Our study focused on exploring the ability of quasi-stable EEG microstate based frontal alpha hemispherical asymmetry measures against standard EEG frontal alpha asymmetry measures in explaining the resting state affect and approach/ withdrawal behavior for healthy young male volunteers during 1-time measurement. The standard alpha topographic maps (CSD referenced) and microstate alpha topographic maps are shown in Figure 4.3. Evidently, the maps of standard alpha topography (CSD referenced) in Figure 4.3b reveal the typical parietal-occipital alpha activity for eyes-closed resting-state conditions (Rashed-Al-Mahfuz et al., 2013; Tenke et al., 2015). However, the parietal-alpha activity is typical of standard alpha topographic maps and has not been observed and reported by any researchers in microstate alpha topographic maps so far. For assessing the association of EEG microstate based frontal hemispheric

asymmetry with affect and approach/withdrawal behavior, robust correlation of PANAS and BAS, BIS measures with standard and EEG microstate FA and FTA was estimated. Subsequently, to better understand the neural mechanisms underlying the proposed microstate and standard hemispherical asymmetry measures, they were subjected to the EEG informed fMRI, and their neural underpinnings were estimated. Further, to gain insights into the hemodynamic lateralization associated with the neural underpinnings and its linkage with affect and approach/withdrawal measures, HLI of both asymmetry measures neural underpinnings' was calculated and subsequently subjected to the robust correlation with PANAS and BAS, BIS measures.

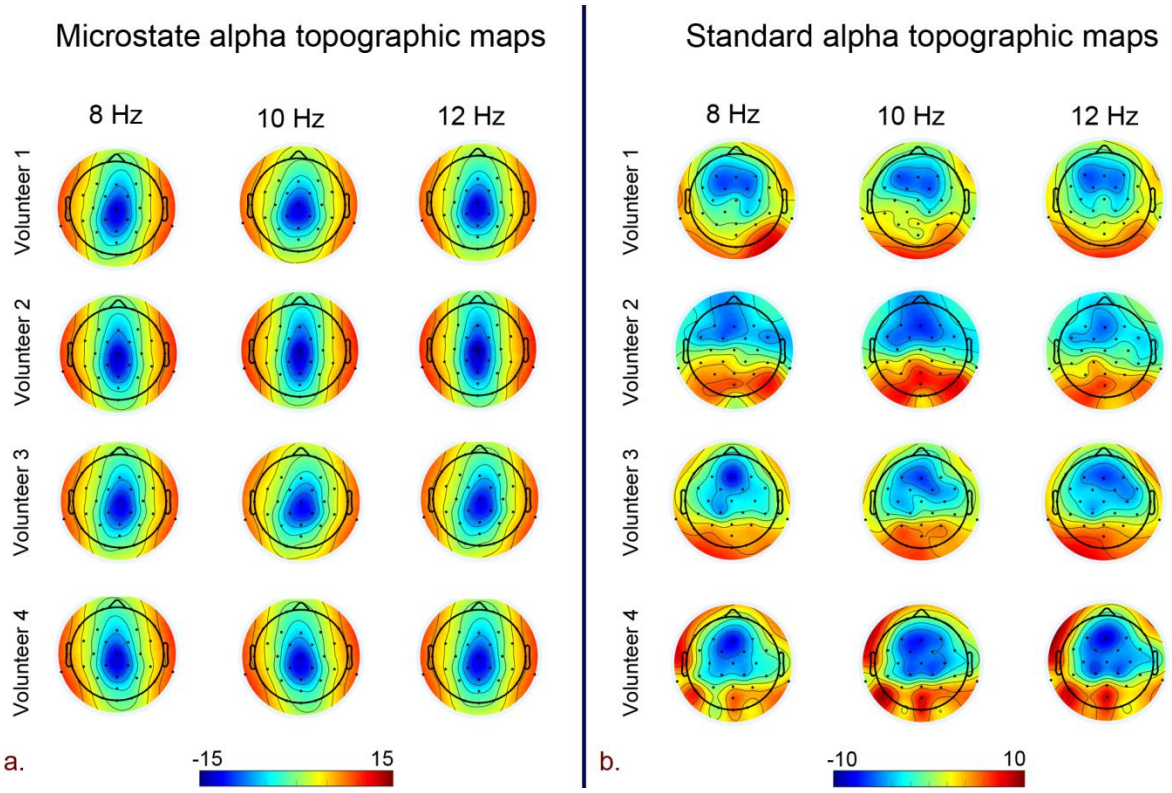


**Figure 4.3** Topographic EEG maps of spectral power density for the alpha band for a. proposed microstate based analysis and b. Standard analysis (CSD referenced). The color bar represents the log-transformed spectral power density (10*log10 (µv2/Hz)) where red represents the maximum and blue represents the minimum values (Kaur et al., 2020).

### *4.4.1 ROBUST CORRELATION OF FRONTAL HEMISPHERICAL ASYMMETRY MEASURES WITH PSYCHOLOGICAL MEASURES*

The robust correlation (Pearson, bend, spearman, and skipped) of proposed microstate and standard frontal hemispheric asymmetry measures with PANAS and BIS/BAS psychological scores is tabulated in Table 4.3.

Standard FA and FTA revealed no statistically significant correlation with PANAS as well as BIS/BAS measures. Similarly, proposed microstate based FA and FTA yielded insignificant low correlation with positive affect score.

Howbeit, negative affect scores revealed a strong and significant correlation with proposed microstate based FA and FTA. Specifically, microstates based FA yielded high pearson, bend and spearman correlations (Figure 4.4a: pearson r=0.35, 95% CI= [0.07; 0.58], pcorr=0.04; Figure 4.4b: bend r=0.33, 95% CI= [-0.02; 0.61], pcorr=0.05; Figure 4.4c: spearman r=0.36, 95% CI= [0.04; 0.62], pcorr=0.03). Similarly, skipped pearson and spearman robust correlations of microstates based FA with negative affect scores has also yielded stronger correlations (Figure 4.4d: pearson skipped=0.35, 95% CI= [0.04; 0.57]; spearman skipped=0.36, 95% CI= [0.005; 0.62]). In addition, a strong robust pearson, bend and spearman correlation of microstates based FTA with negative affect scores was observed (Figure 4.5a: pearson r=0.42, 95% CI= [0.13; 0.67], pcorr=0.01; Figure 4.5b: Bend r=0.42, 95% CI= [0.05; 0.70], pcorr=0.01; Figure 4.5c: spearman r=0.38, 95% CI= [0.02; 0.68], pcorr=0.02). Skipped (pearson and spearman) correlations among microstates-derived FTA and negative affect scores has also yielded stronger correlations (Figure 4.5d: Pearson skipped=0.42, 95% CI= [0.14; 0.67]; Spearman skipped=0.38, 95% CI= [0.04; 0.68]).

However, BAS measures yielded a statistically insignificant low correlation with proposed microstate asymmetry. The analysis with BIS measures for both FA and FTA revealed high correlation, but the p-values remained insignificant.

**Table 4.3** Robust correlation (Pearson, bend, spearman and skipped) of standard and proposed microstate based frontal hemispheric asymmetry measures with psychological scores (Kaur et al., 2020).

| EEG alpha frontal asymmetry | Channel pair | Behavioral measure | Pearson Correlation | | Bend correlation | | Spearman correlation | | Skipped correlation | | | |
|---|---|---|---|---|---|---|---|---|---|---|---|---|
| | | | | | | | | | Pearson | | Spearman | |
| | | | r | p | r | p | r | p | r | t | r | t |
| Standard | F4/F3 (FA) | Positive affect | 0.22 | 0.21 | 0.2 | 0.23 | 0.09 | 0.54 | 0.22 | 1.27 | 0.09 | 0.54 |
| | | Negative affect | -0.1 | 0.54 | -0.04 | 0.8 | -0.05 | 0.75 | -0.1 | -0.6 | -0.05 | -0.31 |
| | | BAS | -0.25 | 0.37 | -0.16 | 0.56 | -0.17 | 0.56 | -0.25 | -0.92 | -0.17 | -0.59 |
| | | BIS | -0.03 | 0.9 | 0.09 | 0.75 | 0.09 | 0.73 | -0.03 | -0.12 | 0.09 | 0.34 |
| | | | | | | | | | | | | |
| | F8/F7 (FTA) | Positive affect | 0.03 | 0.83 | -0.11 | 0.52 | -0.12 | 0.47 | 0.03 | 0.21 | -0.12 | -0.73 |
| | | Negative affect | -0.05 | 0.75 | 0.01 | 0.92 | -0.004 | 0.97 | -0.05 | -0.31 | -0.004 | -0.02 |
| | | BAS | 0.18 | 0.52 | 0.17 | 0.55 | 0.13 | 0.65 | 0.18 | 0.65 | 0.13 | 0.46 |
| | | BIS | -0.14 | 0.62 | -0.14 | 0.61 | -0.3 | 0.28 | -0.14 | -0.5 | -0.3 | -1.12 |
| | | | | | | | | | | | | |
| Microstates | F4/F3 (FA) | Positive affect | 0.03 | 0.84 | 0.08 | 0.61 | 0.12 | 0.46 | 0.03 | 0.2 | 0.12 | 0.73 |
| | | Negative affect | 0.35 | 0.04 | 0.33 | 0.05 | 0.36 | 0.03 | 0.35 | 2.13 | 0.36 | 2.2 |
| | | BAS | -0.09 | 0.74 | -0.04 | 0.86 | 0 | 1 | -0.09 | -0.32 | 0 | 0 |
| | | BIS | -0.3 | 0.29 | -0.41 | 0.14 | -0.28 | 0.32 | -0.3 | -1.09 | -0.28 | -1.01 |
| | | | | | | | | | | | | |
| | F8/F7 (FTA) | Positive affect | 0.0003 | 0.99 | -0.01 | 0.91 | -0.01 | 0.92 | 0.0003 | 0.0018 | -0.01 | -0.09 |
| | | Negative affect | 0.42 | 0.01 | 0.42 | 0.01 | 0.38 | 0.02 | 0.42 | 2.64 | 0.38 | 2.34 |
| | | BAS | -0.17 | 0.54 | -0.18 | 0.52 | -0.18 | 0.53 | -0.17 | -0.62 | -0.18 | -0.64 |
| | | BIS | -0.32 | 0.25 | -0.45 | -1.7 | -0.33 | -1.22 | -0.32 | -1.19 | -0.33 | -1.22 |

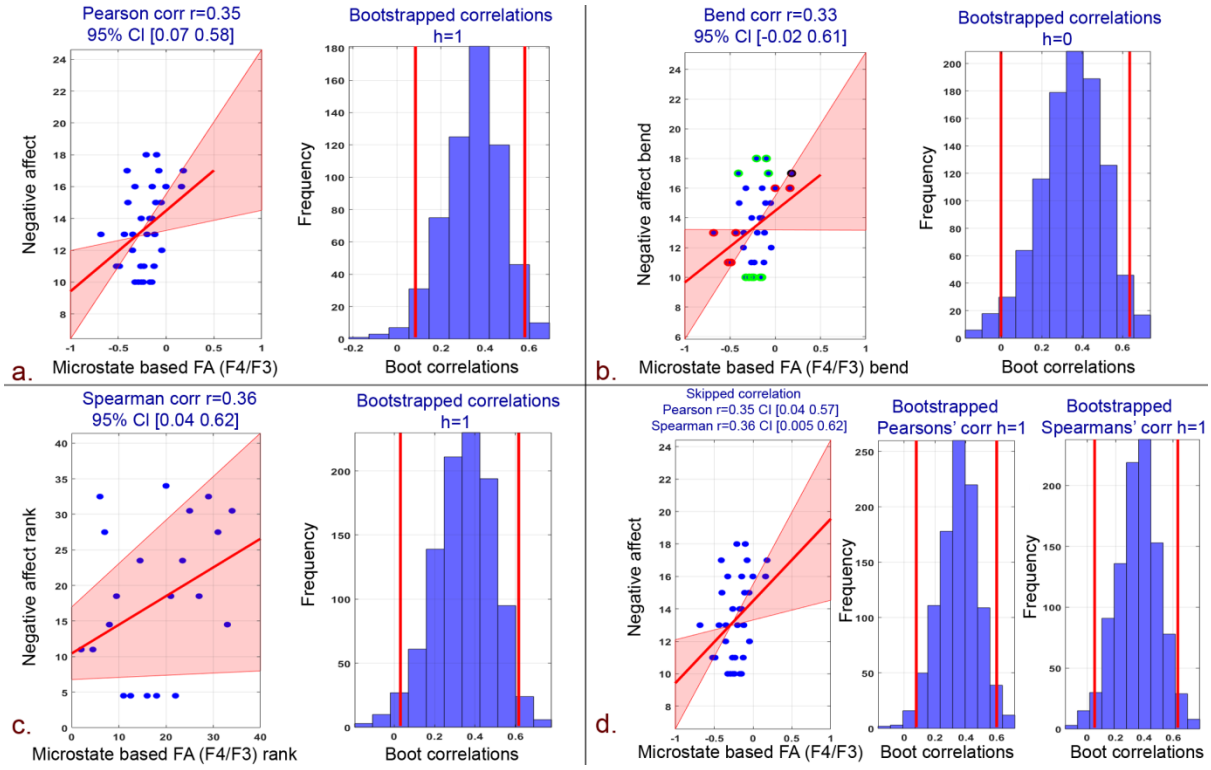


**Figure 4.4** Correlation plots between negative affect scores and microstate based FA (F4/F3) and associated histograms of correlations for bootstrapped data. a. Pearson correlation b. 20% Bend correlation c. Spearman correlation d. Skipped (Pearson and Spearman) correlations (Kaur et al., 2020).

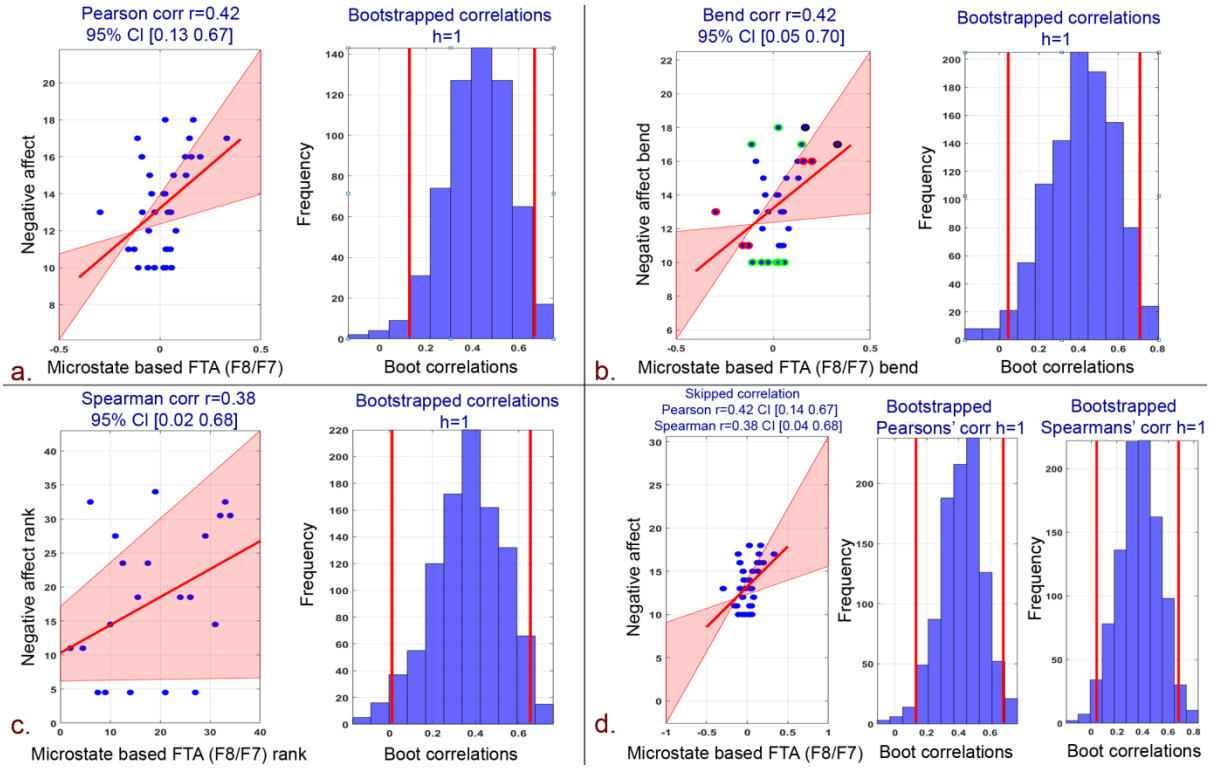


**Figure 4.5** Correlation plots between negative affect scores and microstate based FTA (F8/F7) and associated histograms of correlations for bootstrapped data. a. Pearson correlation b. 20% Bend correlation c. Spearman correlation d. Skipped (Pearson and Spearman) correlations (Kaur et al., 2020).

### *4.4.2 EEG INFORMED FMRI ANALYSIS*

The proposed microstate and standard hemispherical asymmetry measures were subjected to the EEG informed fMRI analysis to assess their neural underpinnings, respectively. The observed neural underpinnings were inferred with FDR corrected p-values less than 0.05, and a cluster size of more than 20 voxels were considered for analysis.

#### 4.4.2.1 Neural underpinnings of standard hemispheric asymmetry

The neural underpinnings of standard FA encompassed right as well as left-hemispheric regions (Figure 4.6a). Supplementary Table S4.1 (see Appendix 2) comprises of these areas, their peak coordinates, and cluster size. Specifically, in the right hemisphere, EEG frontal

asymmetry negatively correlated with BOLD activity in the occipital cortex with major clusters in the lateral occipital cortex and occipital pole. Additionally, BOLD activity in the temporal cortex also correlated negatively with standard FA. However, the BOLD of parietal cortex regions, particularly the postcentral gyrus, correlated positively with standard FA. Withal, in the left hemisphere, standard FA correlated positively with BOLD activity in the postcentral gyrus. However, activity in the occipital fusiform gyrus and temporal lobe regions correlated negatively with this alpha asymmetry measure. Majority of frontal lobe regions correlated negatively. However, superior frontal gyrus correlated positively (high t-value compared to the right hemisphere) with standard FA.

Figure 4.6b shows the neural underpinnings of standard FTA. Both right and left hemispheres revealed positive and negative correlations between BOLD activity and standard FTA (Supplementary Table S4.2; see Appendix 2). In the right hemisphere, BOLD activity in occipital lobe regions (cuneal cortex, lingual gyrus, and superior division of lateral occipital cortex) correlated negatively with standard FTA. Major clusters in the frontal lobe, specifically the frontal pole and activity in the precuneus cortex, also found a negative correlation with this frontal asymmetry index. In the left hemisphere, standard FTA correlated negatively with BOLD activity in the Inferior frontal gyrus. Few clusters in the parietal, occipital, and temporal pole also correlated negatively with standard FTA. The neural underpinnings of standard FA showed left-hemispheric dominance whilst FTA revealed right-hemispheric dominance.

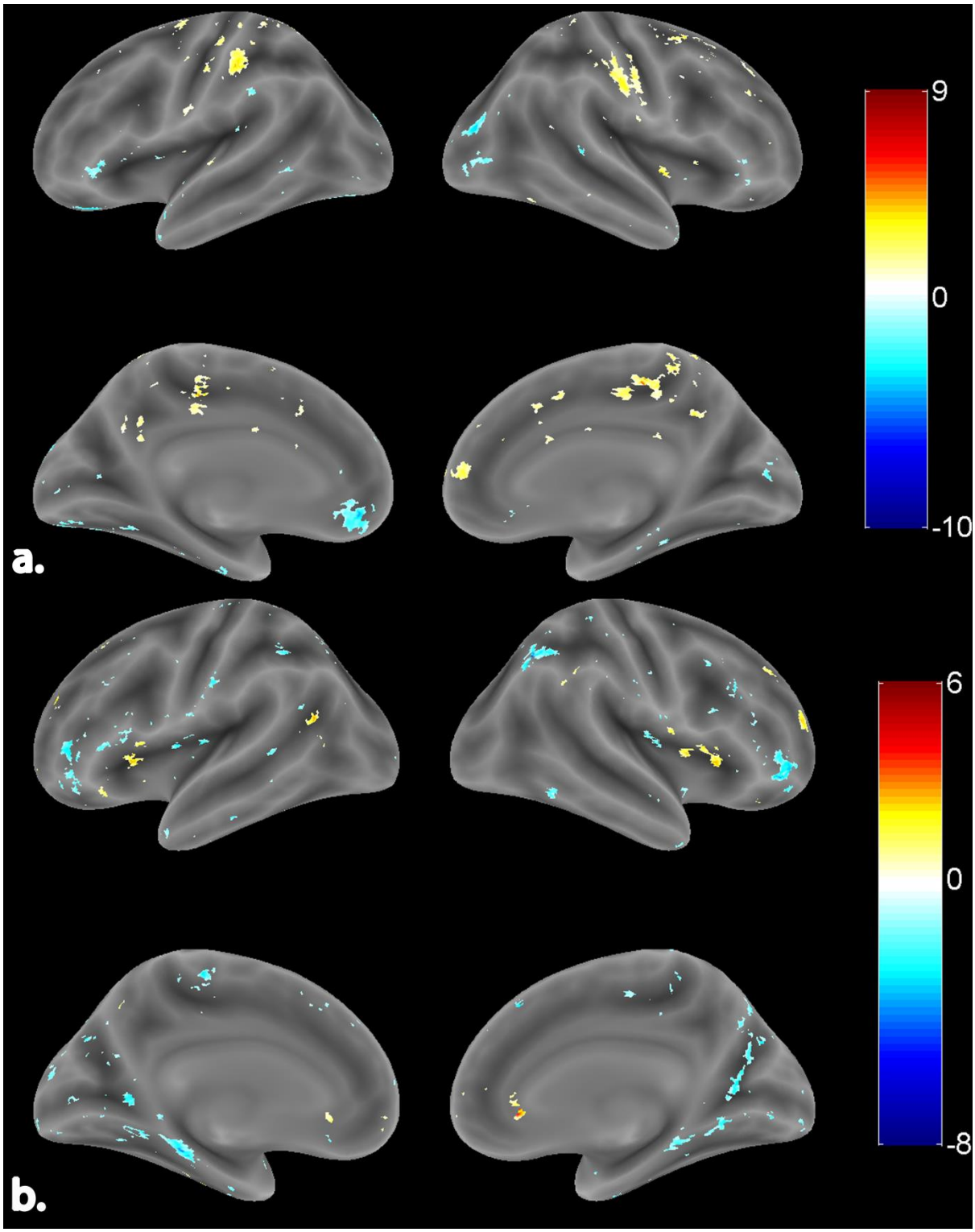


**Figure 4.6** Surface rendered view of neural underpinnings of standard a. FA (channel pair F4/F3) b. FTA (channel pair F8/F7). The color bar indicates the t-values with blue being the least and red being the highest. The activations are represented at FDR corrected $p<0.05$ (Kaur et al., 2020).

#### 4.4.2.2 Neural underpinnings of microstate based EEG asymmetry

Right and left-lateralized neural underpinnings of microstate based FA are shown in Figure 4.7a. A complete list of activation clusters is provided in Supplementary Table S4.3 (see Appendix 2). In the right hemisphere, microstate based FA correlated negatively with BOLD activity in the frontal medial cortex and frontal pole regions of the frontal lobe. Similarly, BOLD activity in the posterior division of the cingulate gyrus has also correlated negatively. However, few clusters in the frontal lobe, occipital lobe, and temporal pole revealed a positive correlation with microstate FA. In the left hemisphere, resting-state microstate based FA correlated positively with major clusters in all lobes, with the frontal lobe having the maximum cluster extent. This is evident as microstates are known to represent the global brain activity.

Figure 4.7b shows the neural underpinnings in both right and left hemispheres for resting-state microstate based FTA. Supplementary Table S4.4 (see Appendix 2) comprises of these areas, their peak coordinates, and cluster size. In the right hemisphere, activity in the frontal lobe and limbic lobe regions correlated negatively with this EEG alpha asymmetry. BOLD of specific regions of the parietal lobe (Angular gyrus) and temporal lobe (Planum temporale) correlated negatively with microstate based FTA. Pertaining to the left hemisphere, activations in the frontal lobe and limbic lobe (a posterior division of cingulate gyrus) correlated negatively with microstate based FTA. Negative correlation also emanated from BOLD activity in specific regions of the parietal lobe (Angular gyrus, Superior parietal lobule) and lateral occipital cortex of the occipital lobe. The neural underpinnings for microstate based FA and FTA showed left-hemispheric dominance.

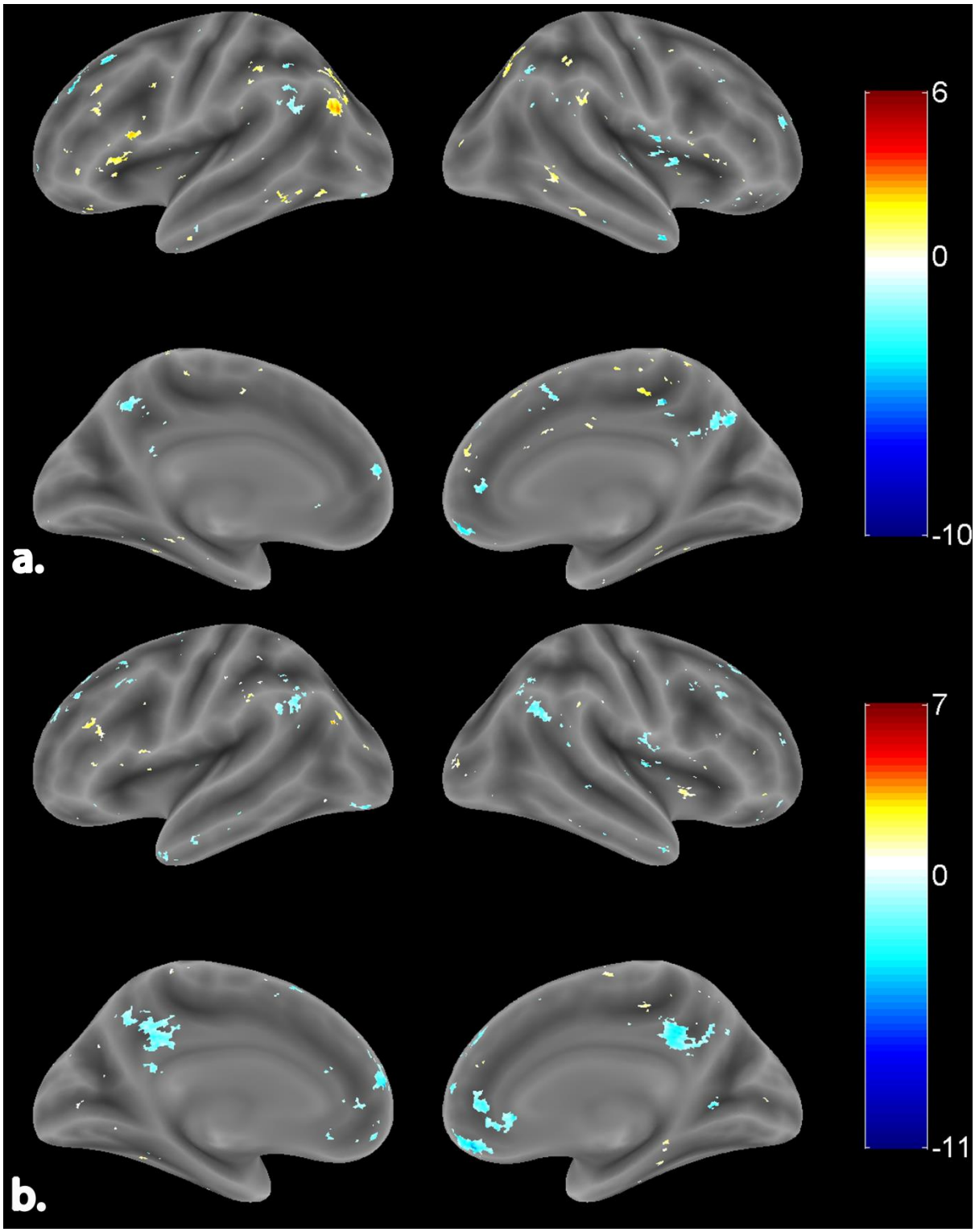


**Figure 4.7** Surface rendered view of neural underpinnings of proposed microstate based a. FA (channel pair F4/F3) b. FTA (channel pair F8/F7). The color bar indicates the t-values with blue being the least and red being the highest. The activations are represented at FDR corrected $p<0.05$ (Kaur et al., 2020).

### *4.4.3 ROBUST CORRELATION OF HLI WITH PANAS, BIS/BAS MEASURES*

The correlation and p-values for all the significant results obtained for this analysis are tabulated in Table 4.4. The robust correlation between negative affect measure and HLI of neural underpinnings of microstate frontal alpha asymmetry yielded a significantly strong negative correlation in the anterior division of the middle temporal gyrus. Further, superior frontal gyrus emerged as the positive correlate for correlation among positive affect scores and HLI pertaining to neural underpinnings of microstate alpha asymmetry. Moreover, the correlation of BIS measure with HLI pertaining to neural underpinnings of microstate frontal alpha asymmetry yielded a significantly strong positive correlation in the inferior frontal gyrus (pars triangularis) and frontal medial cortex. Further, the HLI of occipital fusiform gyrus correlated negatively with the BAS measure.

However, the robust correlation between negative affect and HLI of neural underpinnings of standard frontal alpha asymmetry yielded a low and insignificant correlation with all cortical regions. While the correlation of positive affect scores with HLI pertaining to standard alpha asymmetry revealed a significant positive correlation with the insular cortex. Further, the correlation of BAS and BIS measures with HLI revealed a low and insignificant correlation with all cortical regions pertaining to standard alpha asymmetry.

**Table 4.4** Robust correlation (Pearson, bend, spearman, and skipped) of HLI based on standard and proposed microstate based frontal hemispheric asymmetry measures with psychological scores (Kaur et al., 2020).

| Hemodynamic Lateralization Index (HLI) | Behavioral measure | Cortical regions | Pearson Correlation | | Bend correlation | | Spearman correlation | | Skipped correlation | | | |
|---|---|---|---|---|---|---|---|---|---|---|---|---|
| | | | | | | | | | Pearson | | Spearman | |
| | | | r | p | r | p | r | p | r | t | r | t |
| Standard neural underpinnings | Negative affect | No region survived | - | - | - | - | - | - | - | - | - | - |
| | BIS | No region survived | - | - | - | - | - | - | - | - | - | - |
| | | | | | | | | | | | | |
| | Positive affect | Insular cortex | 0.44 | 0.004 | 0.44 | 0.005 | 0.4 | 0.01 | 0.53 | 3.82 | 0.41 | 2.75 |
| | BAS | No region survived | - | - | - | - | - | - | - | - | - | - |
| | | | | | | | | | | | | |
| Microstates Neural underpinnings | Negative affect | Middle temporal gyrus, anterior division | -0.4 | 0.01 | -0.38 | 0.01 | -0.43 | 0.006 | -0.4 | -2.67 | -0.43 | -2.91 |
| | BIS | Inferior frontal gyrus | 0.69 | 0.005 | 0.63 | 0.01 | 0.69 | 0.005 | 0.69 | 3.36 | 0.69 | 3.39 |
| | | Frontal medial cortex | 0.71 | 0.004 | 0.76 | 0.001 | 0.75 | 0.001 | 0.71 | 3.53 | 0.75 | 4.04 |
| | | | | | | | | | | | | |
| | Positive affect | Superior frontal gyrus | 0.36 | 0.02 | 0.3 | 0.05 | 0.31 | 0.05 | 0.36 | 2.37 | 0.31 | 2.01 |
| | BAS | Occipital fusiform gyrus | -0.58 | 0.02 | -0.57 | 0.03 | -0.55 | 0.03 | -0.58 | -2.51 | -0.55 | -2.32 |

### *4.4.4 ROBUST CORRELATION AMONG FRONTAL HEMISPHERICAL ASYMMETRY MEASURES*

Figure 4.8 shows the Pearson robust correlation of proposed microstate frontal hemispheric asymmetry with standard frontal hemispheric asymmetry measures. Proposed microstate based FA and FTA yielded insignificant low correlation with standard FA and FTA.

Pearson correlation among standard and microstate based FA and FTA revealed correlation coefficients and p-values as Pearson r= -0.14, 0.013; pcorr=0.37, 0.93 respectively.

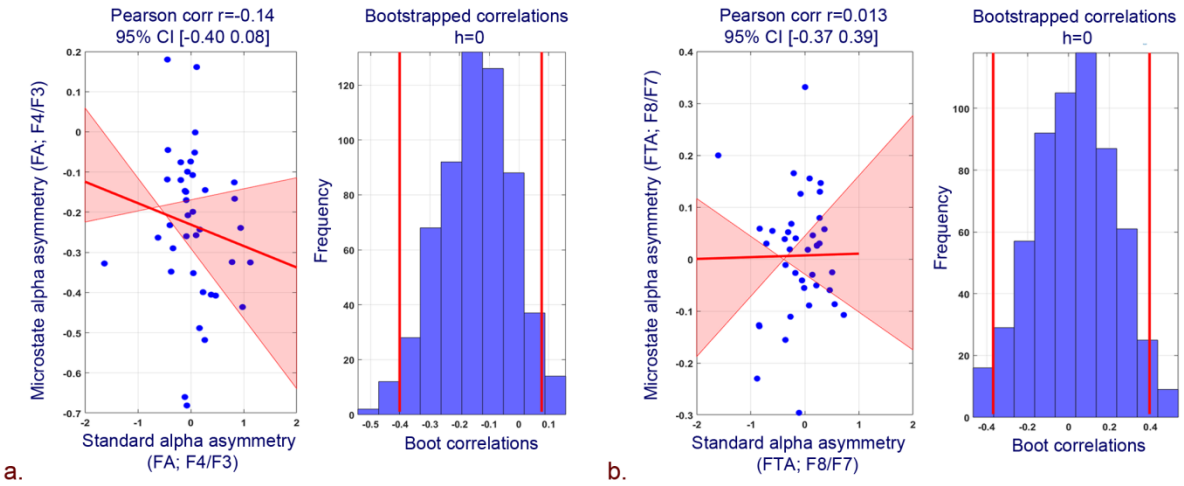


**Figure 4.8** Pearson correlation plots and associated histograms for bootstrapped data for correlation between a. Standard and microstate based FA (F4/F3) b. Standard and microstate based FTA (F8/F7) (Kaur et al., 2020).

## 4.5 DISCUSSION

Valence (Baijal & Srinivasan, 2011; J. Davidson, 1992; Richard J. Davidson et al., 1987; Wyczesany et al., 2018) and motivation hypothesis (Harmon-Jones et al., 2010) propose that higher values of positive affect/approach behavior and negative affect/withdrawal behavior are associated with the greater relative left and right cortical activation, respectively. These hypotheses are established in task-based EEG alpha asymmetry studies where the implications are based on alpha inhibition (desynchronization w.r.t BOLD) in event-specific regions (Fink et al., 2005; Wright et al., 2015). Thus, following this abstraction, the above-mentioned hypothesis holds when standard frontal hemispheric asymmetry ($\ln(\alpha^{Right}) - \ln(\alpha^{Left})$) correlates

positively with positive affect/ approach behavior and negatively with negative affect/withdrawal behavior. Howbeit, the validity of these hypotheses in resting-state recordings which involves sole perception and not induction of valence/behavior still remains vacillating. The inconsistent results of the relationship between the standard resting frontal asymmetry and affect and approach/withdrawal behavior are tabulated in Table 4.5. The line of studies by Tomarken and colleagues ( a J. Tomarken et al., 1992; A. J. Tomarken et al., 1992) and Jacobs & Snyder (1996) supported the above hypothesis. Similarly, for approach/withdrawal dichotomy, Harmon-Jones & Allen (1997), Shackman et al. (2009), and De Pascalis et al. (2013) supported the above-mentioned hypotheses. Nonetheless, Sutton & Davidson (1997) and Schneider et al. (2016) observed no association of affect, approach/withdrawal dichotomy with frontal asymmetry, respectively. Conversely, the study by Hagemann et al. (1999) proposed that subjects with high negative affect exhibited high left cortical activation. Further, Hewig et al. (2006) propounded a higher approach measure to be associated with the bilateral frontal cortical activity. Hence, in order to bring more clarity, the present study aims to assess the capability of quasi-stable microstates based frontal hemispheric asymmetry in explaining the affect and approach/withdrawal dichotomy as against standard frontal hemispheric asymmetry.

**Table 4.5** List of studies for positive/negative affect and approach/withdrawal dichotomy (Kaur et al., 2020).

| STUDY | ALPHA EEG ASYMMETRY (R-L) | MOOD MEASURES | SUBJECTS | MAIN RESULTS |
|---|---|---|---|---|
| A. J. Tomarken, Davidson, & Henriques (1990) | FA (F4/F3); | Acquisition of resting EEG followed by the presentation of affective clips to obtain subjective ratings for emotional reactions | 32 females, Cohort A: 17 to 41 years Cohort B: 20 to 54 years | Resting FA significantly predicted self-reported global NA |
| a J. Tomarken et al., (1992a) | FA (F4/F3); ATA (T4/T3) | Resting EEG on two occasions; 3 weeks apart; PANAS | 90 females, 17-21 years | FA: ↓NA ATA: ↑ PA |
| A. J. Tomarken et al. (1992b) | Same as in Tokarman et al. (1992a) | Same as in Tomarken et al. (1992a) | 85 females, 17-21 years | Same as in Tomarken et al. (1992a) |
| Jacobs & Snyder (1996) | FA (F4/F3); FTA (F8/F7) | Resting EEG on 1-time measurement; PANAS | 40 males, 18-53 years | FTA: ↓NA |
| Sutton & Davidson (1997) | FA (F4/F3) | Resting EEG on two occasions 6 weeks apart PANAS first session; BIS/BAS scales the second session | 46 (23 females) 18–22 years | No correlation between FA and PA, NA, BAS, BIS |

| | | | | |
|---|---|---|---|---|
| Hagemann et al. (1998) | FA (F4/F3); ATA (T4/T3) | Acquisition of resting EEG followed by the presentation of affective slides to obtain subjective ratings for emotional reactions | 37 (22 females: 15 males: Mean age 24.5) | Subjects with greater relative left-sided anterior temporal cortical activation reported more intense NA in response to negative stimuli |
| Hagemann et al.(1999) | FA (F4/F3); ATA (T4/T3) | Resting EEG; PANAS | 36 (24 females) Mean age 24.7 | Subjects with high NA exhibited high left cortical activation at the anterior temporal site |
| Hall & Petruzello (1999) | FA (F4/F3) | Resting EEG and measures of physical activity; PANAS | 41 (26 females) Mean age 68.7 | FA positively predicted PA |
| Harmon-Jones & Allen (1997) | FA (F4/F3); | Resting EEG from females who scored in the upper or lower third of the distribution of social anxiety scores; BAS,BIS | 37 female | FA: ↑ BAS |
| Hewig et al. (2006) | FA (F4/F3); FTA (F8/F7); ATA (T4/T3) | Resting EEG on four occasions; four weeks apart; BAS, BIS | 59 (30 females: Mean age 23; 29 males: Mean age 25) | Higher BAS associated with bilateral frontal cortical activity |

| | | | | |
|---|---|---|---|---|
| Shackman et al. (2009) | FA (F4/F3); FTA (F8/F7) | Resting EEG on two occasions; several weeks apart; BAS, BIS | 51 female Mean age 19.5 | A significant relationship between BIS and FA. Higher BIS associated with right posterior DLPFC |
| De Pascalis et al. (2013) | FA (F4/F3); FTA (F8/F7) | Resting EEG; BAS,BIS | 51 female Mean age 24.1 | FA: ↑ BAS, Higher BAS associated with left-sided activation in MFG |
| Schneider et al. (2016) | FA (F4/F3); | Two assessments of resting EEG; BAS, BIS | 99 (50 females; 49 males aged 10-12 years) | No correlation of BAS, BIS measures with FA |

EEG, Electroencephelography; ↑ Positive correlation; ↓ Negative correlation; FA, Frontal Asymmetry (F4/F3); FTA, Frontal Temporal Asymmetry (F8/F7); ATA, Anterior Temporal Asymmetry (T4/T3); BAS, Behavioral Activation System; BIS, Behavioral Inhibition System; PA, Positive Affect; NA, Negative Affect; DLPFC, Dorsolateral Prefrontal Cortex; MFG, Middle Frontal Gyrus

### *4.5.1 PRELUDE TO THE PRESENT RESEARCH STUDY*

This study primarily focuses on exploring the ability of EEG microstates based frontal hemispherical asymmetry measure against standard Davidson's approach in explaining mechanisms of the resting state affect and approach/ withdrawal behavior. The rationale for examining EEG microstates-derived frontal asymmetry was based on the specific observation that affect and approach/withdrawal measures associated significantly with stable EEG signatures. Microstate analysis estimates the global pattern of coherence across entire EEG

channels from temporal EEG data and thus assesses patterns of quasi-stable activities. The interaction within a large-scale brain network involves a rapid change in the dynamics of these quasi-stable activity patterns. Further, the neural mechanism associated with any cognitive process generally involves the coordinated activity of many neural assemblies located at different cortexes. Correspondingly, the neural mechanisms of resting-state affect and approach/ withdrawal behavior result from one such coordinated activity of the large scale brain networks.

Thus, in this study, a novel approach is explored, which assesses the hemispherical frontal asymmetry of quasi-stable activity patterns (microstates) from large scale brain interactions of the resting state affect and approach/ withdrawal behavior. These EEG microstates based frontal hemispherical asymmetry measures are further subjected to the EEG informed fMRI analysis to estimate their neural underpinnings. Subsequently, the lateralization index, which measures the hemispherical asymmetry of these large scale brain networks based on their hemodynamic information, is measured and correlated with affect and approach/ withdrawal psychological measures. Lastly, the insights brought by the proposed EEG microstates based approach is compared with the standard EEG asymmetry measures to understand the effectiveness of microstate derived asymmetry measures in explaining resting-state affect and approach/ withdrawal behavior. The insights of the present study are summarized in the following sections.

### *4.5.2 STANDARD ALPHA ASYMMETRY AND ITS HLI REVEAL NO CORRELATION WITH PANAS AND BIS/BAS MEASURES*

The current study is in line with the observation of Davidson and colleagues (Sutton & Davidson, 1997) and other earlier studies (Palmiero & Piccardi, 2017; C. W.E.M. Quaedflieg et

al., 2015; Schneider et al., 2016), where no correlation was observed for affect and BIS/BAS measures with standard hemispheric asymmetry. However, these previous studies never explored the neurovascular underpinnings and associated hemodynamic asymmetry of these underpinnings. In the present study, the absence of linkage of standard hemispheric asymmetry with affect and BIS/BAS measures is further strengthened by the lack of correlation of HLI of neural underpinnings of standard alpha asymmetry with PANAS, BIS, and BAS measures. This supports the understanding that neural mechanisms that are measured as standard EEG frontal alpha asymmetry may not be the marker to explain the affect and/or approach-withdrawal measures during resting state. It might possibly are influenced by the neural activity associated with other ongoing resting-state neural mechanisms, which limit its sensitivity towards the neural mechanisms associated with affect and approach-withdrawal measures during resting state. Thus, our finding strengthens the understanding that the standard EEG alpha asymmetry model, especially in the male population, is effectual in explaining affect or approach-withdrawal measures only when arousing situations such as those relying on mood induction procedures are present.

### *4.5.3 MICROSTATES BASED ASYMMETRY CORRELATES WITH AND DELINEATES THE NEURAL MECHANISMS OF NEGATIVE AFFECT*

In contradistinction to the standard hemispheric asymmetry, the proposed microstates based measure brings better insights into the global coordinated activity of large scale brain networks pertaining to negative affect. In this study, the robust correlational analysis revealed a positive correlation of negative affect with microstates based frontal hemispheric asymmetry. This implies that negative affect increases with an increase in right hemispheric alpha activity or a decrease in left-hemispheric alpha activity. Further, the most common neurovascular

hypotheses state that when engaged in the task, the brain region exhibits suppression in alpha power with an increase in the BOLD signal (Fink et al., 2005). This causes a negative correlation between alpha power and BOLD signal and is termed as alpha-BOLD desynchronization. Figure 4.9 depicts these underlying dynamics for the association between alpha asymmetry measures and the BOLD signal during alpha-BOLD synchronization/desynchronization. Following this, the positive correlation of negative affect with microstates based frontal hemispheric asymmetry implies left-hemispheric interaction with negative affect. These observations do not support the valence hypothesis explained in the earlier section but goes in line with the observations by Hagemann et al. (1999), wherein negative affect has been linked to the left-hemisphere. Our results were also in line with a mood induction study by Gale et al. (2001), where negative mood increased with an increase in left frontal activation. Further, recently Farahi et al. (2019) showed the associativity of fear positively with the left hemisphere.

Additionally, neural underpinnings of microstate derived asymmetry revealed the involvement of temporal lobe regions. In this study, HLI ($HRF\_Amp_n^R - HRF\_Amp_n^L$ ), which was estimated by utilizing the amplitude of the HRF of each neural underpinning of microstate based frontal asymmetry linked negatively to the HLI of the anterior division of middle temporal gyrus neural underpinning to negative affect. This implies that relatively left-lateralized HRF amplitude of temporal underpinning of microstate based frontal asymmetry is associated with negative affect. Studies in the past have connected left anterior temporal cortical activation as well as temporal lobe per se to the negative affect (Hennion et al., 2019; Ives-Deliperi & Jokeit, 2019; Meador et al., 2015; Ritchey et al., 2019); this proves the efficacy of microstate based frontal asymmetry in explaining the neurovascular mechanism of negative affect which remains absent in the previous literature. Batut et al. (2006) signaled the involvement of mesial temporal

regions in emotional processes; further, Yun et al. (2017) showed that the angst for social communication in social anxiety disorder could be resultant of the imbalanced functional connectivity of left middle temporal gyrus. The association of anterior division of middle temporal gyrus with negative affect is plausible as studies (Buchanan et al., 2006; Dolcos et al., 2005, 2011) have indicated the interaction between the middle temporal gyrus and amygdala for better prediction of memory for emotional events. Hence, the middle temporal gyrus may be more tightly functionally coupled with affect specific regions for the memory of negative events. The significant correlation of negative affect with temporal region's HLI, which is independently measured from resting fMRI data for neural underpinnings of microstate frontal asymmetry and its relative left lateralization, also strengthens the finding of positive correlation of negative affect with microstate based frontal asymmetry measures (FA and FTA).

| Dynamics of Alpha asymmetry index and BOLD signal for alpha-BOLD desynchronization | | |
|---|---|---|
| Alpha asymmetry index [Right (alpha)-Left (alpha)] | Dominant BOLD activity trend | Cerebral Lateralization |
| ↑ | ↑ **Left Hemisphere** | Positively correlating Left hemispheric activation |
| ↓ | ↑ **Right Hemisphere** | Negatively correlating Right hemispheric activation |
| **Dynamics of Alpha asymmetry index and BOLD signal for alpha-BOLD synchronization** | | |
| Alpha asymmetry index [Right (alpha)-Left (alpha)] | Dominant BOLD activity trend | Cerebral Lateralization |
| ↑ | ↑ **Right Hemisphere** | Positively correlating Right hemispheric activation |
| ↓ | ↑ **Left Hemisphere** | Negatively correlating Left hemispheric activation |

**Figure 4.9** Underlying dynamics associated with alpha asymmetry index and BOLD signal (Kaur et al., 2020).

### *4.5.4 MICROSTATE BASED ASYMMETRY REVEALS NO CORRELATION WITH BIS, POSITIVE AFFECT, AND BAS*

Microstate based asymmetry showed a high but insignificant correlation with BIS measure. It also showed no correlation with positive affect and BAS measure. One possible explanation for these findings is the fact that the positive affect scale is a diverse measure with components of joy, interest, and activation. Each of these components might involve distinct and sometimes even opposite whole-brain activations (Egloff et al., 2003). Similarly, BAS is also

composed of varied components (reward, drive, and fun) (Taubitz et al., 2015). These varied brain activation patterns might not be producing definite patterns at cortical levels to be picked by the alpha power.

### *4.5.5 HLI OF MICROSTATES NEURAL UNDERPINNINGS REVEALS SIGNIFICANT ASSOCIATION WITH BIS, POSITIVE AFFECT, AND BAS MEASURES*

The hemodynamic lateralization measure of neural underpinnings of the proposed technique revealed a high and positive correlation of BIS in frontal cortical regions. Frontal cortical regions play a very important role in inhibition systems, and it has been one of the cornerstones of neuroscience research (Andreas & Hewig, 2017; J. A. Coan & Allen, 2004; Harmon-Jones & Gable, 2018). Further, Fuentes et al. (2012) also emphasized the association of individual differences in the behavioral inhibition system with the orbitofrontal cortex. Hence, our results suggest that the HLI, which constitutes the voxel-level hemispheric differences in HRF amplitude of neural underpinnings of microstates based asymmetry, better manifests BIS measure. Further, though microstate based alpha asymmetry found no significant correlation with positive affect and BAS measure, the HLI of occipital fusiform gyrus was found to correlate with BAS measure strongly. This is consonant with the hypothesis where the BAS system is proposed to be modulated by occipital cortices (Barrós-Loscertales et al., 2010). The nature of correlation was strong but negative and thus was inverse of the BIS system. Moreover, positive affect was correlated positively with hemodynamic lateralization measures in superior frontal gyrus. The link of the prefrontal cortex with positive affect is consistent with recent studies. Wager et al. (2015) showed the association of the prefrontal cortex with positive affect as compared to negative affect. Similarly, Roy et al. (2012) observed more frequent activity was found in the prefrontal cortex during positive as compared with negative feelings. Hence,

hemodynamic lateralization measures of microstates neural underpinnings bring better insight into the positive affect and BAS as compared to the standard EEG based hemispherical asymmetry measures.

Interestingly, the neural underpinnings (middle temporal gyrus (anterior division), inferior frontal gyrus, frontal medial cortex) whose HLI revealed significant correlation (r-value) with negative affect and BIS scores have been observed to be undergoing only the alpha-BOLD desynchronization process. They were found to be either correlating positively in the left hemisphere or negatively in the right hemisphere. On the other hand, the neural underpinnings whose HLI correlated with positive affect and BAS scores have revealed both alpha-BOLD synchronization and desynchronization. Particularly, the superior frontal gyrus, which correlated with positive affect, underwent both alpha-BOLD synchronization and desynchronization. However, the occipital fusiform gyrus correlated negatively in the left hemisphere, which thus undergoes alpha-BOLD synchronization. Thus, the neural mechanisms involved in negative affect/withdrawal in the resting state exhibited only alpha-BOLD desynchronization. On the contrary, the positive affect and an approach relevant region involved both alpha-BOLD synchronization and desynchronization. However, the underlying innate cause of these mechanisms remains elusive and needs to be explored in the future. Thus, our finding implicates that microstates based frontal alpha asymmetry may provide newer insights into the association of alpha asymmetry with mood and personality measures in both healthy and clinical populations. The plausible explanation is that different cognitive states, including affect and approach/withdrawal behavior, generally involve coordinated activity of many neural assemblies located at the different cortex, and the microstate prototypes could represent these cognitive states.

### *4.5.6 ABSENCE OF CORRELATION AMONG PROPOSED MICROSTATE AND STANDARD FRONTAL HEMISPHERIC ASYMMETRY MEASURES*

The proposed microstate based FA and FTA yielded an insignificant low correlation with standard FA and FTA. The proposed microstate based FA and FTA measure the quasi-stable coordinated brain activity and, in the present study, brings better insights into the large scale brain networks of negative affect. Previous works of literature ( a J. Tomarken et al., 1992; Wheeler et al., 1993) have also emphasized the prominence of stability in the standard EEG patterns in bringing forth the linkage among standard frontal alpha asymmetry and affect and approach/withdrawal measures. Hence, the lack of correlation among proposed microstate and standard frontal hemispheric asymmetry measures might be caused by the unstable nature of standard EEG and its frontal alpha asymmetry indices, which is caused by a substantial interference from many other cognitive factors. As this interference is different at different time points across volunteers, the standard EEG and its frontal alpha asymmetry are likely to correlate less with the quasi-stable patterns assessed by the proposed microstate frontal alpha asymmetry indices.

### *4.5.7 LIMITATION OF STUDY*

The present study utilizes 39 volunteers' data to validate the role of microstate based resting frontal alpha asymmetry in understanding the neural mechanisms of affect and approach/withdrawal behavior. However, affect and approach/withdrawal behavior is known to be elicited by mood induction tasks. Hence, it is necessary to carry out future studies to validate the proposed microstate based frontal alpha asymmetry during such task engagements. Further, the current research involves healthy volunteers from the Indian urban population. Many studies

(Consedine et al., 2002; Deer et al., 2018; Thayer & Koenig, 2019) in the past have revealed the association of affect and approach/withdrawal behavior with the cultural, ethnic, and social background of the individuals. Thus, it is required to examine the proposed microstate based frontal alpha asymmetry approach in a larger population dataset, which includes individuals from various cultural, ethnic, and social backgrounds.

Also, the topographies of average-referenced, pre-processed standard EEG are known to represent the posterior alpha than frontal alpha, and these topographies have also been studied in comparison with other referencing schemes (Barzegaran et al., 2017; Tenke et al., 2015). However, the microstate analysis employed in the current study uses an average referencing scheme for frontal alpha asymmetry estimation. The present study follows average referencing for microstate analysis as various studies (Al Zoubi et al., 2019; Michel & Koenig, 2018) adequately understand the cognitive phenomena through average-referenced microstate estimations. Further, the effect of different EEG referencing schemes on microstate estimations is still not clearly understood. Extensive, systematic work needs to be undertaken to properly understand the role of varying EEG reference montages based microstate analysis in explaining frontal, posterior, and temporal EEG frequency signatures and topographies.

## 4.6 CONCLUSION

The above study validates the effectiveness of resting quasi-stable microstate based asymmetry in explaining the neural mechanisms of affect and approach/withdrawal behavior for healthy young male volunteers during 1-time measurement. The novelty of our work emanates from the fact that we estimated the frontal asymmetry of the alpha power from the average GFP amplitude of the quasi-stable microstates topographies, which might reflect the degree of

coordination of the neurons underlying alpha-neural underpinnings. Microstate frontal alpha asymmetry correlated positively with negative affect scores, which are defended by the negative correlation of HLI based on microstates' temporal neural underpinning with negative affect. Further, a significant association of HLI based on microstate neural underpinnings with positive affect, BAS and BIS measures concludes that the neural mechanisms of affect and approach/withdrawal dichotomy are better explained by the synchronized global firing of neurons and on-going activity of entire brain networks as assessed by quasi-stable microstates frontal alpha asymmetry. This study also stands unique in exploring the underlying neurovascular synchronization/desynchronization mechanisms of microstate based frontal asymmetry measures. The analysis revealed that neural underpinnings involved both positively and negatively correlating brain regions, thus satisfying alpha-BOLD desynchronization and synchronization criteria. However, specifically the microstates neural underpinnings whose HLI correlated with negative affect and inhibition involved alpha-BOLD desynchronization, however the positive affect and approach relevant regions involved alpha-BOLD synchronization as well as desynchronization.

Thus, the microstates-based frontal asymmetry model better explains the neural mechanisms underlying the affect and approach/withdrawal measures. Further, subcortical regions and their interactions with the cortical areas also may play an essential role in understanding the mechanisms of affect and approach/withdrawal measures. However, since the detection of deep-rooted subcortical regions through conventional EEG is still dubious, we carried a subsequent study, covered in the next chapter where the subcortical structures, subcortical-cortical interactions, and the architecture of the hemispheric asymmetry of their

functional connectivity dominating affect and approach/withdrawal mechanisms was studied using resting-fMRI functional connectivity estimates.

## REFERENCES


Aben, H. P., Reijmer, Y. D., Visser-Meily, J. M. A., Spikman, J. M., Biessels, G. J., de Kort, P. L. M., & Study Group, P. (2017). Impaired Emotion Recognition after Left Hemispheric Stroke: A Case Report and Brief Review of the Literature. *Case Reports in Neurological Medicine*, *2017*, 1–6. https://doi.org/10.1155/2017/1045039

Abreu, R., Leal, A., & Figueiredo, P. (2018). *EEG-Informed fMRI : A Review of Data Analysis Methods*. *12*(February), 1–23. https://doi.org/10.3389/fnhum.2018.00029

Adolph, D., & Margraf, J. (2017). The differential relationship between trait anxiety, depression, and resting frontal α-asymmetry. *Journal of Neural Transmission*, *124*(3), 379–386. https://doi.org/10.1007/s00702-016-1664-9

Al Zoubi, O., Mayeli, A., Tsuchiyagaito, A., Misaki, M., Zotev, V., Refai, H., Paulus, M., & Bodurka, J. (2019). EEG Microstates Temporal Dynamics Differentiate Individuals with Mood and Anxiety Disorders From Healthy Subjects. *Frontiers in Human Neuroscience*, *13*(February), 1–10. https://doi.org/10.3389/fnhum.2019.00056

Allen, J. J. B., Keune, P. M., Sch, M., & Nusslock, R. (2018). *Frontal EEG alpha asymmetry and emotion : From neural underpinnings and methodological considerations to psychopathology and social cognition*. *October 2017*, 1–6. https://doi.org/10.1111/psyp.13028

Allen, P. J., Josephs, O., & Turner, R. (2000). A method for removing imaging artifact from continuous EEG recorded during functional MRI. In *NeuroImage* (Vol. 12, Issue 2, pp. 230–239). https://doi.org/10.1006/nimg.2000.0599

Allen, P. J., Polizzi, G., Krakow, K., Fish, D. R., & Lemieux, L. (1998). Identification of EEG events in the MR scanner: The problem of pulse artifact and a method for its subtraction. *NeuroImage*, *8*(3), 229–239. https://doi.org/10.1006/nimg.1998.0361

Andreas, M., & Hewig, J. (2017). *Mind the movement : Frontal asymmetry stands for behavioral motivation , bilateral frontal activation for behavior*. *May*, 1–19. https://doi.org/10.1111/psyp.12908

Arakaki, X., Shoga, M., Li, L., Zouridakis, G., Tran, T., Fonteh, A. N., Dawlaty, J., Goldweber, R., Pogoda, J. M., & Harrington, M. G. (2018). Alpha desynchronization/synchronization during working memory testing is compromised in acute mild traumatic brain injury (mTBI). *PLoS ONE*, *13*(2), 1–19. https://doi.org/10.1371/journal.pone.0188101

Baijal, S., & Srinivasan, N. (2011). Emotional and hemispheric asymmetries in shifts of attention: An ERP study. *Cognition and Emotion*, *25*(2), 280–294. https://doi.org/10.1080/02699931.2010.492719

Balconi, M., Vanutelli, M. E., & Grippa, E. (2017). Resting state and personality component (BIS/BAS) predict the brain activity (EEG and fNIRS measure) in response to emotional cues. *Brain and Behavior*, *7*(5), 1–15. https://doi.org/10.1002/brb3.686

Barrós-Loscertales, A., Ventura-Campos, N., Sanjuán-Tomás, A., Belloch, V., Parcet, M. A., & Ávila, C. (2010). Behavioral activation system modulation on brain activation during appetitive and aversive stimulus processing. *Social Cognitive and Affective Neuroscience*, *5*(1), 18–28. https://doi.org/10.1093/scan/nsq012

Barzegaran, E., Vildavski, V. Y., & Knyazeva, M. G. (2017). Fine Structure of Posterior Alpha Rhythm in Human EEG: Frequency Components, Their Cortical Sources, and Temporal Behavior. *Scientific Reports*, *7*(1), 1–12. https://doi.org/10.1038/s41598-017-08421-z

Batut, A. C., Gounot, D., Namer, I. J., Hirsch, E., Kehrli, P., & Metz-Lutz, M. N. (2006). Neural responses associated with positive and negative emotion processing in patients with left versus right temporal lobe epilepsy. *Epilepsy and Behavior*, *9*(3), 415–423. https://doi.org/10.1016/j.yebeh.2006.07.013

Benedek, M., Bergner, S., Könen, T., Fink, A., & Neubauer, A. C. (2011). EEG alpha synchronization is related to top-down processing in convergent and divergent thinking. *Neuropsychologia*, *49*(12), 3505–3511. https://doi.org/10.1016/j.neuropsychologia.2011.09.004

Bradshaw, A. R., Bishop, D. V. M., & Woodhead, Z. V. J. (2017). Methodological considerations in assessment of language lateralisation with fMRI: a systematic review. *PeerJ*, *5*, e3557. https://doi.org/10.7717/peerj.3557

Branco, D. M., Suarez, R. O., Whalen, S., O'Shea, J. P., Nelson, A. P., da Costa, J. C., & Golby, A. J. (2006). Functional MRI of memory in the hippocampus: Laterality indices may be more meaningful if calculated from whole voxel distributions. *NeuroImage*, *32*(2), 592–602. https://doi.org/10.1016/j.neuroimage.2006.04.201

Brodbeck, V., Kuhn, A., von Wegner, F., Morzelewski, A., Tagliazucchi, E., Borisov, S., Michel, C. M., & Laufs, H. (2012). EEG microstates of wakefulness and NREM sleep. *NeuroImage*, *62*(3), 2129–2139. https://doi.org/10.1016/j.neuroimage.2012.05.060

Brzezicka, A., Kamiński, J., Kamińska, O. K., Wołyńczyk-Gmaj, D., & Sedek, G. (2017). Frontal EEG alpha band asymmetry as a predictor of reasoning deficiency in depressed people. *Cognition and Emotion*, *31*(5), 868–878. https://doi.org/10.1080/02699931.2016.1170669

Buchanan, T. W., Tranel, D., & Adolphs, R. (2006). Memories for emotional autobiographical events following unilateral damage to medial temporal lobe. *Brain*, *129*(1), 115–127. https://doi.org/10.1093/brain/awh672

Calhoun, V. D., Stevens, M. C., Pearlson, G. D., & Kiehl, K. A. (2004). fMRI analysis with the general linear model: Removal of latency-induced amplitude bias by incorporation of hemodynamic derivative terms. *NeuroImage*, *22*(1), 252–257. https://doi.org/10.1016/j.neuroimage.2003.12.029

Carver, C. S., & Harmon-Jones, E. (2009). Anger Is an Approach-Related Affect: Evidence and Implications. *Psychological Bulletin*, *135*(2), 183–204. https://doi.org/10.1037/a0013965

Christov, I. I. (2004). Real time electrocardiogram QRS detection using combined adaptive threshold. *BioMedical Engineering Online*, *3*, 1–9. https://doi.org/10.1186/1475-925X-3-28

Coan, J. (2003). *Coan JA , Allen JJB . Frontal EEG asymmetry and behavioral activation and inhibition systems . Frontal EEG asymmetry and the behavioral activation and inhibition systems*. *40*(FEBRUARY), 106–114. https://doi.org/10.1111/1469-8986.00011

Coan, J. A., & Allen, J. J. B. (2004). Frontal EEG asymmetry as a moderator and mediator of emotion. *Biological Psychology*, *67*(1–2), 7–49. https://doi.org/10.1016/j.biopsycho.2004.03.002

Consedine, N. S., Magai, C., Cohen, C. I., & Gillespie, M. (2002). Ethnic variation in the impact of negative affect and emotion inhibition on the health of older adults. *Journals of Gerontology - Series B Psychological Sciences and Social Sciences*, *57*(5), P396–P408. https://doi.org/10.1093/geronb/57.5.P396

Cooper, A., Gomez, R., & Aucote, H. (2007). The Behavioural Inhibition System and Behavioural Approach System (BIS/BAS) Scales: Measurement and structural invariance across adults and adolescents. *Personality and Individual Differences*, *43*(2), 295–305. https://doi.org/10.1016/j.paid.2006.11.023

Davidson, J. (1992). *Anterior cerebral asymmetry and the nature of emotion*. *151*, 125–151.

Davidson, R. J., Kalin, N. H., & Shelton, S. E. (1993). Lateralized response to diazepam predicts temperamental style in rhesus monkeys. *Behavioral Neuroscience*, *107*(6), 1106–1110. https://doi.org/10.1037/0735-7044.107.6.1106

Davidson, R J, Saron, C. D., Senulis, J. A., Ekman, P., & Friesen, W. V. (1990). Approach/withdrawal and cerebral asymmetry: Emotional\rexpression and brain physiology: I. *Journal of Personality and Social Psychology*, *58*(2), 330–341. https://doi.org/10.1037/0022-3514.58.2.330

Davidson, Richard J. (2004). What does the prefrontal cortex "do" in affect: Perspectives on frontal EEG asymmetry research. *Biological Psychology*, *67*(1–2), 219–234. https://doi.org/10.1016/j.biopsycho.2004.03.008

Davidson, Richard J., Mednick, D., Moss, E., Saron, C., & Schaffer, C. E. (1987). Ratings of emotion in faces are influenced by the visual field to which stimuli are presented. *Brain and Cognition*, *6*(4), 403–411. https://doi.org/10.1016/0278-2626(87)90136-9

De Pascalis, V., Cozzuto, G., Caprara, G. V., & Alessandri, G. (2013). Relations among EEG-alpha asymmetry, BIS/BAS, and dispositional optimism. *Biological Psychology*, *94*(1), 198–209. https://doi.org/10.1016/j.biopsycho.2013.05.016

Deer, L. K., Shields, G. S., Ivory, S. L., Hostinar, C. E., & Telzer, E. H. (2018). Racial/ethnic disparities in cortisol diurnal patterns and affect in adolescence. *Development and Psychopathology*, *30*(5), 1977–1993. https://doi.org/10.1017/S0954579418001098

Dolcos, F., Iordan, A. D., & Dolcos, S. (2011). *Neural correlates of emotion Á cognition interactions : A review of evidence from brain imaging investigations*. *23*(6), 669–694.

Dolcos, F., Labar, K. S., & Cabeza, R. (2005). Remembering one year later: Role of the amygdala and the medial temporal lobe memory system in retrieving emotional memories. *Proceedings of the National Academy of Sciences of the United States of America*, *102*(7), 2626–2631. https://doi.org/10.1073/pnas.0409848102

Eftekhari, E., Tran, A., & McGregor, I. (2017). Decentering increases approach motivation among distressed individuals. *Personality and Individual Differences*, *119*, 236–241. https://doi.org/10.1016/j.paid.2017.07.035

Egloff, B., Schmukle, S. C., Burns, L. R., Kohlmann, C. W., & Hock, M. (2003). Facets of Dynamic Positive Affect: Differentiating Joy, Interest, and Activation in the Positive and Negative Affect

Schedule (PANAS). *Journal of Personality and Social Psychology*, *85*(3), 528–540. https://doi.org/10.1037/0022-3514.85.3.528

Farahi, S. M. M., Ebrahimabad, M. J. A., Gorji, A., Bigdeli, I., & Farahi, S. M. M. M. (2019). Neuroticism and frontal EEG asymmetry correlated with dynamic facial emotional processing in adolescents. *Frontiers in Psychology*, *10*(FEB), 1–9. https://doi.org/10.3389/fpsyg.2019.00175

Fedorowicz, G. (2012). *The Effects of Mindfulness Meditation on Mental Health*. https://sophia.stkate.edu/cgi/viewcontent.cgi?referer=https://scholar.google.co.nz/&httpsredir=1&article=1124&context=msw_papers

Fink, A., Grabner, R. H., Neuper, C., & Neubauer, A. C. (2005). EEG alpha band dissociation with increasing task demands. *Cognitive Brain Research*, *24*(2), 252–259. https://doi.org/10.1016/j.cogbrainres.2005.02.002

Flasbeck, V., Popkirov, S., & Brüne, M. (2017). Frontal EEG asymmetry in borderline personality disorder is associated with alexithymia. *Borderline Personality Disorder and Emotion Dysregulation*, *4*(1), 4–9. https://doi.org/10.1186/s40479-017-0071-7

Frenkel, T. I., Koss, K. J., Donzella, B., Frenn, K. A., Lamm, C., Fox, N. A., & Gunnar, M. R. (2017). ADHD Symptoms in Post-Institutionalized Children Are Partially Mediated by Altered Frontal EEG Asymmetry. *Journal of Abnormal Child Psychology*, *45*(5), 857–869. https://doi.org/10.1007/s10802-016-0208-y

Fritsch, V., Da Mota, B., Loth, E., Varoquaux, G., Banaschewski, T., Barker, G. J., Bokde, A. L. W., Brühl, R., Butzek, B., Conrod, P., Flor, H., Garavan, H., Lemaitre, H., Mann, K., Nees, F., Paus, T., Schad, D. J., Schümann, G., Frouin, V., … Thirion, B. (2015). Robust regression for large-scale neuroimaging studies. *NeuroImage*, *111*, 431–441. https://doi.org/10.1016/j.neuroimage.2015.02.048

Fuentes, P., Barrós-Loscertales, A., Bustamante, J. C., Rosell, P., Costumero, V., & Avila, C. (2012). Individual differences in the Behavioral Inhibition System are associated with orbitofrontal cortex and precuneus gray matter volume. *Cognitive, Affective and Behavioral Neuroscience*, *12*(3), 491–498. https://doi.org/10.3758/s13415-012-0099-5

Gabard-Durnam, L. J., Leal, A. S. M., Wilkinson, C. L., & Levin, A. R. (2018). The harvard automated processing pipeline for electroencephalography (HAPPE): Standardized processing software for developmental and high-artifact data. *Frontiers in Neuroscience*, *12*(February), 1–24. https://doi.org/10.3389/fnins.2018.00097

Gale, A., Edwards, J., Morris, P., Moore, R., & Forrester, D. (2001). Extraversion-introversion, neuroticism-stability, and EEG indicators of positive and negative empathic mood. *Personality and Individual Differences*, *30*(3), 449–461. https://doi.org/10.1016/S0191-8869(00)00036-2

Gawlowska, M., Domagalik, A., Beldzik, E., Marek, T., & Mojsa-Kaja, J. (2018). Dynamics of error-related activity in deterministic learning - an EEG and fMRI study. *Scientific Reports*, *8*(1), 2–11. https://doi.org/10.1038/s41598-018-32995-x

Gollan, J. K., Hoxha, D., Chihade, D., Pflieger, M. E., Rosebrock, L., & Cacioppo, J. (2014). Frontal alpha EEG asymmetry before and after behavioral activation treatment for depression. *Biological Psychology*, *99*(1), 198–208. https://doi.org/10.1016/j.biopsycho.2014.03.003

Greimel, E., Grünewald, B. D., Trinkl, M., Schulte-Körne, G., Bartling, J., & Großheinrich, N. (2018).

Resting frontal EEG asymmetry patterns in adolescents with and without major depression. *Biological Psychology*, *132*, 212–216. https://doi.org/10.1016/j.biopsycho.2018.01.003

Hagemann, D., Naumann, E., Becker, G., Maier, S., & Bartussek, D. (1998). Frontal brain asymmetry and affective style: A conceptual replication. *Psychophysiology*, *35*(4), 372–388. https://doi.org/10.1017/S0048577298970755

Hagemann, D., Naumann, E., Lürken, A., Becker, G., Maier, S., & Bartussek, D. (1999). EEG asymmetry, dispositional mood and personality. *Personality and Individual Differences*, *27*(3), 541–568. https://doi.org/10.1016/S0191-8869(98)00263-3

Hall, E. E., & Petruzello, S. J. (1999). Frontal Asymmetry, Dispositional Affect and Physical Activity in Older Adults. *Journal of Aging and Physical Activity*, *7*, 76–90.

Harmon-Jones, E., & Allen, J. J. B. (1997). Behavioral activation sensitivity and resting frontal EEG asymmetry: Covariation of putative indicators related to risk for mood disorders. *Journal of Abnormal Psychology*, *106*(1), 159–163. https://doi.org/10.1037/0021-843X.106.1.159

Harmon-Jones, E., & Gable, P. A. (2018). On the role of asymmetric frontal cortical activity in approach and withdrawal motivation: An updated review of the evidence. *Psychophysiology*, *55*(1). https://doi.org/10.1111/psyp.12879

Harmon-Jones, E., Gable, P. A., & Peterson, C. K. (2010). The role of asymmetric frontal cortical activity in emotion-related phenomena: A review and update. *Biological Psychology*, *84*(3), 451–462. https://doi.org/10.1016/j.biopsycho.2009.08.010

Hennion, S., Szurhaj, W., Skrobala, E., Davière, J., Tyvaert, L., Derambure, P., & Delbeuck, X. (2019). Experiences of self-conscious emotions in temporal lobe epilepsy. *Epilepsy and Behavior*, *90*, 1–6. https://doi.org/10.1016/j.yebeh.2018.10.028

Hewig, J. (2018). Intentionality in frontal asymmetry research. *Psychophysiology*, *55*(1), 1–18. https://doi.org/10.1111/psyp.12852

Hewig, J., Hagemann, D., Seifert, J., Naumann, E., & Bartussek, D. (2006). The relation of cortical activity and BIS/BAS on the trait level. *Biological Psychology*, *71*(1), 42–53. https://doi.org/10.1016/j.biopsycho.2005.01.006

Ives-Deliperi, V. L., & Jokeit, H. (2019). Impaired Social Cognition in Epilepsy: A Review of What We Have Learnt From Neuroimaging Studies. *Frontiers in Neurology*, *10*(September). https://doi.org/10.3389/fneur.2019.00940

Jacob, T. J. C., Bointon, E. S., Dong, S., Warden-Smith, J., Cole, R. H., Paul, L., John, S. R., & Olukogbon, K. (2017). Light and smell stimulus protocol reduced negative frontal EEG asymmetry and improved mood. *Open Life Sciences*, *12*(1), 51–61. https://doi.org/10.1515/biol-2017-0006

Jacobs, G. D., & Snyder, D. (1996). Frontal brain asymmetry predicts affective style in men. *Behavioral Neuroscience*, *110*(1), 3–6. https://doi.org/10.1037/0735-7044.110.1.3

Jansen, A., Menke, R., Sommer, J., Förster, A. F., Bruchmann, S., Hempleman, J., Weber, B., & Knecht, S. (2006). The assessment of hemispheric lateralization in functional MRI-Robustness and reproducibility. *NeuroImage*, *33*(1), 204–217. https://doi.org/10.1016/j.neuroimage.2006.06.019

John, R., & Julie, D. (2004). The Positive and Negative Affect Schedule (PANAS): Construct validity , measurement properties and normative data in a large non-clinical sample. *British Journal of*

*Clinical Psychology*, *43*, 245–265.

Jones, S. E., Mahmoud, S. Y., & Phillips, M. D. (2011). A practical clinical method to quantify language lateralization in fMRI using whole-brain analysis. *NeuroImage*, *54*(4), 2937–2949. https://doi.org/10.1016/j.neuroimage.2010.10.052

Kaur, A., Chinnadurai, V., & Chaujar, R. (2020). Microstates-based resting frontal alpha asymmetry approach for understanding affect and approach/withdrawal behavior. *Scientific Reports*, *10*(1), 1–25. https://doi.org/10.1038/s41598-020-61119-7

Kayser, J., & Tenke, C. E. (2006a). Principal components analysis of Laplacian waveforms as a generic method for identifying ERP generator patterns: I. Evaluation with auditory oddball tasks. *Clinical Neurophysiology*, *117*(2), 348–368. https://doi.org/10.1016/j.clinph.2005.08.034

Kayser, J., & Tenke, C. E. (2006b). Principal components analysis of Laplacian waveforms as a generic method for identifying ERP generator patterns: II. Adequacy of low-density estimates. *Clinical Neurophysiology*, *117*(2), 369–380. https://doi.org/10.1016/j.clinph.2005.08.033

Kelley, N. J., & Schmeichel, B. J. (2014). The effects of negative emotions on sensory perception: fear but not anger decreases tactile sensitivity. *Frontiers in Psychology*, *5*(August), 1–8. https://doi.org/10.3389/fpsyg.2014.00942

Khanna, A. (2016). *Microstates in Resting-State EEG: Current Status and Future Directions*. 105–113. https://doi.org/10.1016/j.neubiorev.2014.12.010.Microstates

Killgore, W. D. S., & Yurgelun-Todd, D. A. (2007). The right-hemisphere and valence hypotheses: Could they both be right (and sometimes left)? *Social Cognitive and Affective Neuroscience*, *2*(3), 240–250. https://doi.org/10.1093/scan/nsm020

Kim, K. H., Yoon, H. W., & Park, H. W. (2004). Improved ballistocardiac artifact removal from the electroencephalogram recorded in fMRI. *Journal of Neuroscience Methods*, *135*(1–2), 193–203. https://doi.org/10.1016/j.jneumeth.2003.12.016

Klimesch, W., Doppelmayr, M., Schwaiger, J., Auinger, P., & Winkler, T. (1999). "Paradoxical" alpha synchronization in a memory task. *Cognitive Brain Research*, *7*(4), 493–501. https://doi.org/10.1016/S0926-6410(98)00056-1

Kok, P., Van Lieshout, L. L. F., & De Lange, F. P. (2016). Local expectation violations result in global activity gain in primary visual cortex. *Scientific Reports*, *6*(August), 1–10. https://doi.org/10.1038/srep37706

Kretowski, M. (2019). *Decision Trees in Data Mining*. https://doi.org/10.1007/978-3-030-21851-5_2

Lachman, M. E., van Reekum, C. M., Hostinar, C. E., Seeman, T. E., Miller, G. E., Davidson, R. J., Graham, E. K., & Mroczek, D. K. (2016). Frontal brain asymmetry, childhood maltreatment, and low-grade inflammation at midlife. *Psychoneuroendocrinology*, *75*, 152–163. https://doi.org/10.1016/j.psyneuen.2016.10.026

Laufs, H., Kleinschmidt, A., Beyerle, A., Eger, E., Salek-Haddadi, A., Preibisch, C., & Krakow, K. (2003). EEG-correlated fMRI of human alpha activity. *NeuroImage*, *19*(4), 1463–1476. https://doi.org/10.1016/S1053-8119(03)00286-6

Lehmann, D., Strik, W. K., Henggeler, B., Koenig, T., & Koukkou, M. (1998). Brain electric microstates and momentary conscious mind states as building blocks of spontaneous thinking: I. Visual imagery

and abstract thoughts. *International Journal of Psychophysiology*, *29*(1), 1–11. https://doi.org/10.1016/S0167-8760(97)00098-6

Lenartowicz, A., Lu, S., Rodriguez, C., Lau, E. P., Walshaw, P. D., McCracken, J. T., Cohen, M. S., & Loo, S. K. (2016). Alpha desynchronization and fronto-parietal connectivity during spatial working memory encoding deficits in ADHD: A simultaneous EEG-fMRI study. *NeuroImage: Clinical*, *11*, 210–223. https://doi.org/10.1016/j.nicl.2016.01.023

Lindquist, K. A., Satpute, A. B., Wager, T. D., Weber, J., & Barrett, L. F. (2016). The Brain Basis of Positive and Negative Affect: Evidence from a Meta-Analysis of the Human Neuroimaging Literature. *Cerebral Cortex*, *26*(5), 1910–1922. https://doi.org/10.1093/cercor/bhv001

Lindquist, M. A., & Wager, T. D. (2007). Validity and power in hemodynamic response modeling: A comparison study and a new approach. *Human Brain Mapping*, *28*(8), 764–784. https://doi.org/10.1002/hbm.20310

Meador, K. J., Kapur, R., Loring, D. W., Kanner, A. M., & Morrell, M. J. (2015). Quality of life and mood in patients with medically intractable epilepsy treated with targeted responsive neurostimulation. *Epilepsy and Behavior*, *45*, 242–247. https://doi.org/10.1016/j.yebeh.2015.01.012

Michel, C. M., & Koenig, T. (2018). EEG microstates as a tool for studying the temporal dynamics of whole-brain neuronal networks: A review. *NeuroImage*, *180*, 577–593. https://doi.org/10.1016/j.neuroimage.2017.11.062

Milz, P., Pascual-Marqui, R. D., Achermann, P., Kochi, K., & Faber, P. L. (2017). The EEG microstate topography is predominantly determined by intracortical sources in the alpha band. *NeuroImage*, *162*, 353–361. https://doi.org/10.1016/j.neuroimage.2017.08.058

Mullen, T. (2012). *CleanLine EEGLAB Plugin. San Diego, CA: Neuroimaging Informatics Toolsand Resources Clearinghouse (NITRC).*

Murray, M. M., Brunet, D., & Michel, C. M. (2008). Topographic ERP analyses: A step-by-step tutorial review. *Brain Topography*, *20*(4), 249–264. https://doi.org/10.1007/s10548-008-0054-5

Murta, T., Leite, M., & Carmichael, D. W. (2014). *Electrophysiological Correlates of the BOLD Signal for EEG-Informed fMRI*. *00*. https://doi.org/10.1002/hbm.22623

Musso, F., Brinkmeyer, J., Mobascher, A., Warbrick, T., & Winterer, G. (2010). Spontaneous brain activity and EEG microstates. A novel EEG/fMRI analysis approach to explore resting-state networks. *NeuroImage*, *52*(4), 1149–1161. https://doi.org/10.1016/j.neuroimage.2010.01.093

Niazy, R. K., Beckmann, C. F., Iannetti, G. D., Brady, J. M., & Smith, S. M. (2005). Removal of FMRI environment artifacts from EEG data using optimal basis sets. *NeuroImage*, *28*(3), 720–737. https://doi.org/10.1016/j.neuroimage.2005.06.067

Nijboer, T. C. W., & Jellema, T. (2012). Unequal impairment in the recognition of positive and negative emotions after right hemisphere lesions: A left hemisphere bias for happy faces. *Journal of Neuropsychology*, *6*(1), 79–93. https://doi.org/10.1111/j.1748-6653.2011.02007.x

Palmiero, M., & Piccardi, L. (2017). Frontal EEG Asymmetry of Mood: A Mini-Review. *Frontiers in Behavioral Neuroscience*, *11*(November), 1–8. https://doi.org/10.3389/fnbeh.2017.00224

Palva, S., & Palva, J. M. (2011). Functional roles of alpha-band phase synchronization in local and large-scale cortical networks. *Frontiers in Psychology*, *2*(SEP), 1–15.

https://doi.org/10.3389/fpsyg.2011.00204

Pernet, C. R., Wilcox, R., & Rousselet, G. A. (2013). *Robust correlation analyses : false positive and power validation using a new open source Matlab toolbox*. *3*(January), 1–18. https://doi.org/10.3389/fpsyg.2012.00606

Pessoa, L. (2014). Understanding brain networks and brain organization. *Physics of Life Reviews*, *11*(3), 400–435. https://doi.org/10.1016/j.plrev.2014.03.005

Pisauro, M. A., Fouragnan, E., Retzler, C., & Philiastides, M. G. (2017). Neural correlates of evidence accumulation during value-based decisions revealed via simultaneous EEG-fMRI. *Nature Communications*, *8*(May), 15808. https://doi.org/10.1038/ncomms15808

Poulsen, A. T., Pedroni, A., Langer, N., & Hansen, L. K. (2018). Microstate EEGlab toolbox: An introductory guide. *BioRxiv*, 289850. https://doi.org/10.1101/289850

Quaedflieg, C. W.E.M., Meyer, T., Smulders, F. T. Y., & Smeets, T. (2015). The functional role of individual-alpha based frontal asymmetry in stress responding. *Biological Psychology*, *104*, 75–81. https://doi.org/10.1016/j.biopsycho.2014.11.014

Quaedflieg, Conny W.E.M., Meyer, T., Merckelbach, H. L. G. J., Giesbrecht, T., Meijer, E. H., Smeets, T., & Smulders, F. T. Y. (2015). The role of frontal EEG asymmetry in post-traumatic stress disorder. *Biological Psychology*, *108*, 62–77. https://doi.org/10.1016/j.biopsycho.2015.03.018

Rashed-Al-Mahfuz, M., Islam, M. R., Hirose, K., & Molla, M. K. I. (2013). Artifact suppression and analysis of brain activities with electroencephalography signals. *Neural Regeneration Research*, *8*(16), 1500–1513. https://doi.org/10.3969/j.issn.1673-5374.2013.16.007

Renger, R. (1993). A review of the profile of mood states (POMS) in the prediction of athletic success. *Journal of Applied Sport Psychology*, *5*(1), 78–84. https://doi.org/10.1080/10413209308411306

Rey, B., Clemente, M., Wrzesien, M., Rodríguez, A., & Alcañiz, M. (2014). Assessing brain activations associated with emotional regulation during virtual reality mood induction procedures. *Expert Systems with Applications*, *42*(3), 1699–1709. https://doi.org/10.1016/j.eswa.2014.10.006

Ritchey, M., Wang, S. F., Yonelinas, A. P., & Ranganath, C. (2019). Dissociable medial temporal pathways for encoding emotional item and context information. *Neuropsychologia*, *124*, 66–78. https://doi.org/10.1016/j.neuropsychologia.2018.12.015

Ritter, P., Becker, R., Freyer, F., & Villringer, A. (2010). EEG quality: The image acquisition artefact. *EEG - FMRI: Physiological Basis, Technique, and Applications*, 153–171. https://doi.org/10.1007/978-3-540-87919-0_9

Ritter, P., Becker, R., Graefe, C., & Villringer, A. (2007). Evaluating gradient artifact correction of EEG data acquired simultaneously with fMRI. *Magnetic Resonance Imaging*, *25*(6), 923–932. https://doi.org/10.1016/j.mri.2007.03.005

Rohr, C. S., Okon-Singer, H., Craddock, R. C., Villringer, A., & Margulies, D. S. (2013). Affect and the Brain's Functional Organization: A Resting-State Connectivity Approach. *PLoS ONE*, *8*(7). https://doi.org/10.1371/journal.pone.0068015

Roy, M., Shohamy, D., & Wager, T. D. (2012). Ventromedial prefrontal-subcortical systems and the generation of affective meaning. *Trends in Cognitive Sciences*, *16*(3), 147–156. https://doi.org/10.1016/j.tics.2012.01.005

Schneider, M., Chau, L., Mohamadpour, M., Stephens, N., Arya, K., & Grant, A. (2016). EEG asymmetry and BIS/BAS among healthy adolescents. *Biological Psychology*, *120*, 142–148. https://doi.org/10.1016/j.biopsycho.2016.09.004

Sclocco, R., Tana, M. G., Visani, E., Gilioli, I., Panzica, F., Franceschetti, S., Cerutti, S., & Bianchi, A. M. (2014). EEG-informed fMRI analysis during a hand grip task: Estimating the relationship between EEG rhythms and the BOLD signal. *Frontiers in Human Neuroscience*, *8*(1 APR), 1–13. https://doi.org/10.3389/fnhum.2014.00186

Seghier, M. L. (2008). Laterality index in functional MRI: methodological issues. *Magnetic Resonance Imaging*, *26*(5), 594–601. https://doi.org/10.1016/j.mri.2007.10.010

Shackman, A. J., McMenamin, B. W., Maxwell, J. S., Greischar, L. L., & Davidson, R. J. (2009). Right dorsolateral prefrontal cortical activity and behavioral inhibition. *Psychological Science*, *20*(12), 1500–1506. https://doi.org/10.1111/j.1467-9280.2009.02476.x

Shafi, M. M., Benwell, C. S. Y., Musaeus, C. S., Farzan, F., Matham, S., Davila, P., Pascual-Leone, A., Santarnecchi, E., & Khanna, A. R. (2017). EEG Microstate Correlates of Fluid Intelligence and Response to Cognitive Training. *Brain Topography*, *30*(4), 502–520. https://doi.org/10.1007/s10548-017-0565-z

Sigman, M., & Dehaene, S. (2008). Brain Mechanisms of Serial and Parallel Processing during Dual-Task Performance. *Journal of Neuroscience*, *28*(30), 7585–7598. https://doi.org/10.1523/jneurosci.0948-08.2008

Smith, E. E., Reznik, S. J., Stewart, J. L., & Allen, J. J. B. (2017). Assessing and conceptualizing frontal EEG asymmetry: An updated primer on recording, processing, analyzing, and interpreting frontal alpha asymmetry. *International Journal of Psychophysiology*, *111*, 98–114. https://doi.org/10.1016/j.ijpsycho.2016.11.005

Stewart, J. L., & Allen, J. J. B. (2018). Resting frontal brain asymmetry is linked to future depressive symptoms in women. *Biological Psychology*, *136*(September 2017), 161–167. https://doi.org/10.1016/j.biopsycho.2018.06.004

Studer, B., Pedroni, A., & Rieskamp, J. (2013). Predicting Risk-Taking Behavior from Prefrontal Resting-State Activity and Personality. *PLoS ONE*, *8*(10), 1–8. https://doi.org/10.1371/journal.pone.0076861

Sutton, S. K., & Davidson, R. J. (1997). Prefrontal brain asymmetry: A Biological Substrate of the Behavioral Approach and Inhibition Systems. *Psychological Science*, *8*(3), 204–210. https://doi.org/10.1111/j.1467-9280.1997.tb00413.x

Taubitz, L. E., Pedersen, W. S., & Larson, C. L. (2015). BAS Reward Responsiveness: A unique predictor of positive psychological functioning. *Personality and Individual Differences*, *80*, 107–112. https://doi.org/10.1016/j.paid.2015.02.029

Tenke, C. E., Kayser, J., Abraham, K., Alvarenga, J. E., & Bruder, G. E. (2015). Posterior EEG alpha at rest and during task performance: Comparison of current source density and field potential measures. *International Journal of Psychophysiology*, *97*(3), 299–309. https://doi.org/10.1016/j.ijpsycho.2015.05.011

Thayer, J. F., & Koenig, J. (2019). Resting Cerebral Blood Flow and Ethnic Differences in Heart Rate Variability: Links to Self-Reports of Affect and Affect Regulation. *NeuroImage*, *202*(August),

116154. https://doi.org/10.1016/j.neuroimage.2019.116154

Tomarken, a J., Davidson, R. J., Wheeler, R. E., & Doss, R. C. (1992). Individual-Differences in Anterior Brain Asymmetry and Fundamental Dimensions of Emotion. *Journal of Personality and Social Psychology*, *62*(4), 676–687. https://doi.org/10.1037/0022-3514.62.4.676

Tomarken, A. J., Davidson, R. J., & Henriques, J. B. (1990). Resting frontal brain asymmetry predicts affective responses to films. *Journal of Personality and Social Psychology*, *59*(4), 791–801. https://doi.org/10.1037/0022-3514.59.4.791

Tomarken, A. J., Davidson, R. J., Wheeler, R. E., & Kinney, L. (1992). Psychometric Properties of Resting Anterior EEG Asymmetry: Temporal Stability and Internal Consistency. In *Psychophysiology* (Vol. 29, Issue 5, pp. 576–592). https://doi.org/10.1111/j.1469-8986.1992.tb02034.x

Tuccitto, D. E., Giacobbi, P. R., & Leite, W. L. (2010). The Internal Structure of Positive and Negative Affect: A Confirmatory Factor Analysis of the PANAS. *Educational and Psychological Measurement*, *70*(1), 125–141. https://doi.org/10.1177/0013164409344522

Van De Ville, D., Britz, J., & Michel, C. M. (2010). EEG microstate sequences in healthy humans at rest reveal scale-free dynamics. *Proceedings of the National Academy of Sciences of the United States of America*, *107*(42), 18179–18184. https://doi.org/10.1073/pnas.1007841107

van der Vinne, N., Vollebregt, M. A., van Putten, M. J. A. M., & Arns, M. (2017). Frontal alpha asymmetry as a diagnostic marker in depression: Fact or fiction? A meta-analysis. *NeuroImage: Clinical*, *16*(April), 79–87. https://doi.org/10.1016/j.nicl.2017.07.006

Wager, T. D., Barrett, L. F., Weber, J., Lindquist, K. A., & Satpute, A. B. (2015). The Brain Basis of Positive and Negative Affect: Evidence from a Meta-Analysis of the Human Neuroimaging Literature. *Cerebral Cortex*, *26*(5), 1910–1922. https://doi.org/10.1093/cercor/bhv001

Wager, T. D., Keller, M. C., Lacey, S. C., & Jonides, J. (2005). Increased sensitivity in neuroimaging analyses using robust regression. *NeuroImage*, *26*(1), 99–113. https://doi.org/10.1016/j.neuroimage.2005.01.011

Watson, D., & Clark, L. A. (1988). *Development and Validation of Brief Measures of Positive and Negative Affect : The PANAS Scales*. *54*(6), 1063–1070.

Wheeler, R. E., Davidson, R. J., & Tomarken, A. J. (1993). Frontal brain asymmetry and emotional reactivity: A biological substrate of affective style. In *Psychophysiology* (Vol. 30, Issue 1, pp. 82–89). https://doi.org/10.1111/j.1469-8986.1993.tb03207.x

Winkler, I., Brandl, S., Horn, F., Waldburger, E., Allefeld, C., & Tangermann, M. (2014). Robust artifactual independent component classification for BCI practitioners. *Journal of Neural Engineering*, *11*(3). https://doi.org/10.1088/1741-2560/11/3/035013

Winkler, I., Haufe, S., & Tangermann, M. (2011). Automatic Classification of Artifactual ICA-Components for Artifact Removal in EEG Signals. *Behavioral and Brain Functions*, *7*, 1–15. https://doi.org/10.1186/1744-9081-7-30

Wright, D., Makin, A. D. J., & Bertamini, M. (2015). Right-lateralized alpha desynchronization during regularity discrimination: Hemispheric specialization or directed spatial attention? *Psychophysiology*, *52*(5), 638–647. https://doi.org/10.1111/psyp.12399

Wu, G. R., Deshpande, G., Laureys, S., & Marinazzo, D. (2015). Retrieving the Hemodynamic Response Function in resting state fMRI: Methodology and application. *Proceedings of the Annual International Conference of the IEEE Engineering in Medicine and Biology Society, EMBS*, *2015-Novem*, 6050–6053. https://doi.org/10.1109/EMBC.2015.7319771

Wyczesany, M., Capotosto, P., Zappasodi, F., & Prete, G. (2018). Hemispheric asymmetries and emotions: Evidence from effective connectivity. *Neuropsychologia*, *121*, 98–105. https://doi.org/10.1016/j.neuropsychologia.2018.10.007

Wymbs, N. F., Bassett, D. S., Mucha, P. J., Porter, M. A., & Grafton, S. T. (2012). Differential Recruitment of the Sensorimotor Putamen and Frontoparietal Cortex during Motor Chunking in Humans. *Neuron*, *74*(5), 936–946. https://doi.org/10.1016/j.neuron.2012.03.038

Yun, J. Y., Kim, J. C., Ku, J., Shin, J. E., Kim, J. J., & Choi, S. H. (2017). The left middle temporal gyrus in the middle of an impaired social-affective communication network in social anxiety disorder. *Journal of Affective Disorders*, *214*(January), 53–59. https://doi.org/10.1016/j.jad.2017.01.043

# CHAPTER FIVE

# THE ARCHITECTURE OF SUBCORTICAL-CORTICAL INTERACTIONS AND FUNCTIONAL ASYMMETRY DOMINATING AFFECT AND APPROACH/WITHDRAWAL BEHAVIOR: GRAPH THEORY APPROACH

## 5.1 ABSTRACT

The relevance of subcortical structures and interhemispheric subcortical-cortical interactions among positive/negative affect and approach/withdrawal tendencies during resting-state are not fully understood. Gaining this knowledge may foster the know-how on their role in subsequent task-engagement and also on the interlinkage among affective measures and approach/withdrawal dichotomy. Here we report the neuroimaging finding based on ROI-based analysis and graph-theory estimates for global and subnetworks on healthy 39 male-volunteers who recorded resting fMRI and self-reported measures of PANAS and BAS-BIS scores. The ROI-to-ROI connectivity, in our study, revealed the connectivity of subcortical neural substrates of PANAS and BAS-BIS scores with bi-lateralized cortical regions. However, on probing the lateralization of strength of degree-measures of the cortical-regions vital for subcortical-cortical interaction, we found, for positive affect, a left-hemispheric proclivity. Further, higher connectivity within the left-hemisphere was also observed for the left-lateralized critical cortical regions of negative affect. Our study also revealed the association of emotion and memory-related subcortical-cortical interactions in positive and negative affect. Right amygdala-right thalamus-frontotemporal cortical areas emanated in positive affect, and right putamen-left hippocampus-frontotemporal cortical regions network stemmed for negative affect. Then, we

show the involvement of basal-ganglia structures in approach-withdrawal dichotomy with tight coupling of right-caudate, left-accumbens with anterior cingulate, and insular regions for withdrawal/inhibition system. Further, distinct involvement of the insula (posterior) in affective states while insula (anterior) in approach/withdrawal systems builds-up for the existence of a feedback-loop between affective and approach/withdrawal systems.

## 5.2 INTRODUCTION

The innate resting neural interactions have been shown to influence subsequent task engagement and decision making (Grossman et al., 2019; Hasson, Nusbaum, & Small, 2009; Kuschpel et al., 2015; López Zunini, Thivierge, Kousaie, Sheppard, & Taler, 2013; Schultz & Cole, 2016). However, it is not clear whether these interactions possess the neural signatures of affective (positive/negative) and approach/withdrawal states of an individual. Affective and approach/withdrawal states exhibit neural engagements that are regulated by strong interhemispheric subcortical-cortical interactions. An existing body of research involving task engagement provides a valuable foundation for understanding these subcortical-cortical neural interactions encompassing the affective and approach/withdrawal measures (Balconi et al., 2012; Chikazoe et al., 2014; Citron et al., 2016; Helfinstein et al., 2012; Kensinger and Schacter, 2006; Laricchiuta and Petrosini, 2014). However, the association of the resting neural interactions with affect and approach/withdrawal measures of an individual is still not established. Specifically, the outlook on the resting subcortical-cortical interactions with their interhemispheric functional connectivities for these measures remains unfathomed. Attaining this knowledge would facilitate the understanding of their predictive effect on subsequently performed tasks.

In addition, the present study also derives its motivation from our previous study (Kaur, Chinnadurai, & Chaujar, 2020), wherein we estimated the efficacy of microstates derived resting frontal electroencephalography (EEG) alpha asymmetry against the standard alpha asymmetry measure in understanding affect and approach-withdrawal behavior. Howbeit, the current study focusses on the resting subcortical-cortical neural interactions and the associated asymmetry in the functional connectivities which dominate the processing of self-reported measures of Positive and Negative Affect Schedule (PANAS) and Behavioral Activation System (BAS) / Behavioral Inhibition System (BIS) psychological scales (Carver & White, 1994; Watson & Clark, 1988). Further, there also exist several theories that interlink the affect measures with the approach, withdrawal behavior (Baumeister, Vohs, DeWall, & Zhang, 2007; Gable, Reis, & Elliot, 2000; Gomez & Gomez, 2002; Maio & Esses, 2001; Meyer & Shack, 1989; Zelenski & Larsen, 1999). One of the arguments posits that positive and negative affect can act as a go or stop signal for any goal-directed (approach/withdrawal) behavior (Henk & Elliot, 2012; Orehek, Bessarabova, Chen, & Kruglanski, 2011). Further, Carver (2001) proposed that during a goal-directed task, affective states influence the approach/withdrawal behavior through a feedback mechanism. This specific feedback process compares a signal during an approach or withdrawal situation against a reference rate. Hence, the error signal in this loop is manifested as either positive/negative affect (see Figure 5.1). For example, in the presence of stimuli that cues reward (or absence of punishment) and mediates approach behavior, the attainment of goal would lead to happiness (positive affect; PA), while the otherwise would elicit sadness (negative affect; NA). Though the above observations were insightful, still, these works of literature bring no clarity on how the neural feedback interactions are manifested during resting-state and further on the association of these interactions with affect, approach/withdrawal behavior of an individual.

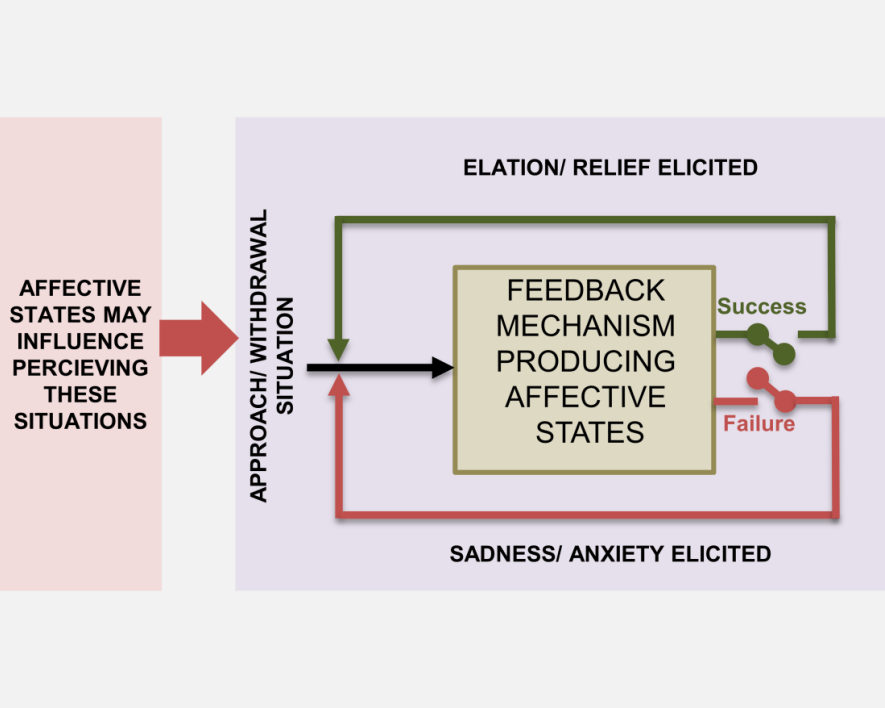


**Figure 5.1** Schema is indicative of the feedback loop between affective states and approach/withdrawal dichotomy.

Also, studies in the recent past have independently analyzed the varied aspects of neural engagements involved in affect (positive and negative) and approach/withdrawal measures during resting-state and task engagement. Rohr et al. (2013), in a resting-state study, showed that positive and negative affect as assessed through PANAS covaried with functional connectivity of a shared set of regions. Subsequently, Lindquist et al. (2016), in a task-based meta-analysis study, explored the brain basis for positive and negative affect. The study mentioned above emphasized the role of the prefrontal cortex, insular region, and subcortical regions of the amygdala and thalamus in elaborating the functions of positive and negative affective stimuli. On the other hand, Angelides et al. (2017) demonstrated the correlation of BAS (fun-seeking) measures with resting-state connectivity between the middle orbitofrontal cortex and putamen. In another task-based study, Laricchiuta and Petrosini (2014) showed approach and withdrawal

behaviors to be modulated by a network of subcortical structures (amygdala, dorsal striatum, hypothalamus, and cerebellum). The above study further proposed that nodes of the network of these subcortical structures are strongly interconnected, and the weight associated with the nodes decides whether the final output would lead to approach or withdrawal behavior. Nevertheless, the knowledge of the network of subcortical and cortical regions involved in processing the affective and approach/withdrawal measures during resting-state still requires exploration.

Hence, in the present study, distinct resting subcortical-cortical interactions and functional connectivity associated with affect and approach/ withdrawal behavior were assessed. For this purpose, self-report inventories that independently measure positive and negative affect (PANAS) and BAS and BIS measures were utilized, and the relationship between these measures and resting Bold-oxygenated level-dependent (BOLD) signal was gauged. To assess subcortical-cortical interactions associated with neural underpinnings of affect and approach/ withdrawal behavior independently, ROI-to-ROI analysis and graph theory metrics (degree and betweenness centrality) were employed. Further, an existing body of literature (Balconi et al., 2017; J. Davidson, 1992; R. J. Davidson, Saron, Senulis, Ekman, & Friesen, 1990; Killgore & Yurgelun-Todd, 2007) supports the hemispheric lateralization of affective processes and personality measures where the left hemisphere dominates PA and BAS measures. In contrast, the right hemispheric region dominates NA and BIS measures. However, the validity of lateralization for affect and approach/withdrawal behavior in resting-state remains elusive. To refine this understanding further, the Estimation of the asymmetry in the functional connectivity measures of the subcortical and the critical cortical substrates dominating subcortical-cortical interaction of affect and approach/ withdrawal behavior was performed.

## 5.3 METHODS

The schematic of the methodology followed in the present study is explained in Figure 5.2.

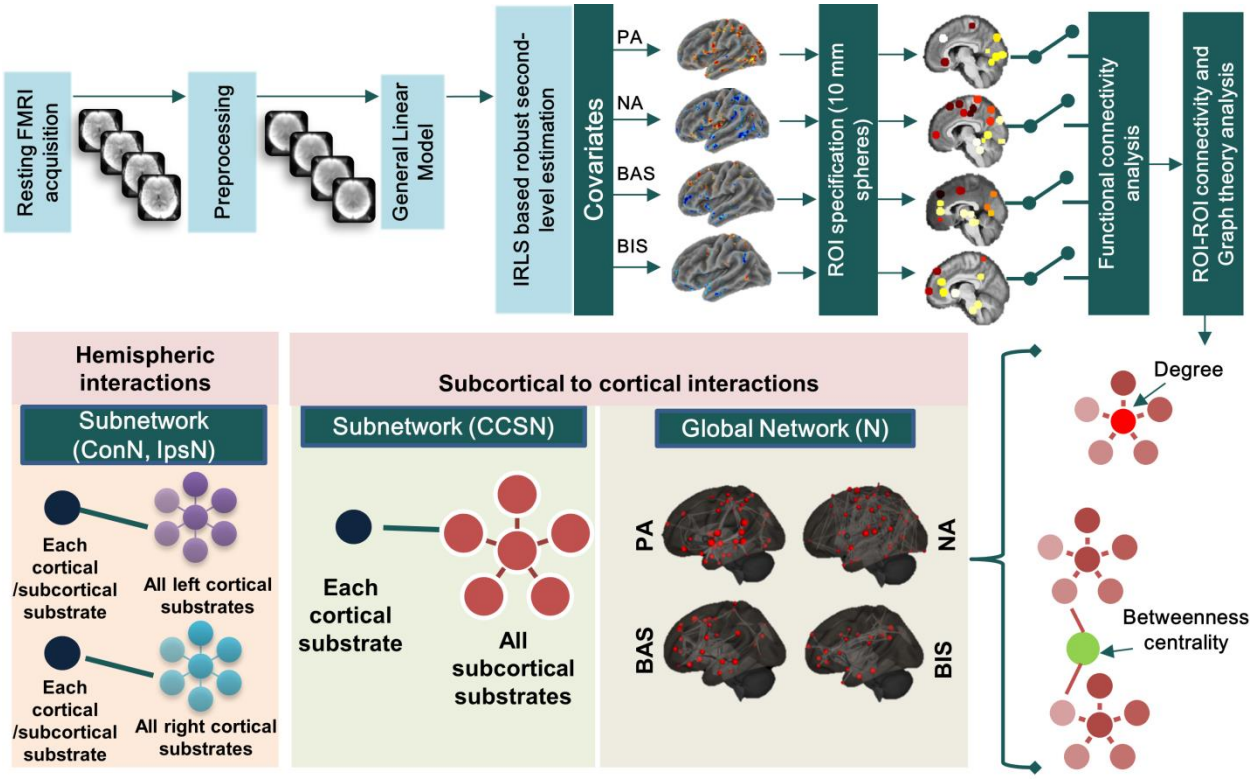


**Figure 5.2** Schematic of the methodology followed in the present study.

### *5.3.1 SAMPLE AND PROCEDURE*

The sample consists of the same subjects which were utilized for the study included in Chapter four. Thus, thirty-nine healthy adults with a mean age of 19.57 ± 1.28 were recruited for this study. The study included all right-handed male subjects with no history of depression or other severe diseases. The study adhered to the Declaration of Helsinki and was approved by the local institutional ethical committee. All subjects submitted a written informed consent.

### *5.3.2 BEHAVIORAL MEASURES*

As explained in Chapter four, participants were asked to complete Positive and Negative Affect (PANAS) and Behavioral approach system (BAS)/ Behavioral inhibition system (BIS) questionnaires before resting fMRI acquisition to assess the dispositional affect and approach/withdrawal parameters in resting state. PANAS consists of ten positive and negative adjectives each that are rated on a Likert scale ranging from very slightly or not at all (1) to extremely (5) and assesses the affect at the present moment (Crawford & Henry, 2004; Watson & Clark, 1988). BAS and BIS scales (Carver & White, 1994) include twenty-four items in total (twenty score-items and four fillers, each measured on a four-point Likert scale), among them seven items (range = 7–28) measure BIS and thirteen items BAS (range = 13–52; 13 items). PA, NA, BIS, and BAS scores showed good internal consistency (Cronbach's alpha's= 0.89; 0.91; 0.93; 0.92).

### *5.3.3 DATA ACQUISITION AND PRE-PROCESSING STEPS*

As described in Chapter four, we acquired resting-fMRI data using a Siemens 3T scanner. Anatomical scans included a high-resolution T1-weighted structural image with the following parameters: MPRAGE sequence, 0.9 x 0.9 x 0.9 mm resolution ; FoV: 240 mm; slice TR/TE=1900ms/2.49ms; FA:$90^{o}$; 160 slices with slice thickness 0.9mm and distance factor of 50%). Functional T2*-weighted images were obtained using a 6-minute resting-state echo-planar imaging (EPI) sequence with the following parameters: T2* EPI sequence, 3.8 x 3.8 x 5.0 mm resolution; FoV: 240 mm; slice TR/TE=2000ms/30ms; FA: $90^{o}$; 30 slices with thickness 5mm and distance factor of 0%).

Functional scans were pre-processed and analyzed using the Functional Connectivity Toolbox (CONN) (Whitfield-Gabrieli & Nieto-Castanon, 2012). Data from the resting-fMRI scan underwent the default pre-processing pipeline for volume-based analysis (realignment and unwarping, slice-time correction, direct normalization to MNI space, and spatial smoothening with 8 mm full width half maximum Gaussian kernel filter).

### *5.3.4 DATA ANALYSIS*

The present study aims to decipher the distinct subcortical-cortical interactions and asymmetry in functional connectivity dominating the affect and approach/ withdrawal behavior. For this purpose, at first, the cortical and subcortical neural underpinnings of PANAS and BAS/BIS measures were estimated. Subsequently, ROI-to-ROI functional connectivity analysis and the graph theory metrics (degree and betweenness centrality) was employed to understand the connectivity among subcortical-cortical regions of affect and approach/withdrawal measures.

After assessing the neural substrates, we employed a global network wherein the nodes comprised all the neural substrates (region of interest) of a particular psychological measure. Besides, subnetworks constituting the amalgamation of each cortical substrate with all subcortical substrates for a specific psychological measure were examined to understand the interaction among subcortical and cortical substrates and pinning down the vital subcortical and cortical regions for the same. Further, to estimate the hemispheric asymmetry of functional connections associated with the neural substrates of positive and negative affect (PANAS) and BAS and BIS measures, other subnetworks were constituted which involved the concatenation of an individual neural substrate of a particular psychological measure first with all the left-lateralized cortical substrates and subsequently with all the right-lateralized cortical substrates.

Thus, the merger of left-lateralized cortical substrates would constitute the ipsilateral functional connection for left-lateralized cortical regions and the contralateral functional connection for right-lateralized cortical areas. Therefore, to analyze the hemispheric dominance for the functional associations of each cortical region, the ratio quantifying the ipsilateral and contralateral functional connections was estimated.

#### 5.3.4.1 Estimation of neural substrates of PANAS and BIS/BAS measures

We examined the robust correlations of PANAS and BAS-BIS scores with the Bold Oxygen Level Dependent (BOLD) signal of resting-state fMRI to establish the cortical and subcortical neural basis for PA, NA, BAS, and BIS measures. The first-level analysis of resting-state fMRI data was performed in SPM12 using the General linear model (GLM). The model also incorporated the six motion regressors. The above step yielded, for each subject, the first-level statistical parametric maps accommodated with their temporal and dispersion derivative terms. The first-level statistical maps were then subjected to the Canlab Core toolbox to extract amplitude measures from the basis sets (Calhoun, Stevens, Pearlson, & Kiehl, 2004). The robust second-level group analysis was employed next, utilizing the contrast images for amplitude summary measure, in Canlab core's robust regression toolbox (Wager, Keller, Lacey, & Jonides, 2005). PA, NA, BAS, and BIS measures were passed as covariates in second-level analysis in four separate models, respectively, to estimate their neural underpinnings. Canlab core's robust regression toolbox detects the extreme outliers through iteratively re-weighted least squares (IRLS) method. IRLS minimizes the probability of negative findings and false-positives while retaining power. It reduces the effect of extreme outliers and has proved effective with small samples (n=10), and the benefits increase with an increase in sample size (n=40). Subsequently, the amplitude contrast image was subjected for the whole brain analysis corrected with voxel-

wise False Discovery Rate (FDR) thresholded at q < .05, yielding the neural substrates f PA, NA, BAS, and BIS.

#### 5.3.4.2 Functional connectivity analysis

##### *5.3.4.2.1 Definition of Region of Interest (ROI's) and ROI-to-ROI connectivity*

The CONN Functional Connectivity Toolbox (Whitfield-Gabrieli & Nieto-Castanon, 2012) was utilized to parcellate the brain into ROI's, consisting of 10 mm diameter spheres, based on neural substrates of psychological measures (PA, NA, BAS, and BIS). The above step yielded four independent atlases consisting of ROI's of neural substrates of PA, NA, and BAS and BIS measures. Functional connectivity analyses were performed independently on all four ROI atlases.

Further, to analyze the interaction among subcortical and cortical regions, we utilized the CONN Functional Connectivity Toolbox (Whitfield-Gabrieli & Nieto-Castanon, 2012) to estimate the significance and strength of bivariate Pearson correlation among pairs of ROI's within each subject's data. For ROI-to-ROI connectivity, the BOLD time-series was extracted from each neural substrate and was correlated with the BOLD time-series signal of every other cortical and subcortical neural substrate of a psychological measure. This resulted in a correlation matrix showing connectivity between each region within the network for each participant. The bivariate regression coefficient is represented as follows

$$r(i,j) = \frac{\sum_t NS_i(t)NS_j(t)}{\sqrt{\sum_t NS_i(t)^2 NS_j(t)^2}} \quad \text{Equation 5.1}$$

$$Z(i,j) = \tanh^{-1} r(i,j) \quad \text{Equation 5.2}$$

with $NS_i(t) =$ BOLD time series within the $i^{th}$ neural substrate, centered to zero mean, $r(i,j) =$ correlation coefficients between the $i^{th}$ and $j^{th}$ ROI's (cortical/subcortical neural substrate) and $Z(i,j) =$ Fisher-transformed correlation coefficient. In the second-level analysis step, the first-level connectivity-measure matrix for each participant (effect of rest condition) was thresholded at $p < 0.05$ corrected for multiple comparisons (FDR).

#### *5.3.4.2.2 Graph theory analysis*

In the current study, we employed graph theory to understand the subcortical and cortical neural interactions for PA, NA, BAS, and BIS measures. Graph theory is a mathematical technique that represents brain networks as maps composed of nodes (i.e., regions of interest, ROI) and edges (i.e., connections between them) (Farahani et al., 2019; Wang et al., 2010). Thus, for a given ROI, graph theory captures large-scale properties of information flow by accounting for that ROI's relationship with the entire brain network rather than individual regions.

To construct a functional brain network, CONN Functional Connectivity Toolbox was utilized (Whitfield-Gabrieli & Nieto-Castanon, 2012). The unweighted ROI-to-ROI correlation matrices were first thresholded at a cost value of 0.15. The adjacency matrices were built using two-sided analysis thresholds for accounting for the possible effects of negative correlations. For the following explanation, the network is represented as a graph by G (N, K) with N denoting the total number of nodes in the graph, and K the number of edges. Further, $C = \{C_1, C_2, \dots \dots C_n\}$ denotes an array of cortical regions and $SC = \{SC_1, SC_2, \dots \dots SC_m\}$ is an array of subcortical regions where n,m are the total number of cortical and subcortical neural substrates, respectively.

This graph G (N, K) is computed independently for all the self-reported psychological measures. Thus, the graph-theoretical matrices which have been assessed are as follows

a. Degree, which is the total number of edges linked to any node $i$ and is calculated as follows

$$D_i = \sum_{j \in G} adjacency_{ij} \qquad \text{Equation 5.3}$$

where, $D_i =$ (degree of the i$^{th}$ node)/ROI, $adjacency_{ij}$ is the i$^{th}$ row and j$^{th}$ column element of adjacency matrix $A$. Graph adjacency matrix $A(i,j)$ is computed by thresholding the ROI-to-ROI analysis correlation matrix $r(i,j)$.

b. Betweenness centrality is defined as the proportion of all shortest paths in a network that pass through a particular neural substrate ROI, indicating the importance of this ROI in information flow. Betweenness centrality is represented as follows

$$BC_i = \frac{\sum_{j \in G, k \neq i} [i \in P_{j,k}]}{(N-1)(N-2)} \qquad \text{Equation 5.4}$$

where $BC_i =$ (betweenness centrality of the i$^{th}$ node )/ROI and, $P_{j,k} =$ set of nodes in minimum distance path between j$^{th}$ and k$^{th}$ nodes. Results were considered significant after p<.05 FDR correction.

*5.3.4.2.2.1 Defining network and sub-network nodes*

A global network encompassing all cortical and subcortical substrates of a specific psychological measure was utilized to assess the vital subcortical regions for subcortical-cortical interactions. The network for gauging subcortical-cortical interactions was defined as follows

$$N = G(N, K) \qquad \text{Equation 5.5}$$

where $N$ is the network formed by the concatenation of all cortical substrates and subcortical substrates of a particular psychological measure as defined in the previous section. Thus, N (n+m) depicts the total neural underpinnings of a specific psychological measure, and K represents the respective edges of this network.

Subsequently, to delineate the vital cortical substrates which communicate with the subcortical areas, a discrete subnetwork was constructed, independently for each psychological measure as described below in Equation 5.6

$$CSCN_i = G(m_i, k_i) \quad \text{Equation 5.6}$$

where i $= 1{:}n$ ; $n$ is the number of cortical regions, $m_i$=$\{C_i, SC\}$ is formed by the concatenation of the i$^{th}$ cortical substrate and all subcortical substrates ($SC$) of a particular psychological measure and $k_i$ represents the respective edges.

At last, the subnetwork for understanding ipsilateral and contralateral hemispheric interactions among cortical neural substrates was formed as

$$ConN_i = G(mcon_i, kcon_i) \quad \text{Equation 5.7}$$

$$IpsN_i = G(mips_i, kips_i) \quad \text{Equation 5.8}$$

where i $= 1{:}s$ ; $s$ is the total neural substrates of a particular psychological measure, i.e., $s = n + m$; $mcon_i$=$\{s_i, C_{con}\}$ is formed by the concatenation of the i$^{th}$ substrate and all the contralateral cortical substrates ($C_{con}$) of a particular psychological measure and $kcon_i$ represents the respective edges. Supposedly, if a left-lateralized region is considered then, the specific *ConN* network would include this region and all the right-lateralized cortical areas. Similarily, $mips_i$=$\{s_i, C_{ips}\}$ is formed by the concatenation of the i$^{th}$ substrate and all the ipsilateral cortical substrates ($C_{ips}$) of that particular psychological measure and $kips_i$ represents

the respective edges. For the same left-lateralized region, the specific *IpsN* network would include this region and all the left-lateralized cortical areas. Finally, the hemispherical interactions (*HI)* for the cortical substrates were quantified utilizing the degree measures of these subnetworks as described below

$$HI_{con_i} = \frac{ConN_{Degree_i}}{ConN_{Degree_i} + IpsN_{Degree_i}} \quad \text{Equation 5.9}$$

$$HI_{ips_i} = \frac{IpsN_{Degree_i}}{ConN_{Degree_i} + IpsN_{Degree_i}} \quad \text{Equation 5.10}$$

where $i = 1{:}\, n$ ; $n$ is the total cortical substrates of a particular psychological measure.

Finally, the laterality index ($LI_{fun\_conn}$) based on the *HI's* was estimated as described in Equation 5.11. Only the cortical regions vital for subcortical-cortical interactions as assessed via ROI-to-ROI connectivity analysis and degree measures of global *(N)* as well as subnetwork *CSCN* were considered for estimation of $LI_{fun\_conn}$.

$$LI_{fun\_conn_i} = HI_{ips_i} - HI_{con_i} \quad \text{Equation 5.11}$$

where i=1:v, v is the cortical regions vital for subcortical to cortical interaction and $LI_{fun\_conn}$ is the functional connectivity based laterality index.

We also estimated the laterality index ($LI_{active\_voxels}$) based on the number of active voxels/lobe for each psychological measure (see Equation 5.12).

$$LI_{active\_voxels} = \frac{NV_{left} - NV_{right}}{NV_{left} + NV_{right}} \quad \text{Equation 5.12}$$

where $NV_{left}$ and $NV_{right}$ are the number of active voxels in the left and right hemispheres, respectively, for a particular lobe.

## 5.4 RESULTS

The present study estimates the distinct subcortical-cortical interactions and asymmetry in functional connectivity associated with affect and approach/ withdrawal behavior. Initially, the cortical and subcortical neural underpinnings of PANAS and BAS/BIS measures were assessed. Then, to understand the subcortical-cortical interactions and the critical regions which facilitate the same, ROI-to-ROI analysis and the graph theory metrics (degree and betweenness centrality) were utilized. Subsequently, hemispheric dominance of functional connections associated with the vital cortical substrates of PANAS and BAS and BIS measures were assessed and analyzed. The following subsections summarize the results obtained after carrying out the analysis.

### *5.4.1 RESTING NEURAL SUBSTRATES ASSOCIATED WITH AFFECT AND APPROACH/WITHDRAWAL MEASURES*

Figure 5.3a accommodates the resting neural substrates for PA, NA, BAS, and BIS measures. The associated extent (no. of voxels) for resting neural substrates for PA, NA, BAS, and BIS measures has been depicted as a heatmap in Figure 5.4, and Supplementary Figure S5.1 (see Appendix 3) illustrates the concomitant t-values. The abbreviations for the region names used in Figure 5.4 and Supplementary Figure S5.1 are provided as Abbreviations at the end of this chapter. The tabulation of neural substrates for the psychological measures have also been presented as supplementary material (see Supplementary Tables S5.1-S5.4; see Appendix 3). We report the most significant results after applying a false discovery rate ($p<0.05$) to solve the problem of multiple comparisons. Regions with cluster size >20 were considered for analysis.

The subcortical neural substrates for PA were pinned majorly at the right amygdala and left hippocampus. Few subcortical clusters were also found in the right and left-lateralized

thalamus. Major cortical substrates for PA included left and right-lateralized regions of the occipital lobe (Temporal occipital and occipital fusiform gyrus, cuneal cortex, lingual gyrus), frontal lobe (inferior frontal gyrus pars opercularis, frontal pole, frontal orbital cortex, precentral gyrus), anterior division of superior temporal gyrus, central operculum cortex and middle temporal gyrus (posterior division) of the temporal lobe and few clusters in the postcentral gyrus. Activations also elicited in limbic regions of the parahippocampal gyrus, posterior division of the cingulate gyrus and insular cortex. Subcortical regions of the brain-stem, right putamen, and left hippocampus activated in association with NA. Insular cortex (posterior division) also emerged as a significant neurophysiological correlate for this psychological measure. Cortical neural substrates for NA were pinned at substantial clusters in the occipital lobe (a superior division of lateral occipital cortex, intracalcarine cortex, and lingual gyrus), temporal lobe (inferior temporal gyrus (temporooccipital part), planum temporale), frontal lobe (precentral gyrus, middle frontal gyrus, inferior frontal gyrus pars opercularis, frontal operculum cortex) and parietal regions such as postcentral gyrus, supramarginal gyrus (anterior division) and precuneus cortex.

BAS subcortical neural substrates were primarily pinned at the right and left thalamus and brain stem. Few clusters were also found in the left and right putamen and left hippocampus. Limbic regions such as the parahippocampal gyrus, anterior division of cingulate gyrus, insular cortex, and paracingulate gyrus were found to be strongly associated with BAS. Major cortical substrates were found in frontal lobe regions (superior frontal gyrus, frontal pole, and medial frontal cortex) and parietal lobe regions (superior parietal lobule, postcentral gyrus, angular gyrus). Other significant cortical substrates included temporal fusiform and temporal occipital fusiform cortex.

On the other hand, right caudate, brain stem, left accumbens, and left thalamus emerged as subcortical neurophysiological substrates for BIS. Anterior as well as the posterior division of cingulate gyrus along with insular and paracingulate regions activated for BIS. Cortical substrates for BIS, similar to BAS, were pinned majorly at frontal lobe regions (precentral gyrus, frontal pole, and inferior frontal gyrus pars opercularis). Other activations included the posterior division of the middle and inferior temporal gyrus, superior division of lateral occipital cortex, and parietal regions (angular gyrus, postcentral gyrus).

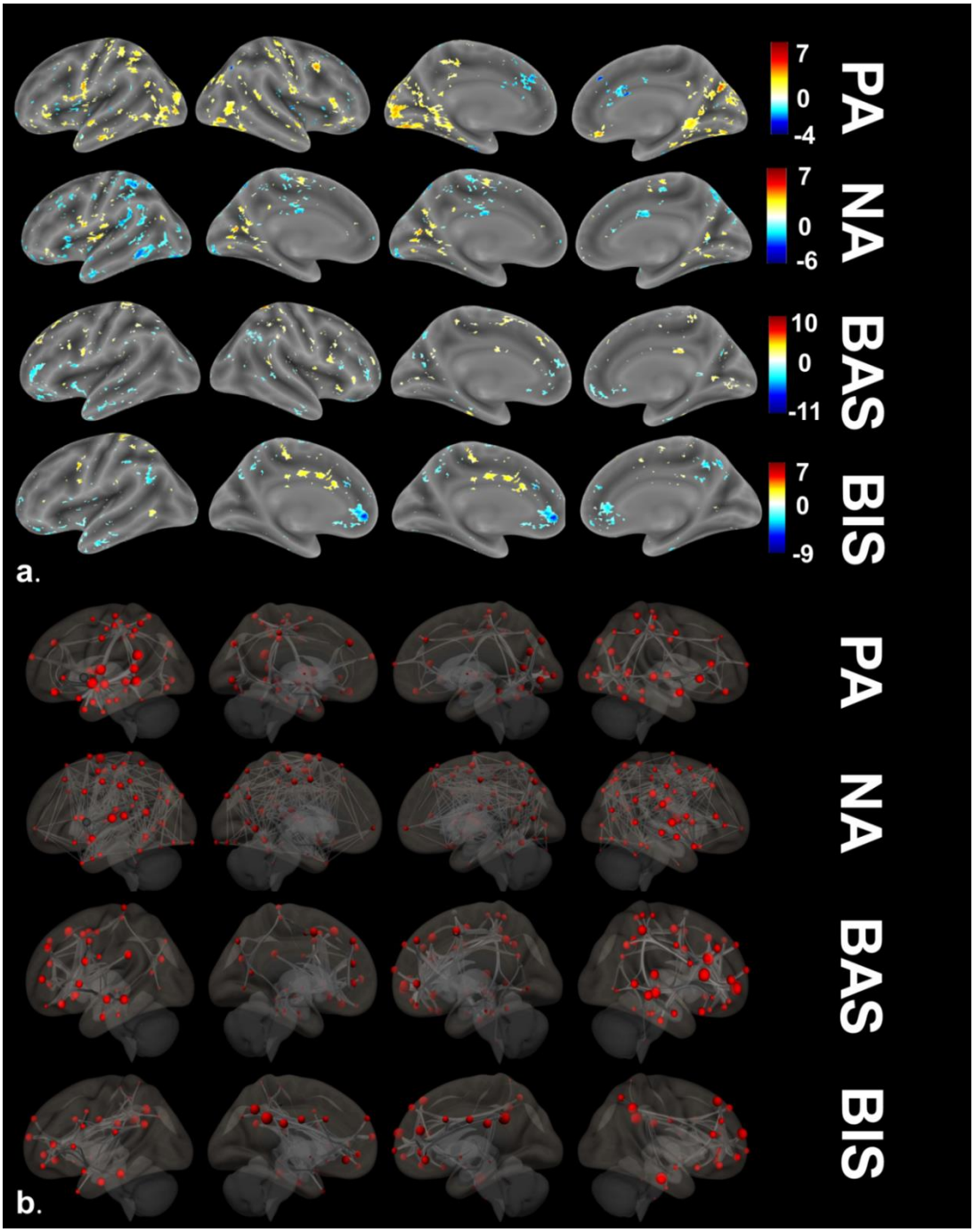


**Figure 5.3** (a) Surface rendered view of neural substrates of PA, NA, BAS, and BIS. The color bar indicates the t-values, and the activations are represented at FDR corrected $p<0.05$ (b) The nodes and edges of PA, NA, BAS, and BIS for global graph analysis.

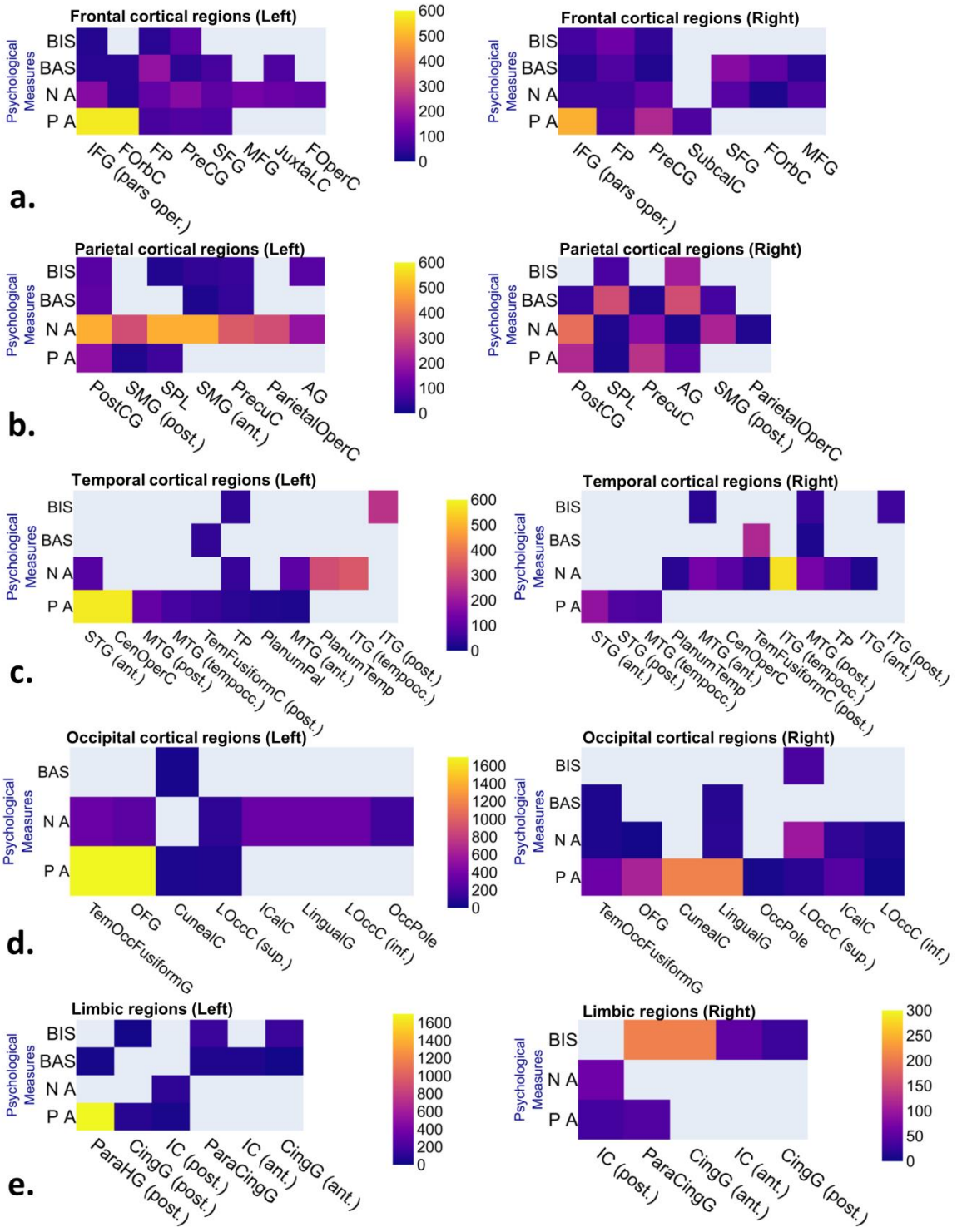


**Figure 5.4** Heatmaps for the representation of the extent (no. of voxels) of neural substrates of PA, NA, BAS, and BIS measures for (a) frontal regions, (b) parietal regions, (c) temporal regions, (d) occipital regions (e) limbic regions.

### *5.4.2 FUNCTIONAL CONNECTIVITY ANALYSIS*

To attain the objectives of the present study, ROI-to-ROI analysis and graph theory analysis was implemented on the global network and subnetworks of neural substrates for PA, NA, BAS, and BIS measures. Figure 5.3b shows the nodes and edges for a global network (N) formed by all neural substrates of particular psychological measures. The results of the analyses are explained below.

#### 5.4.2.1 Subcortical hubs for subcortical-cortical interaction

Figure 5.5 and Figure 5.6 illustrates the violin plots for degree and betweenness centrality associated with all the subcortical substrates of PA, NA, BAS, and BIS for a global network (N). The violin plot constitutes both the kernel density plot and box plot for the entire dataset of 39 volunteers' degree and betweenness centrality values. Thus, the violin plot represents the full distribution of the data along with statistical parameters such as mean, median, and interquartile ranges.

Among the subcortical neural substrates of PA right amygdala and right thalamus emanated as correlate showing high degree (right amygdala, β: 10.15; T: 12.63, right thalamus β: 8.79; T: 8.09) and betweenness centrality (right amygdala, β: 0.013; T: 6.07, right thalamus, β: 0.018; T: 4.99) in a global network N (see Figure 5.5a and 5.6a). In NA, the right putamen and left hippocampus emerged as the substrates exhibiting high degree (right putamen, β: 11.54; T: 13.87, left hippocampus, β: 9.17; T: 8.55) as well as betweenness centrality (right putamen, β: 0.004: T: 7.98, left hippocampus, β: 0.006; T: 5.58) (see Figure 5.5b and 5.6b). Further, the brain stem showed low betweenness centrality, and thus it's representation has been omitted in Fig 5b.

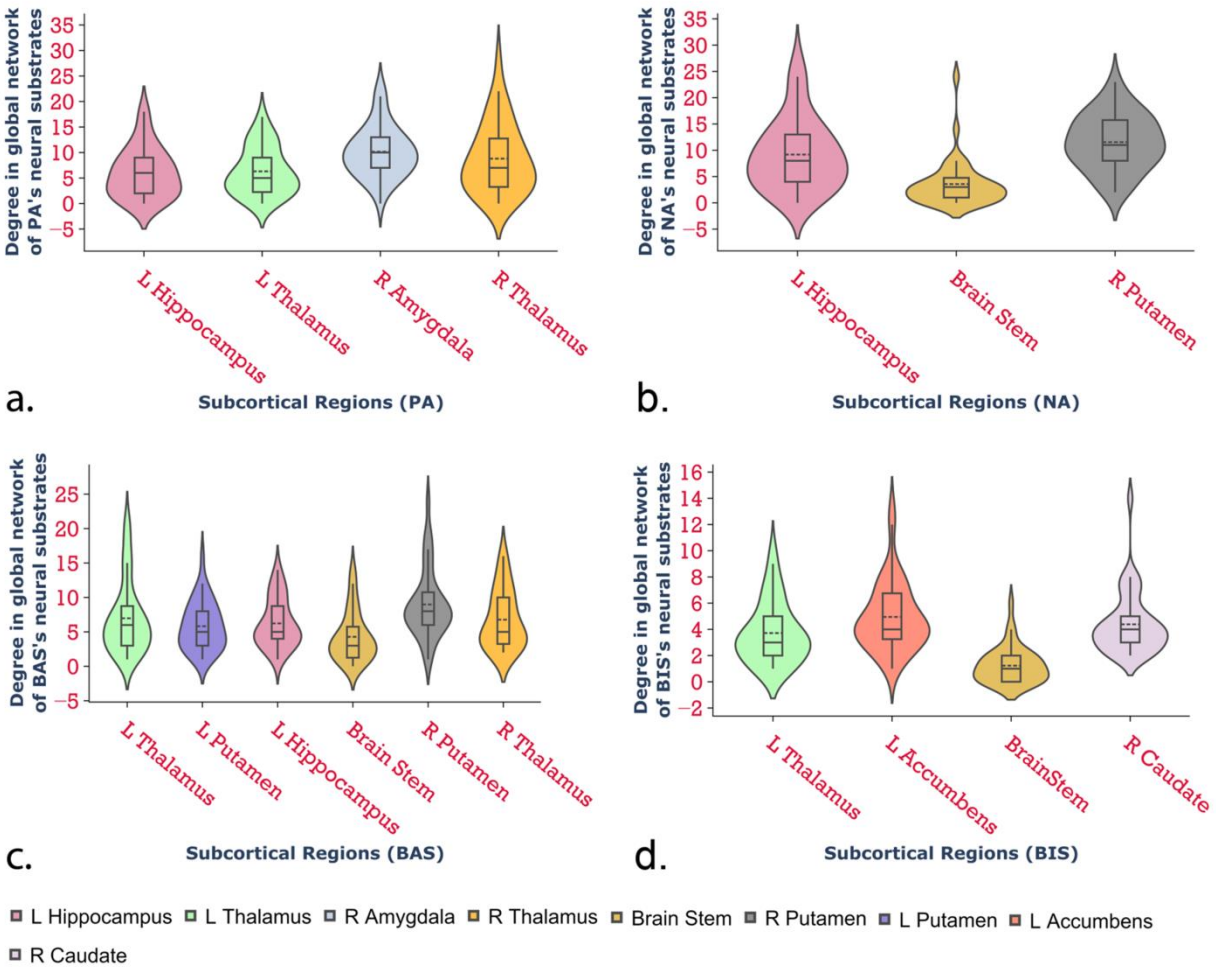


**Figure 5.5** Violin plots (kernel density plot and box plot) representing degree in the global network (N) for subcortical substrates of (a) PA (b) NA (c) BAS (d) BIS.

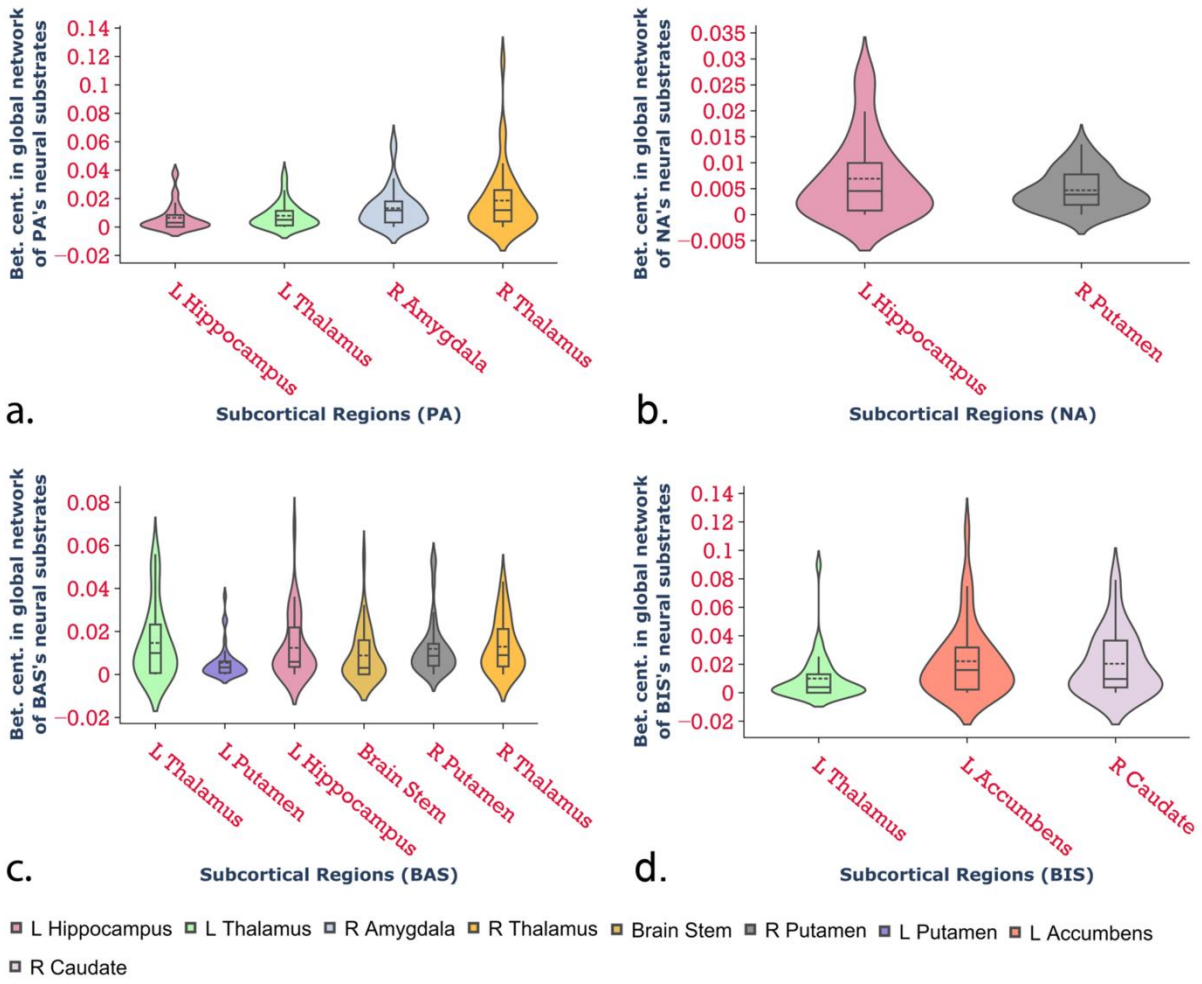


**Figure 5.6** Violin plots (kernel density plot and box plot) representing betweenness centrality in the global network (N) for subcortical substrates of (a) PA (b) NA (c) BAS (d) BIS.

Graph theory analysis for the global network (N) in BAS revealed right putamen and left thalamus exhibiting high degree (right putamen, β: 8.97; T: 11.26, left thalamus, β: 8.05; T: 8.98) and the left thalamus showed high betweenness centrality (left thalamus, β: 0.014; T: 5.92) (see Figure 5.5c and 5.6c). Left accumbens and right caudate showed a high degree (left accumbens, β: 4.95; T: 12, right caudate, β: 4.38; T: 11.50) and betweenness centrality (left accumbens, β: 0.022; T: 5.42, right caudate, β: 0.020; T: 5.81) among the other subcortical substrates of BIS (see Figure 5.5d and 5.6d).

### 5.4.2.2 Cortical hubs for subcortical-cortical interaction

#### *5.4.2.2.1 ROI-to-ROI connectivity analysis in the global network*

Figure 5.7a shows the Sankey diagram for ROI-to-ROI connectivity analysis between subcortical and cortical regions for all the psychological measures in which the width of the flows is proportional to the correlation values. The results reported are at FDR corrected $p<.05$ and correlation coefficient value $r>0.2$. Supplementary Table S5.5 (see Appendix 3) shows the tabulation of data for the above analysis. The abbreviations for the cortical regions, for Figure 5.7, are provided in the Abbreviations section at the end of this chapter.

The ROI-to-ROI functional connectivity analysis for PA revealed the significant coupling of the right amygdala with cortical regions of the left and right-lateralized insular cortex (posterior), medial and anterolateral temporal lobe regions (left-lateralized planum palore, posterior division parahippocampal gyrus, central opercular cortex, temporal pole, and right-lateralized anterior division of superior temporal gyrus), prefrontal cortex regions (right and left-lateralized inferior frontal gyrus (pars opercularis), right-lateralized subcallosal cortex). The posterior division of left-lateralized parahippocampal gyrus also showed significant connectivity with the subcortical region left hippocampus. Left thalamus connected with the insular cortex (left, posterior) and the right thalamus with the right and left-lateralized insular cortex (posterior). The ROI-to-ROI analysis for NA showed the strong connection of the subcortical region, right putamen with prefrontal cortex regions (bilateral frontal orbital cortex, precentral gyrus), bilateral insular cortex (posterior), and right lateralized central operculum cortex. The left hippocampus also showed significant connectivity towards a few temporal regions and left-lateralized frontal orbital cortex.

BAS's ROI-to-ROI analysis showed a significant correlation of right putamen with frontal regions (juxtapositional lobule cortex (left), frontal orbital cortex (right)), anterior division of insular cortex (left-lateralized). Further, the left putamen also showed connectivity to the anterior division of the insular cortex (left-lateralized) and prefrontal regions. The left Hippocampus is connected to the temporal areas such as the posterior division of the parahippocampal gyrus (left) and temporal fusiform cortex (left). The left thalamus showed association with the temporal fusiform cortex (right) and occipital regions. BIS's functional connectivity showed a high correlation of left accumbens with bilateral anterior cingulate gyrus, paracingulate gyrus (left), insular cortex (right, anterior division). Also, the right caudate showed a significant association with the bilateral anterior cingulate gyrus and right lateralized insular cortex.

Figure 5.7b shows the Sankey diagram for ROI-to-ROI connectivity analysis among subcortical regions for all the psychological measures in which the width of the arrows is proportional to the correlation values. The results reported are at FDR corrected $p<.05$ and correlation coefficient value $r>0.2$. In PA, the right amygdala and right thalamus connected to the left thalamus. Similarily in BAS, the left thalamus found its connectivity with the right thalamus, left hippocampus, and brain-stem. Right caudate, left accumbens and left thalamus associated with each other in BIS.

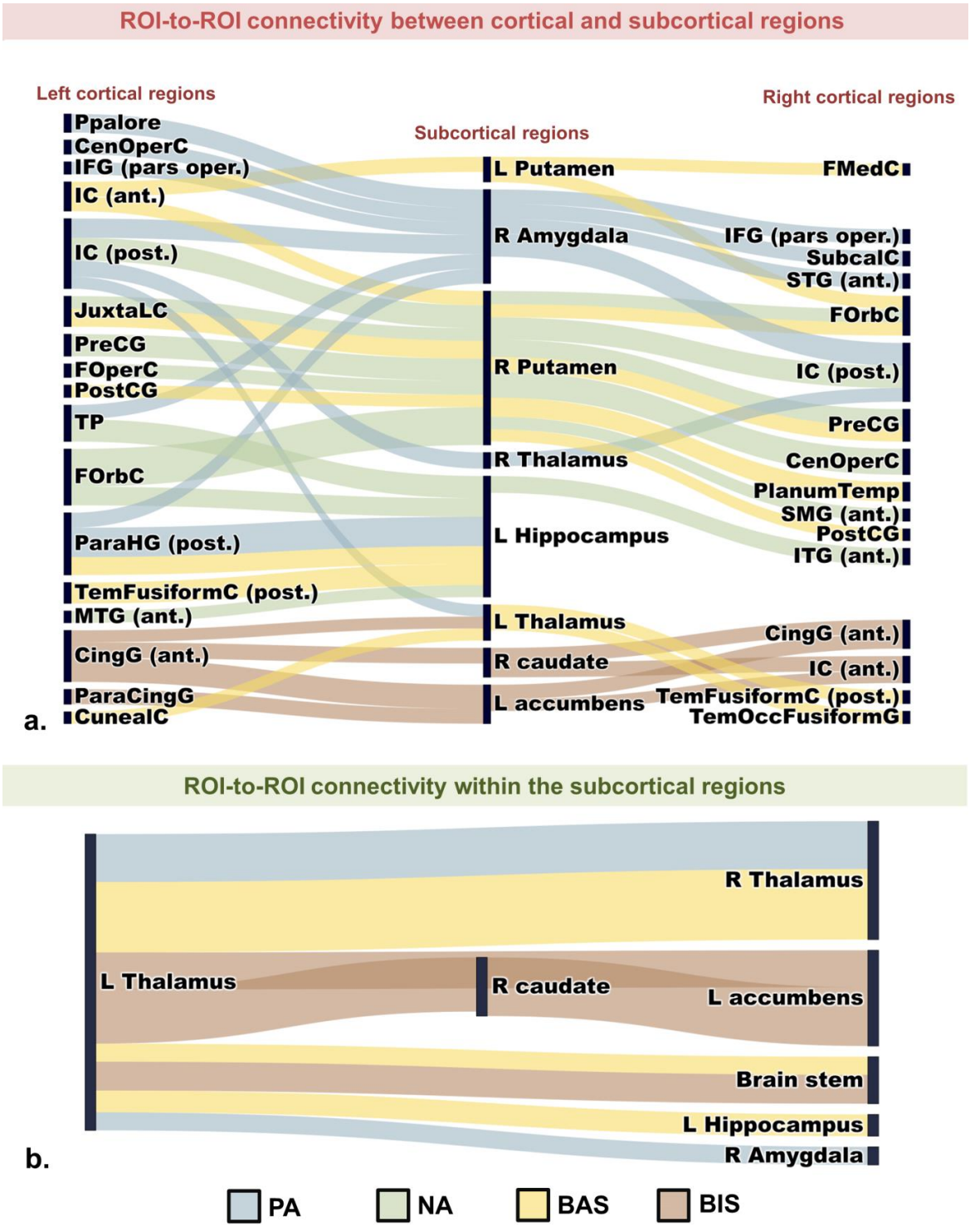


**Figure 5.7** Sankey diagram for ROI-to-ROI connectivity analysis for PA, NA, BAS, and BIS (a) between subcortical and cortical regions (b) within subcortical regions. The width of the flow is proportional to the correlation values.

#### *5.4.2.2.2 Cortical hubs in network analysis of CSCN network*

The vital cortical regions for subcortical-cortical interaction were analyzed through a discrete subnetwork ($CSCN_i$), which was constructed independently for each psychological measure by the concatenation of the $i^{th}$ cortical substrate and all subcortical substrates of a particular psychological measure. The graph theory measures (degree and betweenness centrality) for cortical neural substrates for their interaction with subcortical substrates are provided in Supplementary Table S5.6 (see Appendix 3). Figure 5.8a and 5.8b depict Sankey diagrams for this analysis, where the flow represents the beta-values for degree and betweenness centrality measures at $p<0.05$ for the cortical regions of all psychological measures. The abbreviations for the cortical regions, for Figure 5.8, are provided in the Abbreviations section at the end of this chapter.

In PA, a high degree, which correlates to dense functional connections were found in the posterior division of left-lateralized parahippocampal gyrus and other temporal regions (medial and anterolateral temporal lobe regions), posterior division of left and right-lateralized insular cortex and subcallosal cortex (right). Among these regions, high betweenness centrality, which pinpoints the critical cortical hubs which communicate with subcortical areas, was exhibited by the posterior division of left-lateralized parahippocampal gyrus and superior temporal gyrus, and posterior division of left and right-lateralized insular cortex. Graph theory analysis for the CSCN network revealed a higher degree within the NA in the left and right-lateralized insular cortex (posterior), prefrontal, and temporal regions. Among them, the left-lateralized temporal pole, frontal orbital cortex, and posterior insula exhibited high betweenness centrality.

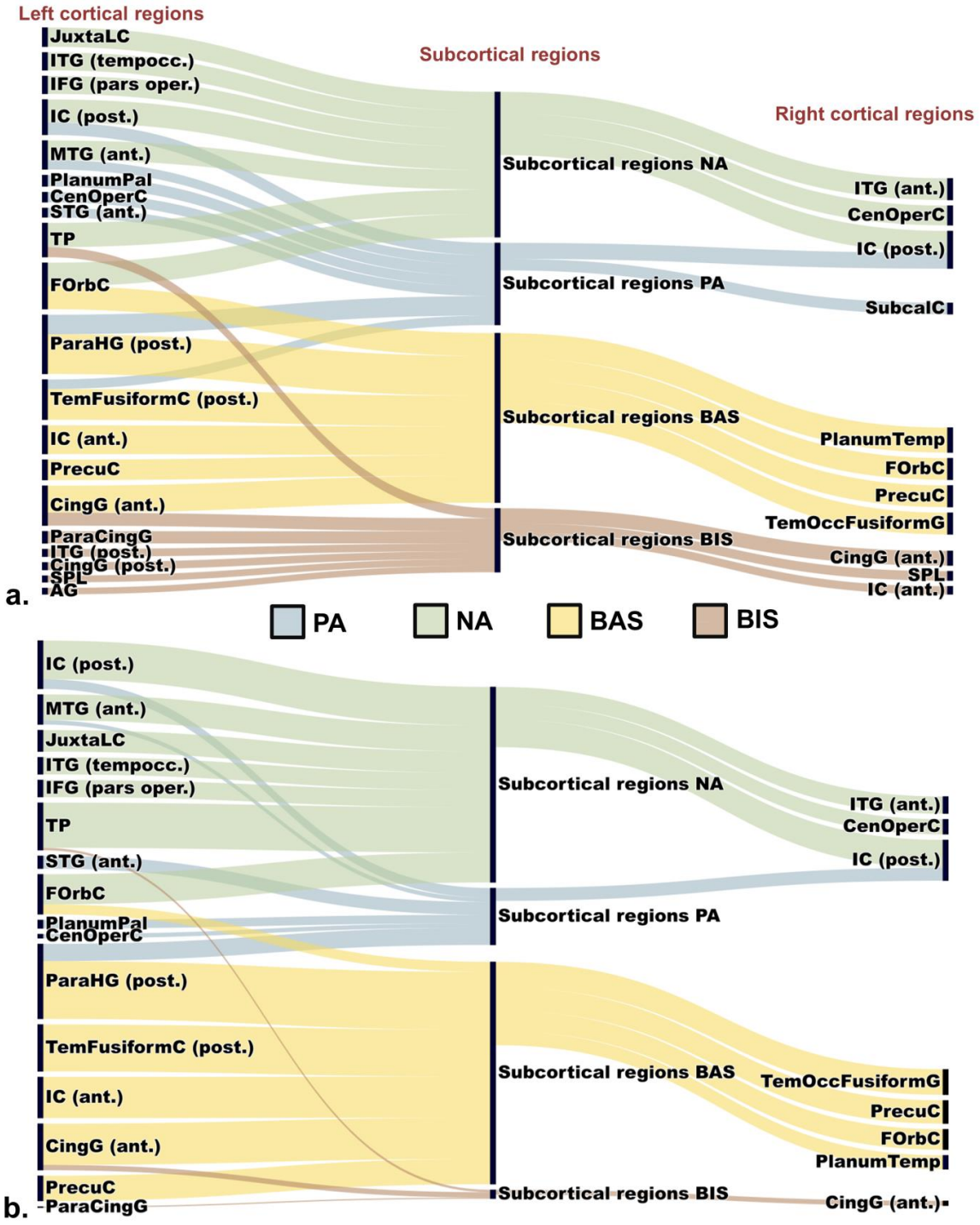


**Figure 5.8** Sankey diagram for subcortical-cortical interaction for discrete subnetwork *(CSCN)* where the flow represents (a) the degree and (b) the betweenness centrality measures for the cortical regions of all psychological measures.

Similar to psychological measure, PA, a higher degree, was exhibited by the left-lateralized parahippocampal gyrus and temporal fusiform cortex (posterior) in BAS. The anterior division of left-lateralized cingulate gyrus and insula also showed a high degree. Other regions included the bi-lateral frontal orbital and precuneous cortex. Among the areas mentioned above, the left-lateralized parahippocampal gyrus and temporal fusiform cortex (posterior), anterior division of left-lateralized cingulate gyrus, and insula showed high betweenness centrality. BIS exhibited dense connections of the bi-lateral anterior cingulate gyrus, anterior insular cortex (left), paracingulate gyrus (right), and superior parietal lobule (right) with subcortical substrates. The bilateral anterior cingulate gyrus showed high betweenness centrality for this network.

#### 5.4.2.3 Hemispheric dominance of functional connections

##### *5.4.2.3.1 Lateralization predilection of subcortical regions*

The subnetwork for understanding contralateral ($ConN$) and ipsilateral ($IpsN$) hemispheric interactions were formed independently for each psychological measure by the concatenation of each neural substrate first with all left-lateralized cortical regions and subsequently with all right-lateralized cortical areas. Figure 5.9 shows this analysis for all the subcortical neural substrates for all psychological measures. The figure depicts no specific lateralization for NA and BAS measures, barring the left hippocampus, which shows a higher mean degree value for left-lateralized cortical regions for PA, NA, and BAS measures. In PA, the right amygdala is more affine towards left-lateralized areas, while the right thalamus shows a higher mean degree for right lateralized regions. In BIS, all the subcortical regions connected more to left-lateralized cortical regions.

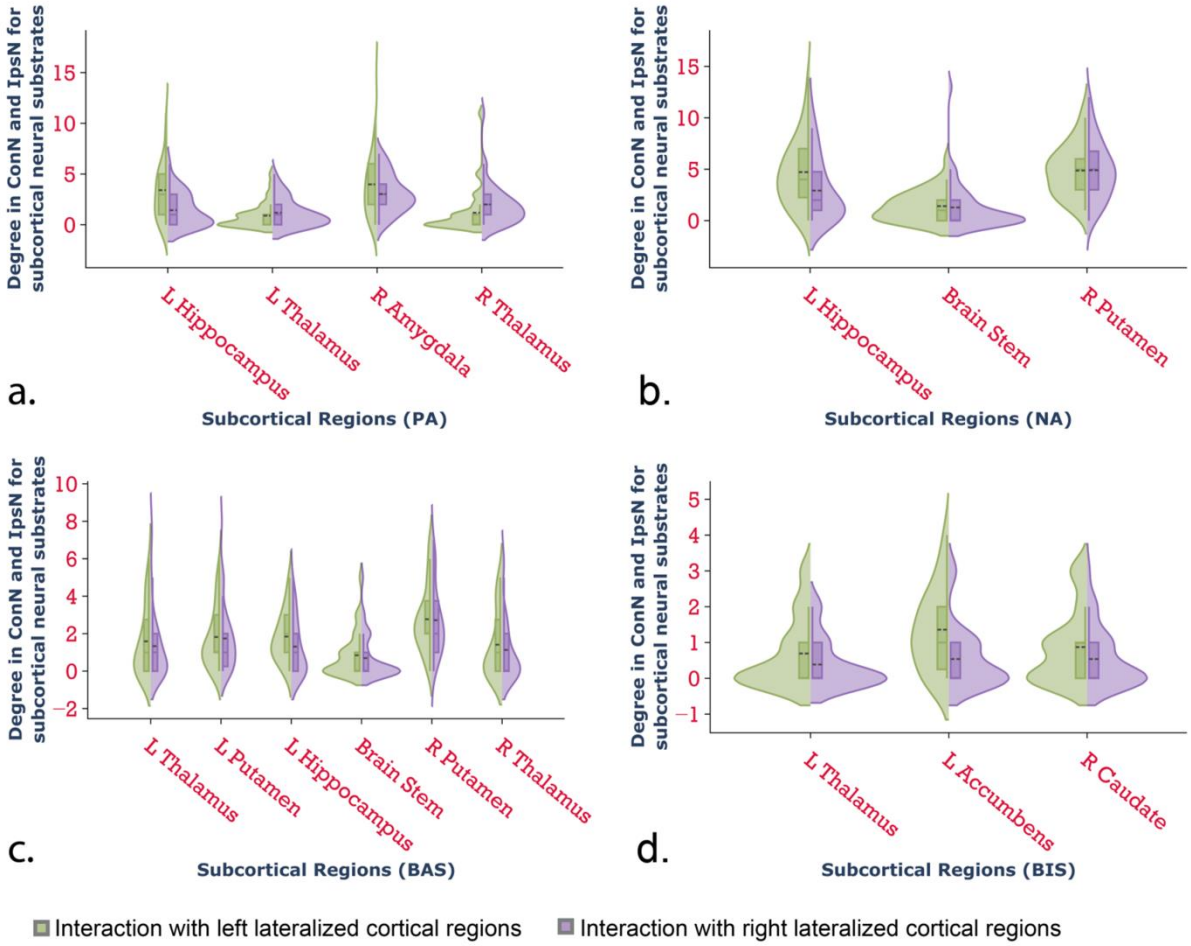


**Figure 5.9** Violin plots (kernel density plot and box plot) representing degree in contralateral ($ConN$) and ipsilateral ($IpsN$) networks for the interaction of subcortical substrates with left and right lateralized cortical regions in (a) PA (b) NA (c) BAS (d) BIS.

### *5.4.2.3.2 Lateralization predilection of cortical regions vital for subcortical-to-cortical interactions*

In the previous analyses, the cortical areas which exhibited dense connections with subcortical regions were considered, and their laterality index ($LI_{fun\_conn}$) based on interhemispheric parameters $HI_{ips}$ and $HI_{con}$ was assessed. Figure 5.10 depicts the $LI_{fun\_conn}$ for vital cortical regions for all psychological measures. Figure 5.10 reveals the dense

connectivity of left and right lateralized cortical regions critical for subcortical-cortical interactions in PA with the left hemisphere. Further, specifically, the left-lateralized vital cortical regions in NA showed a greater laterality index depicting their higher connectedness to left hemispheric operations.

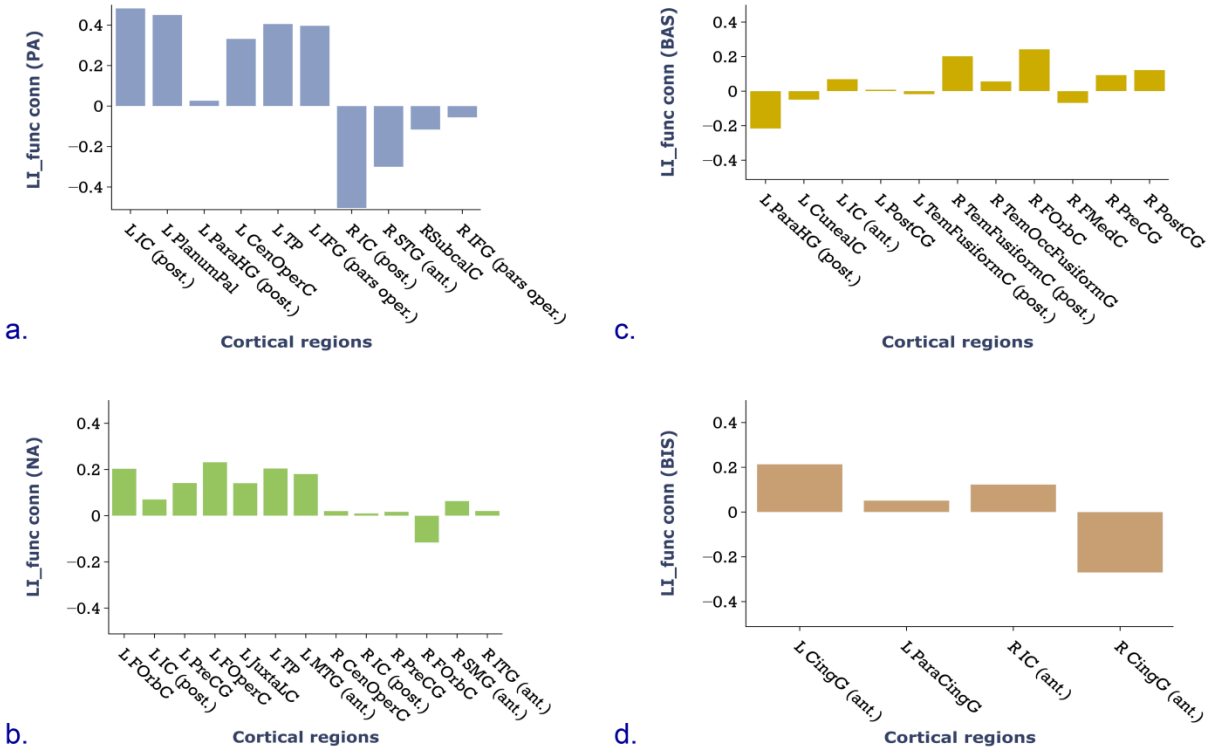


**Figure 5.10** The functional connectivity based laterality index for cortical regions vital for subcortical-cortical interaction for (a) PA (b) NA (c) BAS (d) BIS.

The laterality index ($LI_{active\_voxel}$) based on the number of active voxels per lobe was also estimated for all psychological measures and is shown in Figure 5.11.

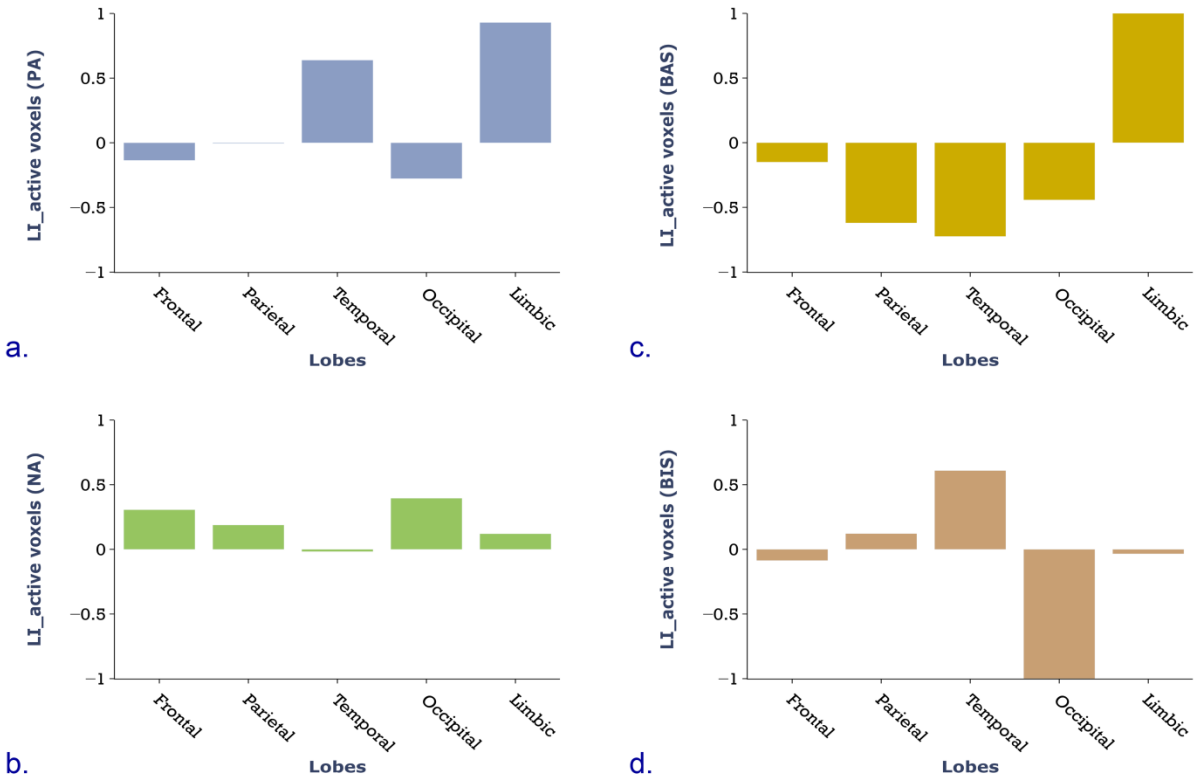


**Figure 5.11** The number of active voxels based laterality index for each lobe for (a) PA (b) NA (c) BAS (d) BIS.

## 5.5 DISCUSSION

In this study, to assess the pre-task affect (positive/negative) and approach/withdrawal neural systems that dominate the brain, we established the neural mechanisms underlying PA, NA, BAS, and BIS self-reported measures in resting-state fMRI recording. The rationale for this estimation is that emotional processes facilitate learning and memory processing (Osaka, Yaoi, Minamoto, & Osaka, 2013), which integrates with other secondary processes and finally mature to higher-order cognitive functions to create productive solutions for living. It has been reported that positive emotions facilitate academic achievement and learning, being mediated by the self-

motivation levels, and satisfaction with learning materials (Um, Plass, Hayward, & Homer, 2012). Conversely, a recent study (D'Mello, Lehman, Pekrun, & Graesser, 2014) reported that a state such as confusion improves learning and leads to higher performances on the post and transfer tests because of the increase in focus of attention on materials of learning.

Specifically, the present study brings more clarity in understanding resting subcortical-to-cortical neural interactions that serve these resting self-reported affective and approach/withdrawal measures. Further, the hemispheric asymmetry of the functional connections of these neural substrates dominating a particular psychological measure was also analyzed. The key observations from the analysis in this study are discussed below.

### *5.5.1 LATERALIZATION OF CONNECTIVITY OF CORTICAL REGIONS VITAL FOR SUBCORTICAL-CORTICAL INTERACTIONS*

In our study, both left and right cortical neural substrates in PA, which were significantly associated with the subcortical substrates, were found to show dense connectivity with all the left hemispheric cortical substrates, hinting the crucial role of left-hemispheric connectivity in processing PA. Further, the left-lateralized vital cortical neural substrates of NA showed higher connectivity with the left hemispheric cortical regions, while no specific asymmetry was observed for the right-lateralized regions. Also, relatively more voxels activated for the left hemisphere for the majority of lobes in NA.

### *5.5.2 THE EMERGENCE OF THE AMYGDALA, HIPPOCAMPUS, AND PUTAMEN AS SUBCORTICAL HUBS FOR PA AND NA*

The right amygdala (see Figure 5.5a and Figure5.6a) and right thalamus appear as the hub subcortical neural substrate for PA among other substrates, namely the left hippocampus and thalamus. However, for NA, the amygdala seemed to be absent, and the right putamen along with the left hippocampus appeared as subcortical neural substrates. Our results are in line with the study of Bonnet et al. (2015), wherein it was revealed that the amygdala is sensitive to changes in emotional intensity while viewing positively valenced stimuli. However, Rohr et al. (2013) found feeble connectivity of the right amygdala with PA as well as NA. In this study, PANAS, which was used to assess the positive and negative affective states, involves labeling events in the past or present to evaluate the current self-mood state. Although the amygdala has been associated with both positive and negatively valenced stimuli in many task-based studies (Banks, Eddy, Angstadt, Nathan, & Luan Phan, 2007; Berntson, Bechara, Damasio, Tranel, & Cacioppo, 2007; Okada et al., 2011), present research reveals that right amygdala is involved significantly during labeling of current events which are decisive of an individual's resting positive valence. Also, the thalamo-amygdala pathway exhibits long-term potentiation, a form of synaptic plasticity that might constitute the circuit's emotional learning functions (LeDoux, 1993).

On the other hand, the right putamen came across as the hub subcortical region interacting with NA's cortical neural substrates (see Fig 5.5b and Figure 5.6b). Putamen forms a part of basal ganglia, which is known to be involved in emotional regulation. A recent study by Eimontaite et al. (2019) found that left amygdala activation may indicate an increase in cooperative behavior and emotion augmentation, and the left putamen may help suppress an

emotion to engage in cooperation. Our study suggests the role of the right amygdala during PA and right putamen during NA. The differential lateralization of the current research with the study mentioned above can be due to the present study's resting-state nature.

Further, the left hippocampus appeared to play a part as the subcortical substrate for both PA and NA. A plausible explanation for the association of the left hippocampus with both PA and NA is that memories of the past can influence an individual's current affective mood state. Hippocampus is a significant contributor to keeping memories of past events (Hamm & Mattfeld, 2019; Squire et al., 2010). Many studies (Dolcos, Labar, & Cabeza, 2005; Phelps, 2004; Richardson, Strange, & Dolan, 2004; Zheng et al., 2017) suggest that the amygdala, in combination with the hippocampus and prefrontal cortex, plays a vital role in the retrieval of memories for emotional events. Together they act in concert when emotion meets memory. In the present study, we postulate that the dynamics of the amygdala and Hippocampus interactions are associated with the positive event's memory, which gets translated to the current resting positive affect score for an individual. In contrast, the putamen and hippocampus system might transform memories of adverse events to current resting negative affect.

### *5.5.3 FRONTAL AND TEMPORAL REGIONS' ROLE IN PA AND NA*

The temporal and frontal regions for PA and NA interacted significantly with the subcortical neural substrates. The left-lateralized parahippocampal gyrus (posterior division), connected considerably with the amygdala and Hippocampus for PA. Parahippocampal gyrus is known to be a part of the Papez circuit, one of the significant pathways of the limbic system, involved in cortical control of emotion as well as maintaining new information in memory (Citron, Gray, Critchley, Weekes, & Ferstl, 2014). The parahippocampal gyrus' involvement

signifies its interaction with the amygdala and other subcortical regions for retrieval of emotional memory and transferal of this information for forming the current PA of an individual. The right amygdala also showed connectedness with bilateral inferior frontal gyrus and few temporal regions. The existence of the temporal-amygdala-orbitofrontal network (Catani, Dell'Acqua, & Thiebaut de Schotten, 2013) has also been observed in the limbic system model for the amalgamation of visceral sensation and emotion with semantic memory and behavior.

However, in NA, the frontal orbital cortex and few other frontal regions (prefrontal gyrus) appeared to be significantly connected with the right putamen. Beucke et al. (2013), in their study, observed greater connectivity in the orbitofrontal cortex and putamen. Further, the orbitofrontal cortex's connectivity and putamen positively correlated with global obsessive-compulsive disorder's symptom severity. This substantiates the association of NA with greater connectivity of putamen and further with other frontal regions. The frontal orbital cortex, in addition to other few temporal areas, also found strong connections with the left hippocampus subcortical neural substrate for NA (Ross, Lopresti, Schon, & Stern, 2013). Thus, the memories that form an individual's negative affectivity are managed by the hippocampus-basal ganglia pathway, which has been associated with the domain of emotion and memory in the past (Foerde & Shohamy, 2011; Kafkas & Montaldi, 2015; Xiao & Barbas, 2002).

Thus, in the current study, the high linkage of the temporal, frontal regions with subcortical regions was found for both PA and NA. The frontal and temporal areas form the part of significant pathways of the limbic system, which are responsible for the management of emotion and memory (Kensinger, 2009). NA network, besides, showed connectivity with a few parietal regions (supramarginal gyrus, superior parietal lobule, and precuneous cortex), which was consonant with the study of Rohr et al. (2013). Our results were also equivalent to the study

by Citron et al. (2014). In the study mentioned above, the interaction of valence and arousal was explored at the neural level, during implicit emotion-word processing. The results of this study stated the occurrence of frontal-temporal regions (language network) during the contrast between words and pseudowords. Although ours was a resting-state study, the PANAS questionnaire does involve words like ‘interested,’ ‘distressed,’ ‘ashamed,’ which too may elicit particular valence (positive and negative) and arousal associated with these words and can bring in more connectivity of frontal and temporal regions.

### *5.5.4 THE SPECIFIC ROLE OF BASAL GANGLIA IN BAS AND BIS*

In this study, the critical subcortical neural substrates of BAS were mainly found in the right putamen and left-lateralized thalamus (Figure 5.5c and Fig 5.6c). Putamen forms a part of the striatum, and previous research has exhibited the striatum's crucial roles in high-level processing of learning, reward, and decision-making (Berkman, Lieberman, & Gable, 2009). Graybiel (2017) reported that many cognitive functions count on the striatum and its connectivity between various subcortical and cortical networks. Angelides et al. (2017), in their study, employed ROI-to-ROI functional connectivity analysis for assessing the neural mechanisms of appetitive motivation and approach behavior as reflected in BIS/BAS measures during resting-state. Their results demonstrated a correlation between BAS-fun seeking and resting-state connectivity between the middle orbitofrontal cortex and putamen. This observation is in line with our results for integrated BAS scores wherein bi-lateralized putamen formed higher connections with medial and orbitofrontal regions. Also, the right and left putamen is significantly connected to the anterior division of the insula. This confirms that the functional link for BAS measure is driven by putamen during resting-state.

On the other hand, BIS was driven by right-lateralized caudate and left-lateralized accumbens and thalamus at the sub-cortical level (Figure 5.5d and Fig 5.6d). Carretié et al. (2009) demonstrated that the caudate nucleus was sensitive to negative pictures compared to positive and neutral images. Their study concluded that striatum (specifically caudate) plays a crucial role in withdrawal situations. Caudate activation has been shown to interfere with the elaboration of goal-directed behavior (Aron et al., 2003; Jahanshahi, Obeso, Rothwell, & Obeso, 2015). In another study, the indirect pathway from the caudate tail was found to mediate the rejection of bad objects in the periphery (Amita & Hikosaka, 2019). Moreover, the ventral striatum's (accumbens) role in controlling behavioral inhibition has been studied in the past (Guyer et al., 2006; Verharen, Van Den Heuvel, Luijendijk, Vanderschuren, & Adan, 2019). Our study thus confirms the role of the dorsal striatum (caudate) and ventral striatum (accumbens) in constantly comparing perceptual inputs with representations of goals and detection of goal conflicts.

### *5.5.5 ROLE OF ANTERIOR CINGULATE AND ANTERIOR DIVISION OF INSULA IN BAS AND BIS*

The regions showing significant involvement with the subcortical neural substrates for both BIS were the anterior division of the cingulate gyrus and insular cortex. At the same time, BAS showed connectedness to majorly anterior division of the insular cortex, frontal regions and left thalamus in BAS connected to anterior division of the cingulate gyrus. Anterior cingulate gyrus has been known to control a wide range of behaviors based on reward, punishment, and uncertainty (Monosov, 2017; Orr & Hester, 2012; Swick & Turken, 2002). Our study shows that the anterior cingulate and insula are tightly coupled with the subcortical neural substrates of BIS as compared to BAS.

Further, the anterior insula may be playing an important role in switching between different functional networks, based on current needs, by directing highly connected hubs to activate them or to deactivate them. In their work, Medford and Critchley (2010) reviewed the anterior cingulate and insula's conjoint activity in response and awareness. Thus, the anterior insula and cingulate may be playing a role in the feedback system, which eventually generates the approach/avoidance behavior.

### *5.5.6 POINTER FOR THE EXISTENCE OF FEEDBACK MECHANISM AMONG AFFECTIVE AND APPROACH/WITHDRAWAL STATES*

The involvement of the posterior portion of the insula in both PA and NA and the anterior part of the insula in both approach and withdrawal behavior points to the feedback mechanism which may exist among affective and approach/withdrawal states. Cauda et al. (2011) documented the existence of two major networks for insula in the resting brain. One network connected the anterior insula with the anterior cingulate and to the middle and inferior temporal cortex, and the second links the middle-posterior insula to the sensorimotor, premotor, supplementary motor, and middle posterior cingulate cortices, specifying its linkage with sensorimotor integration. Further, it has been proposed (Craig, 2002; Namkung et al., 2017; Uddin, Nomi, Hébert-Seropian, Ghaziri, & Boucher, 2017) that the integration of visceral information in the insula follows a posterior-to-anterior progression, wherein the primary interoceptive signals are first represented in its posterior portion, then attended in the middle and anterior parts, where integrated perceptual maps of the organism state are more refined. Another study (Ying et al., 2018) on moral disgust suggested the association of posterior insula in primary and anterior insula in the secondary level of moral disgust. Thus the involvement of the posterior portion of the insula, specifically in PA and NA, and the anterior part of the insula in

both approach and withdrawal behavior suggests the existence of a feedback loop among affective and approach/withdrawal states where the affective states in the background involve explicit neural mechanisms for translation into behavior.

## 5.6 CONCLUSION

The present study explores the distinct subcortical-cortical interactions and assesses the asymmetry in functional connections among PA, NA, BAS, and BIS measures. The ROI-to-ROI connectivity revealed the connectivity of subcortical neural substrates of PANAS and BAS-BIS scores with bi-lateralized cortical regions. However, the lateralization of the strength of degree-measures of the cortical-regions vital for subcortical-cortical interaction, a left-hemispheric inclination, was observed for positive affect. Further, higher connectivity within the left-hemisphere was also observed for the left-lateralized critical cortical regions of negative affect. ROI-to-ROI analysis and graph theory analysis revealed the connectedness among the right amygdala, right thalamus, and majorly frontal-temporal regions for PA. The left hippocampus also emerged as a subcortical substrate for PA and connected substantially to the parahippocampal gyrus. Similarily right putamen, left hippocampus, and majorly frontal-temporal regions emerged as having significant interactions for NA. This highlights the importance of emotion and memory associated areas with the affective states. BAS measure constitutes dense coupling of the right putamen, left thalamus, frontal regions, and anterior insula and cingulate regions. At the same time, BIS showed strong connectedness among right caudate, left accumbens, frontal regions, and anterior insula and cingulate regions. These observations strengthen the role of basal ganglia's structures in approach and inhibition tendencies. Further, in our study, the association of posterior insula and major subcortical regions with affective

measures and the linkage of the anterior insula with approach/withdrawal measures underscores the existence of feedback mechanisms among affect and approach/withdrawal measures. This study's key findings may serve as the basis for exploration in the clinical population and during task engagement.

## 5.7 ABBREVIATIONS

| Cortical regions | Abbreviations |
|---|---|
| Inferior frontal gyrus (pars oper.) | IFG (pars oper.) |
| Frontal orbital cortex | FOrbC |
| Frontal pole | FP |
| Precetral gyrus | PreCG |
| Superior frontal gyrus | SFG |
| Middle frontal gyrus | MFG |
| Juxtapositional lobule | JuxtaLC |
| Frontal operculum cortex | FOpercC |
| Subcallosal cortex | SubcalC |
| Postcentral gyrus | PostCG |
| Supramarginal gyrus, anterior division | SMG (ant.) |
| Superior parietal lobule | SPL |
| Supramarginal gyrus, posterior division | SMG (post.) |
| Precuneous cortex | PrecuC |
| Parietal operculum cortex | ParietalOperC |
| Angular gyrus | AG |
| Superior temporal gyrus, anterior division | STG (ant.) |

| | |
|---|---|
| Central operculum cortex | CenOperC |
| Middle temporal gyrus, posterior division | MTG (post.) |
| Middle temporal gyrus, temporooccipital division | MTG (tempocc.) |
| Temporal fusiform cortex, posterior division) | TemFusiformC (post.) |
| Temporal pole | TP |
| Middle temporal gyrus, anterior division | MTG (ant.) |
| Planum temporale | PlanumTemp |
| Inferior temporal gyrus, temporooccipital part | ITG (tempocc.) |
| Inferior temporal gyrus, posterior division | ITG (post.) |
| Superior temporal gyrus, posterior division | STG (post.) |
| Inferior temporal gyrus, anterior division | ITG (ant.) |
| Planum palore | PlanumPal |
| Temporal occipital fusiform gyrus | TemOccFusiformG |
| Occipital fusiform gyrus | OFG |
| Cuneal cortex | CunealC |
| Lateral occipital cortex, superior division | LOccC (sup.) |
| Intracalcarine cortex | ICalC |
| Lingual gyrus | LingualG |
| Lateral occipital cortex, inferior division | LOccC (inf.) |
| Occipital pole | OccPole |
| Parahippocampal gyrus, posterior division | ParaHG (post.) |
| Cingulate gyrus, posterior division | CingG (post.) |
| Insular cortex, posterior division | IC (post.) |
| Paracingulate gyrus | ParacingG |
| Insular cortex, anterior division | IC (ant.) |

| Cingulate gyrus, anterior division | CingG (ant.) |
|---|---|
| **Laterality** | **Abbreviations** |
| L | Left |
| R | Right |

## REFERENCES


Amita, H., & Hikosaka, O. (2019). Indirect pathway from caudate tail mediates rejection of bad objects in periphery. *Science Advances*, *5*(8), 1–8. https://doi.org/10.1126/sciadv.aaw9297

Angelides, N. H., Gupta, J., & Vickery, T. J. (2017). Associating resting-state connectivity with trait impulsivity. *Social Cognitive and Affective Neuroscience*, *12*(6), 1001–1008. https://doi.org/10.1093/scan/nsx031

Aron, A. R., Schlaghecken, F., Fletcher, P. C., Bullmore, E. T., Eimer, M., Barker, R., … Robbins, T. W. (2003). Inhibition of subliminally primed responses is mediated by the caudate and thalamus: Evidence from functional MRI and Huntington's disease. *Brain*, *126*(3), 713–723. https://doi.org/10.1093/brain/awg067

Balconi, M., Falbo, L., & Conte, V. A. (2012). BIS and BAS correlates with psychophysiological and cortical response systems during aversive and appetitive emotional stimuli processing. *Motivation and Emotion*, *36*(2), 218–231. https://doi.org/10.1007/s11031-011-9244-7

Balconi, M., Vanutelli, M. E., & Grippa, E. (2017). Resting state and personality component (BIS/BAS) predict the brain activity (EEG and fNIRS measure) in response to emotional cues. *Brain and Behavior*, *7*(5), 1–15. https://doi.org/10.1002/brb3.686

Banks, S. J., Eddy, K. T., Angstadt, M., Nathan, P. J., & Luan Phan, K. (2007). Amygdala-frontal connectivity during emotion regulation. *Social Cognitive and Affective Neuroscience*, *2*(4), 303–312. https://doi.org/10.1093/scan/nsm029

Baumeister, R. F., Vohs, K. D., DeWall, C. N., & Zhang, L. (2007). How Emotion Shapes Behavior: Feedback, Anticipation, and Reflection, Rather Than Direct Causation. *Personality and Social Psychology Review*, *11*(2), 167–203. https://doi.org/10.1177/1088868307301033

Berkman, E. T., Lieberman, M. D., & Gable, S. L. (2009). BIS, BAS, and response conflict: Testing predictions of the revised reinforcement sensitivity theory. *Personality and Individual Differences*, *46*(5–6), 586–591. https://doi.org/10.1016/j.paid.2008.12.015

Berntson, G. G., Bechara, A., Damasio, H., Tranel, D., & Cacioppo, J. T. (2007). Amygdala contribution to selective dimensions of emotion. *Social Cognitive and Affective Neuroscience*, *2*(2), 123–129. https://doi.org/10.1093/scan/nsm008

Beucke, J. C., Sepulcre, J., Talukdar, T., Linnman, C., Zschenderlein, K., Endrass, T., … Kathmann, N. (2013). Abnormally high degree connectivity of the orbitofrontal cortex in obsessive-compulsive disorder. *JAMA Psychiatry*, *70*(6), 619–629. https://doi.org/10.1001/jamapsychiatry.2013.173

Bonnet, L., Comte, A., Tatu, L., Millot, J. L., Moulin, T., & Medeiros De Bustos, E. (2015). The role of

the amygdala in the perception of positive emotions: An "intensity detector." *Frontiers in Behavioral Neuroscience*, *9*(JULY), 1–12. https://doi.org/10.3389/fnbeh.2015.00178

Calhoun, V. D., Stevens, M. C., Pearlson, G. D., & Kiehl, K. A. (2004). fMRI analysis with the general linear model: Removal of latency-induced amplitude bias by incorporation of hemodynamic derivative terms. *NeuroImage*, *22*(1), 252–257. https://doi.org/10.1016/j.neuroimage.2003.12.029

Carretié, L., Ríos, M., de la Gándara, B. S., Tapia, M., Albert, J., López-Martín, S., & Álvarez-Linera, J. (2009). The striatum beyond reward: caudate responds intensely to unpleasant pictures. *Neuroscience*, *164*(4), 1615–1622. https://doi.org/10.1016/j.neuroscience.2009.09.031

Carver, C. S. (2001). Affect and the functional bases of behavior: On the dimensional structure of affective experience. *Personality and Social Psychology Review*, *5*(4), 345–356. https://doi.org/10.1207/S15327957PSPR0504_4

Carver, C. S., & White, T. L. (1994). Behavioral Inhibition, Behavioral Activation, and Affective Responses to Impending Reward and Punishment: The BIS/BAS Scales. *Journal of Personality and Social Psychology*, *67*(2), 319–333. https://doi.org/10.1037/0022-3514.67.2.319

Catani, M., Dell'Acqua, F., & Thiebaut de Schotten, M. (2013). A revised limbic system model for memory, emotion and behaviour. *Neuroscience and Biobehavioral Reviews*, *37*(8), 1724–1737. https://doi.org/10.1016/j.neubiorev.2013.07.001

Cauda, F., D'Agata, F., Sacco, K., Duca, S., Geminiani, G., & Vercelli, A. (2011). Functional connectivity of the insula in the resting brain. *NeuroImage*, *55*(1), 8–23. https://doi.org/10.1016/j.neuroimage.2010.11.049

Chikazoe, J., Lee, D. H., Kriegeskorte, N., & Anderson, A. K. (2014). Population coding of affect across stimuli, modalities and individuals. *Nature Neuroscience*, *17*(8), 1114–1122. https://doi.org/10.1038/nn.3749

Citron, F. M. M., Abugaber, D., & Herbert, C. (2016). Approach and withdrawal tendencies during written word processing: Effects of task, emotional valence, and emotional arousal. *Frontiers in Psychology*, *6*(JAN), 1–11. https://doi.org/10.3389/fpsyg.2015.01935

Citron, F. M. M., Gray, M. A., Critchley, H. D., Weekes, B. S., & Ferstl, E. C. (2014). Emotional valence and arousal affect reading in an interactive way: Neuroimaging evidence for an approach-withdrawal framework. *Neuropsychologia*, *56*(1), 79–89. https://doi.org/10.1016/j.neuropsychologia.2014.01.002

Coutanche, M. N., & Thompson-Schill, S. L. (2015). Creating concepts from converging features in human cortex. *Cerebral Cortex*, *25*(9), 2584–2593. https://doi.org/10.1093/cercor/bhu057

Craig, A. D. (2002). How do you feel? Interoception: The sense of the physiological condition of the body. *Nature Reviews Neuroscience*, *3*(8), 655–666. https://doi.org/10.1038/nrn894

Crawford, J. R., & Henry, J. D. (2004). The Positive and Negative Affect Schedule (PANAS): Construct validity, measurement properties and normative data in a large non-clinical sample. *British Journal of Clinical Psychology*, *43*(3), 245–265. https://doi.org/10.1348/0144665031752934

D'Mello, S., Lehman, B., Pekrun, R., & Graesser, A. (2014). Confusion can be beneficial for learning. *Learning and Instruction*, *29*, 153–170. https://doi.org/10.1016/j.learninstruc.2012.05.003

Davidson, J. (1992). *Anterior cerebral asymmetry and the nature of emotion*. *151*, 125–151.

Davidson, R. J., Saron, C. D., Senulis, J. A., Ekman, P., & Friesen, W. V. (1990). Approach/withdrawal and cerebral asymmetry: Emotional\rexpression and brain physiology: I. *Journal of Personality and Social Psychology*, *58*(2), 330–341. https://doi.org/10.1037/0022-3514.58.2.330

Dolcos, F., Labar, K. S., & Cabeza, R. (2005). Remembering one year later: Role of the amygdala and the medial temporal lobe memory system in retrieving emotional memories. *Proceedings of the National Academy of Sciences of the United States of America*, *102*(7), 2626–2631. https://doi.org/10.1073/pnas.0409848102

Eimontaite, I., Schindler, I., De Marco, M., Duzzi, D., Venneri, A., & Goel, V. (2019). Left amygdala and putamen activation modulate emotion driven decisions in the iterated prisoner's dilemma game. *Frontiers in Neuroscience*, *13*(JUL), 1–12. https://doi.org/10.3389/fnins.2019.00741

Farahani, F. V., Karwowski, W., & Lighthall, N. R. (2019). Application of graph theory for identifying connectivity patterns in human brain networks: A systematic review. *Frontiers in Neuroscience*, *13*(JUN), 1–27. https://doi.org/10.3389/fnins.2019.00585

Fliessbach, K., Buerger, C., Trautner, P., Elger, C. E., & Weber, B. (2010). Differential effects of semantic processing on memory encoding. *Human Brain Mapping*, *31*(11), 1653–1664. https://doi.org/10.1002/hbm.20969

Foerde, K., & Shohamy, D. (2011). The role of the basal ganglia in learning and memory: Insight from Parkinson's disease. *Neurobiology of Learning and Memory*, *96*(4), 624–636. https://doi.org/10.1016/j.nlm.2011.08.006

Gable, S. L., Reis, H. T., & Elliot, A. J. (2000). Behavioral activation and inhibition in everyday life. *Journal of Personality and Social Psychology*, *78*(6), 1135–1149. https://doi.org/10.1037/0022-3514.78.6.1135

Gomez, A., & Gomez, R. (2002). Personality traits of the behavioural approach and inhibition systems: Associations with processing of emotional stimuli. *Personality and Individual Differences*, *32*(8), 1299–1316. https://doi.org/10.1016/S0191-8869(01)00119-2

Graybiel, A. M. (2017). Chapter 10 - The Basal Ganglia. *Conn's Translational Neuroscience*, 219–225. https://doi.org/10.1016/B978-0-12-802381-5.00018-X

Grossman, S., Yeagle, E. M., Harel, M., Espinal, E., Harpaz, R., Noy, N., … Malach, R. (2019). The Noisy Brain: Power of Resting-State Fluctuations Predicts Individual Recognition Performance. *Cell Reports*, *29*(12), 3775-3784.e4. https://doi.org/10.1016/j.celrep.2019.11.081

Guyer, A. E., Nelson, E. E., Perez-Edgar, K., Hardin, M. G., Roberson-Nay, R., Monk, C. S., … Ernst, M. (2006). Striatal functional alteration in adolescents characterized by early childhood behavioral inhibition. *Journal of Neuroscience*, *26*(24), 6399–6405. https://doi.org/10.1523/JNEUROSCI.0666-06.2006

Hamm, A. G., & Mattfeld, A. T. (2019). Distinct Neural Circuits Underlie Prospective and Concurrent Memory-Guided Behavior. *Cell Reports*, *28*(10), 2541-2553.e4. https://doi.org/10.1016/j.celrep.2019.08.002

Hasson, U., Nusbaum, H. C., & Small, S. L. (2009). Task-dependent organization of brain regions active during rest. *Proceedings of the National Academy of Sciences of the United States of America*, *106*(26), 10841–10846. https://doi.org/10.1073/pnas.0903253106

Helfinstein, S. M., Fox, N. A., & Pine, D. S. (2012). Approach-withdrawal and the role of the striatum in the temperament of behavioral inhibition. *Developmental Psychology*, *48*(3), 815–826. https://doi.org/10.1037/a0026402

Henk, A., & Elliot, A. J. (2012). Goal-Directed Behavior. In *Frontiers of Social Psychology*.

Jahanshahi, M., Obeso, I., Rothwell, J. C., & Obeso, J. A. (2015). A fronto-striato-subthalamic-pallidal network for goal-directed and habitual inhibition. *Nature Reviews Neuroscience*, *16*(12), 719–732. https://doi.org/10.1038/nrn4038

Kafkas, A., & Montaldi, D. (2015). Striatal and midbrain connectivity with the hippocampus selectively boosts memory for contextual novelty. *Hippocampus*, *25*(11), 1262–1273. https://doi.org/10.1002/hipo.22434

Kaur, A., Chinnadurai, V., & Chaujar, R. (2020). Microstates-based resting frontal alpha asymmetry approach for understanding affect and approach/withdrawal behavior. *Scientific Reports*, *10*(1), 1–25. https://doi.org/10.1038/s41598-020-61119-7

Kensinger, E. A. (2009). Remembering the details: Effects of emotion. *Emotion Review*, *1*(2), 99–113. https://doi.org/10.1177/1754073908100432

Kensinger, E. A., & Schacter, D. L. (2006). Amygdala activity is associated with the successful encoding of item, but not source, information for positive and negative stimuli. *Journal of Neuroscience*, *26*(9), 2564–2570. https://doi.org/10.1523/JNEUROSCI.5241-05.2006

Killgore, W. D. S., & Yurgelun-Todd, D. A. (2007). The right-hemisphere and valence hypotheses: Could they both be right (and sometimes left)? *Social Cognitive and Affective Neuroscience*, *2*(3), 240–250. https://doi.org/10.1093/scan/nsm020

Kuschpel, M. S., Liu, S., Schad, D. J., Heinzel, S., Heinz, A., & Rapp, M. A. (2015). Differential effects of wakeful rest, music and video game playing on working memory performance in the n-back task. *Frontiers in Psychology*, *6*(OCT), 1–11. https://doi.org/10.3389/fpsyg.2015.01683

Laricchiuta, D., & Petrosini, L. (2014). Individual differences in response to positive and negative stimuli: Endocannabinoid-based insight on approach and avoidance behaviors. *Frontiers in Systems Neuroscience*, *8*(DEC), 1–22. https://doi.org/10.3389/fnsys.2014.00238

LeDoux, J. E. (1993). Emotional memory systems in the brain. *Behavioural Brain Research*, *58*(1–2), 69–79. https://doi.org/10.1016/0166-4328(93)90091-4

Lindquist, K. A., Satpute, A. B., Wager, T. D., Weber, J., & Barrett, L. F. (2016). The Brain Basis of Positive and Negative Affect: Evidence from a Meta-Analysis of the Human Neuroimaging Literature. *Cerebral Cortex*, *26*(5), 1910–1922. https://doi.org/10.1093/cercor/bhv001

López Zunini, R. A., Thivierge, J. P., Kousaie, S., Sheppard, C., & Taler, V. (2013). Alterations in Resting-State Activity Relate to Performance in a Verbal Recognition Task. *PLoS ONE*, *8*(6), 1–8. https://doi.org/10.1371/journal.pone.0065608

Maio, G. R., & Esses, V. M. (2001). The Need for Affect: Individual Differences in the Motivation to Approach or Avoid Emotions. *Journal of Personality*, *69*(4), 583–614. https://doi.org/10.1111/1467-6494.694156

Medford, N., & Critchley, H. D. (2010). Conjoint activity of anterior insular and anterior cingulate cortex: awareness and response. *Brain Structure & Function*, *214*(5–6), 535–549.

https://doi.org/10.1007/s00429-010-0265-x

Meyer, G. J., & Shack, J. R. (1989). Structural Convergence of Mood and Personality: Evidence for Old and New Directions. *Journal of Personality and Social Psychology*, *57*(4), 691–706. https://doi.org/10.1037/0022-3514.57.4.691

Monosov, I. E. (2017). Anterior cingulate is a source of valence-specific information about value and uncertainty. *Nature Communications*, *8*(1), 1–11. https://doi.org/10.1038/s41467-017-00072-y

Naccache, L., Gaillard, R., Adam, C., Hasboun, D., Clémenceau, S., Baulac, M., … Cohen, L. (2005). A direct intracranial record of emotions evoked by subliminal words. *Proceedings of the National Academy of Sciences of the United States of America*, *102*(21), 7713–7717. https://doi.org/10.1073/pnas.0500542102

Namkung, H., Kim, S. H., & Sawa, A. (2017). The Insula: An Underestimated Brain Area in Clinical Neuroscience, Psychiatry, and Neurology. *Trends in Neurosciences*, *40*(4), 200–207. https://doi.org/10.1016/j.tins.2017.02.002

Okada, G., Okamoto, Y., Kunisato, Y., Aoyama, S., Nishiyama, Y., Yoshimura, S., … Yamawaki, S. (2011). The effect of negative and positive emotionality on associative memory: An fMRI study. *PLoS ONE*, *6*(9). https://doi.org/10.1371/journal.pone.0024862

Orehek, E., Bessarabova, E., Chen, X., & Kruglanski, A. W. (2011). Positive affect as informational feedback in goal pursuit. *Motivation and Emotion*, *35*(1), 44–51. https://doi.org/10.1007/s11031-010-9197-2

Orr, C., & Hester, R. (2012). Error-related anterior cingulate cortex activity and the prediction of conscious error awareness. *Frontiers in Human Neuroscience*, *6*(JUNE 2012), 1–12. https://doi.org/10.3389/fnhum.2012.00177

Osaka, M., Yaoi, K., Minamoto, T., & Osaka, N. (2013). When do negative and positive emotions modulate working memory performance? *Scientific Reports*, *3*, 1–8. https://doi.org/10.1038/srep01375

Phelps, E. A. (2004). Human emotion and memory: Interactions of the amygdala and hippocampal complex. *Current Opinion in Neurobiology*, *14*(2), 198–202. https://doi.org/10.1016/j.conb.2004.03.015

Ralph, M. A. L., Jefferies, E., Patterson, K., & Rogers, T. T. (2016). The neural and computational bases of semantic cognition. *Nature Reviews Neuroscience*, *18*(1), 42–55. https://doi.org/10.1038/nrn.2016.150

Richardson, M. P., Strange, B. A., & Dolan, R. J. (2004). Encoding of emotional memories depends on amygdala and hippocampus and their interactions. *Nature Neuroscience*, *7*(3), 278–285. https://doi.org/10.1038/nn1190

Rohr, C. S., Okon-Singer, H., Craddock, R. C., Villringer, A., & Margulies, D. S. (2013). Affect and the Brain's Functional Organization: A Resting-State Connectivity Approach. *PLoS ONE*, *8*(7). https://doi.org/10.1371/journal.pone.0068015

Ross, R. S., Lopresti, M. L., Schon, K., & Stern, C. E. (2013). Role of the Hippocampus and orbitofrontal cortex during the disambiguation of social cues in working memory. *Cognitive, Affective and Behavioral Neuroscience*, *13*(4), 900–915. https://doi.org/10.3758/s13415-013-0170-x

Schultz, D. H., & Cole, M. W. (2016). Higher intelligence is associated with less task-related brain network reconfiguration. *Journal of Neuroscience*, *36*(33), 8551–8561. https://doi.org/10.1523/JNEUROSCI.0358-16.2016

Squire, L. R., Van Der Horst, A. S., McDuff, S. G. R., Frascino, J. C., Hopkins, R. O., & Mauldin, K. N. (2010). Role of the Hippocampus in remembering the past and imagining the future. *Proceedings of the National Academy of Sciences of the United States of America*, *107*(44), 19044–19048. https://doi.org/10.1073/pnas.1014391107

Swick, D., & Turken, U. (2002). Dissociation between conflict detection and error monitoring in the human anterior cingulate cortex. *Proceedings of the National Academy of Sciences of the United States of America*, *99*(25), 16354–16359. https://doi.org/10.1073/pnas.252521499

Uddin, L. Q., Nomi, J. S., Hébert-Seropian, B., Ghaziri, J., & Boucher, O. (2017). Structure and Function of the Human Insula. *Journal of Clinical Neurophysiology*, *34*(4), 300–306. https://doi.org/10.1097/WNP.0000000000000377

Um, E. R., Plass, J. L., Hayward, E. O., & Homer, B. D. (2012). Emotional Design in Multimedia Learning. *Journal of Educational Psychology*, *104*(2), 485–498. https://doi.org/10.1037/a0026609

Verharen, J. P. H., Van Den Heuvel, M. W., Luijendijk, M., Vanderschuren, & Adan, R. A. H. (2019). Corticolimbic mechanisms of behavioral inhibition under threat of punishment. *Journal of Neuroscience*, *39*(22), 4353–4364. https://doi.org/10.1523/JNEUROSCI.2814-18.2019

Wager, T. D., Keller, M. C., Lacey, S. C., & Jonides, J. (2005). Increased sensitivity in neuroimaging analyses using robust regression. *NeuroImage*, *26*(1), 99–113. https://doi.org/10.1016/j.neuroimage.2005.01.011

Wang, J., Zuo, X., & He, Y. (2010). Graph-based network analysis of resting-state functional MRI. *Frontiers in Systems Neuroscience*, *4*(June), 1–14. https://doi.org/10.3389/fnsys.2010.00016

Watson, D., & Clark, L. A. (1988). *Development and Validation of Brief Measures of Positive and Negative Affect : The PANAS Scales*. *54*(6), 1063–1070.

Whitfield-Gabrieli, S., & Nieto-Castanon, A. (2012). Conn: A Functional Connectivity Toolbox for Correlated and Anticorrelated Brain Networks. *Brain Connectivity*, *2*(3), 125–141. https://doi.org/10.1089/brain.2012.0073

Xiao, D., & Barbas, H. (2002). Pathways for emotions and memory II. Afferent input to the anterior thalamic nuclei from prefrontal, temporal, hypothalamic areas and the basal ganglia in the rhesus monkey. *Thalamus and Related Systems*, *2*(01), 33. https://doi.org/10.1017/s1472928802000304

Ying, X., Luo, J., Chiu, C. yue, Wu, Y., Xu, Y., & Fan, J. (2018). Functional dissociation of the posterior and anterior insula in moral disgust. *Frontiers in Psychology*, *9*(JUN), 1–10. https://doi.org/10.3389/fpsyg.2018.00860

Zelenski, J. M., & Larsen, R. J. (1999). Susceptibility to affect: A comparison of three personality taxonomies. *Journal of Personality*, *67*(5), 761–791. https://doi.org/10.1111/1467-6494.00072

Zheng, J., Anderson, K. L., Leal, S. L., Shestyuk, A., Gulsen, G., Mnatsakanyan, L., … Lin, J. J. (2017). Amygdala-hippocampal dynamics during salient information processing. *Nature Communications*, *8*. https://doi.org/10.1038/ncomms14413

# CHAPTER SIX

# CONCLUSIONS AND RECOMMENDATIONS FOR FUTURE WORK

## 6.1 CONCLUSIONS

The hemispheric asymmetry of cognitive, affective, and several high-order functions is a vital feature of the human brain and offers innumerable directions to explore (Toga et al., 2009). This thesis examines resting-state EEG/fMRI hemispheric asymmetry models and utilizes EEG-fMRI data integration approaches and simultaneous EEG-fMRI acquisitions. Since the EEG data used to estimate the resting-state EEG hemispheric models was recorded simultaneously with fMRI, we devised an EEG preprocessing pipeline streamlined to mitigate the Magnetic resonance gradient artifact, Cardioballistic artifact, and other conventional EEG-related artifacts, which is enclosed in **Chapter two**. The chapter also validated the pipeline by estimating the power spectrum from 0-50 Hz and analyzing the quality report generated after the supervised usage of functionalities of The Harvard Automated Processing Pipeline for Electroencephalography toolbox (Gabard-Durnam et al., 2018). The chapter concluded that the final artifact corrected data was appropriately cleaned without any significant loss of data following this pipeline's use.

Next, primarily in this thesis, the EEG-based resting-state hemispheric asymmetry models were estimated. Further, their capability to comprehend the human response to an external task, and the potential of their real-time recordings to reflect specific human psychological states was gauged, for application in domains such as military/aviation. EEG measurements hold the advantage of being cheap, non-invasive, portable, and has a high

temporal resolution to enable real-time recordings. Though fMRI has a high spatial resolution, it is still costly, non-portable, and thus not fit for real-time recordings (Rosa et al., 2010). Therefore, for these EEG-based resting-state hemispheric asymmetry models, we utilized the EEG-informed fMRI approach for further exploring the mapping between EEG and fMRI, which might aid the use of these models for real-time applications while still restoring the related fMRI features.

The resting-state frontal asymmetry model based on EEG's alpha signature was first examined before a Situational Awareness (SA) task, and its linkage with the SA-task outcome was tested in **Chapter three**. SA has gained considerable attention in the field of ergonomics, and is vital for operation in the military/aviation domain (Sarter, 1990; Wickens, 2002). Thus assessing the linkage of SA with pre-task parameters may improve SA. The chapter concluded a strong association of the neural mechanisms underlying pre-SA task resting alpha power and its frontal asymmetry model with subsequently performed SA-task which was designed to have influence from Stroop effect. Hence, the pre-task resting alpha frontal asymmetry displayed potential as a reliable parameter that can be estimated to assess an individual's performance in the tasks involving the maintenance of good situational awareness. The following were the key highlights of this work:

- The performance measures of SA-task, i.e., the reaction time and the SA-index correlated positively with the measure of pre-task resting frontal alpha hemispheric asymmetry, suggesting that pre-task alpha frontal asymmetry is a vital parameter that, when observed before tasks calling for the maintenance of good SA, can reduce human errors associated with the task.

- Further, the functional connectivity analysis revealed a strong association of the neural underpinnings of pre-task resting alpha and its frontal asymmetry with visual, memory, and high-order cognition underpinnings of the SA task. In specifics, connectivity analysis among the neural underpinnings of pre-task frontal alpha asymmetry and SA task divulged that the pre-task frontal alpha asymmetry parameters could cause modulation in the integration of perceived contextual information, emotion, and retrieval of memory associated with the situational awareness.

Following the assessment of the effect of neural mechanisms of resting frontal alpha asymmetry model on subsequently performed SA-task, the connectedness of this model with self-reported measures of affect and approach/withdrawal behavior was assessed. Frontal alpha asymmetry assessed during task engagement and in the clinical population has been linked to affect and approach/withdrawal behavior (Reznik & Allen, 2017). However, the standard resting frontal alpha asymmetry model's linkage with these measures of affect and approach/withdrawal behavior in healthy population is dubious. Our analysis also concluded no association of standard resting frontal alpha asymmetry model, and it’s Hemodynamic Lateralization Index (HLI) (assessed from the neural underpinnings of standard resting frontal alpha asymmetry model) with affect and approach/withdrawal behavior.

We further hypothesized that EEG patterns' stability might be one of the vital methodological parameters responsible for the inconsistent results obtained for the association of standard resting frontal alpha asymmetry model with affect and approach/withdrawal behavior as unstable EEG patterns might possess interference from other cognitive processes. Thus, we assessed a novel microstates-based resting frontal alpha asymmetry model as EEG microstates

are short durations of stable scalp topography (Khanna, 2016). The study is encompassed in **Chapter four** and concluded that the microstates-based resting frontal alpha asymmetry model better assess the mechanisms of affect and approach/withdrawal behavior and can potentially reflect them in real-time analysis. The vital highlights from this study were:

- The negative affect scores' robust positive correlation exclusively with resting microstates-based frontal alpha asymmetry and its negative correlation with hemodynamic lateralization of microstates' temporal neural underpinning revealed that the degree of coordinated neuronal activity underlying alpha underpinnings is better represented by the quasi-stable microstates topographies.
- The linkage between hemodynamic lateralization of microstates' neural underpinnings and the positive affect, approach, and withdrawal measures concluded that the synchronized firing of neurons as assessed by the quasi-stable resting microstates-based frontal alpha asymmetry better explains the neural mechanisms of affect and approach/withdrawal dichotomy.
- The analysis also concluded the involvement of processes of alpha synchronization and desynchronization among the neural underpinnings of microstates as well as standard alpha asymmetry measures. However, precisely the microstates neural underpinnings whose hemodynamic lateralization correlated with negative affect and inhibition behavior involved alpha-BOLD desynchronization; however, the positive affect and approach relevant regions involved alpha-BOLD synchronization as well as desynchronization.

After analyzing the association of EEG based resting hemispheric asymmetry models with affect and approach/withdrawal dichotomy, our objective was to assess the critical role of

subcortical structures, their interactions with cortical areas and functional hemispheric asymmetry of cortical regions vital for subcortical-cortical interactions dominating affect and approach/withdrawal behavior. As it is challenging to capture stronger subcortical signals using conventional 32-channel EEG (Seeber et al., 2019), this study, as included in **Chapter five,** was exclusively based on estimating the hemispheric asymmetry model from resting fMRI graph theory functional connectivity metrics. The following key findings may form the basis for task-based studies and in the clinical population:

- The ROI-to-ROI connectivity revealed the connectivity of subcortical neural substrates of affect and approach/withdrawal behavior with bi-lateralized cortical regions. However, the hemispheric asymmetry index based on the degree measure of functional connectivity analysis revealed the left hemisphere's dense connectedness for affective measures. This also goes in line with Chapter four's observation, where the nature of the correlation of negative affect with microstates-based frontal alpha asymmetry measure and its HLI indicated its significant interactions with the left hemisphere.
- Further, the specific role of subcortical structures and subcortical-cortical interactions dominating the positive and negative affect, approach, and withdrawal behavior was deciphered, and it was concluded that:
    - ► The right amygdala, right thalamus, and majorly frontal-temporal regions showed dense connectivity for positive affect.
    - ► The right putamen left hippocampus, and majorly frontal-temporal regions emerged as having significant interactions for negative affect. This highlights the importance of emotion and memory associated areas with the affective states.

- ► Approach measure constituted dense coupling of the right putamen, left thalamus, frontal regions, anterior insula, and anterior cingulate regions. Also, inhibition measures showed strong connectedness among right caudate, left accumbens, frontal regions, anterior insula, and anterior cingulate regions. These observations strengthen the role of basal ganglia's structures in approach and inhibition tendencies.

## 6.2 RECOMMENDATIONS FOR FUTURE WORK

This thesis's main objective was to estimate the resting EEG/fMRI hemispheric asymmetry models and gauge their capability to understand and influence human actions during task-engagement and to assess the potential of their real-time recordings to reflect specific human psychological states. Though these objectives were majorly accomplished, still, the following aspects can be explored in the future.

- **Demographic Effect:** The current research work involves healthy volunteers from the Indian urban population. Thus, it is required to observe the results presented here in a larger population dataset, which includes individuals from various cultural, ethnic, and social backgrounds.
- **Additional state-trait variables for SA:** The association of standard resting asymmetry measures with other state and trait measures such as anxiety, curiosity, fatigue can be explored in future studies.
- **EEG referencing out-turn on microstate analysis:** Future works can incorporate the role of different EEG referencing schemes on microstate based estimations of frontal asymmetry measures and thus in elucidating EEG frequency signatures and topographies.

- **Validation in a clinical population and task studies:** The results presented for various hemispheric asymmetry models can be tested further for studies involving mood-induction tasks as well as in the clinical population.

## REFERENCES


Gabard-Durnam, L. J., Leal, A. S. M., Wilkinson, C. L., & Levin, A. R. (2018). The harvard automated processing pipeline for electroencephalography (HAPPE): Standardized processing software for developmental and high-artifact data. *Frontiers in Neuroscience*, *12*(February), 1–24. https://doi.org/10.3389/fnins.2018.00097

Khanna, A. (2016). *Microstates in Resting-State EEG: Current Status and Future Directions*. 105–113. https://doi.org/10.1016/j.neubiorev.2014.12.010.Microstates

Reznik, S. J., & Allen, J. J. B. (2017). Frontal asymmetry as a mediator and moderator of emotion: An updated review. *Psychophysiology*, *January*. https://doi.org/10.1111/psyp.12965

Rosa, M. J., Daunizeau, J., & Friston, K. J. (2010). EEG-fMRI integration: A critical review of biophysical modeling and data analysis approaches. *Journal of Integrative Neuroscience*, *9*(4), 453–476. https://doi.org/10.1142/S0219635210002512

Sarter, N. B. (1990). Situation awareness. A critical but ill-defined phenomenon. *Proceedings of the Human Factors Society*, 23.

Seeber, M., Cantonas, L. M., Hoevels, M., Sesia, T., Visser-Vandewalle, V., & Michel, C. M. (2019). Subcortical electrophysiological activity is detectable with high-density EEG source imaging. *Nature Communications*, *10*(1), 1–7. https://doi.org/10.1038/s41467-019-08725-w

Toga, A. W., Narr, K. L., Thompson, P. M., & Luders, E. (2009). Brain asymmetry: Evolution. *Encyclopedia of Neuroscience*, 303–311. https://doi.org/10.1016/B978-008045046-9.00936-0

Wickens, C. D. (2002). Situation awareness and workload in aviation. *Current Directions in Psychological Science*, *11*(4), 128–133. https://doi.org/10.1111/1467-8721.00184

# APPENDICES

# APPENDIX 1: SUPPLEMENTARY MATERIAL FOR CHAPTER THREE

**Supplementary Table S3.1** Correlation (r) and Significance (p) values for electrodes finding strong correlation of their PRAA with behavioral SA Index (Kaur et al., 2019).

| **Electrodes** | **Pearson correlation** | | **Spearman correlation** | | **Skipped correlation** | |
|---|---|---|---|---|---|---|
| | r | p | r | p | r | t |
| Fp2 | 0.58 | 0.01 | 0.55 | 0.01 | 0.55 | 2.69 |
| C4 | 0.52 | 0.02 | 0.5 | 0.03 | 0.64 | 3.37 |
| O1 | 0.53 | 0.02 | 0.52 | 0.02 | 0.71 | 4.05 |
| SP7 | 0.53 | 0.02 | 0.48 | 0.04 | 0.6 | 3.07 |
| Pz | 0.53 | 0.02 | 0.48 | 0.04 | 0.63 | 3.32 |
| Oz | 0.53 | 0.02 | 0.5 | 0.03 | 0.49 | 2.3 |
| Cp1 | 0.53 | 0.02 | 0.5 | 0.03 | 0.43 | 1.91 |
| POz | 0.58 | 0.01 | 0.57 | 0.01 | 0.77 | 4.91 |

**Supplementary Table S3.2** Neural underpinnings of Situational Awareness (SA) task. The activations are represented at FWE Corrected p<0.05. The coordinates reported are in Montreal Neurological Institute (MNI) space (Kaur et al., 2019).

| REGION LABEL | CLUSTER NUMBER | EXTENT | T-VALUE | MNI COORDINATES | | | LATERALITY |
|---|---|---|---|---|---|---|---|
| | | | | X | Y | Z | |
| **FRONTAL LOBE** | | | | | | | |
| Superior Frontal Gyrus | 1 | 636 | 22.727 | 2 | 22 | 50 | L |
| Inferior Frontal Gyrus, pars opercularis | 1 | 219 | 26.867 | -44 | 6 | 26 | L |
| Middle Frontal Gyrus | 1 | 211 | 29.805 | -30 | -6 | 54 | L |
| Precentral Gyrus | 2 | 127 | 24.759 | 36 | -2 | 58 | R |
| | 1 | 124 | 24.492 | -52 | -8 | 48 | L |
| | 2 | 124 | 24.413 | -38 | -18 | 62 | L |
| | 3 | 30 | 19.234 | 44 | 8 | 32 | R |
| **PARIETAL LOBE** | | | | | | | |
| Precuneous Cortex | 1 | 18 | 21.188 | -8 | -56 | 64 | L |
| | 2 | 8 | 19.876 | 6 | -50 | 54 | R |
| | 3 | 5 | 19.848 | -4 | -44 | 60 | L |
| Superior Parietal Lobule | 1 | 8 | 18.979 | -30 | -44 | 44 | L |
| Parietal Operculum Cortex | 1 | 7 | 18.391 | -60 | -26 | 18 | L |
| **TEMPORAL LOBE** | | | | | | | |
| Inferior Temporal Gyrus, temporooccipital part | 1 | 8 | 20.546 | -44 | -50 | -10 | L |
| **OCCIPITAL LOBE** | | | | | | | |
| Occipital fusiform gyrus | 1 | 3843 | 46.216 | -28 | -70 | -12 | L |
| | 2 | 1452 | 44.349 | 26 | -76 | -12 | R |
| Lateral Occipital Cortex, inferior division | 1 | 3843 | 38.899 | -40 | -84 | 8 | L |
| Intracalcarine Cortex | 1 | 3843 | 36.932 | 4 | -86 | 2 | R |
| | 2 | 12 | 17.864 | -16 | -64 | 10 | L |
| Temporal Occipital Fusiform Cortex | 1 | 1452 | 43.344 | 28 | -50 | -14 | R |
| Lateral Occipital Cortex, superior division | 1 | 1452 | 42.125 | 38 | -82 | 12 | R |

| | | | | | | | |
|---|---|---|---|---|---|---|---|
| | 2 | 219 | 42.358 | 28 | -58 | 54 | R |
| | 3 | 145 | 19.302 | 32 | -86 | 24 | R |
| | 4 | 138 | 31.954 | 16 | -66 | 62 | R |
| Juxtapositional Lobule Cortex | 1 | 636 | 32.122 | -4 | -2 | 52 | L |
| **SUBCORTICAL REGIONS** | | | | | | | |
| Right Thalamus | 1 | 9 | 19.081 | 10 | -16 | 8 | |

**Supplementary Table S3.3** Neural underpinnings of pre-task resting alpha frontal asymmetry (PRAFA) through EEG informing SA-task based fMRI. The activations are represented at uncorrected p<0.001. The coordinates reported are in MNI space (Kaur et al., 2019).

| REGION LABEL | CLUSTER NUMBER | EXTENT | T-VALUE | MNI COORDINATES | | | LATERALITY |
|---|---|---|---|---|---|---|---|
| | | | | X | Y | Z | |
| **PARIETAL LOBE** | | | | | | | |
| Precuneous cortex | 1 | 23 | 16.08 | 12 | -50 | 14 | R |
| Parietal operculum cortex | 1 | 6 | 17.995 | -36 | -32 | 20 | L |
| **LIMBIC LOBE** | | | | | | | |
| Parahippocampal gyrus, posterior division | 1 | 23 | 28.405 | -18 | -30 | -20 | L |
| Insular cortex | 1 | 7 | 16.96 | -36 | 8 | -16 | L |

**Supplementary Table S3.4** Neural underpinnings of pre-task resting absolute alpha (PRAA) power through EEG informing SA-task based fMRI. The activations are represented at uncorrected p<0.001. The coordinates reported are in MNI space (Kaur et al., 2019).

| REGION LABEL | CLUSTER NUMBER | EXTENT | T-VALUE | MNI COORDINATES | | | LATERALITY |
|---|---|---|---|---|---|---|---|
| | | | | X | Y | Z | |
| **FRONTAL LOBE** | | | | | | | |
| Frontal Pole | 1 | 88 | 22.631 | 22 | 40 | 44 | R |
| | 2 | 45 | 23.765 | -20 | 44 | 42 | L |
| | 3 | 30 | 23.64 | 36 | 60 | 12 | R |
| | 4 | 27 | 25.706 | 38 | 50 | -18 | R |
| | 5 | 25 | 52.7 | -12 | 68 | 6 | L |
| | 6 | 16 | 16.718 | 26 | 36 | -20 | R |
| Middle Frontal Gyrus | 1 | 88 | 21.838 | 26 | 18 | 48 | R |
| | 2 | 22 | 23.402 | 40 | 10 | 50 | R |
| | 3 | 14 | 18.613 | -42 | 14 | 46 | L |
| | 4 | 12 | 22.327 | 36 | 4 | 42 | R |
| | 5 | 7 | 14.495 | -34 | 8 | 56 | L |
| | 6 | 6 | 14.621 | -36 | 36 | 34 | L |
| | 7 | 5 | 14.723 | -48 | 20 | 34 | L |
| Superior Frontal Gyrus | 1 | 51 | 25.006 | 2 | 42 | 44 | L |
| | 2 | 26 | 39.144 | -18 | 34 | 52 | L |
| | 3 | 12 | 15.027 | 4 | 14 | 62 | R |
| | 4 | 5 | 13.194 | 22 | 16 | 64 | R |
| Inferior Frontal Gyrus, pars opercularis | 1 | 11 | 19.37 | 44 | 20 | 24 | R |
| **PARIETAL LOBE** | | | | | | | |
| Postcentral Gyrus | 1 | 21 | 24.729 | 50 | -22 | 56 | R |
| | 2 | 19 | 23.454 | 46 | -22 | 44 | R |
| | 3 | 12 | 16.575 | 56 | -12 | 50 | R |
| Precuneous Cortex | 1 | 20 | 23.712 | -6 | -50 | 54 | L |
| Superior Parietal Lobule | 1 | 8 | 14.716 | -30 | -42 | 48 | L |

| | | | | | | | |
|---|---|---|---|---|---|---|---|
| **TEMPORAL LOBE** | | | | | | | |
| Inferior Temporal Gyrus, posterior division | 1 | 115 | 33.605 | 60 | -8 | -34 | R |
| Temporal Fusiform Cortex, posterior division | 1 | 115 | 21.658 | 38 | -10 | -38 | R |
| Middle Temporal Gyrus, posterior division | 1 | 24 | 25.518 | -54 | -46 | 4 | L |
| | 2 | 21 | 27.991 | -62 | -24 | -18 | L |
| | 3 | 8 | 16.989 | 52 | -36 | -2 | R |
| Middle Temporal Gyrus, anterior division | 1 | 20 | 33.302 | 54 | 2 | -38 | R |
| Temporal pole | 1 | 14 | 19.004 | -50 | 6 | -22 | L |
| | 2 | 6 | 17.258 | 42 | 18 | -36 | R |
| | 3 | 6 | 17.203 | -50 | 8 | -32 | L |
| **OCCIPITAL LOBE** | | | | | | | |
| Lateral Occipital Cortex, superior division | 1 | 24 | 16.916 | -38 | -72 | 38 | L |
| **LIMBIC LOBE** | | | | | | | |
| Cingulate Gyrus, posterior division | 1 | 20 | 17.348 | -4 | -20 | 44 | L |
| **SUBCORTICAL REGIONS** | | | | | | | |
| Right Hippocampus | 1 | 20 | 26.765 | 24 | -16 | -24 | |
| Right Thalamus | 1 | 13 | 17.714 | 2 | -24 | 6 | |
| | 2 | 8 | 15.125 | 6 | -18 | 12 | |
| Left Thalamus | 1 | 6 | 17.056 | -4 | -10 | 4 | |

# APPENDIX 2: SUPPLEMENTARY MATERIAL FOR CHAPTER FOUR

**Supplementary Table S4.1** Neural underpinnings of standard FA (channel pair F4/F3). The activations after correction for multiple comparisons are represented at p<.05 (FDR corrected). The coordinates reported are in MNI space (Kaur et al., 2020).

| RIGHT HEMISPHERIC ACTIVATIONS | | | | | | |
|---|---|---|---|---|---|---|
| **REGION LABEL** | **CLUSTER NUMBER** | **EXTENT** | **T-VALUE** | **MNI COORDINATES** | | |
| | | | | **X** | **Y** | **Z** |
| **FRONTAL LOBE** | | | | | | |
| Superior frontal gyrus | 1 | 43 | 4.271 | 22 | 4 | 48 |
| **PARIETAL LOBE** | | | | | | |
| Postcentral gyrus | 1 | 246 | 6.414 | 50 | -20 | 38 |
| | 2 | 97 | 8.087 | 16 | -28 | 44 |
| | 3 | 33 | 3.886 | 14 | -44 | 60 |
| | 4 | 23 | -3.349 | 48 | -26 | 64 |
| Superior parietal lobule | 1 | 48 | 4.345 | 18 | -46 | 64 |
| **TEMPORAL LOBE** | | | | | | |
| Temporal pole | 1 | 20 | -2.74 | 42 | 14 | -32 |
| **OCCIPITAL LOBE** | | | | | | |
| Lateral occipital cortex, superior division | 1 | 96 | -4.214 | 38 | -86 | 14 |
| Lateral occipital cortex, inferior division | 1 | 31 | -2.84 | 36 | -72 | -30 |
| | 2 | 20 | -3.317 | 46 | -80 | 2 |
| Occipital pole | 1 | 96 | -4.04 | 22 | -90 | 26 |
| Intracalcarine cortex | 1 | 27 | -2.747 | 10 | -80 | 10 |

| | | | | | | |
|---|---|---|---|---|---|---|
| **LIMBIC LOBE** | | | | | | |
| Paracingulate gyrus | 1 | 34 | 3.121 | 12 | 50 | 10 |
| Insular cortex | 1 | 38 | 9.396 | 34 | -6 | -2 |
| **LEFT HEMISPHERIC ACTIVATIONS** | | | | | | |
| **REGION LABEL** | **CLUSTER NUMBER** | **EXTENT** | **T-VALUE** | **MNI COORDINATES** | | |
| | | | | **X** | **Y** | **Z** |
| **FRONTAL LOBE** | | | | | | |
| Superior frontal gyrus | 1 | 118 | 7.828 | -24 | -4 | 62 |
| | 2 | 26 | -3.36 | -6 | 56 | 30 |
| Frontal medial cortex | 1 | 117 | -5.587 | -12 | 42 | -10 |
| Frontal orbital cortex | 1 | 60 | -6.658 | -22 | 26 | -18 |
| Precentral gyrus | 1 | 60 | 6.636 | -16 | -26 | 40 |
| Inferior frontal gyrus | 1 | 27 | -3.36 | -46 | 30 | -2 |
| **PARIETAL LOBE** | | | | | | |
| Postcentral gyrus | 1 | 147 | 5.015 | -46 | -26 | 38 |
| | 2 | 36 | 3.992 | -36 | -28 | 70 |
| | 3 | 21 | 2.715 | -62 | -8 | 22 |
| Superior parietal lobule | 1 | 132 | 7.511 | -30 | -46 | 64 |
| **TEMPORAL LOBE** | | | | | | |
| Temporal Occipital Fusiform Cortex | 1 | 159 | -2.946 | -28 | -66 | -22 |
| Temporal Fusiform cortex, posterior division | 1 | 39 | -3.441 | -36 | -14 | -26 |
| **OCCIPITAL LOBE** | | | | | | |
| Occipital fusiform gyrus | 1 | 159 | -3.179 | -22 | -84 | -10 |
| Occipital pole | 1 | 29 | -3.58 | -16 | -90 | 30 |
| | 2 | 20 | -2.736 | -2 | -98 | 0 |
| **LIMBIC LOBE** | | | | | | |
| Cingulate gyrus, posterior division | 1 | 34 | 4.73 | -8 | -54 | 28 |

**Supplementary Table S4.2** Neural underpinnings of standard FTA (channel pair F8/F7). The activations after correction for multiple comparisons are represented at p<.05 (FDR corrected). The coordinates reported are in MNI space (Kaur et al., 2020).

| RIGHT HEMISPHERIC ACTIVATIONS | | | | | | |
|---|---|---|---|---|---|---|
| **REGION LABEL** | **CLUSTER NUMBER** | **EXTENT** | **T-VALUE** | **MNI COORDINATES** | | |
| | | | | **X** | **Y** | **Z** |
| **FRONTAL LOBE** | | | | | | |
| Frontal pole | 1 | 67 | 3.822 | 26 | 54 | 22 |
| | 2 | 385 | -5.757 | 46 | 38 | 10 |
| | 3 | 385 | -5.113 | 30 | 48 | -12 |
| | 4 | 385 | -2.962 | 50 | 44 | -10 |
| Subcallosal cortex | 1 | 25 | 6.522 | 6 | 30 | -4 |
| | 2 | 20 | -3.574 | 6 | 14 | -4 |
| Middle frontal gyrus | 1 | 94 | -8.063 | 50 | 14 | 36 |
| Precentral gyrus | 1 | 27 | -3.411 | 50 | 6 | 40 |
| **PARIETAL LOBE** | | | | | | |
| Precuneous cortex | 1 | 392 | -4.401 | 28 | -52 | 10 |
| | 2 | 392 | -2.89 | 22 | -66 | 26 |
| Supramarginal gyrus, posterior gyrus | 1 | 36 | 3.054 | 64 | -46 | 32 |
| **TEMPORAL LOBE** | | | | | | |
| Inferior temporal gyrys, temporooccipital part | 1 | 39 | -3.061 | 56 | -54 | -14 |
| Central operculum cortex | 1 | 28 | -2.751 | 36 | -12 | 22 |
| **OCCIPITAL LOBE** | | | | | | |
| Cuneal cortex | 1 | 392 | -5.546 | 8 | -78 | 38 |
| Lateral occipital cortex, superior division | 1 | 174 | -6.328 | 34 | -62 | 46 |
| Occipital fusform cortex | 1 | 149 | -4.764 | 26 | -68 | -26 |
| Lingual gyrus | 1 | 210 | -2.931 | 14 | -58 | -4 |
| | 2 | 48 | -2.582 | 2 | -76 | 0 |
| Occipital pole | 1 | 20 | -2.553 | 8 | -96 | 2 |

| | | | | | | |
|---|---|---|---|---|---|---|
| **LIMBIC LOBE** | | | | | | |
| Insular cortex | 1 | 56 | 3.558 | 30 | 20 | 8 |
| **LEFT HEMISPHERIC ACTIVATIONS** | | | | | | |
| **FRONTAL LOBE** | | | | | | |
| Inferior frontal gyrus | 1 | 305 | -3.912 | -50 | 32 | 16 |
| | 2 | 20 | -2.703 | -46 | 16 | 26 |
| Middle frontal gyrus | 1 | 42 | -3.196 | -52 | 22 | 30 |
| | 2 | 21 | -3.502 | -50 | 14 | 36 |
| Frontal operculum cortex | 1 | 46 | 3.808 | -34 | 18 | 12 |
| Precentral gyrus | 1 | 36 | -2.984 | -6 | -26 | 52 |
| | 2 | 22 | -3.16 | -32 | -20 | 72 |
| **PARIETAL LOBE** | | | | | | |
| Supramarginal gyrus, posterior division | 1 | 32 | -2.772 | -36 | -44 | 36 |
| Postcentral gyrus | 1 | 24 | -2.86 | -62 | -14 | 36 |
| **TEMPORAL LOBE** | | | | | | |
| Temporal pole | 1 | 40 | -3.633 | -50 | 10 | -28 |
| **OCCIPITAL LOBE** | | | | | | |
| Occipital pole | 1 | 60 | -2.882 | -4 | -94 | 22 |
| Lateral occipital cortex, superior division | 1 | 26 | -2.893 | -8 | -86 | 38 |
| Lingual gyrus | 1 | 42 | -2.896 | -24 | -54 | 2 |
| **LIMBIC LOBE** | | | | | | |
| | | | | | | |
| Parahippocampal gyrus, posterior division | 1 | 175 | -5.375 | -10 | -38 | -22 |
| Parahippocampal gyrus, anterior division | 1 | 23 | -3.412 | -30 | -10 | -30 |
| Cingulate gyrus, posterior division | 1 | 22 | -2.716 | -10 | -40 | 2 |

**Supplementary Table S4.3** Neural underpinnings of proposed microstate based FA (channel pair F4/F3). The activations after correction for multiple comparisons are represented at p<.05 (FDR corrected). The coordinates reported are in MNI space (Kaur et al., 2020).

| RIGHT HEMISPHERIC ACTIVATIONS | | | | | | |
|---|---|---|---|---|---|---|
| **REGION LABEL** | **CLUSTER NUMBER** | **EXTENT** | **T-VALUE** | **MNI COORDINATES** | | |
| | | | | **X** | **Y** | **Z** |
| **FRONTAL LOBE** | | | | | | |
| Middle frontal gyrus | 1 | 32 | 5.93 | 42 | 34 | 40 |
| | 2 | 26 | 3.035 | 44 | 4 | 58 |
| Superior frontal gyrus | 1 | 24 | 3.421 | 4 | 14 | 60 |
| Frontal operculum cortex | 1 | 20 | 3.036 | 40 | 22 | 4 |
| Frontal medial cortex | 1 | 59 | -6.743 | 4 | 44 | -14 |
| Frontal pole | 1 | 20 | -3.366 | 22 | 48 | 18 |
| **PARIETAL LOBE** | | | | | | |
| Precuneous cortex | 1 | 23 | 4.279 | 6 | -50 | 66 |
| **TEMPORAL LOBE** | | | | | | |
| Temporal occipital fusiform cortex | 1 | 60 | 3.691 | 32 | -40 | -28 |
| Middle temporal gyrus, temporoccipital part | 1 | 42 | 4.211 | 62 | -50 | -8 |
| Inferior temporal gyrus,temporoccipital part | 1 | 22 | 3.538 | 54 | -38 | -18 |
| Central operculum cortex | 1 | 22 | -4.769 | 50 | -8 | 10 |
| Middle temporal gyrus, anterior division | 1 | 23 | -5.849 | 52 | 0 | -36 |
| **OCCIPITAL LOBE** | | | | | | |
| Lateral occipital cortex, superior division | 1 | 64 | 4.138 | 22 | -58 | 48 |
| **LIMBIC LOBE** | | | | | | |
| Insular cortex | 1 | 48 | 6.748 | 40 | 14 | -4 |
| | 2 | 29 | -3.17 | 36 | 2 | 4 |
| Parahippocampal gyrus, posterior division | 1 | 27 | 5.738 | 36 | -28 | -10 |
| Cingulate gyrus, posterior division | 1 | 106 | -3.381 | 8 | -52 | 28 |

| LEFT HEMISPHERIC ACTIVATIONS | | | | | | |
|---|---|---|---|---|---|---|
| **REGION LABEL** | **CLUSTER NUMBER** | **EXTENT** | **T-VALUE** | **MNI COORDINATES** | | |
| | | | | **X** | **Y** | **Z** |
| **FRONTAL LOBE** | | | | | | |
| Inferior frontal gyrus | 1 | 82 | 5.142 | -54 | 10 | 14 |
| Frontal operculum cortex | 1 | 37 | 3.055 | -40 | 24 | 6 |
| Middle frontal gyrus | 1 | 29 | 2.89 | -42 | 30 | 42 |
| | 2 | 42 | -7.953 | -24 | 24 | 36 |
| Frontal pole | 1 | 42 | -4.002 | -22 | 40 | 32 |
| Precentral gyrus | 1 | 41 | -3.66 | -36 | -10 | 66 |
| **PARIETAL LOBE** | | | | | | |
| Supramarginal gyrus, anterior division | 1 | 57 | 3.13 | -60 | -30 | 46 |
| | 2 | 23 | 3.112 | -44 | -36 | 44 |
| Postcentral gyrus | 1 | 23 | 3.168 | -14 | -38 | 76 |
| Supramarginal gyrus, posterior division | 1 | 22 | 3.485 | -54 | -42 | 54 |
| | 2 | 35 | -3.261 | -38 | -48 | 36 |
| Precuneous cortex | 1 | 144 | -4.005 | -4 | -58 | 42 |
| **TEMPORAL LOBE** | | | | | | |
| Temporal fusiform cortex, posterior division | 1 | 66 | 3.132 | -38 | -48 | -32 |
| Inferior temporal gyrus, temporoocipital part | 1 | 23 | 2.967 | -58 | -54 | -14 |
| **OCCIPITAL LOBE** | | | | | | |
| Lateral occipital cortex, superior division | 1 | 74 | 4.041 | -42 | -74 | 28 |
| | 2 | 50 | 2.992 | -28 | -62 | 30 |
| | 3 | 41 | 3.427 | -30 | -78 | 36 |
| Lateral occipital cortex, inferior division | 1 | 24 | -3.625 | -30 | -82 | -28 |
| Occipital fusiform gyrus | 1 | 21 | -3.382 | -34 | -86 | -20 |
| **LIMBIC LOBE** | | | | | | |
| Parahippocampal Gyrus, posterior division | 1 | 66 | 3.035 | -22 | -36 | -20 |

**Supplementary Table S4.4** Neural underpinnings of proposed microstate based FTA (channel pair F8/F7). The activations after correction for multiple comparisons are represented at p<.05 (FDR corrected). The coordinates reported are in MNI space (Kaur et al., 2020).

| **RIGHT HEMISPHERIC ACTIVATIONS** | | | | | | |
|---|---|---|---|---|---|---|
| **REGION LABEL** | **CLUSTER NUMBER** | **EXTENT** | **T-VALUE** | **MNI COORDINATES** | | |
| | | | | **X** | **Y** | **Z** |
| **FRONTAL LOBE** | | | | | | |
| Frontal medial cortex | 1 | 192 | -11.711 | 2 | 42 | -12 |
| Frontal pole | 1 | 81 | -3.819 | 8 | 50 | 42 |
| | 2 | 25 | -2.958 | 8 | 58 | 14 |
| Subcallosal cortex | 1 | 68 | -4.043 | 6 | 28 | -4 |
| Superior frontal gyrus | 1 | 23 | -3.107 | 16 | 32 | 56 |
| **PARIETAL LOBE** | | | | | | |
| Angular gyrus | 1 | 104 | -3.685 | 50 | -56 | 28 |
| **TEMPORAL LOBE** | | | | | | |
| Planum Temporale | 1 | 124 | -3.416 | 62 | -12 | 6 |
| **OCCIPITAL LOBE** | | | | | | |
| Lingual gyrus | 1 | 20 | -3.676 | 26 | -56 | 2 |
| **LIMBIC LOBE** | | | | | | |
| Cingulate gyrus, posterior division | 1 | 203 | -5.841 | 4 | -44 | 38 |
| Insular cortex | 1 | 124 | -5.241 | 36 | -12 | 14 |
| **LEFT HEMISPHERIC ACTIVATIONS** | | | | | | |
| **REGION LABEL** | **CLUSTER NUMBER** | **EXTENT** | **T-VALUE** | **MNI COORDINATES** | | |
| | | | | **X** | **Y** | **Z** |

| | | | | | | |
|---|---|---|---|---|---|---|
| **FRONTAL LOBE** | | | | | | |
| Middle frontal gyrus | 1 | 25 | 3.014 | -42 | 34 | 24 |
| | 2 | 51 | -3.049 | -26 | 20 | 38 |
| | 3 | 25 | -3.022 | -42 | 18 | 48 |
| Superior Frontal Gyrus | 1 | 138 | -3.021 | -4 | 52 | 36 |
| | 2 | 30 | -4.585 | -6 | 40 | 50 |
| | 3 | 21 | -3.298 | -2 | 14 | 66 |
| Frontal pole | 1 | 138 | -6.323 | -8 | 58 | 14 |
| | 2 | 75 | -3.548 | -20 | 52 | 30 |
| | 3 | 21 | -2.748 | -20 | 44 | 38 |
| Precentral gyrus | 1 | 21 | -2.877 | -36 | -12 | 68 |
| **PARIETAL LOBE** | | | | | | |
| Supramarginal gyrus, anterior division | 1 | 87 | 7.244 | -62 | -28 | 40 |
| | 2 | 41 | 2.927 | -44 | -36 | 46 |
| Angular gyrus | 1 | 181 | -3.641 | -46 | -56 | 54 |
| | 2 | 181 | -3.615 | -58 | -54 | 36 |
| Superior Parietal Lobule | 1 | 181 | -2.478 | -34 | -52 | 38 |
| **TEMPORAL LOBE** | | | | | | |
| Temporal pole | 1 | 47 | -4.092 | -44 | 10 | -36 |
| **OCCIPITAL LOBE** | | | | | | |
| Lateral occipital cortex, inferior division | 1 | 91 | -3.47 | -30 | -88 | -18 |
| **LIMBIC LOBE** | | | | | | |
| Cingulate gyrus, posterior division | 1 | 386 | -5.096 | -6 | -48 | 36 |
| | 2 | 386 | -2.506 | -4 | -44 | 14 |

# APPENDIX 3: SUPPLEMENTARY MATERIAL FOR CHAPTER FIVE

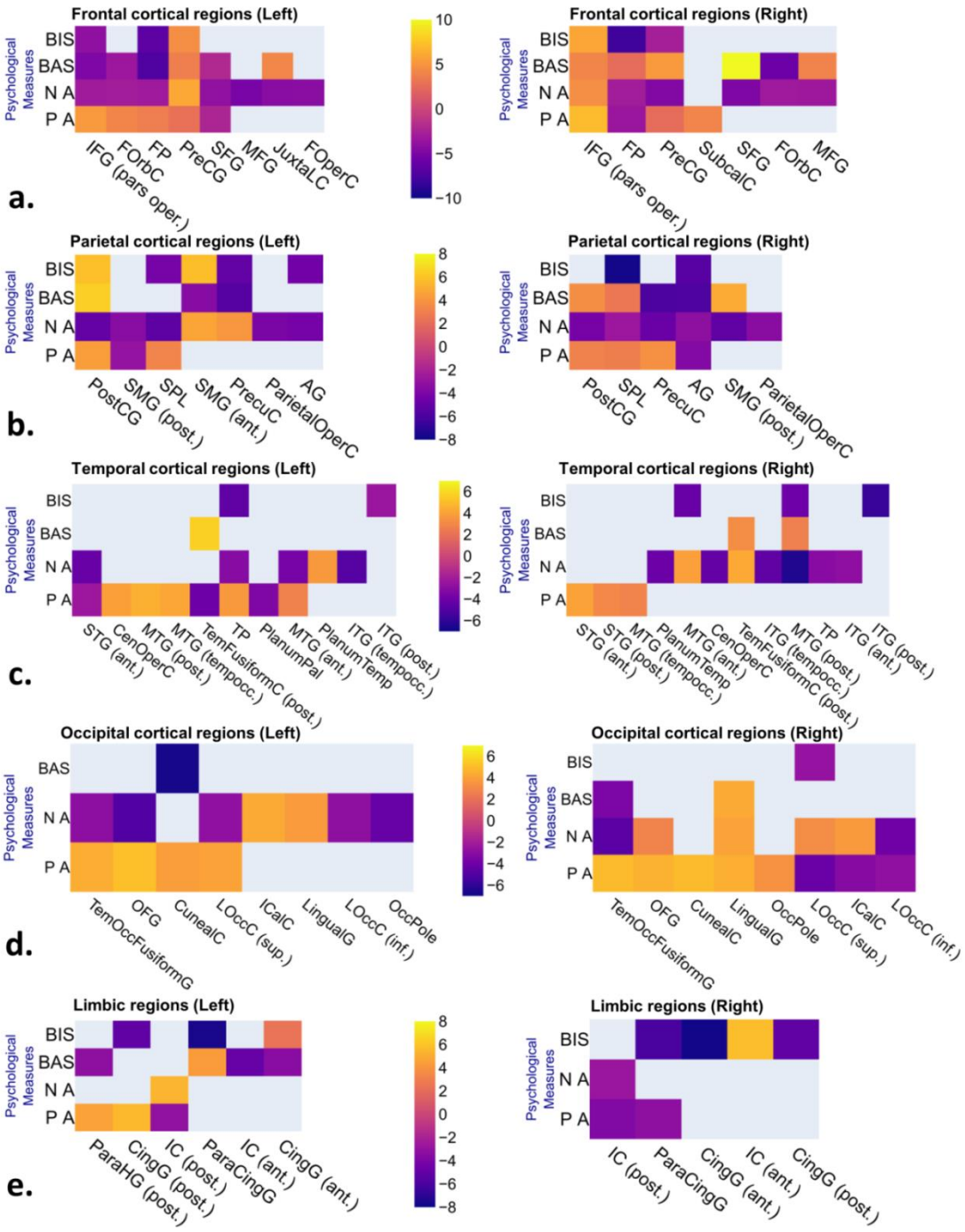


**Supplementary Figure S5.1** Heatmaps for the representation of the t-values of neural substrates of PA, NA, BAS and BIS measures for (a) frontal regions (b) parietal regions (c) temporal regions (d) occipital regions (e) limbic regions.

**Supplementary Table S5.1** Neural substrates of Positive affect (PA). The activations after correction for multiple comparisons are represented at p<.05 (FDR corrected). The coordinates reported are in MNI space.

| REGION LABEL | CLUSTER NUMBER | EXTENT | T-VALUE | MNI COORDINATES | | | LATERALITY |
|---|---|---|---|---|---|---|---|
| | | | | X | Y | Z | |
| **FRONTAL LOBE** | | | | | | | |
| Inferior Frontal Gyrus, pars opercularis | 1 | 580 | 5.24 | -56 | 8 | 0 | L |
| | 2 | 493 | 7.03 | 52 | 18 | -2 | R |
| | 3 | 493 | 3.53 | 54 | 30 | 14 | R |
| Frontal Orbital Cortex | 1 | 580 | 4.10 | -36 | 30 | 0 | L |
| Frontal Pole | 1 | 493 | 4.03 | 38 | 44 | -16 | R |
| | 2 | 35 | 3.99 | -12 | 62 | 22 | L |
| | 3 | 31 | 3.75 | 16 | 68 | 14 | R |
| | 4 | 69 | 3.60 | -46 | 38 | -18 | L |
| | 5 | 69 | -3.43 | 26 | 40 | 42 | R |
| Precentral Gyrus | 1 | 239 | 2.57 | 44 | -12 | 38 | R |
| | 2 | 85 | 2.83 | -24 | -30 | 56 | L |
| | 3 | 82 | 3.24 | 56 | -6 | 46 | R |
| | 4 | 73 | 3.28 | -40 | -16 | 50 | L |
| | 5 | 27 | 2.97 | 12 | -30 | 66 | R |
| Subcallosal Cortex | 1 | 79 | 4.04 | 6 | 30 | -14 | R |
| Superior Frontal Gyrus | 1 | 26 | 3.11 | -22 | -2 | 60 | L |
| | 2 | 78 | -2.31 | -6 | 38 | 36 | L |
| **PARIETAL LOBE** | | | | | | | |
| Postcentral Gyrus | 1 | 239 | 3.09 | 46 | -28 | 64 | R |
| | 2 | 146 | 3.24 | -60 | -10 | 42 | L |
| | 3 | 146 | 2.36 | -50 | -24 | 54 | L |
| | 4 | 85 | 3.76 | -46 | -24 | 64 | L |
| | 5 | 71 | 3.60 | 42 | -30 | 52 | R |
| Supramarginal Gyrus, posterior division | 1 | 174 | 4.38 | -44 | -42 | 42 | L |
| | 2 | 68 | -2.76 | -64 | -44 | 10 | L |
| | 3 | 23 | -3.02 | -64 | -48 | 22 | L |

| | | | | | | | |
|---|---|---|---|---|---|---|---|
| | 4 | 20 | -3.19 | -56 | -46 | 50 | L |
| Superior Parietal Lobule | 1 | 57 | 3.24 | -38 | -52 | 58 | L |
| | 2 | 46 | 2.97 | -36 | -38 | 52 | L |
| | 3 | 21 | 2.92 | 40 | -46 | 66 | R |
| Precuneous Cortex | 1 | 258 | 3.78 | 20 | -52 | 8 | R |
| Angular Gyrus | 1 | 97 | -3.73 | 58 | -46 | 48 | R |
| **TEMPORAL LOBE** | | | | | | | |
| Superior Temporal Gyrus, anterior division | 1 | 580 | -2.33 | -50 | -14 | -6 | L |
| | 2 | 184 | 3.99 | 58 | -2 | -14 | R |
| Central Opercular Cortex | | 580 | 3.93 | -48 | -10 | 8 | L |
| Middle Temporal Gyrus, posterior division | 1 | 112 | 4.49 | -62 | -18 | -24 | L |
| | 2 | 31 | 2.89 | -50 | -36 | -4 | L |
| Superior Temporal Gyrus, posterior division | 1 | 83 | 2.95 | 50 | -28 | 2 | R |
| Middle Temporal Gyrus, temporooccipital part | 1 | 74 | 2.73 | 58 | -56 | 4 | R |
| | 2 | 68 | 4.15 | -62 | -46 | -2 | L |
| Temporal Fusiform Cortex, posterior division | 1 | 53 | -4.07 | -40 | -12 | -34 | L |
| Temporal Pole | 1 | 35 | 3.64 | -50 | 8 | -32 | L |
| | 2 | 24 | 3.21 | -48 | 12 | -22 | L |
| Planum Polare | 1 | 23 | 2.10 | -48 | -2 | -4 | L |
| | 2 | 23 | -3.42 | -48 | -6 | -6 | L |
| Middle Temporal Gyrus, anterior division | 1 | 20 | 2.70 | -48 | 0 | -26 | L |
| **OCCIPITAL LOBE** | | | | | | | |
| Temporal Occipital Fusiform Cortex | 1 | 1693 | 4.41 | -40 | -52 | -22 | L |
| | 2 | 346 | 4.90 | 32 | -40 | -22 | R |
| | 3 | 346 | 3.75 | 44 | -58 | -20 | R |
| Occipital Fusiform Gyrus | 1 | 1693 | 5.10 | -20 | -78 | -8 | L |
| | 2 | 638 | 4.57 | 30 | -82 | -10 | R |
| Cuneal Cortex | 1 | 1178 | 4.88 | 18 | -72 | 26 | R |
| | 2 | 1178 | 4.56 | 10 | -84 | 40 | R |
| | 3 | 52 | 3.81 | -16 | -80 | 34 | L |
| Lingual Gyrus | 1 | 1178 | 4.48 | 4 | -82 | -2 | R |
| | 2 | 638 | 4.59 | 22 | -62 | -10 | R |
| | 3 | 258 | 3.67 | 22 | -40 | -14 | R |
| | 4 | 22 | 3.08 | 0 | -72 | -14 | R |
| Occipital Pole | 1 | 40 | 3.37 | 10 | -96 | 2 | R |
| Lateral Occipital Cortex, superior division | 1 | 62 | 4.05 | -24 | -60 | 64 | L |
| | 2 | 24 | 3.60 | -40 | -76 | 20 | L |
| | 3 | 97 | -4.22 | 36 | -70 | 48 | R |
| | 4 | 23 | 3.57 | 38 | -86 | 10 | R |

| | | | | | | | |
|---|---|---|---|---|---|---|---|
| Intracalcarine Cortex | 1 | 258 | -3.16 | 14 | -64 | 10 | R |
| Lateral Occipital Cortex, inferior division | 1 | 23 | -2.81 | 32 | -86 | 6 | R |
| **LIMBIC LOBE** | | | | | | | |
| Parahippocampal Gyrus, posterior division | 1 | 1693 | 4.57 | -16 | -34 | -12 | L |
| | 2 | 36 | 4.55 | -30 | -26 | -22 | L |
| Cingulate Gyrus, posterior division | 1 | 90 | 5.50 | -12 | -34 | 38 | L |
| | 2 | 90 | -2.06 | -10 | -34 | 42 | L |
| Insular Cortex | 1 | 27 | 3.31 | -42 | -8 | 4 | L |
| | 2 | 43 | -3.10 | -36 | -14 | -4 | L |
| | 3 | 37 | -3.53 | -34 | 0 | 6 | L |
| | 4 | 32 | -3.82 | 36 | -16 | 2 | R |
| | 5 | 27 | -2.65 | -42 | -10 | -2 | L |
| Paracingulate Gyrus | 1 | 42 | -3.25 | 6 | 34 | 38 | R |
| **SUBCORTICAL REGIONS** | | | | | | | |
| Right Amygdala | 1 | 77 | 5.03 | 24 | -6 | -16 | |
| Left Hippocampus | 1 | 1693 | -1.94 | -20 | -30 | -8 | |
| Left Thalamus | 1 | 29 | -3.13 | 0 | -8 | 4 | |
| Right Thalamus | 1 | 28 | -3.84 | 14 | -10 | 4 | |

**Supplementary Table S5.2** Neural substrates of Negative affect (NA). The activations after correction for multiple comparisons are represented at p<.05 (FDR corrected). The coordinates reported are in MNI space.

| REGION LABEL | CLUSTER NUMBER | EXTENT | T-VALUE | MNI COORDINATES | | | LATERALITY |
|---|---|---|---|---|---|---|---|
| | | | | X | Y | Z | |
| **FRONTAL LOBE** | | | | | | | |
| Precentral Gyrus | 1 | 164 | 6.02 | -58 | 6 | 6 | L |
| | 2 | 79 | 4.33 | -36 | -6 | 56 | L |
| | 3 | 23 | 3.87 | 60 | 2 | 12 | R |
| | 4 | 23 | 3.63 | -52 | 8 | 36 | L |
| | 5 | 21 | 3.37 | 58 | 10 | 34 | R |
| | 6 | 151 | -3.82 | -52 | -10 | 46 | L |
| | 7 | 107 | -4.71 | 48 | -10 | 36 | R |
| | 8 | 100 | -3.90 | 22 | -12 | 74 | R |
| | 9 | 100 | -2.17 | 32 | -6 | 56 | R |
| | 10 | 79 | -2.87 | -30 | -10 | 56 | L |
| | 11 | 72 | -3.62 | -6 | -28 | 58 | L |
| | 12 | 46 | -2.94 | 6 | -18 | 48 | R |
| | 13 | 27 | -2.69 | -12 | -22 | 46 | L |
| Superior Frontal Gyrus | 1 | 81 | 2.27 | 20 | -10 | 64 | R |
| | 2 | 33 | 2.88 | -22 | -8 | 68 | L |
| | 3 | 105 | -3.90 | -4 | 26 | 62 | L |
| | 4 | 105 | -2.90 | -6 | 4 | 68 | L |
| | 5 | 92 | -4.88 | 10 | 32 | 58 | R |
| | 6 | 40 | -3.54 | 22 | 10 | 52 | R |
| | 7 | 33 | -3.32 | -24 | 0 | 70 | L |
| Inferior Frontal Gyrus, pars triangularis | 1 | 57 | 4.61 | 54 | 32 | 12 | R |
| | 2 | 164 | -3.04 | -48 | 10 | 10 | L |
| Frontal Orbital Cortex | 1 | 31 | 3.24 | -40 | 18 | -14 | L |
| | 2 | 32 | -2.92 | -24 | 4 | -14 | L |
| | 3 | 20 | -3.10 | 30 | 16 | -18 | R |
| Middle Frontal Gyrus | 1 | 21 | 2.61 | 30 | 20 | 48 | R |

| | | | | | | | |
|---|---|---|---|---|---|---|---|
| | 2 | 138 | -5.18 | -30 | 28 | 48 | L |
| | 3 | 138 | -3.84 | -46 | 24 | 36 | L |
| | 4 | 81 | -3.27 | 30 | 4 | 58 | R |
| | 5 | 21 | -2.56 | 28 | 26 | 44 | R |
| Juxtapositional Lobule Cortex | 1 | 121 | -4.34 | -6 | -6 | 48 | L |
| Frontal Pole | 1 | 111 | -3.11 | -24 | 48 | -12 | L |
| | 2 | 57 | -2.94 | 52 | 40 | 4 | R |
| | 3 | 25 | -3.38 | -4 | 58 | 0 | L |
| Frontal Operculum Cortex | 1 | 106 | -4.25 | -36 | 16 | 10 | L |
| **PARIETAL LOBE** | | | | | | | |
| Supramarginal Gyrus, anterior division | 1 | 491 | 4.67 | -54 | -28 | 42 | L |
| | 2 | 378 | 4.54 | 64 | -18 | 42 | R |
| | 3 | 226 | -5.19 | 64 | -22 | 24 | R |
| | 4 | 21 | -3.14 | 54 | -32 | 34 | R |
| Postcentral Gyrus | 1 | 378 | 3.03 | 48 | -30 | 58 | R |
| | 2 | 226 | 2.22 | 58 | -18 | 28 | R |
| | 3 | 35 | 2.97 | -16 | -38 | 74 | L |
| | 4 | 491 | -4.98 | -42 | -38 | 46 | L |
| | 5 | 378 | -4.25 | 44 | -32 | 52 | R |
| | 6 | 57 | -3.48 | -44 | -22 | 60 | L |
| | 7 | 57 | -2.42 | -22 | -32 | 64 | L |
| | 8 | 35 | -4.28 | -8 | -38 | 78 | L |
| Precuneous Cortex | 1 | 341 | 4.06 | -8 | -68 | 30 | L |
| | 2 | 120 | 2.96 | 20 | -52 | 6 | R |
| | 3 | 34 | 2.96 | 10 | -62 | 24 | R |
| | 4 | 168 | -4.82 | 6 | -74 | 46 | R |
| | 5 | 114 | -4.12 | -4 | -70 | 56 | L |
| | 6 | 34 | -2.24 | 12 | -60 | 22 | R |
| Parietal Operculum Cortex | 1 | 48 | 4.81 | -44 | -24 | 18 | L |
| | 2 | 313 | -4.08 | -44 | -40 | 22 | L |
| | 3 | 24 | -3.44 | 32 | -28 | 20 | R |
| Superior Parietal Lobule | 1 | 491 | -5.20 | -36 | -50 | 64 | L |
| | 2 | 24 | -2.66 | 24 | -46 | 64 | R |
| Supramarginal Gyrus, posterior division | 1 | 313 | -3.51 | -64 | -44 | 30 | L |
| Angular Gyrus | 1 | 185 | -4.26 | -54 | -54 | 16 | L |
| | 2 | 20 | -3.27 | 62 | -50 | 28 | R |
| **TEMPORAL LOBE** | | | | | | | |
| Planum Temporale | 1 | 313 | 3.65 | -62 | -20 | 10 | L |
| | 2 | 313 | -2.71 | -62 | -30 | 12 | L |
| | 3 | 34 | -4.15 | 62 | -12 | 6 | R |

| | | | | | | | |
|---|---|---|---|---|---|---|---|
| Middle Temporal Gyrus, anterior division | 1 | 139 | 3.91 | 64 | -8 | -8 | R |
| | 2 | 97 | 2.22 | -56 | 0 | -30 | L |
| | 3 | 97 | -3.71 | -56 | -4 | -28 | L |
| Central Opercular Cortex | 1 | 64 | 4.13 | 44 | 8 | 6 | R |
| | 2 | 96 | -4.38 | 42 | -18 | 20 | R |
| Temporal Fusiform Cortex, posterior division | 1 | 35 | 4.28 | 24 | -38 | -18 | R |
| Inferior Temporal Gyrus, temporooccipital part | 1 | 566 | -4.49 | 54 | -44 | -16 | R |
| | 2 | 338 | -4.83 | -56 | -54 | -8 | L |
| | 3 | 110 | -4.37 | 62 | -50 | 6 | R |
| Middle Temporal Gyrus, posterior division | 1 | 139 | -6.45 | 66 | -22 | -4 | R |
| Superior Temporal Gyrus, anterior division | 1 | 88 | -4.24 | -54 | 0 | -10 | L |
| Temporal Pole | 1 | 80 | -3.09 | 56 | 10 | -18 | R |
| | 2 | 48 | -3.11 | -46 | 10 | -34 | L |
| Inferior Temporal Gyrus, anterior division | 1 | 26 | -2.87 | 40 | -6 | -36 | R |
| **OCCIPITAL LOBE** | | | | | | | |
| Lateral Occipital Cortex, superior division | 1 | 566 | 3.13 | 46 | -74 | 18 | R |
| | 2 | 51 | 4.00 | -44 | -76 | 26 | L |
| | 3 | 114 | -2.79 | -18 | -80 | 40 | L |
| | 4 | 65 | -3.68 | 16 | -70 | 48 | R |
| | 5 | 42 | -3.30 | 34 | -68 | 34 | R |
| | 6 | 42 | -3.22 | 18 | -82 | 38 | R |
| | 7 | 32 | -3.45 | 18 | -60 | 62 | R |
| | 8 | 28 | -2.69 | -22 | -70 | 38 | L |
| Intracalcarine Cortex | 1 | 341 | 4.28 | -16 | -68 | 6 | L |
| | 2 | 120 | 3.70 | 12 | -72 | 10 | R |
| Lingual Gyrus | 1 | 341 | 3.73 | -14 | -52 | -12 | L |
| | 2 | 99 | 3.99 | 20 | -60 | -14 | R |
| | 3 | 341 | -3.04 | -8 | -62 | 0 | L |
| Occipital Fusiform Gyrus | 1 | 27 | 2.77 | 28 | -74 | -10 | R |
| | 2 | 278 | -5.01 | -14 | -90 | -14 | L |
| | 3 | 27 | -3.98 | 28 | -82 | -10 | R |
| | 4 | 26 | -3.32 | 14 | -86 | -22 | R |
| Temporal Occipital Fusiform Cortex | 1 | 338 | -2.89 | -42 | -48 | -22 | L |
| | 2 | 58 | -4.72 | 38 | -50 | -26 | R |
| Lateral Occipital Cortex, inferior division | 1 | 338 | -2.86 | -46 | -72 | 4 | L |
| | 2 | 278 | -3.84 | -36 | -82 | -14 | L |
| | 3 | 53 | -3.98 | 32 | -84 | 2 | R |
| | 4 | 23 | -3.19 | -44 | -70 | -18 | L |
| Occipital Pole | 1 | 168 | -4.31 | -6 | -90 | 32 | L |
| | 2 | 28 | -4.23 | -14 | -98 | -14 | L |

| | | | | | | | |
|---|---|---|---|---|---|---|---|
| **LIMBIC LOBE** | | | | | | | |
| Insular Cortex | 1 | 109 | 5.34 | -36 | -14 | 8 | L |
| | 2 | 64 | 2.35 | 40 | -14 | 6 | R |
| | 3 | 64 | -2.72 | 42 | -12 | 8 | R |
| | 4 | 54 | -2.34 | -36 | 6 | -8 | L |
| **SUBCORTICAL REGIONS** | | | | | | | |
| Brain-Stem | 1 | 29 | 5.54 | -10 | -44 | -34 | |
| | 2 | 28 | 3.49 | -2 | -36 | -16 | |
| Right Putamen | 1 | 29 | 3.69 | 28 | 0 | -4 | |
| Left Hippocampus | 1 | 33 | -3.54 | -30 | -8 | -26 | |

**Supplementary Table S5.3** Neural substrates of Behavioral activation system (BAS). The activations after correction for multiple comparisons are represented at p<.05 (FDR corrected). The coordinates reported are in MNI space.

| REGION LABEL | CLUSTER NUMBER | EXTENT | T-VALUE | MNI COORDINATES | | | LATERALITY |
|---|---|---|---|---|---|---|---|
| | | | | X | Y | Z | |
| **FRONTAL LOBE** | | | | | | | |
| Superior Frontal Gyrus | 1 | 165 | 10.14 | 16 | 4 | 66 | R |
| | 2 | 165 | 6.70 | 24 | -8 | 52 | R |
| | 3 | 31 | 4.55 | -4 | 42 | 42 | L |
| | 4 | 27 | 3.17 | -22 | 8 | 48 | L |
| | 5 | 26 | 3.77 | 22 | 26 | 44 | R |
| | 6 | 70 | -2.08 | -18 | 22 | 50 | L |
| Frontal Pole | 1 | 82 | 2.56 | 38 | 54 | 0 | R |
| | 2 | 71 | 4.90 | -20 | 44 | 36 | L |
| | 3 | 22 | 2.11 | 24 | 42 | -16 | R |
| | 4 | 186 | -7.24 | -44 | 50 | 8 | L |
| | 5 | 82 | -5.13 | 26 | 54 | 2 | R |
| | 6 | 81 | -3.87 | 44 | 50 | 6 | R |
| | 7 | 47 | -7.40 | -30 | 46 | -16 | L |
| | 8 | 27 | -3.26 | 14 | 54 | 38 | R |
| | 9 | 25 | -4.50 | 20 | 64 | 16 | R |
| | 10 | 22 | -5.10 | 26 | 44 | -14 | R |
| Juxtapositional Lobule Cortex | 1 | 79 | 4.17 | -8 | -6 | 50 | L |
| | 2 | 79 | -2.07 | -6 | -2 | 50 | L |
| Precentral Gyrus | 1 | 39 | 3.70 | -54 | 6 | 24 | L |
| | 2 | 32 | 5.19 | -46 | 2 | 42 | L |
| | 3 | 24 | 5.24 | 62 | 8 | 22 | R |
| | 4 | 21 | 5.61 | 42 | 2 | 34 | R |
| Middle Frontal Gyrus | 1 | 36 | 3.96 | 42 | 26 | 26 | R |
| | 2 | 36 | -6.31 | 44 | 34 | 34 | R |
| Inferior Frontal Gyrus, pars triangularis | 1 | 33 | 4.10 | 52 | 30 | -8 | R |
| Frontal Orbital Cortex | 1 | 27 | 4.46 | 28 | 24 | -6 | R |
| | 2 | 55 | -11.28 | 20 | 28 | -18 | R |

| | | | | | | | |
|---|---|---|---|---|---|---|---|
| | 3 | 34 | -3.31 | -36 | 30 | -14 | L |
| Frontal Medial Cortex | 1 | 105 | -5.91 | 6 | 42 | -14 | R |
| Inferior Frontal Gyrus, pars opercularis | 1 | 34 | -4.94 | -50 | 12 | 4 | L |
| | 2 | 28 | -4.17 | 54 | 22 | 12 | L |
| **PARIETAL LOBE** | | | | | | | |
| Superior Parietal Lobule | 1 | 314 | 2.58 | 34 | -48 | 42 | R |
| | 2 | 109 | 8.62 | 20 | -46 | 62 | R |
| | 3 | 109 | 2.84 | 40 | -40 | 64 | R |
| Postcentral Gyrus | 1 | 105 | 6.43 | -24 | -34 | 72 | L |
| | 2 | 52 | 3.64 | 60 | -6 | 38 | R |
| | 3 | 33 | 4.74 | 44 | -32 | 64 | R |
| | 4 | 105 | -2.09 | -16 | -32 | 64 | L |
| | 5 | 30 | -4.57 | -58 | -8 | 28 | L |
| Supramarginal Gyrus, posterior division | 1 | 66 | 5.00 | 48 | -40 | 52 | R |
| Precuneous Cortex | 1 | 38 | 5.48 | -8 | -62 | 14 | L |
| | 2 | 46 | -5.58 | -8 | -76 | 42 | L |
| | 3 | 26 | -5.94 | 14 | -60 | 28 | R |
| Angular Gyrus | 1 | 314 | -5.87 | 50 | -56 | 38 | R |
| Supramarginal Gyrus, anterior division | 1 | 21 | -3.57 | -60 | -38 | 30 | L |
| **TEMPORAL LOBE** | | | | | | | |
| Temporal Fusiform Cortex, posterior division | 1 | 235 | 3.16 | 26 | -34 | -22 | R |
| | 2 | 45 | 5.65 | -40 | -28 | -24 | L |
| | 3 | 26 | 4.19 | 42 | -30 | -22 | R |
| Middle Temporal Gyrus, posterior division | 1 | 21 | 2.60 | 68 | -34 | -6 | R |
| **OCCIPITAL LOBE** | | | | | | | |
| Lingual Gyrus | 1 | 86 | 4.28 | 4 | -70 | 0 | R |
| Temporal Occipital Fusiform Cortex | 1 | 235 | -2.09 | 26 | -48 | -18 | R |
| Lateral Occipital Cortex, inferior division | 1 | 55 | -3.54 | 52 | -66 | -2 | R |
| Cuneal Cortex | 1 | 38 | -6.76 | -18 | -72 | 26 | L |
| Middle Temporal Gyrus, posterior division | 1 | 86 | -7.29 | -60 | -12 | -26 | L |
| | 2 | 74 | -4.42 | -66 | -34 | -10 | L |
| | 3 | 22 | -5.14 | 64 | -8 | -22 | R |
| | 4 | 21 | -3.04 | 60 | -28 | -4 | R |
| | 5 | 20 | -4.85 | -58 | -16 | -10 | L |
| | 6 | 57 | -3.94 | 54 | -22 | -28 | R |
| Temporal Pole | 1 | 35 | -4.66 | 50 | 20 | -20 | R |
| Middle Temporal Gyrus, temporooccipital part | 1 | 28 | -5.12 | 64 | -48 | 4 | R |
| Planum Temporale | 1 | 25 | -4.91 | 48 | -28 | 12 | R |

| | | | | | | | |
|---|---|---|---|---|---|---|---|
| **LIMBIC LOBE** | | | | | | | |
| Paracingulate Gyrus | 1 | 62 | 4.27 | -8 | 42 | 22 | L |
| Insular Cortex | 1 | 63 | -4.94 | -32 | 16 | -6 | L |
| Parahippocampal Gyrus, posterior division | 1 | 34 | -3.26 | -34 | -38 | -10 | L |
| Cingulate Gyrus, anterior division | 1 | 20 | -3.46 | -2 | 42 | 4 | L |
| **SUBCORTICAL REGIONS** | | | | | | | |
| Right Thalamus | 1 | 186 | 6.91 | 8 | -24 | 2 | |
| Brain-Stem | 1 | 186 | 3.75 | 4 | -36 | -20 | |
| | 2 | 92 | 4.76 | 10 | -38 | -46 | |
| | 3 | 186 | -2.29 | -2 | -30 | -20 | |
| Left Thalamus | 1 | 132 | 6.86 | -6 | -10 | 0 | |
| | 2 | 30 | 4.02 | -8 | -26 | -2 | |
| | 3 | 25 | -4.45 | -20 | -36 | 0 | |
| Left Putamen | 1 | 26 | 4.93 | -20 | 18 | -8 | |
| Right Putamen | 1 | 23 | -6.16 | 32 | -8 | -4 | |
| Left Hippocampus | 1 | 21 | -3.53 | -34 | -14 | -22 | |

**Supplementary Table S5.4** Neural substrates of Behavioral inhibition system (BIS). The activations after correction for multiple comparisons are represented at p<.05 (FDR corrected). The coordinates reported are in MNI space.

| REGION LABEL | CLUSTER NUMBER | EXTENT | T-VALUE | MNI COORDINATES | | | LATERALITY |
|---|---|---|---|---|---|---|---|
| | | | | X | Y | Z | |
| **FRONTAL LOBE** | | | | | | | |
| Precentral Gyrus | 1 | 102 | 4.60 | -8 | -32 | 48 | L |
| | 2 | 71 | 5.31 | -52 | 6 | 26 | L |
| | 3 | 71 | 3.16 | -38 | 2 | 40 | L |
| | 4 | 42 | -2.78 | 60 | -2 | 18 | R |
| Inferior Frontal Gyrus, pars triangularis | 1 | 64 | 5.94 | 50 | 32 | 18 | R |
| | 2 | 22 | 3.86 | -44 | 36 | 8 | L |
| | 3 | 27 | -3.96 | -54 | 16 | 6 | L |
| Frontal Pole | 1 | 32 | 3.37 | 40 | 42 | 32 | R |
| | 2 | 25 | 3.64 | 24 | 64 | 20 | R |
| | 3 | 125 | -8.01 | 12 | 50 | 46 | R |
| | 4 | 56 | -4.25 | 22 | 38 | 52 | R |
| | 5 | 40 | -3.62 | 36 | 58 | -4 | R |
| | 6 | 38 | -6.15 | 12 | 68 | 2 | R |
| | 7 | 35 | -6.56 | -38 | 48 | -16 | L |
| | 8 | 31 | -4.70 | 32 | 38 | -10 | R |
| | 9 | 30 | -4.46 | -16 | 62 | 16 | L |
| | 10 | 23 | -3.72 | -8 | 58 | 34 | L |
| **PARIETAL LOBE** | | | | | | | |
| Postcentral Gyrus | 1 | 95 | 5.80 | -26 | -32 | 64 | L |
| Supramarginal Gyrus, anterior division | 1 | 43 | 5.75 | -62 | -26 | 20 | L |
| Superior Parietal Lobule | 1 | 22 | 2.66 | -34 | -42 | 54 | L |
| | 2 | 72 | -7.79 | 16 | -52 | 72 | R |
| | 3 | 25 | -4.22 | -12 | -52 | 70 | L |
| Angular Gyrus | 1 | 210 | -5.48 | 52 | -50 | 44 | R |
| | 2 | 93 | -4.44 | -48 | -56 | 28 | L |
| Precuneous Cortex | 1 | 50 | -5.07 | -6 | -58 | 42 | L |

| | | | | | | | |
|---|---|---|---|---|---|---|---|
| | 2 | 32 | -3.55 | -8 | -70 | 36 | L |
| **TEMPORAL LOBE** | | | | | | | |
| Middle Temporal Gyrus, posterior division | 1 | 259 | -6.10 | -56 | -12 | -28 | L |
| | 2 | 52 | -4.02 | 60 | -20 | -24 | R |
| Inferior Temporal Gyrus, posterior division | 1 | 259 | -2.37 | -60 | -32 | -20 | L |
| | 2 | 59 | -5.81 | 46 | -16 | -34 | R |
| Temporal Pole | 1 | 42 | -4.53 | -54 | 6 | -18 | L |
| | 2 | 37 | -4.90 | -40 | 12 | -38 | L |
| Middle Temporal Gyrus, anterior division | 1 | 34 | -4.26 | 58 | -6 | -14 | R |
| **OCCIPITAL LOBE** | | | | | | | |
| Lateral Occipital Cortex, superior division | 1 | 210 | -2.59 | 32 | -62 | 54 | R |
| **LIMBIC LOBE** | | | | | | | |
| Cingulate Gyrus, anterior division | 1 | 154 | 2.39 | -4 | 34 | -6 | L |
| | 2 | 94 | 5.87 | -4 | 14 | 32 | L |
| | 3 | 33 | 3.47 | -2 | -10 | 30 | L |
| | 4 | 207 | -7.82 | 4 | 36 | 0 | R |
| Insular Cortex | 1 | 52 | 5.73 | 30 | 16 | -14 | R |
| Paracingulate Gyrus | 1 | 207 | -6.03 | 12 | 40 | 22 | R |
| | 2 | 154 | -7.64 | -12 | 44 | -2 | L |
| Cingulate Gyrus, posterior division | 1 | 28 | -5.15 | 2 | -46 | 34 | R |
| | 2 | 26 | -5.18 | -2 | -28 | 26 | L |
| **SUBCORTICAL REGIONS** | | | | | | | |
| Brain-Stem | 1 | 58 | 3.96 | 12 | -40 | -28 | |
| | 2 | 38 | 4.10 | 8 | -28 | -40 | |
| | 3 | 21 | 3.37 | -2 | -32 | -8 | |
| Left Thalamus | 1 | 32 | 3.45 | -2 | -2 | -4 | |
| | 2 | 29 | 3.94 | -6 | -24 | 10 | |
| Right Caudate | 1 | 151 | -4.30 | 6 | 10 | -2 | |
| Left Accumbens | 1 | 31 | -4.01 | -8 | 16 | -8 | |

**Supplementary Table S5.5** ROI-to-ROI correlations of subcortical with cortical regions and other subcortical areas for Positive affect (PA), Negative affect (NA), Behavioral activation system (BAS), and Behavioral inhibition system (BIS) psychological measures.

| SUBCORTICAL REGIONS (SEED REGIONS) | CORTICAL REGION LABELS | ABBREVIATIONS OF CORTICAL REGION LABELS | SUBCORTICAL REGIONS | CORR. VALUES (p<.05) |
|---|---|---|---|---|
| **PA** | | | | |
| Right Amygdala | Insular cortex, posterior division (R) | IC (post.) | | 0.38 |
| | Insular cortex, posterior division (L) | IC (post.) | | 0.32 |
| | Planum Palore (L) | Ppalore | | 0.31 |
| | Parahippocampal gyrus, posterior division (L) | ParaHG | | 0.25 |
| | Superior temporal gyrus, anterior division (R) | STG (ant.) | | 0.25 |
| | Subcallosal cortex (R) | SubcalC | | 0.25 |
| | Inferior Frontal Gyrus, pars opercularis (R) | IFG (pars oper.) | | 0.24 |
| | Central Opercular Cortex (L) | CenOperC | | 0.24 |
| | Temporal Pole (L) | TP | | 0.24 |
| | Inferior Frontal Gyrus, pars opercularis (L) | IFG (pars oper.) | | 0.21 |
| | | | | |
| Left Hippocampus | Parahippocampal gyrus, posterior division (L) | ParaHG (post.) | | 0.49 |
| | | | | |
| Left Thalamus | | | Right thalamus | 0.53 |
| | | | Right amygdala | 0.2 |
| | Insular cortex, posterior division (L) | IC (post.) | | 0.2 |
| | | | | |
| Right Thalamus | | | Left Thalamus | 0.53 |
| | Insular cortex, posterior division (L) | IC (post.) | | 0.27 |
| | Insular cortex, posterior division (R) | IC (post.) | | 0.23 |
| | | | | |
| **NA** | | | | |
| Right Putamen | Frontal orbital cortex (L) | FOrbC | | 0.63 |

| | | | | |
|---|---|---|---|---|
| | Central opercular cortex (R) | CenOperC | | 0.43 |
| | Insular cortex, posterior division (R) | IC (post.) | | 0.37 |
| | Insular cortex, posterior division (L) | IC (post.) | | 0.38 |
| | Precentral gyrus (L) | PreCG | | 0.27 |
| | Precentral gyrus (R) | PreCG | | 0.29 |
| | Frontal operculum cortex (L) | FOperC | | 0.23 |
| | Frontal orbital cortex (R) | FOrbC | | 0.22 |
| | Supramarginal gyrus, anterior division (R) | SMG (ant.) | | 0.21 |
| | Juxtapositional lobule cortex (L) | JuxtaLC | | 0.21 |
| | | | | |
| Left Hippocampus | Temporal pole (L) | TP | | 0.37 |
| | Frontal orbital cortex (L) | FOrbC | | 0.31 |
| | Inferior temporal gyrus, anterior division (R) | ITG (ant.) | | 0.28 |
| | Middle temporal gyrus, anterior division (L) | MTG (ant.) | | 0.2 |
| | | | | |
| **BAS** | | | | |
| Brain-stem | | | Left thalamus | 0.2 |
| Left thalamus | | | Right thalamus | 0.78 |
| Left thalamus | | | Left hippocampus | 0.24 |
| | Paahippocampal gyrus, posterior division (L) | ParaHG (post.) | | 0.4 |
| | Temporal fusiform gyrus, posterior division (R) | TemFusiformC (post.) | | 0.22 |
| | Temporal occipital fusiform gyrus (R) | TemOccFusiformG | | 0.21 |
| | Cuneal cortex (L) | CunealC | | 0.2 |
| | | | | |
| Left Putamen | Insular cortex, anterior division (L) | IC (ant.) | | 0.25 |
| | Frontal orbital cortex (R) | FOrbC | | 0.22 |
| | Frontal medial cortex (R) | FMedC | | 0.2 |
| | | | | |
| Right putamen | Planum temporale (R) | PlanumTemp | | 0.32 |
| | Juxtapositional lobule cortex (L) | JuxtaLC | | 0.3 |
| | Precentral gyrus (R) | PreCG | | 0.25 |
| | Insular cortex, anterior division (L) | IC (ant.) | | 0.24 |
| | Frontal orbital cortex (R) | FOrbC | | 0.22 |
| | Postcentral gyrus (L) | PostCG | | 0.21 |
| | Postcentral gyrus (R) | PostCG | | 0.2 |
| | | | | |
| Left Hippocampus | Temporal Fusiform Cortex, posterior division (L) | TemFusiformC (post.) | | 0.35 |
| | Parahippocampal Gyrus, posterior division (L) | ParaHG (post.) | | 0.3 |

| | | | | |
|---|---|---|---|---|
| | | | Left thalamus | 0.24 |
| | | | | |
| Brain stem | | | Left thalamus | 0.32 |
| | | | | |
| **BIS** | | | | |
| Left thalamus | | | Right caudate | 0.6 |
| | | | Left accumbens | 0.41 |
| | | | Brain stem | 0.31 |
| | Cingulate gyrus, anterior division (L) | CingG (ant.) | | 0.2 |
| | | | | |
| | | | | |
| Right caudate | | | Left accumbens | 0.65 |
| | | | Left thalamus | 0.6 |
| | Cingulate gyrus, anterior division (L) | CingG (ant.) | | 0.26 |
| | Insular cortex, anterior division (R) | IC (ant.) | | 0.25 |
| | Cingulate gyrus, anterior division (R) | CingG (ant.) | | 0.24 |
| | | | | |
| | | | | |
| Left accumbens | | | Right caudate | 0.65 |
| | | | Left thalamus | 0.41 |
| | Cingulate gyrus, anterior division (L) | CingG (ant.) | | 0.4 |
| | Paracingulate gyrus (L) | ParaCingG | | 0.25 |
| | Cingulate gyrus, anterior division (R) | CingG (ant.) | | 0.24 |
| | Insular cortex, anterior division (R) | IC (ant.) | | 0.2 |

**Supplementary Table S5.6** Graph theory measures (degree and betweenness centrality) for the subnetwork *CSCN* (each cortical substrate with all subcortical neural substrates) of Positive affect (PA), Negative affect (NA), Behavioral activation system (BAS), and Behavioral inhibition system (BIS) psychological measures.

| REGION LABELS | LATERALITY | BETA VALUES (p<.05) | | |
|---|---|---|---|---|
| | | DEGREE | COST | BETWEENNESS CENTRALITY |
| **PA** | | | | |
| Parahippocampal Gyrus, posterior division | L | 0.641 | 0.160 | 0.013 |
| Insular Cortex | R | 0.500 | 0.125 | 0.013 |
| Insular Cortex | L | 0.462 | 0.115 | 0 |
| Subcallosal cortex | R | 0.462 | 0.115 | 0.009 |
| Planum Polare | L | 0.410 | 0.103 | 0.004 |
| Central Opercular Cortex | L | 0.385 | 0.096 | 0.013 |
| Superior Temporal Gyrus, anterior division | L | 0.385 | 0.096 | 0 |
| Temporal Fusiform Cortex, posterior division | L | 0.385 | 0.096 | 0.004 |
| Middle Temporal Gyrus, anterior division | L | 0.385 | 0.096 | 0.004 |
| Superior Temporal Gyrus, anterior division | R | 0.372 | 0.093 | 0.002 |
| Inferior Frontal Gyrus, pars opercularis | R | 0.359 | 0.090 | 0.004 |
| **NA** | | | | |
| Temporal Pole | L | 0.974 | 0.244 | 0.030 |
| Frontal Orbital Cortex | L | 0.936 | 0.234 | 0.038 |
| Insular Cortex | L | 0.923 | 0.231 | 0.038 |
| Inferior Temporal Gyrus, anterior division | R | 0.872 | 0.218 | 0.017 |
| Insular Cortex | R | 0.872 | 0.218 | 0.028 |
| Central Opercular Cortex | R | 0.795 | 0.199 | 0.015 |
| Middle Temporal Gyrus, anterior division | L | 0.782 | 0.196 | 0.026 |
| Juxtapositional Lobule Cortex | L | 0.769 | 0.192 | 0.021 |
| Inferior Temporal Gyrus, temporooccipital part | L | 0.718 | 0.179 | 0.017 |
| Inferior Frontal Gyrus, pars triangularis | L | 0.718 | 0.179 | 0.017 |

| | | | | |
|---|---|---|---|---|
| Frontal Orbital Cortex | R | 0.692 | 0.173 | 0.026 |
| Frontal Operculum Cortex | L | 0.692 | 0.173 | 0.017 |
| **BAS** | | | | |
| Supramarginal Gyrus, posterior division | R | 16.85 | 0.225 | 0.027 |
| Middle Frontal Gyrus | R | 16.41 | 0.219 | 0.020 |
| Middle Temporal Gyrus, posterior division | R | 16.15 | 0.215 | 0.022 |
| Inferior Frontal Gyrus, pars opercularis | L | 15.38 | 0.205 | 0.022 |
| Angular Gyrus | R | 15.10 | 0.201 | 0.022 |
| Middle Temporal Gyrus, temporooccipital part | R | 14.64 | 0.195 | 0.021 |
| Middle Temporal Gyrus, posterior division | L | 14.39 | 0.192 | 0.020 |
| Inferior Frontal Gyrus, pars triangularis | R | 14.36 | 0.191 | 0.019 |
| Frontal Pole | R | 13.79 | 0.184 | 0.019 |
| Middle Temporal Gyrus, posterior division | R | 13.56 | 0.181 | 0.018 |
| Temporal Pole | R | 13.03 | 0.174 | 0.016 |
| Superior Parietal Lobule | R | 12.84 | 0.171 | 0.018 |
| **BIS** | | | | |
| Cingulate Gyrus, posterior division | R | 14.03 | 0.286 | 0.051 |
| Angular Gyrus | L | 11.85 | 0.242 | 0.044 |
| Cingulate Gyrus, anterior division | R | 11.13 | 0.227 | 0.050 |
| Angular Gyrus | R | 10.77 | 0.220 | 0.043 |
| Middle Temporal Gyrus, posterior division | R | 10.62 | 0.217 | 0.035 |
| Paracingulate Gyrus | R | 10.44 | 0.213 | 0.033 |
| Middle Temporal Gyrus, posterior division | L | 10.38 | 0.212 | 0.033 |
| Paracingulate Gyrus | L | 9.62 | 0.196 | 0.035 |
| Frontal Pole | L | 9.00 | 0.184 | 0.030 |
| Inferior Temporal Gyrus, posterior division | L | 8.92 | 0.182 | 0.027 |
| Cingulate Gyrus, anterior division | L | 8.91 | 0.182 | 0.035 |
| Cingulate Gyrus, posterior division | L | 8.56 | 0.175 | 0.026 |

# REFERENCES

Kaur, A., Chaujar, R., & Chinnadurai, V. (2019). Effects of Neural Mechanisms of Pretask Resting EEG Alpha Information on Situational Awareness: A Functional Connectivity Approach. *Human Factors*. https://doi.org/10.1177/0018720819869129

Kaur, A., Chinnadurai, V., & Chaujar, R. (2020). Microstates-based resting frontal alpha asymmetry approach for understanding affect and approach/withdrawal behavior. *Scientific Reports*, *10*(1), 1–25. https://doi.org/10.1038/s41598-020-61119-7

# Effects of Neural Mechanisms of Pretask Resting EEG Alpha Information on Situational Awareness: A Functional Connectivity Approach

**Ardaman Kaur**, Institute of Nuclear Medicine and Allied Sciences, Delhi, India, **Rishu Chaujar**, Delhi Technological University, India, and **Vijayakumar Chinnadurai**, Institute of Nuclear Medicine and Allied Sciences, Delhi, India

**Objective:** In this study, the influence of pretask resting neural mechanisms on situational awareness (SA)-task is studied.

**Background:** Pretask electroencephalography (EEG) information and Stroop effect are known to influence task engagement independently. However, neural mechanisms of pretask resting absolute alpha (PRAA) and pretask resting alpha frontal asymmetry (PRAFA) in influencing SA-task which is undergoing Stroop effect is still not understood.

**Method:** The study involved pretask resting EEG measurements from 18 healthy individuals followed by functional magnetic resonance imaging (fMRI) acquisition during SA-task. To understand the effect of pretask alpha information and Stroop effect on SA, a robust correlation between mean reaction time, SA Index, PRAA, and PRAFA were assessed. Furthermore, neural underpinnings of PRAA, PRAFA in SA-task, and functional connectivity were analyzed through the EEG-informed fMRI approach.

**Results:** Significant robust correlation of reaction time was observed with SA Index (Pearson: $r = .50$, $p\text{corr} = .05$) and PRAFA (Pearson: $r = .63$; $p\text{corr} = .01$), respectively. Similarly, SA Index significantly correlated with PRAFA (Pearson: $r = .56$, $p\text{corr} = .01$; Spearman: $r = .61$, $p\text{corr} = .007$), and PRAA (Pearson: $r = .59$, $p\text{corr} = .005$; Spearman: $r = .59$, $p\text{corr} = .002$). Neural underpinnings of SA-task revealed regions involved in visual-processing and higher-order cognition. PRAA was primarily underpinned at frontal-temporal areas and functionally connected to SA-task regions pertaining to the emotional regulation. PRAFA has correlated with limbic and parietal regions, which are involved in integration of visual, emotion, and memory information of SA-task.

**Conclusion:** The results suggest a strong association of reaction time with SA-task and PRAFA and strongly support the hypothesis that PRAFA, PRAA, and associated neural mechanisms significantly influence the outcome of SA-task.

**Application:** It is beneficial to study the effect of pretask resting information on SA-task to improve SA.

**Keywords:** situational awareness, cognition, physiological measurement, methods and skills, neuroimaging, neuroergonomics, analysis and evaluation

Address correspondence to Vijayakumar Chinnadurai, Scientist "F," NMR Research Centre, Institute of Nuclear Medicine and Allied Sciences, Lucknow Road, Timarpur, Delhi 110054, India; e-mail: vijayakumar@inmas.drdo.in; vijayafmc@gmail.com.

*HUMAN FACTORS*
Vol. XX, No. X, Month XXXX, pp. 1–21
DOI: 10.1177/0018720819869129
Article reuse guidelines: sagepub.com/journals-permissions


## INTRODUCTION

Neuroergonomics, the field which investigates the behavioral aspects of the human brain by integrating knowledge from both neuroscience and neuroimaging with ergonomics has evolved immensely in the last decade (Gramann, Fairclough, Zander, & Ayaz, 2017; Hancock & Szalma, 2003; Mehta, Parasuraman, Mckinley, & Neuroscience, 2013; Sestito, Harel, Nador, & Flach, 2018). This interdisciplinary approach would be very useful in comprehending human abilities for augmenting their interaction with various environments.

Situational awareness (SA), which is the knowledge about the environment, is one of the constructs that has become the focus of the ergonomics community recently (Endsley, 1995b; Endsley, Bolté, & Jones, 2016). It begins with the perception of the elements in the environment (Level 1), comprehension of their meaning (Level 2), and ends at decision making (Level 3) (Endsley, 1995b; Endsley et al., 2016). Maintenance of SA is essential for optimum performance in the military, aviation domain. However, there are many physiological and psychological factors that can cause loss of SA (Endsley, Bolstad, & Carolina, 1994; Klamklay, 2002). These factors include attention, long-term and working memory, automaticity, and experience of an individual. Previous research majorly examined the association of the aforementioned factors with the loss of SA individually because it is difficult to test the SA model as a whole (Endsley, 2015).

The maintenance of SA primarily depends on the ability of the individual to allocate cognitive resources to perform specific functions by filtering out function-irrelevant stimuli. This cognitive process is better studied through the Stroop

effect which involves performing a less automated task (e.g., recognizing the ink color) while inhibiting the interference arising from a more automated task (e.g., reading the word). Past research (Jensen & Rohwer, 1966; Kang et al., 2013; Scarpina & Tagini, 2017) reported the application of the Stroop test in measuring cognitive functions, such as attention, processing speed, cognitive flexibility, and working memory. Specifically, Klamklay (2002), in their study, reported a high positive correlation of performance and SA with Stroop color and word test. Despite these works, there are many questions that are still needed to be addressed for a better understanding of the maintenance of SA. They are as follows: (1) Does SA gets influenced by the Stroop effect during the SA-task? (2) What are the neural mechanisms of SA when it is influenced by the Stroop effect? (3) What are the pretask factors that can affect the neural mechanisms in SA? Understanding these aspects requires an in-depth analysis of multimodal information acquired from an individual while performing the SA-task that is influenced by the Stroop effect.

Cognitive neuroscience employs divergent assessment techniques such as functional magnetic resonance imaging (fMRI), electroencephalography (EEG), functional near infra-red spectroscopy (fNIRS), and positron emission tomography (PET) to study the functional dynamics of the brain during task engagement. Hence, appropriate use of these techniques will facilitate us in understanding neural mechanisms underlying the Stroop effect on SA and ways to ameliorate it under various environments. Catherwood et al. (2014) employed EEG for mapping brain activity and suggested that there is an early coactivity in high-order and perception areas during the loss of SA. The aforementioned study investigated the association of loss of SA with concurrent activity in high-level cognitive regions and those for perceptual (visual) processing through EEG source analysis. Although this study revealed valuable neural insights of SA, it did not address the association of pretask resting information with the behavioral outcome of the subsequently performed SA-task.

Pretask resting-state information refers to complex and highly nonrandom patterns of intrinsic activity occurring while the brain is not actively involved in a task (Raichle & Snyder, 2007). EEG signatures acquired during pretask resting state have been known as a contributor to the outcome of subsequently performed cognitive tasks. In particular, frontal alpha asymmetry and peak alpha oscillations (8–12 Hz) have been investigated extensively in the past decades (Ambrosini & Vallesi, 2016; Grandy, Werkle-bergner, Chicherio, & Schmiedek, 2013) as a measure to examine emotion-related (Davidson, 1992, 2010; Tomarken, Davidson, Wheeler, & Kinney, 1992), and motivation-related trait individual differences and state-related changes (Davidson, Saron, Senulis, Ekman, & Friesen, 1990; Tomarken, Davidson, & Henriques, 1990). Frontal hemispheric asymmetry has also been conceptualized and, to some extent, proved to be a mediator and moderator of emotion (Coan & Allen, 2004; Gable, Neal, & Threadgill, 2018; Reznik & Allen, 2018). A recent study by Balconi, Vanutelli, and Grippa (2017) elucidated the predictive effect of resting-state activity and approach/withdrawal dichotomy.

Furthermore, absolute power of alpha oscillations from which frontal asymmetry is derived has also been linked to reflect performance in various cognitive functions (Angelakis, Lubar, Stathopoulou, & Kounios, 2004), including attention, arousal, working memory, long-term memory, and reading. There is a shred of clear evidence that alpha and beta bands of resting EEG predict individual differences in attentional blink magnitudes (MacLean, Arnell, & Cote, 2012; Shapiro, Hanslmayr, Enns, & Lleras, 2017). López Zunini, Thivierge, Kousaie, Sheppard, and Taler (2013) explored the mutual relationship between cognitive states and resting-state alpha powers by showing that alpha band resting-state activity before a verbal recognition task can predict accuracy during the task.

However, there are no published works which provide a better understanding of the association of pretask resting EEG alpha information with the performance of subsequently performed SA-task when the task is influenced by the Stroop effect. In addition, there is no clarity in understanding of the influence of neural mechanisms of pretask resting alpha information and associated functional connectivity on subsequently performed SA-task.

Hence, in this work, the association of pretask resting EEG alpha information on the subsequently performed SA-task has been investigated. In particular, the SA-task is designed to have more influence from the Stroop effect; hence, the ability of pretask resting information in assessing the behavioral outcome of SA in those conditions can be studied. To confirm the presence of Stroop effect during the SA-task, the robust correlation of the reaction time which assesses the Stroop effect with the SA Index of the individual during the same task is carried out. Then, as this study primarily aims to understand the effect of pretask alpha information on individual's SA, the pretask information is correlated with SA Index and further subjected to the EEG-informed fMRI analysis for understanding its neural mechanisms. Integration of EEG and fMRI through the EEG-informed fMRI approach has emerged to balance their complementary temporal and spatial resolutions (Abreu, Leal, & Figueiredo, 2018; Huster, Debener, Eichele, & Herrmann, 2012; Jorge, van der Zwaag, & Figueiredo, 2014; Murta, Leite, Carmichael, Patrícia, & Louis, 2015). This technique enables us to assess regions that correspond to the task engagement (neural underpinnings of the SA-task) as well as the regions whose neural activity is manifested as cortical EEG power (neural underpinnings of EEG powers). Subsequently, to understand the modulation of neural underpinnings of SA-task by neural mechanisms underlying pretask resting alpha information, functional connectivity among neural underpinnings of SA-task, pretask alpha power, and its associated hemispheric asymmetry was estimated and analyzed.

## MATERIALS AND METHODS

Schematic diagram of the methodology adopted in this study is illustrated in Figure 1.

### Subjects

Pretask resting-state EEG and task-fMRI studies were performed on 18 healthy volunteers (12 men, 6 women, mean age: 24 years, *SD*: 3 years). All volunteers completed informed consent procedures approved by the local institutional review board. This research complied with the American Psychological Association Code of Ethics.

### Paradigm Information

Catherwood et al. (2014) employed an abstract task, and a real-world urban threat detection task to assess the loss of SA by measuring EEG information for the same. Their study concluded the rapid and early coactivity of visual and higher-order regions for both abstract and more real-world content. Keeping in mind the compatibility of task performance in an MR environment, we chose to employ a modified Stroop test to study SA. Stroop color and word test is a neuropsychological test extensively used to assess the ability to inhibit cognitive interference that occurs when the processing of a specific stimulus feature impedes the simultaneous processing of a second stimulus attribute. Scarpina and Tagini (2017) also report the application of the Stroop test in measuring cognitive functions such as attention, processing speed, cognitive flexibility, and working memory. Similar to the study by Catherwood et al. (2014), in our study, the "situation" is defined in terms of target information within a visual field. The essential requirements resemble many real-world situations requiring perceptual and cognitive processing to identify a target item.

The choice of Stroop test was done, as it requires any volunteer to perform a less automated task while inhibiting the interference arising from a more automated task. This holds parallel to the concept of SA, wherein identifying which elements the operator needs to perceive and understand is an important parameter that facilitates the decision-making process. We modified the basic Stroop test by inserting questions about the presence of an object in the previous environment at random intervals, which is in line with Endsley's original task where random questions are asked to the volunteer about the driving simulation. Hence, in our paradigm, volunteers were exposed to a paradigm wherein each slide, they had to perceive the question being displayed, comprehend its meaning, and answer from a given set of four choices. Each stimulus slide lasted for 4.5 seconds on the screen and was followed by a baseline slide for 3 seconds. The base-

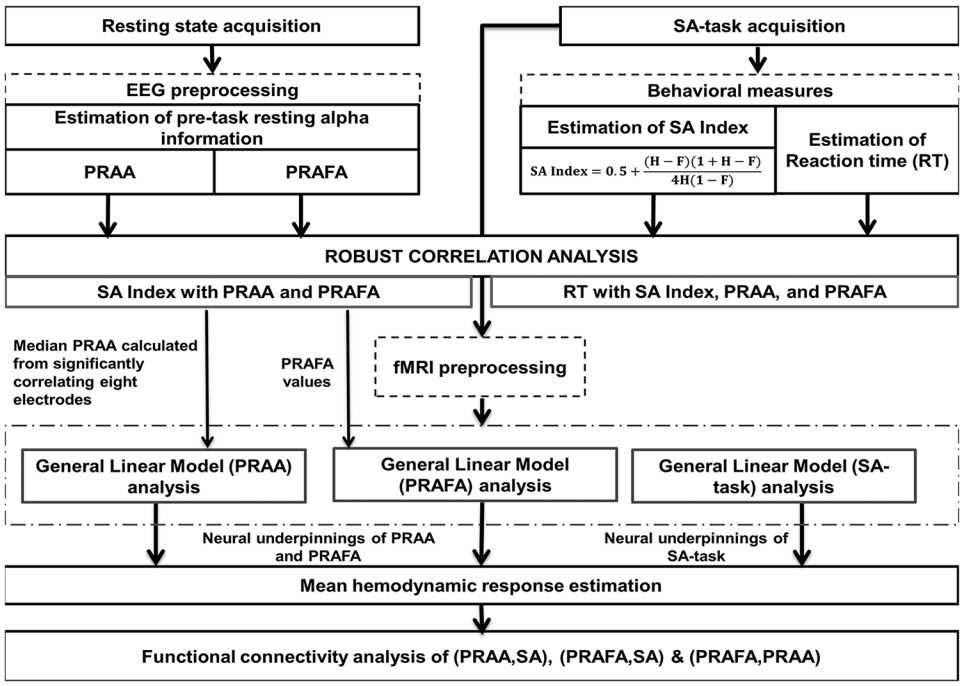


*Figure 1.* Schematic diagram of the methodology adopted in this study.

line slide is the fixation block of the paradigm, where no specific task was carried out by the volunteers except viewing standard blank slide with a cross. In the paradigm, 20 stimulus slides were made, where the volunteer had to observe and orient the true sense of the Stroop color and word test question. Moreover, in five stimulus slides, the volunteer was randomly asked about the presence of an object in the previous environment. In our paradigm, Level 1 SA (perception) was achieved by the visual perception of the questions being placed. Volunteers slowly transited to Level 2 SA (comprehension) while understanding the meaning of the question being asked. For example, one of the slides asked the volunteer to observe the color of text, where the text was "Eight" written in green color as shown in Figure 2. Thus, the volunteer had to observe all the choices, including a green-colored object and number eight and make a final choice by pressing a button in the same slide. At random times during the task, the volunteers were inquired about the particular features in the previous environment with a question such as: did you notice this object in the previous environment? (Figure 2). These questions were modified and drafted to go in sync with Endsley's original task (Endsley, 1995a). These questions particularly triggered the bottom-top process, where the volunteer had to shift the attention to another additional goal, which was to focus on other elements in the environment. Furthermore, volunteers were not trained for the occurrence of these random questions before the experiment.

## Acquisition and Preprocessing Steps

*Pretask resting EEG data acquisition and preprocessing*. Pretask resting-state EEG data were acquired using magnetic resonance imaging (MRI) compatible Brain-Amp EEG amplifier and electrode cap with 31 Ag/AgCl electrodes positioned according to the 10/20 system and 1 electrocardiography (ECG) channel. The reference electrode was placed between Fz and Cz electrodes. Raw EEG data were sampled at 5 kHz using a brain vision recorder, and electrode impedances were kept less than 10 kΩ. We recorded resting EEG on all volunteers while they were at rest in the MRI room. Resting-state EEG recording lasted for 6 minutes and included the eyes-closed condition. The eyes-closed condition was chosen, as alpha rhythm which is the

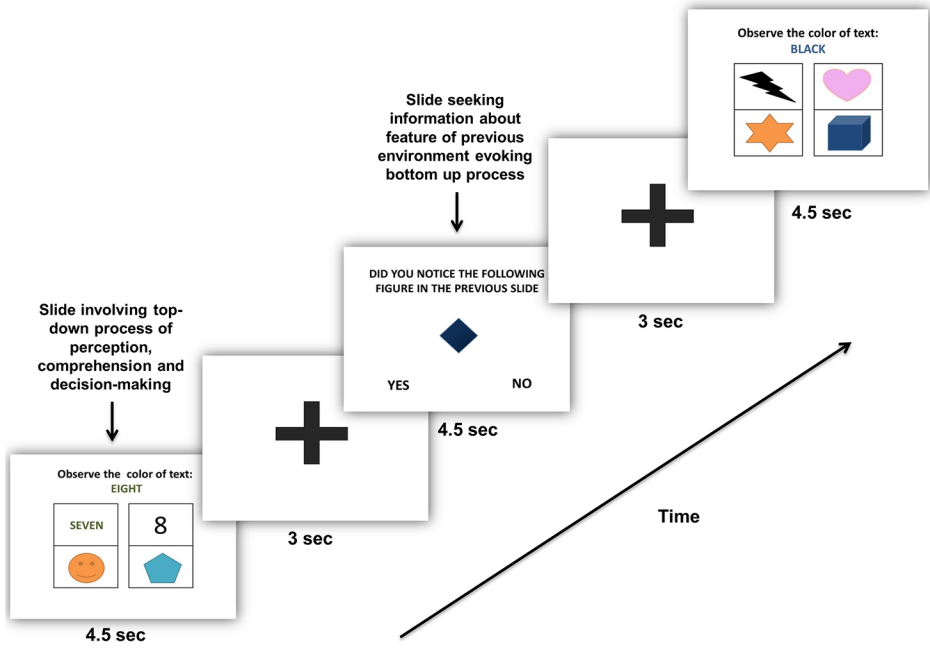


*Figure 2.* Schematic showing functional magnetic resonance imaging (fMRI) stimulus and baseline presentation paradigm for situational awareness (SA) task.

EEG correlate of relaxed wakefulness, is best obtained while the eyes are closed. Furthermore, functional connectivity in the alpha band decreases in the eyes-open condition as compared to eyes-closed condition (Barry & De Blasio, 2017; Gómez-Ramírez, Freedman, Mateos, Pérez-Velázquez, & Valiante, 2017).

The acquired EEG data were corrected for gradient and cardio-ballistic artifacts using brain vision analyzer's (BVA) algorithms, and ocular artifacts were removed using the independent component analysis (ICA) approach in BVA (Gajda, Sroka, Stencel, Wajda, & Zeglen, 2001). Then, the power spectral densities of the alpha band (8–12 Hz) of every channel were computed for the entire duration of resting acquisition using Welch's overlapped segment averaging estimator. The spectral densities of alpha band power were then log transformed for further analysis.

*fMRI data acquisition and preprocessing.* Functional and anatomical MRI was performed in a 3 T MR Siemens scanner. During the SA-task, fMRI scanning was carried out with a T2-weighted echo-planar imaging (EPI) sequence and 247 functional blocks were acquired. The other acquisition parameters were set as number of slices = 36, slice thickness = 3 mm, TR = 3,000 ms, flip angle = 90°, TE = 36 ms, field of view (FOV) = 230 × 230. The whole-brain anatomical scan was also acquired using a T1-weighted sequence with the parameters TR = 1900 ms, flip angle = 9°, TE = 2.49 ms, FOV = 256 × 256. The acquired fMRI data were preprocessed, coregistered, normalized to Montreal Neurological Institute (MNI) template, and smoothed using a Gaussian kernel (6 mm full width half maximum) in SPM12 (https://www.fil.ion.ucl.ac.uk/spm/).

## Data Analysis

*Estimation of the SA Index as a behavioral measure of task.* Quantification of SA in previous literature has been done using Quantitative Assessment of Situational Awareness (QASA; Edgar et al., 2018; Nikolla, Edgar, Catherwood, & Matthews, 2018; Stanislaw & Todorov, 1999). QASA involves the collection and analysis of volunteers' responses to true/false statements

using signal-detection theory (SDT) metrics. As this study aims to understand the Stroop effect on SA-task, we required to keep more than one task-irrelevant option along with the correct answer in the slides to bring more Stroop effect during task engagement. Hence, each slide had one correct answer (signal) and three wrong answers (noise). We have calculated Hits (H) as a ratio between the number of correct answers selected by the individual and the total number of correct answers. To calculate false alarm (F), we have grouped all three task-irrelevant answers in the slide as one false category. Hence, if the individual selects any one of the task-irrelevant stimuli as an answer, then it is considered as a single false category. Thus, a false alarm is estimated as the ratio between the number of task-irrelevant stimuli identified as correct and the total number of false. The purpose of doing this was to ensure that the volunteer uses his/her cognitive resources in observing all the options in addition to the hit. This assessment of true/false from the answers of volunteers for the adaptation of signal-detection theory metrics, and eventual quantification of SA allowed us to assess the Stroop effect during the task engagement. The additional slides which enquired about the presence of a particular object in the previous environment evoked yes-no responses from the volunteers. These yes-no responses on signal trials (when an object was present in the previous environment) and noise trials (when an object was absent in the previous environment) were also added to the proportion of hits (correct identification) and false alarms (incorrect identification). Hence, using the estimated H and F, SA Index was derived as,

$$\text{SA Index} = 0.5 + \frac{(\text{H} - \text{F})(1 + \text{H} - \text{F})}{4\text{H}(1 - \text{F})}$$

Ben-David, Chajut, and Algom (2012) have also employed a similar concept of SDT for analysis of emotional Stroop color and word task, where the percentage of correct identification of color provided the rate of hits (H). In a complementary fashion, the percentage of incorrect identifications of color as word provided the rate of false alarms (F).

Subsequently, the behavioral score of SA-task of each volunteer was combined in a vector form ($SA_{all}$) as,

$$\text{SA}_{all} = \left\{\text{SA Index}_i | i = 1 \text{to N}\right\}$$

where N is the total number of volunteers who participated in the study. These estimations were implemented via programming in Matlab (2013).

*Estimation of reaction time to corroborate Stroop effect on SA-task*. Reaction time was estimated specifically for slides involving the Stroop effect to validate its presence in SA-task. Mean reaction time was calculated for every volunteer and combined in a vector form ($RT_{all}$) as,

$$\text{RT}_{all} = \left\{\text{RT Index}_i | i = 1 \text{ to N}\right\}$$

where N is the total number of volunteers who participated in the study. Subsequently, the robust correlation between response time, SA Index, and pretask alpha information were assessed.

*Estimation of pretask resting alpha information*. As mentioned in earlier sections, this study focuses on understanding the role of the pretask EEG alpha signatures in the outcome of the subsequently performed SA-task. Hence, in this study, the pretask resting alpha information was assessed by measuring pretask resting absolute alpha (PRAA) power and its associated hemispherical asymmetry through pretask resting alpha frontal asymmetry (PRAFA) index. The methods of estimating these two indices are explained as follows:

At first, the average PRAA values of every channel of each volunteer was estimated and organized as,

$$\text{PRAA}_{all} = \left\{\text{PRAA}_{i,j} \middle| \begin{matrix} i = 1 \text{ to N} \\ j = 1 \text{ to M} \end{matrix}\right\}$$

where N and M are the total number of volunteers who participated in the study and the total number of EEG channels, respectively. Each row in the matrix $PRAA_{all}$ contains details about

PRAA of every channel of a particular volunteer.

Furthermore, PRAFA was calculated through PRAFA index based on differences of absolute alpha values measured from frontal hemispheres (Ellis, Kinzel, Salgari, & Loo, 2017; Smith, Reznik, Stewart, & Allen, 2017) as given as follows,

$$\mathrm{PRAFA}_{all} = \{\mathrm{PRAFA}_i | i = 1 \text{ to } \mathrm{N}\}$$

where N is the number of volunteers, and $\mathrm{PRAFA}_i$ is the PRAFA of the *i*th volunteer which is estimated as $\log(\propto_{Right}) - \log(\propto_{Left})$. The $\propto_{Right}$ is the median of absolute alpha values of F4, F8 channels and $\propto_{Left}$ was estimated by computing the median of absolute alpha values of F3, F7 channels for every volunteer. These channels were chosen because hemispheric asymmetry has been linked to mid-frontal (F3, F4) and lateral frontal (F7, F8) sites (Coan & Allen, 2003; Harmon-Jones, Gable, & Peterson, 2010; Wheeler, Davidson, & Tomarken, 1993).

The PRAFA is an ideal index to assess neural mechanisms associated with the hemispherical asymmetry. Higher scores on the PRAFA index indicate relatively higher alpha power and lower inhibition in the right frontal hemisphere as compared to the left hemisphere. Many researchers (Klimesch, 2012; Sadaghiani & Kleinschmidt, 2016; Uusberg, Uibo, Kreegipuu, & Allik, 2013) have observed that neural activity reflected by blood oxygenated level dependent (BOLD) signal, correlates negatively with alpha power. This suggests that higher PRAFA index is suggestive of higher neural activity in the left frontal hemisphere and vice versa. Numerous studies (Balconi, Finocchiaro, & Canavesio, 2014; De Pascalis, Cozzuto, Caprara, & Alessandri, 2013; Ferreira et al., 2006; Harmon-Jones et al., 2010; Jones, Field, & Almeida, 2009; Mennella, Patron, & Palomba, 2017; Papousek et al., 2014; Schneider et al., 2016) reflect the association of greater left frontal activity with a general approach or motivational system, and the greater right frontal activity with avoidance or withdrawal system.

*Robust correlations among reaction time, SA Index, and pretask resting information*. Robust correlations were implemented in the robust correlation Matlab toolbox (Pernet, Wilcox, & Rousselet, 2013). This method protects against bivariate or univariate outliers. Pearson, Spearman, Bend, and Skipped correlation coefficients, as well as their bootstrapped confidence intervals, were computed. Furthermore, both *p* values and confidence intervals were Bonferroni corrected for multiple comparisons.

To substantiate the influence of Stroop effect on SA, the robust correlation of reaction times pertaining to slides evoking Stroop effect was estimated with the SA Index as well as PRAA and PRAFA. Thus, $\mathrm{RT}_{all}$ was correlated with $\mathrm{SA}_{all}$ vector, $\mathrm{PRAA}_{all}$, and $\mathrm{PRAFA}_{all}$. Furthermore, to explore the role of pretask resting information in the behavioral outcome of the subsequently performed SA-task, the robust correlation of SA Index with PRAA and PRAFA was carried out. Each row of $\mathrm{PRAA}_{all}$ was thus correlated with $\mathrm{SA}_{all}$ vector to assess the most informative EEG channels which are associated with the behavioral outcome of subsequently performed task. Eight EEG channels (fp2, poz, c4, pz, p7, cp1, o1, and oz) significantly correlated with the SA Index. Hence, their median was computed for the purpose of passing it as a covariate in the EEG-informed fMRI model to estimate the neural underpinnings of PRAA. Similarly, $\mathrm{PRAFA}_{all}$ was also subjected to the robust correlation analysis with the $\mathrm{SA}_{all}$ Index. The median value of the PRAFA was then used as a covariate in the EEG-informed fMRI model to assess the neural underpinnings of PRAFA.

*Estimation of neural underpinnings of SA-task, PRAFA, and PRAA*. The assessment of the neural underpinnings of the SA-task reveals the brain regions which are involved during the task. This has been estimated by the general linear model approach using statistical parametric model (SPM12). In this model, at first level of analysis, *t*-contrast was specified for testing the SA-task effect (active-baseline); where active comprised all the stimuli, and statistical parametric maps were constructed for canonical hemodynamic response function (HRF) and its temporal and dispersion derivatives. These contrast images of each subject were then passed onto second-level group analyses. Similarly, the neural underpinnings of PRAFA and PRAA were assessed through EEG-informed fMRI approach. Both PRAFA

and PRAA were subjected as a global covariate at the second level to two independent EEG-informed fMRI models. The results of the second-level analysis of the neural underpinnings of the SA-task as well as PRAFA and PRAA were subjected to the one-way analysis of variance (ANOVA) statistical method. The *F*-contrast was computed, and significant activations for the SA-task and PRAFA and PRAA were analyzed at family-wise error (FWE) corrected $p < .05$ significance.

*Functional connectivity analysis*. This study aims to understand the modulation of neural underpinnings of SA-task by neural mechanisms of pretask resting alpha information. Therefore, functional connectivity analysis was carried out to understand the interaction between the neural underpinnings of SA-task with PRAA and PRAFA. It is estimated by assessing the mutual correlations of the mean hemodynamic response of different neural underpinnings pertaining to the SA stimuli. Specifically, the functional connectivity between *x*th neural underpinning of PRAA (PRAA[*x*]) and *y*th neural underpinning of SA, SA(*y*) is estimated as,

$$\text{Functional connectivity}\left[\text{PRAA}(x),\text{SA}(y)\right] = Corr\left(m\text{HR}_{\text{PRAA}}(x), m\text{HR}_{\text{SA}}(y)\right)$$

Similarly, functional connectivity between PRAFA and SA neural underpinnings is estimated as

$$\text{Functional connectivity}\left[\text{PRAFA}(z),\text{SA}(y)\right] = Corr\left(m\text{HR}_{\text{PRAFA}}(z), m\text{HR}_{\text{SA}}(y)\right)$$

In addition, the functional connectivity between *x*th neural underpinning of PRAA (PRAA[*x*]) and *z*th neural underpinning of PRAFA (PRAFA[*z*]) is further estimated as,

$$\text{Functional connectivity}\left[\text{PRAA}(x),\text{PRAFA}(z)\right] = Corr\left(m\text{HR}_{\text{PRAA}}(x), m\text{HR}_{\text{PRAFA}}(z)\right)$$

where $m\text{HR}_{\text{PRAA}}(x)$, $m\text{HR}_{\text{PRAFA}}(z)$, and $m\text{HR}_{\text{SA}}(y)$ are the mean hemodynamic responses of the *x*th, *z*th, and *y*th neural underpinnings of PRAA, PRAFA, and SA, respectively, pertaining to the SA stimuli during the task. The mean hemodynamic responses of every neural underpinning pertaining to PRAA, PRAFA, and SA are estimated by forming a vector whose elements are the average hemodynamic response of all the voxels of that specific neural underpinning corresponding to a particular SA stimuli block (Figure 3). For example, the mean hemodynamic response of *x*th neural underpinning of PRAA, $m\text{HR}_{\text{PRAA}}(x)$ is estimated as,

$$m\text{HR}_{\text{PRAA}}(x) = \left\{ \left| Avg\left(m\text{HR}^{i}_{\text{PRAA}} \mid i = 1:\text{N}x\right)\right|_{\text{Blockindex}} ; \text{Block index} = 1:\text{N}_{\text{SABlocks}} \right\}$$

where $\text{N}x$ is the total number of voxels in the *x*th underpinning of PRAA, and $\text{N}_{\text{SABlocks}}$ is the total number of SA stimuli blocks performed during the task which in our experiment is 25. The mean hemodynamic response of every voxel pertaining to each stimulus was carried out by measuring time to peak (TTP) and width (W) of HRF for each stimulus (Lindquist, Meng, Atlas, & Wager, 2009). The TTP and W of each task stimulus were observed to be having mean values of 3.78 seconds and 1.9 seconds, respectively. This suggests that the hemodynamic response of the task stimuli was very well contained inside the block time of 4.5 seconds during the task. Correlation threshold for the correlation among the neural underpinnings of SA, PRAA, and PRAFA was set more than 0.5, and *t*-test ($p < .05$) for group analysis was performed for the in-depth understanding of the association between underpinnings of PRAA and SA, PRAFA and SA, and PRAFA and PRAA.

## RESULTS

As mentioned in the earlier sections, this study aims to understand the influence of neural mechanisms of pretask resting information on SA. Particularly, the SA-task is designed to have more influence from the Stroop effect; therefore, the ability of pretask resting information in

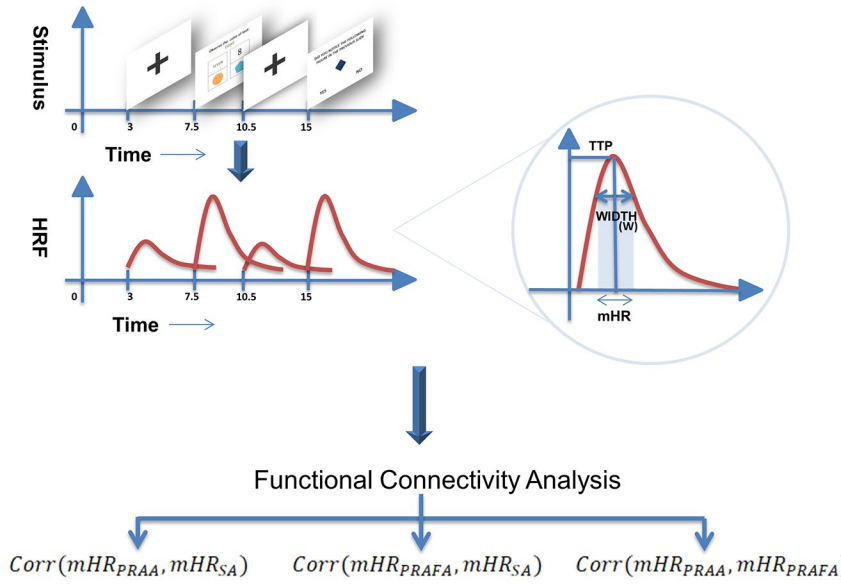


*Figure 3.* Schematic showing the estimation of mean hemodynamic response of each stimulus for functional connectivity analysis.

assessing the behavioral outcome of SA in those conditions can be studied. In addition, this study validated the existence of the Stroop effect in SA-task by correlating the reaction time which assesses the Stroop effect with the SA Index as well as pretask resting parameters. The study also focuses in bringing better clarity of interactions between neural mechanisms associated with SA-task and pretask resting information through functional connectivity analysis. The pretask resting information has been assessed by estimating both PRAA and PRAFA. The following sections present the results of this study in detail.

## Confirmation for the Presence of Stroop Effect During SA-Task

The results of robust correlations revealed significant association among the reaction time of the stimuli evoking Stroop effect in SA-task with an SA Index. Strong and significant Pearson and Pearson-skipped correlation was observed between reaction time and SA Index measures (Figure 4a: Pearson $r$ = .51, 95% CI = [0.07; 0.84], $p$corr = .05; Figure 4b: Pearson-skipped $r_{skipped}$ = .51, 95% CI = [0.06; 0.83]). Bend, Spearman, and Spearman-skipped correlations revealed insignificant $p$ values for this analysis.

Similarly, reaction time revealed significant positive Pearson and Pearson-skipped correlations with PRAFA (Figure 4c: Pearson $r$ = .63, 95% CI = [0.16; 0.87], $p$corr = .011; Figure 4d: Pearson-skipped $r_{skipped}$ = .44, 95% CI = [0.03; 0.75]). However, insignificant $p$ values were revealed for Bend, Spearman, and Spearman-skipped correlations. Furthermore, no significant correlations were observed between reaction time and PRAA. Hence, these results validate the presence of the Stroop effect in SA-task.

## Association of Pretask Resting Information With SA Index

The results of robust correlations revealed a significant role of pretask resting measures with behavioral performance in SA-task. In particular, robust correlation analysis revealed a strong and significant correlation between PRAFA and SA Index measures (Figure 5a: Pearson $r$ = .56, 95% CI = [0.15; 0.79], $p$corr = .01; Figure 5b: Spearman $r$ = .61, 95% CI = [0.12; 0.90], $p$corr = .007). Skipped (Pearson and Spearman) and bend correlations among PRAFA values and SA Index measures also

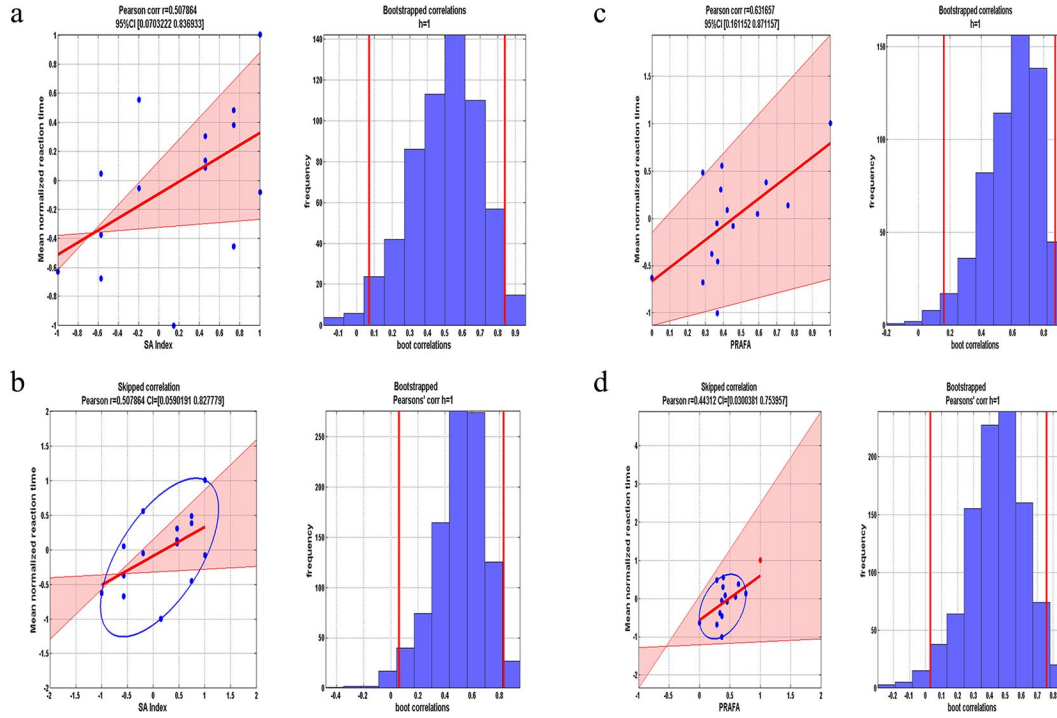


*Figure 4.* Correlation plots between mean normalized reaction time and Situational Awareness Index: (a) Pearson correlation, (b) Skipped (Pearson) correlation. Correlation plots between mean normalized reaction time and pretask resting alpha frontal asymmetry: (c) Pearson correlation, (d) Skipped (Pearson) correlation.

yielded stronger correlations (Figure 5c: Bend correlation coefficient = .51, 95% CI = [0.09; 0.88], *p*corr = .03; Figure 5d: Pearson $r_{skipped}$ = .56, 95% CI = [0.16; 0.79]; Spearman $r_{skipped}$ = .61, 95% CI = [0.12; 0.91]).

Similarly, PRAA was strongly correlating with the SA Index across eight electrodes. The correlation coefficients of all these channels, as well as the respective significance levels, have been tabulated in Supplementary Table 1. Median of PRAA of these strongly correlating eight electrodes have also revealed a significant positive correlation with behavioral SA Index (Figure 6a: Pearson $r$ = .59, 95% CI = [0.23; 0.88], *p*corr = .005; Figure 6b: Spearman $r$ = .59, 95% CI = [0.09; 0.89], *p*corr = .002). Skipped (Pearson and Spearman) and bend correlations among median of PRAA values and SA Index measures also yielded significant correlations (Figure 6c: Bend correlation coefficient = .62, 95% CI = [0.18; 0.89], *p*corr = .004; Figure 6d: Pearson $r_{skipped}$ = .76, 95% CI = [0.55; 0.91]; Spearman $r_{skipped}$ = .79, 95% CI = [0.51; 0.92]). Hence, these results reveal the significant association between pretask resting measures and behavioral performance of the subsequently performed SA-task.

## Neural Underpinnings of SA-Task

Figure 7 shows neural underpinnings of SA-task (FWE corrected $p < .05$), and regions are tabulated in Supplementary Table 2. The significant activations during the SA-task relative to the baseline were analyzed using the categorical approach. The baseline is the neural activity observed during fixation block of the paradigm, where no specific task was carried out except viewing standard blank slide with a cross. The group analysis of the generalized linear model (GLM) model showed significant neural activations in primary and high-level visual-processing areas including occipital fusiform gyrus, lateral occipital cortex (inferior and superior division) and temporal-occipital fusiform gyrus. In

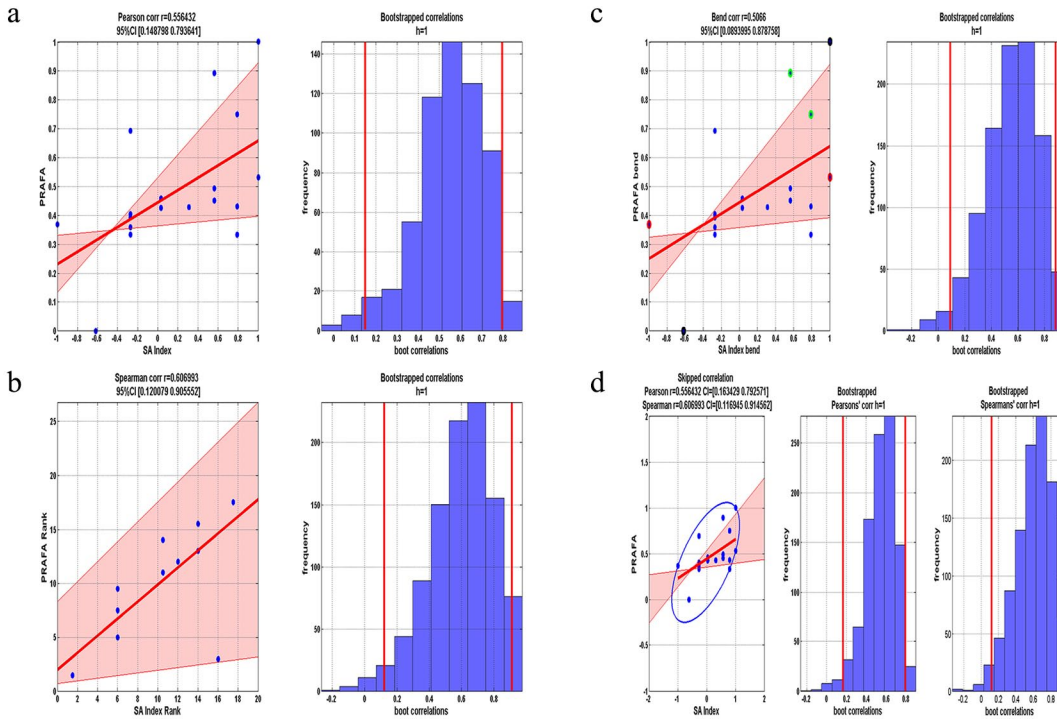


*Figure 5.* Correlation plots between pretask resting alpha frontal asymmetry and Situational Awareness Index and associated histograms of correlations for bootstrapped data: (a) Pearson correlation, (b) Spearman correlation, (c) 20% Bend correlation, and (d) skipped (Pearson and Spearman) correlations.

addition, significant involvement of frontal lobe (inferior, middle, and superior frontal gyrus) was also observed as neural underpinning of SA-task. The presence of activity in the visual cortex and occipital-temporal regions justified the attainment of Level 1 (perception) of SA, where primary and high-level visual-processing regions are involved. The significant activations in motor areas, precuneus, inferior, middle, and superior frontal gyrus, and posterior cingulate gyrus elucidate their role in high-order cognition required to form Level 2 (comprehension) and Level 3 (decision making) of SA.

## Neural Underpinnings of PRAFA and PRAA

Reznik and Allen (2018) explored the frontal hemispherical differences of alpha as a predictor, moderator, and mediator of emotional regulation. However, it is still unclear which brain regions, in particular, are involved in mediating the emotional regulation during the SA-task. Thus, to decipher these neural underpinnings during the SA-task, PRAFA was passed as a global covariate in an independent EEG-informed fMRI model. Figure 8 shows the neural underpinning of PRAFA as assessed by this EEG-informed fMRI model and details of the regions are tabulated in Supplementary Table 3. The significant activations were observed in the parahippocampal gyrus, precuneus cortex, insular cortex, and parietal operculum cortex all at uncorrected $p < .001$.

Similarly, the neural underpinnings of PRAA as assessed by the independent EEG-informed fMRI analysis are shown in Figure 9, and the regions are tabulated in Supplementary Table 4. The neural underpinnings of PRAA revealed significant activations in both frontal and temporal cortex at uncorrected $p < .001$. In particular, frontal pole, middle frontal gyrus, superior frontal gyrus, and inferior frontal gyrus have shown stronger activation in the frontal cortex. In addition, right hippocampus, precuneus cortex,

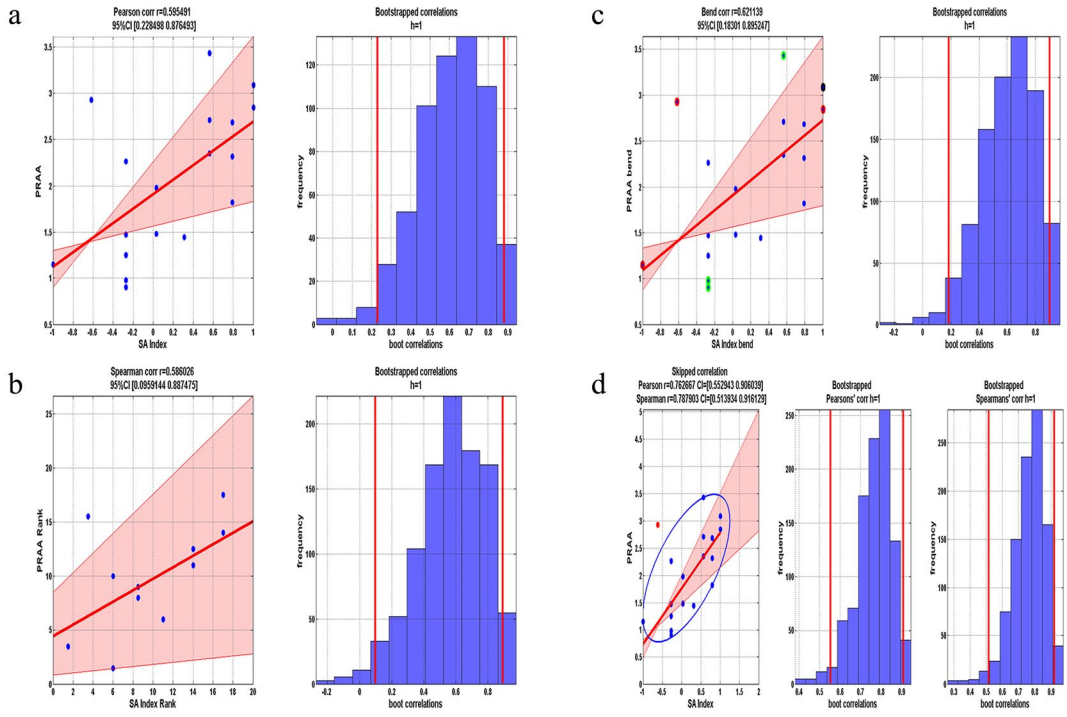


*Figure 6.* Correlation plots between median pretask resting absolute alpha values and Situational Awareness Index and histograms of correlations for bootstrapped data: (a) Pearson correlation, (b) Spearman correlation, (c) 20% Bend correlation, and (d) skipped (Pearson and Spearman) correlations.

cingulate gyrus, thalamus, inferior temporal gyrus, and middle temporal gyrus have also shown significant involvements. These regions are well known for their role in the emotional stability of the individual (Kassam, Markey, Cherkassky, Loewenstein, & Just, 2011; Kohn et al., 2014). Furthermore, the PRAA has also revealed a correlation with neural activity in visual and attention regions such as an occipital pole, lateral occipital cortex, and temporal fusiform cortex.

## Functional Connectivity Analysis

The functional connectivity between neural underpinnings of PRAFA and neural underpinnings of PRAA has revealed strong mutual interaction across those regions. Similarly, the functional connectivity approach brought a better understanding of changes in neural mechanisms of SA-tasks by pretask resting information.

*Connectivity between PRAA and SA neural underpinnings*. Figure 10 shows strong interactions of frontal (frontal pole, middle frontal gyrus, and superior frontal gyrus) and temporal (middle temporal gyrus and temporal pole) underpinnings of PRAA with neural underpinning of SA-task such as inferior frontal gyrus, middle frontal gyrus, precentral gyrus, motor cortex, occipital lobe regions (occipital fusiform gyrus and lateral occipital cortex), and parietal regions (precuneus cortex and postcentral gyrus). Furthermore, the subcortical underpinning of SA-task in left putamen specifically connected to frontal and temporal pole underpinnings of PRAA.

*Connectivity between PRAFA and SA neural underpinnings*. The connectivity results revealed strong interactions of the insula (PRAFA neural underpinning) with postcentral gyrus and left putamen of the SA-task (Figure 10). Parietal operculum cortex of PRAFA neural underpinning significantly correlated with many neural underpinnings of SA-task, such as lateral occipital cortex, occipital fusiform gyrus, postcentral gyrus, and precuneus cortex regions. Another neural underpinning of PRAFA, the precuneus cortex, correlated with the intracalcarine cortex,

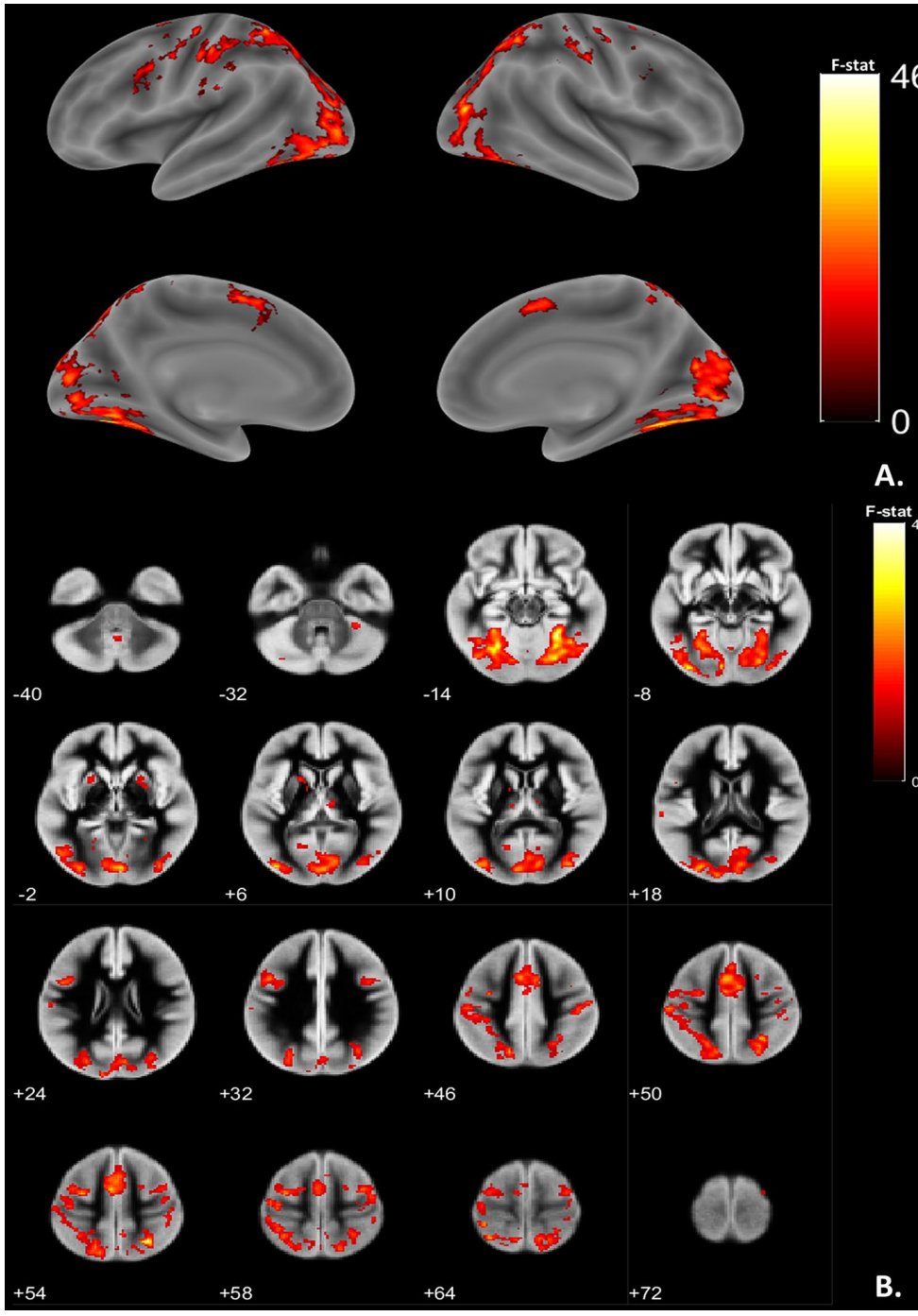


*Figure 7.* Neural underpinnings of situational awareness task as shown in (a) surface rendered view and (b) slice montage view. The activations are represented at family-wise error-corrected $p < .05$.

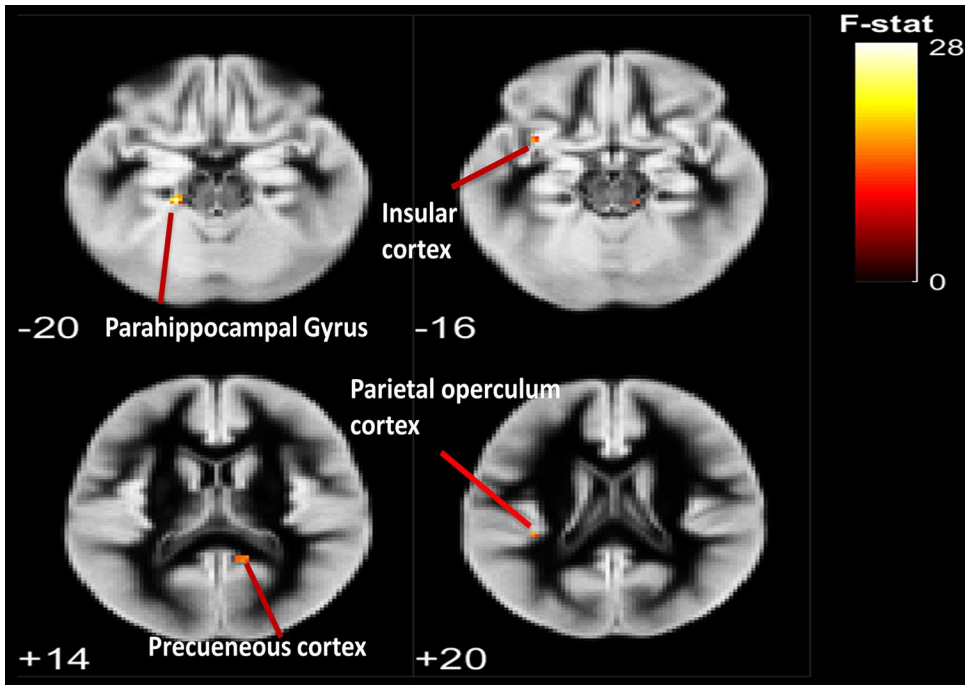


*Figure 8.* Neural underpinnings of pretask resting-state alpha frontal asymmetry through electroencephalography informing situational awareness-task-based functional magnetic resonance imaging as shown in slice montage view.
The activations are represented at uncorrected $p < .001$.

juxtapositional lobule cortex, lateral occipital cortex, middle frontal gyrus, occipital fusiform gyrus, postcentral gyrus, precentral gyrus, precuneus cortex, and right thalamus areas of SA-task. On the contrary, parahippocampal gyrus showed no correlation with SA clusters.

*Connectivity between PRAFA and PRAA neural underpinnings*. Figure 10 shows the connectivity within neural underpinnings of PRAFA and PRAA. The connectivity results ($r > .5$; $p < .05$) revealed a significant correlation of insula, parietal operculum cortex, and precuneus cortex (neural underpinnings of PRAFA) with frontal-temporal underpinnings of PRAA. Parahippocampal gyrus (neural underpinning of PRAFA) correlated explicitly with temporal pole underpinning of PRAA.

## DISCUSSION

Our study aims to explore the influence of pretask resting alpha information such as PRAFA and PRAA on SA. In particular, the SA-task is designed to have more influence from the Stroop effect; hence, the ability of pretask resting information in assessing the behavioral outcome of SA in those conditions can be studied. The study extends to explore the neural underpinnings of the task, pretask resting information, and revealed through functional connectivity analysis that neural underpinnings of PRAFA and PRAA significantly interact with neural underpinnings of SA-task and influence the behavioral outcome of SA.

SA generally possesses alternation between top-down and bottom-up processes. Top-down processing is a goal-driven process, where attention is directed in accordance with active goals. On the contrary, bottom-up is a data-driven process, where perceived cues from the environment activate new goals. In this study, the neural underpinnings of the SA-task revealed significant engagement of visual cortex and occipital-temporal regions. The strong involvement of these regions pertaining to the memory (tempo-

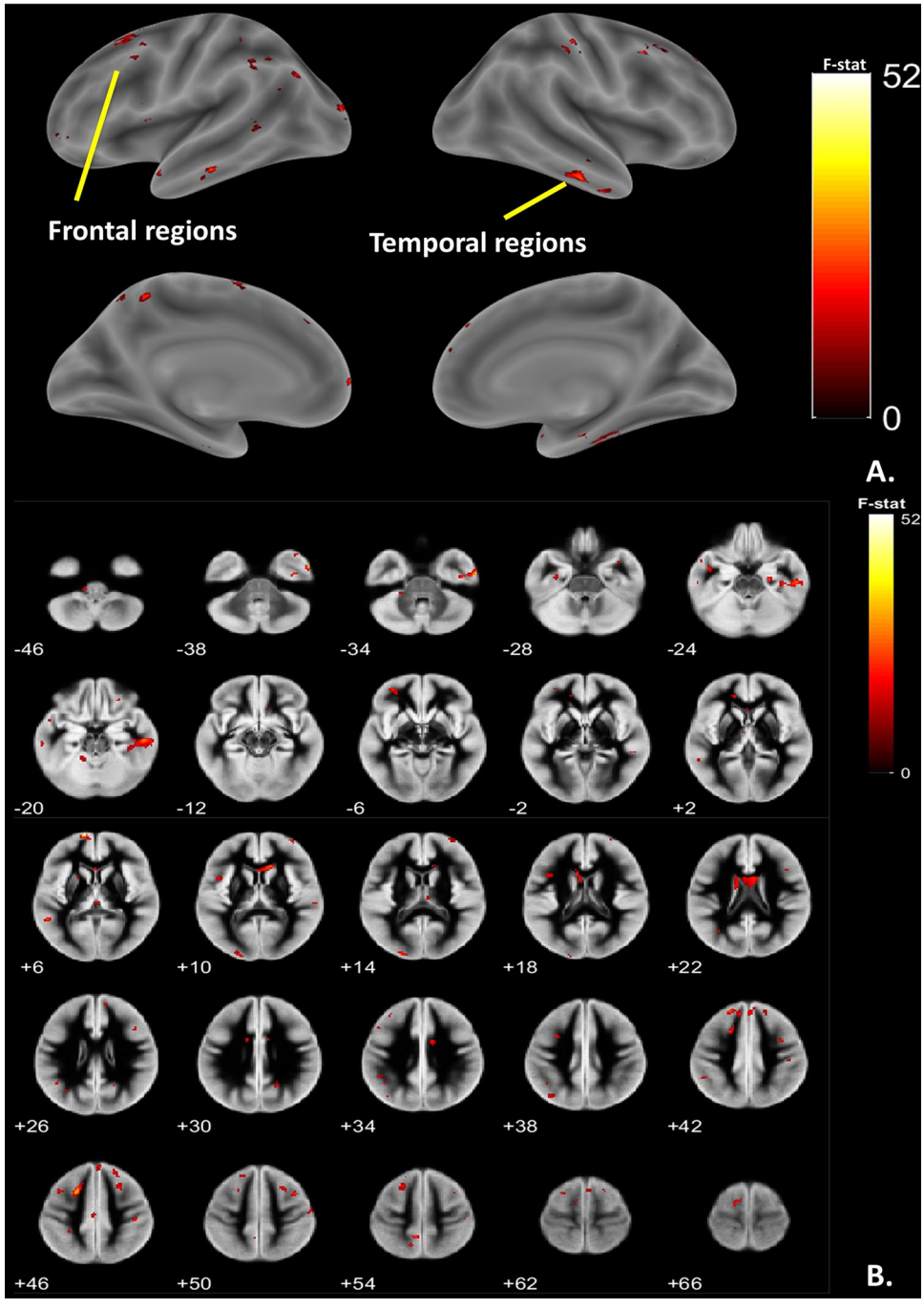


*Figure 9.* Neural underpinnings of pretask resting-state absolute alpha power through electroencephalography informing situational awareness-task-based functional magnetic resonance imaging as shown in (a) surface rendered view and (b) slice montage view. The activations are represented at uncorrected $p < .001$.

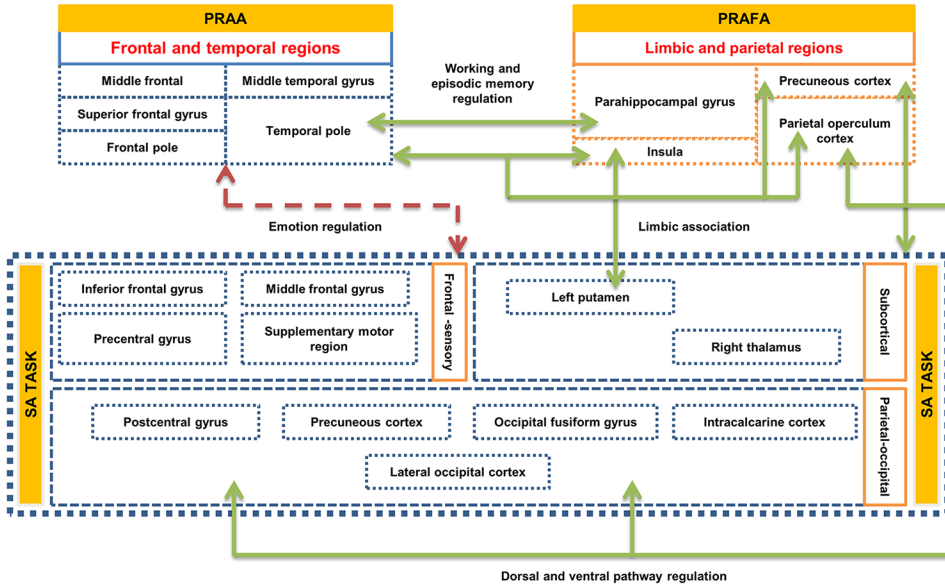


*Figure 10.* Schematic showing functional connectivity of neural underpinnings of SA-task with PRAA and PRAFA underpinnings.
The interregional correlation was done at $r > .5$ ($p < .05$). The dotted arrow illustrates the functional connectivity of PRAA (frontal and temporal regions) with SA regions. The solid arrows illustrate the limbic association of PRAFA regions with SA-task regions and integration of dorsal/ventral pathways, memory regulation. SA = situational awareness; PRAA = pretask resting absolute alpha; PRAFA = pretask resting alpha frontal asymmetry.

ral regions) and visual processing justifies hypothesis of Catherwood et al. (2014) that rapid memory operation is engaged during reversal of bottom-up cognitive operations in SA. Similarly, the strong arousal was observed in sensory, precuneus, frontal gyrus, and posterior cingulate gyrus during the SA-task. These regions have also been observed by Catherwood et al. (2014) and have been linked with cognition under uncertainty. Hence, this study provides neuroimaging validation of regions associated with SA-task engagement as observed in the aforementioned study.

## Validation of Presence of Stroop Effect During SA-Task

In this study, the increase in reaction time during the Stroop effect in SA-task correlated positively with the SA Index. This goes in line with the previous studies where delayed reaction times were observed when the font color and the word were different compared to when they were the same (Klamklay, 2002; Repov, 2004). This happens during the Stroop effect as the processing of a color impedes the simultaneous processing of a second stimulus attribute (word). Thus, our results suggest that the more the reaction time in Stroop effect, the better the performance in the task. Furthermore, Stroop effect's reaction time also correlated positively with pretask EEG alpha parameter PRAFA.

## Role of Pretask Absolute Alpha Information in SA-Task

The changes in alpha EEG oscillation are known to be a marker of inhibition caused by the neural activity. The neural underpinning as assessed by functional imaging facilitates to pinpoint the involvement of cognitive trait and state of the individual in the modulations of alpha oscillations. In this study, changes observed in pretask absolute alpha information have been revealed to be significantly modulating neural mechanisms associated with the subsequently

performed SA-task. This is evident through higher positive robust correlation observed between the SA Index and PRAA of eight channels (mainly posterior).

The neural underpinnings of PRAA observed in this study were primarily from frontal, temporal, and few parietal regions. Figure 10 clearly illustrates the strong functional connectivity between frontal-temporal regions of PRAA with neural underpinnings of SA-task. Although temporal lobe is the hub of memory management, the functional connectivity between frontal and temporal lobes has also been studied (Kennis, Rademaker, & Geuze, 2013; Lacruz, García Seoane, Valentin, Selway, & Alarcón, 2007; Pfeifer et al., 2009) for their association with emotional regulation and arousal of affect. This clearly explains the effect of PRAA on SA-task, as there is a demand for rapid memory management for the purpose of comprehension and understanding of environments. Furthermore, the neural underpinnings of PRAA observed in the parietal regions such as angular gyrus, precuneus have been well studied as main areas involved in mentalization process (Frith & Frith, 2006). This is one of the core cognitive resources recruited during comprehension stage of SA-task.

### Role of PRAFA in SA-Task

The hemispheric asymmetry and lateralization of arousal of task-related neural activity are strongly connected with modulation of many cognitive state and trait behaviors, particularly approach/withdrawal behavior (Alves & Fukusima, 2009; Davidson, 1992; Spielberg, Stewart, Levin, & Miller, 2008). The EEG alpha asymmetry is one of the validated information which estimates the hemispherical asymmetry and associated cognitive state and trait behavior modulations. In this study, the high positive robust correlation of PRAFA with SA Index indicates the possible role of pretask cognitive state/trait behavior as assessed by the EEG asymmetry in the SA-task engagement. This further supports the suggestion of Catherwood et al. (2014) that asymmetry of brain processes is linked with neural mechanisms of SA.

Furthermore, neural underpinnings of PRAFA revealed areas of the limbic lobe (insular cortex and parahippocampal gyrus) and parietal cortex (precuneus and parietal operculum cortex). During SA-task, the perception and attention resources play a very important role in the behavioral outcome of the task (Thilakarathne, 2015). The limbic region has direct access to perceptual information prior to sensory cortical systems and also modulates innate behaviors, including motivation and avoidance behaviors (Nishijo, Rafal, & Tamietto, 2018). In particular, the insula in limbic lobe plays a critical role in integrating bottom-up interceptive prediction error signals with top-down predictions from high-level cortical areas (Gu, Hof, Friston, & Fan, 2013; Klein, Ullsperger, & Danielmeier, 2013; Lu et al., 2016).

Similarly, the role of working and episodic memory in SA-task is nicely explained by the neural underpinning of PRAFA and their functional connectivity with neural underpinnings of SA-task (Figure 10). During SA-task, the individual perceives the environment and encodes the situational information as episodic and working memory (Gutzwiller & Clegg, 2013; Heenan, Herdman, Brown, & Robert, 2014; Johannsdottir & Herdman, 2010). Any decay of this encoded information in episodic and working memory leads to loss of SA which pauses the individual to reassess the situations again (Gartenberg, Breslow, Mccurry, & Trafton, 2013). This is known as the resumption lag. The neural underpinnings of PRAFA (parahippocampal gyrus and posterior parietal cortex) are involved in regulation and maintenance of the episodic (Behrendt, 2013) and working memory (Schon, Newmark, Ross, & Stern, 2016). The situations are assessed by the individual by integrating informational and spatial content of objects in the situations and associated emotional and spatiotemporally information (Behrendt, 2013). Posterior parietal regions which are part of the dorsal visual stream communicates spatial environmental information through the parahippocampal cortex. The integration of objects and contextual emotional information (Aminoff, Kveraga, & Bar, 2013) with parahippocampal cortex are derived from the ventral visual stream (neural underpinning of SA-task) and insula. Thus, it is evidently clear that the neural underpinning of PRAFA controls key regions pertaining to understanding the

situations during the SA-task. Furthermore, a parietal association of PRAFA is also supported by many research work wherein precuneus forms a central hub for the link between the frontal and parietal regions (Bullmore & Sporns, 2009; Gong et al., 2009; Iturria-Medina, Sotero, Canales-Rodríguez, Alemán-Gómez, & Melie-García, 2008).

### Limitation of the Study

In this study, SA-task is designed to have more influence from the Stroop effect; hence, the ability of pretask resting information in assessing the behavioral outcome of SA in those conditions can be studied. The robust correlation of the reaction time with the SA Index of the individual has validated the presence of Stroop effect during the SA-task. However, the possibility of association of pretask resting information with other cognitive traits and states such as fatigue, mental workload (Borghini, Astolfi, Vecchiato, Mattia, & Babiloni, 2014) cannot be ignored. Hence, more elaborate research could be carried out in the future to reveal the role of specific cognitive/affective traits and states independently in the behavioral outcome and neural mechanisms of SA-tasks.

## CONCLUSION

SA is a complex cognitive task, and this study explored the association of the neural mechanisms associated with pretask resting alpha information (PRAA and PRAFA) on SA. SA-task is designed to have more influence from Stroop effect and the ability of pretask resting information in assessing SA in those conditions has been studied. The positive correlation of reaction time with the SA Index as well as PRAFA validates the presence of the Stroop effect in SA-task. Positive robust correlation of behavioral outcome of SA-task with PRAA and PRAFA suggests that the variability in an individual's PRAFA and PRAA are vital parameters to be observed before SA-task. The present findings are also part of the first efforts in understanding the neural underpinnings of the SA-task using functional imaging. Furthermore, the role of PRAA and PRAFA on the SA-task has been reinforced by assessing the functional connectivity of SA-task neural underpinnings with PRAA and PRAFA underpinnings. The connectivity results revealed a strong connection of the neural underpinnings of PRAA and PRAFA which are associated with cognitive and affective state/trait factors, with visual, memory, and high-order cognition regions involved in SA-task. In particular, the connectivity of pretask alpha asymmetry with neural underpinnings of SA-task reveals the modulation of integration of perceived contextual information, emotion, and retrieval of memory associated with the SA by the pretask trait/state information. Our results are encouraging and could be employed in operations which involve maintenance of good SA, wherein neural mechanisms associated with pretask resting alpha information could be used as a reliable predictor of performance of an individual in those operations.

## KEY POINTS

- Pretask resting information correlates positively with SA.
- Pretask absolute alpha correlates with frontal-temporal regions in SA.
- Pretask absolute alpha controls emotional pathways during SA.
- Pretask frontal alpha asymmetry correlates with limbic-parietal regions.
- Pretask resting information facilitates memory-visual integration in SA.

## SUPPLEMENTAL MATERIAL

Supplemental material is available in the online version of the journal.

## REFERENCES

Abreu, R., Leal, A., & Figueiredo, P. (2018). EEG-informed fMRI: A review of data analysis methods. *Frontiers in Human Neuroscience*, *12*, Article 29. doi:10.3389/fnhum.2018.00029

Alves, N. T., & Fukusima, S. S. (2009). Patterns of brain asymmetry in the perception of positive and negative facial expressions. *Laterality: Asymmetries of Body, Brain and Cognition*, *14*, 256–272. doi:10.1080/13576500802362927

Ambrosini, E., & Vallesi, A. (2016). Asymmetry in prefrontal resting-state EEG spectral power underlies individual differences in phasic and sustained cognitive control. *NeuroImage*, *124*, 843–857. doi:10.1016/j.neuroimage.2015.09.035

Aminoff, E. M., Kveraga, K., & Bar, M. (2013). The role of the parahippocampal cortex in cognition. *Trends in Cognitive Sciences*, *17*, 379–390. doi:10.1016/j.tics.2013.06.009

Angelakis, E., Lubar, J. F., Stathopoulou, S., & Kounios, J. (2004). Peak alpha frequency: An electroencephalographic measure of

cognitive preparedness. *Clinical Neurophysiology*, *115*, 887–897. doi:10.1016/j.clinph.2003.11.034

Balconi, M., Finocchiaro, R., & Canavesio, Y. (2014). Reward-system effect (BAS rating), left hemispheric "unbalance" (alpha band oscillations) and decisional impairments in drug addiction. *Addictive Behaviors*, *39*, 1026–1032. doi:10.1016/j.addbeh.2014.02.007

Balconi, M., Vanutelli, M. E., & Grippa, E. (2017). Resting state and personality component (BIS/BAS) predict the brain activity (EEG and fNIRS measure) in response to emotional cues. *Brain and Behavior*, *7*(5), 1–15. doi:10.1002/brb3.686

Barry, R. J., & De Blasio, F. M. (2017). EEG differences between eyes-closed and eyes-open resting remain in healthy ageing. *Biological Psychology*, *129*, 293–304. doi:10.1016/j.biopsycho.2017.09.010

Behrendt, R. (2013). Conscious experience and episodic memory: Hippocampus at the crossroads. *Frontiers in Psychology*, *4*, Article 304. doi:10.3389/fpsyg.2013.00304

Ben-David, B. M., Chajut, E., & Algom, D. (2012). The pale shades of emotion: A signal detection theory analysis of the emotional Stroop task. *Psychology*, *3*, 537–541.

Borghini, G., Astolfi, L., Vecchiato, G., Mattia, D., & Babiloni, F. (2014). Measuring neurophysiological signals in aircraft pilots and car drivers for the assessment of mental workload, fatigue and drowsiness. *Neuroscience and Biobehavioral Reviews*, *44*, 58–75. doi:10.1016/j.neubiorev.2012.10.003

Bullmore, E., & Sporns, O. (2009). Complex brain networks: Graph theoretical analysis of structural and functional systems. *Nature Reviews Neuroscience*, *10*, 186–198. doi:10.1038/nrn2575

Catherwood, D., Edgar, G. K., Nikolla, D., Alford, C., Brookes, D., Baker, S., & White, S. (2014). Mapping brain activity during loss of situation awareness: An EEG investigation of a basis for top-down influence on perception. *Human Factors*, *56*, 1428–1452. doi:10.1177/0018720814537070

Coan, J. A., & Allen, J. J. (2003). Frontal EEG asymmetry and the behavioral activation and inhibition systems. *Psychophysiology*, *40*, 106–114. doi:10.1111/1469-8986.00011

Coan, J. A., & Allen, J. J. (2004). Frontal EEG asymmetry as a moderator and mediator of emotion. *Biological Psychology*, *67*(1–2), 7–49. doi:10.1016/j.biopsycho.2004.03.002

Davidson, R. J. (1992). Anterior cerebral asymmetry and the nature of emotion. *Brain and Cognition*, *20*, 125–151.

Davidson, R. J. (2010). Symposium on emotion hemispheric substrates. *Psychological Science*, *3*, 39–43.

Davidson, R. J., Saron, C. D., Senulis, J. A., Ekman, P., & Friesen, W. V. (1990). Approach/withdrawal and cerebral asymmetry: Emotional\rexpression and brain physiology: I. *Journal of Personality and Social Psychology*, *58*, 330–341. doi:10.1037/0022-3514.58.2.330

De Pascalis, V., Cozzuto, G., Caprara, G. V., & Alessandri, G. (2013). Relations among EEG-alpha asymmetry, BIS/BAS, and dispositional optimism. *Biological Psychology*, *94*, 198–209. doi:10.1016/j.biopsycho.2013.05.016

Edgar, G. K., Catherwood, D., Baker, S., Sallis, G., Bertels, M., Edgar, H. E., & Whelan, A. (2018). Quantitative Analysis of Situation Awareness (QASA): Modelling and measuring situation awareness using signal detection theory. *Ergonomics*, *61*, 762–777. doi:10.1080/00140139.2017.1420238

Ellis, A. J., Kinzel, C., Salgari, G. C., & Loo, S. K. (2017). Frontal alpha asymmetry predicts inhibitory processing in youth with attention deficit/hyperactivity disorder. *Neuropsychologia*, *102*, 45–51. doi:10.1016/j.neuropsychologia.2017.06.003

Endsley, M. R. (1995a). Measurement of situation awareness in dynamic systems. *Human Factors: The Journal of the Human Factors and Ergonomics Society*, *37*, 65–84. doi:10.1518/001872095779049499

Endsley, M. R. (1995b). Toward a theory of situation awareness in dynamic systems. *Human Factors: The Journal of the Human Factors and Ergonomics Society*, *37*, 32–64. doi:10.1518/001872095779049543

Endsley, M. R. (2015). Situation awareness misconceptions and misunderstandings. *Journal of Cognitive Engineering and Decision Making*, *9*(1), 4–32. doi:10.1177/1555343415572631

Endsley, M. R., Bolstad, C. A., & Carolina, N. (1994). Individual differences in pilot situation awareness. *The International Journal of Aviation Psychology*, *4*, 241–264. doi:10.1207/s15327108ijap0403_3

Endsley, M. R., Bolté, B., & Jones, D. G. (2016). *Designing for situation awareness: An approach to user-centered design*. Boca Raton, FL: CRC Press.

Ferreira, C., Deslandes, A., Moraes, H., Cagy, M., Basile, L. F., Piedade, R., & Ribeiro, P. (2006). The relation between EEG prefrontal asymmetry and subjective feelings of mood following 24 hours of sleep deprivation. *Arquivos de Neuro-Psiquiatria*, *64*, 382–387. doi:10.1590/S0004-282X2006000300006

Frith, C. D., & Frith, U. (2006). The neural basis of mentalizing. *Neuron*, *50*, 531–534. doi:10.1016/j.neuron.2006.05.001

Gable, P. A., Neal, L. B., & Threadgill, A. H. (2018). Regulatory behavior and frontal activity: Considering the role of revised-BIS in relative right frontal asymmetry. *Psychophysiology*, *55*(1). doi:10.1111/psyp.12910

Gajda, J., Sroka, R., Stencel, M., Wajda, A., & Zeglen, T. (2001). A vehicle classification based on inductive loop detectors. *Proceedings of the 18th IEEE, IMTC, Budapest*, *1*, 460–464.

Gartenberg, D., Breslow, L., Mccurry, J. M., & Trafton, J. G. (2013). Situation awareness recovery. *Human Factors: The Journal of the Human Factors and Ergonomics Society*, *56*, 710–727. doi:10.1177/0018720813506223

Gómez-Ramírez, J., Freedman, S., Mateos, D., Pérez-Velázquez, J. L., & Valiante, T. (2017). Exploring the alpha desynchronization hypothesis in resting state networks with intracranial electroencephalography and wiring cost estimates. *Scientific Reports*, *7*(1), 1–11. https://doi.org/10.1038/s41598-017-15659-0

Gong, G., He, Y., Concha, L., Lebel, C., Gross, D. W., Evans, A. C., & Beaulieu, C. (2009). Mapping anatomical connectivity patterns of human cerebral cortex using in vivo diffusion tensor imaging tractography. *Cerebral Cortex*, *19*, 524–536. doi:10.1093/cercor/bhn102

Gramann, K., Fairclough, S. H., Zander, T. O., & Ayaz, H. (2017). Editorial: Trends in neuroergonomics. *Frontiers in Human Neuroscience*, *11*, Article 165. doi:10.3389/fnhum.2017.00165

Grandy, T. H., Werkle-bergner, M., Chicherio, C., & Schmiedek, F. (2013). Peak individual alpha frequency qualifies as a stable neurophysiological trait marker in healthy younger and older adults. *Psychophysiology*, *50*, 570–582. doi:10.1111/psyp.12043

Gu, X., Hof, P. R., Friston, K. J., & Fan, J. (2013). Anterior insular cortex and emotional awareness. *Journal of Comparative Neurology*, *521*, 3371–3388. doi:10.1002/cne.23368

Gutzwiller, R. S., & Clegg, B. A. (2013). The role of working memory in levels of situation awareness. *Journal of Cognitive Engineering and Decision Making*, *7*, 141–154. doi:10.1177/1555343412451749

Hancock, P. A., & Szalma, J. L. (2003). The future of neuroergonomics. *Theoretical Issues in Ergonomics Science*, *4*, 238–249. doi:10.1080/1463922021000020927

Harmon-Jones, E., Gable, P. A., & Peterson, C. K. (2010). The role of asymmetric frontal cortical activity in emotion-related

phenomena: A review and update. *Biological Psychology*, *84*, 451–462. doi:10.1016/j.biopsycho.2009.08.010

Heenan, A., Herdman, C. M., Brown, M. S., & Robert, N. (2014). Effects of conversation on situation awareness and working memory in simulated driving. *Human Factors*, *56*, 1077–1092. doi:10.1177/0018720813519265

Huster, J., Debener, S., Eichele, T., & Herrmann, C. S. (2012). Methods for simultaneous EEG-fMRI: An introductory review. *The Journal of Neuroscience*, *32*, 6053–6060. doi:10.1523/JNEUROSCI.0447-12.2012

Iturria-Medina, Y., Sotero, R. C., Canales-Rodríguez, E. J., Alemán-Gómez, Y., & Melie-García, L. (2008). Studying the human brain anatomical network via diffusion-weighted MRI and graph theory. *NeuroImage*, *40*, 1064–1076. doi:10.1016/j.neuroimage.2007.10.060

Jensen, A. R., & Rohwer, W. D. (1966). The stroop color-word test: A review. *Acta Psychologica*, *25*(C), 36–93. https://doi.org/10.1016/0001-6918(66)90004-7

Johannsdottir, K. R., & Herdman, C. M. (2010). The role of working memory in supporting drivers' situation awareness for surrounding traffic. *Human Factors: The Journal of the Human Factors and Ergonomics Society*, *52*, 663–673. doi:10.1177/0018720810385427

Jones, N. A., Field, T., & Almeida, A. (2009). Right frontal EEG asymmetry and behavioral inhibition in infants of depressed mothers. *Infant Behavior and Development*, *32*, 298–304. doi:10.1016/j.infbeh.2009.04.004

Jorge, J., van der Zwaag, W., & Figueiredo, P. (2014). EEG–fMRI integration for the study of human brain function. *NeuroImage*, *102*(Pt. 1), 24–34. doi:10.1016/j.neuroimage.2013.05.114

Kang, C., Lee, G. J., Yi, D., Mcpherson, S., Rogers, S., Tingus, K. D., & Lu, P. H. (2013). Normative data for healthy older adults and an abbreviated version of the Stroop test. *The Clinical Neuropsychologist*, *27*, 276–289.

Kassam, K. S., Markey, A. R., Cherkassky, V. L., Loewenstein, G., & Just, M. A. (2011). Identifying emotions on the basis of neural activation. *PLoS ONE*, *8*(6), e66032.

Kennis, M., Rademaker, A. R., & Geuze, E. (2013). Neuroscience and Biobehavioral Reviews neural correlates of personality: An integrative review. *Neuroscience and Biobehavioral Reviews*, *37*(1), 73–95. https://doi.org/10.1016/j.neubiorev.2012.10.012

Klamklay, J. (2002). *Individual differences and situation awareness*. Retrieved from https://lib.dr.iastate.edu/cgi/viewcontent.cgi?article=2003&context=rtd

Klein, T. A., Ullsperger, M., & Danielmeier, C. (2013). Error awareness and the insula: Links to neurological and psychiatric diseases. *Frontiers in Human Neuroscience*, *7*, Article 14. doi:10.3389/fnhum.2013.00014

Klimesch, W. (2012). Alpha-band oscillations, attention, and controlled access to stored information. *Trends in Cognitive Sciences*, *16*, 606–617. doi:10.1016/j.tics.2012.10.007

Kohn, N., Falkenberg, I., Kellermann, T., Eickhoff, S. B., Gur, R. C., & Habel, U. (2014). Neural correlates of effective and ineffective mood induction. *Social Cognitive and Affective Neuroscience*, *9*, 864–872. doi:10.1093/scan/nst055

Lacruz, M. E., García Seoane, J. J., Valentin, A., Selway, R., & Alarcón, G. (2007). Frontal and temporal functional connections of the living human brain. *European Journal of Neuroscience*, *26*, 1357–1370. doi:10.1111/j.1460-9568.2007.05730.x

Lindquist, M. A., Meng, J., Atlas, L. Y., & Wager, T. D. (2009). Modeling the hemodynamic response function in fMRI: Efficiency, bias and mis-modeling. *NeuroImage*, *45*, S187–S198. doi:10.1016/j.neuroimage.2008.10.065

López Zunini, R. A., Thivierge, J. P., Kousaie, S., Sheppard, C., & Taler, V. (2013). Alterations in resting-state activity relate to performance in a verbal recognition task. *PLoS ONE*, *8*(6), 1–8. doi:10.1371/journal.pone.0065608

Lu, C., Yang, T., Zhao, H., Zhang, M., Meng, F., Fu, H., . . . Xu, H. (2016). Insular cortex is critical for the perception, modulation, and chronification of pain. *Neuroscience Bulletin*, *32*, 191–201. doi:10.1007/s12264-016-0016-y

MacLean, M. H., Arnell, K. M., & Cote, K. A. (2012). Resting EEG in alpha and beta bands predicts individual differences in attentional blink magnitude. *Brain and Cognition*, *78*, 218–229. doi:10.1016/j.bandc.2011.12.010

Matlab. (2013). [Computer software]. Retrieved from https://in.mathworks.com/products/matlab.html

Mehta, R. K., Parasuraman, R., Mckinley, A., & Neuroscience, A. (2013). Neuroergonomics: A review of applications to physical and cognitive work. *Frontiers in Human Neuroscience*, *7*, Article 889. doi:10.3389/fnhum.2013.00889

Mennella, R., Patron, E., & Palomba, D. (2017). Frontal alpha asymmetry neurofeedback for the reduction of negative affect and anxiety. *Behaviour Research and Therapy*, *92*, 32–40. doi:10.1016/j.brat.2017.02.002

Murta, T., Leite, M., Carmichael, D. W., Patrícia, F., & Louis, L. (2015). Electrophysiological correlates of the BOLD signal for EEG-informed fMRI. *Human Brain Mapping*, *36*, 391–414. doi:10.1002/hbm.22623

Nikolla, D., Edgar, G., Catherwood, D., & Matthews, T. (2018). Can bottom-up processes of attention be a source of "interference" in situations where top-down control of attention is crucial? *British Journal of Psychology*, *109*, 85–98. doi:10.1111/bjop.12251

Nishijo, H., Rafal, R., & Tamietto, M. (2018). Editorial: Limbic-brainstem roles in perception, cognition, emotion, and behavior. *Frontiers in Neuroscience*, *12*, Article 395. doi:10.3389/fnins.2018.00395

Papousek, I., Weiss, E. M., Schulter, G., Fink, A., Reiser, E. M., & Lackner, H. K. (2014). Prefrontal EEG alpha asymmetry changes while observing disaster happening to other people: Cardiac correlates and prediction of emotional impact. *Biological Psychology*, *103*, 184–194. doi:10.1016/j.biopsycho.2014.09.001

Pernet, C. R., Wilcox, R., & Rousselet, G. A. (2013). Robust correlation analyses: False positive and power validation using a new open source Matlab toolbox. *Frontiers in Psychology*, *3*, Article 606. doi:10.3389/fpsyg.2012.00606

Pfeifer, J. H., Masten, C. L., Borofsky, L. A., Dapretto, M., Fuligni, A. J., & Lieberman, M. D. (2009). Neural correlates of direct and reflected self-appraisals in adolescents and adults: When social perspective-taking informs self-perception. *Child Development*, *80*, 1016–1038.

Raichle, M. E., & Snyder, A. Z. (2007). A default mode of brain function: A brief history of an evolving idea. *NeuroImage*, *37*, 1083–1090. doi:10.1016/j.neuroimage.2007.02.041

Repov, G. (2004). Naèin odgovarjanja in Stroopov uèinek: analiza reakcijskih èasov [The mode of response and the Stroop effect: A reaction time analysis]. *Horizons*, *114*, 105–114.

Reznik, S. J., & Allen, J. J. B. (2018). Frontal asymmetry as a mediator and moderator of emotion: An updated review. *Psychophysiology*, *55*(1). doi:10.1111/psyp.12965

Sadaghiani, S., & Kleinschmidt, A. (2016). Brain networks and α-oscillations: Structural and functional foundations of cognitive control. *Trends in Cognitive Sciences*, *20*, 805–817. doi:10.1016/j.tics.2016.09.004

Scarpina, F., & Tagini, S. (2017). The Stroop color and word test. *Frontiers in Psychology*, *8*, Article 557. doi:10.3389/fpsyg.2017.00557

Schneider, M., Chau, L., Mohamadpour, M., Stephens, N., Arya, K., & Grant, A. (2016). EEG asymmetry and BIS/BAS among

healthy adolescents. *Biological Psychology*, *120*, 142–148. doi:10.1016/j.biopsycho.2016.09.004

Schon, K., Newmark, R. E., Ross, R. S., & Stern, C. E. (2016). A working memory buffer in parahippocampal regions: Evidence from a load effect during the delay period. *Cerebral Cortex*, *26*, 1965–1974. doi:10.1093/cercor/bhv013

Sestito, M., Harel, A., Nador, J., & Flach, J. (2018). Investigating neural sensorimotor mechanisms underlying flight expertise in pilots: Preliminary data from an EEG study. *Frontiers in Human Neuroscience*, *12*, Article 489. doi:10.3389/fnhum.2018.00489

Shapiro, K. L., Hanslmayr, S., Enns, J. T., & Lleras, A. (2017). Alpha, beta: The rhythm of the attentional blink. *Psychonomic Bulletin & Review*, *24*, 1862–1869. doi:10.3758/s13423-017-1257-0

Smith, E. E., Reznik, S. J., Stewart, J. L., & Allen, J. J. B. (2017). Assessing and conceptualizing frontal EEG asymmetry: An updated primer on recording, processing, analyzing, and interpreting frontal alpha asymmetry. *International Journal of Psychophysiology*, *111*, 98–114. doi:10.1016/j.ijpsycho.2016.11.005

Spielberg, J. M., Stewart, J. L., Levin, R. L., & Miller, G. A. (2008). Prefrontal cortex, emotion, and approach/withdrawal motivation. *Social and Personality Psychology Compass*, *2*, 135–153. doi:10.1111/j.1751-9004.2007.00064.x

Stanislaw, H., & Todorov, N. (1999). Calculation of signal detection theory measures. *Behavior Research Methods, Instruments, & Computers*, *31*, 137–149. doi:10.3758/BF03207704

Thilakarathne, D. J. (2015). Modelling of situation awareness with perception, attention, and prior and retrospective awareness. *Biologically Inspired Cognitive Architectures*, *12*, 77–104. doi:10.1016/j.bica.2015.04.010

Tomarken, A. J., Davidson, R. J., & Henriques, J. B. (1990). Resting frontal brain asymmetry predicts affective responses to films. *Journal of Personality and Social Psychology*, *59*, 791–801. doi:10.1037/0022-3514.59.4.791

Tomarken, A. J., Davidson, R. J., Wheeler, R. E., & Kinney, L. (1992). Psychometric properties of resting anterior EEG asymmetry: Temporal stability and internal consistency. *Psychophysiology*, *29*, 576–592. doi:10.1111/j.1469-8986.1992.tb02034.x

Uusberg, A., Uibo, H., Kreegipuu, K., & Allik, J. (2013). EEG alpha and cortical inhibition in affective attention. *International Journal of Psychophysiology*, *89*, 26–36. doi:10.1016/j.ijpsycho.2013.04.020

Wheeler, R. E., Davidson, R. J., & Tomarken, A. J. (1993). Frontal brain asymmetry and emotional reactivity: A biological substrate of affective style. *Psychophysiology*, *30*, 82–89. doi:10.1111/j.1469-8986.1993.tb03207.x

Ardaman Kaur is a doctoral student in the NMR Research Center, Institute of Nuclear Medicine and Allied Sciences, India. She received her Master's degree in Electronic Science in 2014 from the Department of Electronic Science, University of Delhi, South Campus, India.

Rishu Chaujar is an associate professor in the Department of Engineering Physics, Delhi Technological University, India. She received her PhD degree in Electronic Science in 2009 from the Department of Electronic Science, University of Delhi, South Campus, India.

Vijayakumar Chinnadurai is a scientist in the NMR Research Center, Institute of Nuclear Medicine and Allied Sciences, India. He received his PhD degree in Electronic Science in 2011 from the Department of Electronic Science, University of Pune, Pune, India.

*Date received: October 9, 2018*
*Date accepted: July 19, 2019*

SCIENTIFIC REPORTS
nature research

OPEN

# Microstates-based resting frontal alpha asymmetry approach for understanding affect and approach/withdrawal behavior

Ardaman Kaur[1,2], Vijayakumar Chinnadurai[1*] & Rishu Chaujar[2]

**The role of resting frontal alpha-asymmetry in explaining neural-mechanisms of affect and approach/withdrawal behavior is still debatable. The present study explores the ability of the quasi-stable resting EEG asymmetry information and the associated neurovascular synchronization/desynchronization in bringing more insight into the understanding of neural-mechanisms of affect and approach/withdrawal behavior. For this purpose, a novel frontal alpha-asymmetry based on microstates, that assess quasi-stable EEG scalp topography information, is proposed and compared against standard frontal-asymmetry. Both proposed and standard frontal alpha-asymmetries were estimated from thirty-nine healthy volunteers resting-EEG simultaneously acquired with resting-fMRI. Further, neurovascular mechanisms of these asymmetry measures were estimated through EEG-informed fMRI. Subsequently, the Hemodynamic Lateralization Index (HLI) of the neural-underpinnings of both asymmetry measures was assessed. Finally, the robust correlation of both asymmetry-measures and their HLI's with PANAS, BIS/BAS was carried out. The standard resting frontal-asymmetry and its HLI yielded no significant correlation with any psychological-measures. However, the microstate resting frontal-asymmetry correlated significantly with negative affect and its neural underpinning's HLI significantly correlated with Positive/Negative affect and BIS/BAS measures. Finally, alpha-BOLD desynchronization was observed in neural-underpinning whose HLI correlated significantly with negative affect and BIS. Hence, the proposed resting microstate-frontal asymmetry better assesses the neural-mechanisms of affect, approach/withdrawal behavior.**

Understanding the neural mechanisms associated with functional hemispheric asymmetry of affect, approach/withdrawal measures is one of the core focuses in neuroscience. Numerous studies revealed an association of functional hemispheric asymmetry with positive/negative affect and approach/withdrawal dichotomy. This linkage was initially observed in many studies where left hemispheric lesion affected the perception of positive emotions whilst damage to the right hemisphere impaired the perception of negative emotions[1–3]. Subsequently, there was a surge in elucidating the role of frontal hemispheric asymmetry based on the alpha signature of electroencephalography (EEG) in manifesting the individual differences in affect and approach/withdrawal measures[4–6]. Davidson *et al.*[7–9], in their studies, suggested the lateralization of the prefrontal cortex (PFC) with respect to positive/motivational valence. Thus, the right PFC was observed to be linked with avoidance/negative emotion and left PFC with approach/positive emotion. Nevertheless, Carver and Harmon-Jones[10] showed the association of left hemisphere with negative emotion anger and thus proposed to eliminate the differentiation of positive and negative valence from the affective model. Subsequently, a larger number of studies concentrated on EEG frontal asymmetry through the induction of emotional/motivational states or tasks to understand the neural mechanisms associated with the evoked approach/withdrawal behavior[11–18] and other specific tasks[19]. This has led to ample literature which examined alterations in frontal EEG asymmetry in clinical and healthy populations[20–28].

Although the aforementioned studies have proved EEG based frontal asymmetry assessment as a reliable indicator of affect, approach/withdrawal behavior during emotional tasks, it's validity in healthy individuals during resting still remains ambiguous. In one large resting EEG study, Tomarken *et al.*[29,30] revealed a significant

[1]NMR Research Centre, Institute of Nuclear Medicine and Allied Sciences, Lucknow Road, Timarpur, Delhi, 110054, India. [2]Department of Applied Physics, Delhi Technological University, Shahbad Daulatpur, Main Bawana Road, Delhi, 110042, India. *email: vijayakumar@inmas.drdo.in

negative correlation of resting Frontal asymmetry (FA; channel pair: F4, F3) with negative affect and positive correlation of resting Anterior Temporal Asymmetry (ATA; channel pair: T4, T3) with positive affect for female subjects. Jacobs and Snyder[31], in their study, revealed the negative correlation of resting Frontal Temporal Asymmetry (FTA; channel pair: F8, F7) with negative affect in men, further Hall and Petruzzello[32] showed that resting FA positively predicted the positive affect of both sexes. Pertaining to approach and withdrawal measures, studies by Harmon-Jones and Allen[33] and De Pascalis *et al.*[34] reported a significant positive correlation of approach measure, Behavioral Activation System (BAS) with resting FA. The aforementioned studies are in sync with the hypothesis that positive affect correlates positively with alpha asymmetry ($\ln(\alpha lpha^{Right}) - \ln(\alpha lpha^{Left})$) and links to the left hemisphere, howbeit negative affect correlates negatively with the same and associates with the right hemisphere. Conversely, in another study[35], absolutely no significant relationship was observed between resting FA and measures of positive and negative valence for both sexes. Similarly, Schneider *et al.*[36] observed an absence of correlation between resting alpha FA and measures of approach/withdrawal behavior. In contradiction to the above hypothesis, Hagemann *et al.*[37] showed that subjects exhibiting greater relative left-hemispheric resting cortical activation at the anterior temporal site reported more intense NA in response to negative stimuli. Further, in the same line of research[38], it was found that subjects scoring high on NA, demonstrated greater relative left-sided resting cortical activation at the anterior temporal region than subjects scoring low on NA.

Most findings of the aforementioned literature are based on two fundamental assumptions. Firstly, the above studies assume the acquired EEG to possess only stable cognitive information. Hence, these studies correlate the single session EEG information directly with affect and approach/ withdrawal measures. However, many studies[29,39] revealed that the stable EEG patterns across previous sessions showed the interrelation of affect and approach/ withdrawal measures with frontal alpha asymmetry. This brings the importance of assessing the stable EEG patterns and information from single session recordings as unstable EEG information may be influenced by interference from many cognitive factors. Recent EEG studies of wakeful rest have shown that global electrical brain activity on scalp remains semi-stable for transient periods[40,41]. In specifics, there exists a finite number of scalp potential topographies in spontaneous resting EEG activity that remains stable for a definite time before rapidly shifting to a different topography that once again attains a stable state. These distinct epochs of topographic stability have been referred to as 'EEG microstates'. Lehman *et al.*[42] substantiated that EEG microstates represent blocks of consciousness, and these microstates are modulated by the content of the thoughts. Additionally, Milz *et al.*[43] postulated the role of intracranial sources in the alpha band in predominantly determining these EEG microstate topographies. Further, Shafi *et al.*[44], in their study, highlighted the role of microstates in individual variability of human fluid intelligence and in response to cognitive training. Howbeit, there is no study to date that has explored the quasi-stable state as assessed by EEG microstates for understanding frontal hemispheric asymmetry. Also, their ability over standard EEG frontal asymmetry in explaining affect and approach/withdrawal dichotomy is still unmapped.

Further, the second important assumption is that EEG alpha power is inversely[45–47] related to neural activation. Hence, an increase in neural activation in the left hemisphere is associated with the increase observed in frontal asymmetry scores. This enables us in concluding that the positive correlation of affect and approach/withdrawal measures with frontal asymmetry score ($\ln(\alpha lpha^{Right}) - \ln(\alpha lpha^{Left})$) is the resultant of left hemispherical neuronal activity and vice versa. However, recently, many neuro-vascular studies[48–51] have observed alpha-BOLD synchronization wherein the alpha power correlates positively with neural activation during task engagement. Hence, there is a need to fully understand the neurovascular coupling and neural underpinning associated with frontal EEG asymmetry[5] and how alpha-BOLD synchronization or desynchronization during resting-state associates with affect and approach/withdrawal behavior. Few researchers brought better understanding by studying the role of hemispheric asymmetry in affect, approach/avoidance behavior through functional MR imaging. Rohr *et al.*[52] concluded that the affective elements in the underlying organization of emotion are predominantly associated with the network of right-hemispheric regions. Lindquist *et al.*[53] proposed that the implementation of valence depends on a set of valence-general limbic and paralimbic brain regions. Though the above studies gave significant insights, the congruence between resting-EEG frontal alpha asymmetry and resting-fMRI is still uncharted. This is vital for a better understanding of neuro-vascular aspects of resting frontal asymmetry and their association with affect and approach/withdrawal behavior.

Hence, the present study proposes an EEG microstate based approach for assessment of quasi-stable frontal hemispherical asymmetry measures of resting-state affect and approach/withdrawal behavior. It further aims to compare the performance of microstate based frontal hemispheric asymmetry against the standard resting EEG frontal asymmetry measures. For this purpose, resting EEG was acquired from a sample of 39 healthy male subjects. This multichannel resting-EEG signal from all subjects was parsed into a limited number of distinct quasi-stable microstates. These microstates were back-fitted to each subject's EEG data to obtain microstate time-series data specific to each subject. The microstate time-series was further filtered at alpha frequency band and EEG microstate based frontal asymmetry measures were derived from channel pairs F4/F3 (FA) and F8/F7 (FTA). Further, the robust correlation of both standard and EEG microstate based frontal hemispheric asymmetry with positive/negative affect (PANAS) and approach (BAS)/withdrawal (BIS) behavior was carried out.

Moreover, the study focuses on bringing a better understanding of neural mechanisms associated with functional hemispheric asymmetry of affect and approach/ withdrawal behavior during resting-state. For this purpose, standard and microstates based resting EEG frontal asymmetries were subjected to the EEG informed fMRI approach and the associated neural underpinning of both EEG frontal asymmetries were independently estimated. Thereafter, the hemodynamic lateralization index (HLI) based on the amplitude of hemodynamic response function (HRF) of regions part of the neural underpinning of both EEG frontal asymmetries were assessed. Further, the estimated HLI was subjected to a robust correlation with resting-state affect and approach/withdrawal psychological scores. Finally, the results were analyzed to understand the ability of proposed EEG

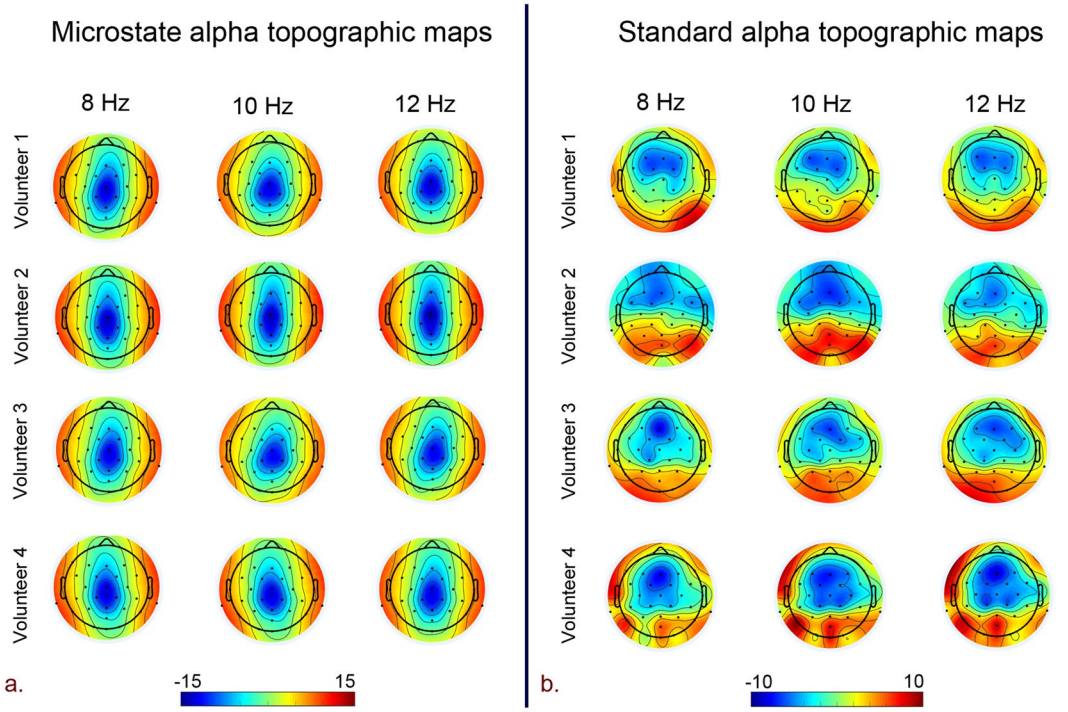


**Figure 1.** Topographic EEG maps of spectral power density for the alpha band for. (**a**) Proposed microstate based analysis and. (**b**) Standard analysis (CSD referenced). The color bar represents the log-transformed spectral power density (10*log10 ($\mu v^2$/Hz)) where red represents the maximum and blue represents the minimum values.

microstate estimates in revealing neural-vascular insights of association of functional hemispherical asymmetry with resting-state affect and approach/ withdrawal behavior.

## Results

Our study focused on exploring the ability of quasi-stable EEG microstate based frontal alpha hemispherical asymmetry measures against standard EEG frontal alpha asymmetry measures in explaining the resting state affect and approach/ withdrawal behavior for healthy young male volunteers during 1-time measurement. The standard alpha topographic maps (CSD referenced) and microstate alpha topographic maps are shown in Fig. 1. Evidently, the maps of standard alpha topography (CSD referenced) in Fig. 1b reveal the typical parietal-occipital alpha activity for eyes-closed resting-state condition[54,55]. However, the parietal-alpha activity is typical of standard alpha topographic maps and has not been observed and reported by any researchers in microstate alpha topographic maps so far. For assessing the association of EEG microstate based frontal hemispheric asymmetry with affect and approach/withdrawal behavior, robust correlation of PANAS and BAS, BIS measures with standard and EEG microstate FA and FTA was estimated. Subsequently, to better understand the neural mechanisms underlying the proposed microstate and standard hemispherical asymmetry measures, they were subjected to the EEG informed fMRI, and their neural underpinnings were estimated. Further, to gain insights into the hemodynamic lateralization associated with the neural underpinnings and its linkage with affect and approach/withdrawal measures, HLI of both asymmetry measures neural underpinnings' was calculated and subsequently subjected to the robust correlation with PANAS and BAS, BIS measures.

**Robust correlation of frontal hemispherical asymmetry measures with psychological measures.** The robust correlation (Pearson, bend, spearman, and skipped) of proposed microstate and standard frontal hemispheric asymmetry measures with PANAS, BIS/BAS psychological scores are tabulated in Table 1.

Standard FA and FTA revealed no statistically significant correlation with PANAS as well as BIS/BAS measures. Similarly, proposed microstate based FA and FTA yielded insignificant low correlation with positive affect score.

Howbeit, negative affect scores revealed a strong and significant correlation with proposed microstate based FA and FTA. Specifically, microstates based FA yielded high pearson, bend and spearman correlations (Fig. 2a: pearson r = 0.35, 95% CI = [0.07; 0.58], pcorr = 0.04; Fig. 2b: bend r = 0.33, 95% CI = [−0.02; 0.61], pcorr = 0.05; Fig. 2c: spearman r = 0.36, 95% CI = [0.04; 0.62], pcorr = 0.03). Similarly, skipped pearson and spearman robust correlations of microstates based FA with negative affect scores has also yielded stronger correlations (Fig. 2d: pearson skipped = 0.35, 95% CI = [0.04; 0.57]; spearman skipped = 0.36, 95% CI = [0.005; 0.62]). In addition, a strong robust pearson, bend and spearman correlation of microstates based FTA with negative affect scores was observed (Fig. 3a: pearson r = 0.42, 95% CI = [0.13; 0.67], pcorr = 0.01; Fig. 3b: Bend r = 0.42, 95% CI = [0.05;

| EEG alpha frontal asymmetry | Channel pair | Behavioral measure | Pearson Correlation | | Bend correlation | | Spearman correlation | | Skipped correlation | | | |
|---|---|---|---|---|---|---|---|---|---|---|---|---|
| | | | | | | | | | Pearson | | Spearman | |
| | | | r | p | r | p | r | p | r | t | r | t |
| Standard | F4/F3 (FA) | Positive affect | 0.22 | 0.21 | 0.2 | 0.23 | 0.09 | 0.54 | 0.22 | 1.27 | 0.09 | 0.54 |
| | | Negative affect | −0.1 | 0.54 | −0.04 | 0.8 | −0.05 | 0.75 | −0.1 | −0.6 | −0.05 | −0.31 |
| | | BAS | −0.25 | 0.37 | −0.16 | 0.56 | −0.17 | 0.56 | −0.25 | −0.92 | −0.17 | −0.59 |
| | | BIS | −0.03 | 0.9 | 0.09 | 0.75 | 0.09 | 0.73 | −0.03 | −0.12 | 0.09 | 0.34 |
| | F8/F7 (FTA) | Positive affect | 0.03 | 0.83 | −0.11 | 0.52 | −0.12 | 0.47 | 0.03 | 0.21 | −0.12 | −0.73 |
| | | Negative affect | −0.05 | 0.75 | 0.01 | 0.92 | −0.004 | 0.97 | −0.05 | −0.31 | −0.004 | −0.02 |
| | | BAS | 0.18 | 0.52 | 0.17 | 0.55 | 0.13 | 0.65 | 0.18 | 0.65 | 0.13 | 0.46 |
| | | BIS | −0.14 | 0.62 | −0.14 | 0.61 | −0.3 | 0.28 | −0.14 | −0.5 | −0.3 | −1.12 |
| Microstates | F4/F3 (FA) | Positive affect | 0.03 | 0.84 | 0.08 | 0.61 | 0.12 | 0.46 | 0.03 | 0.2 | 0.12 | 0.73 |
| | | Negative affect | 0.35 | 0.04 | 0.33 | 0.05 | 0.36 | 0.03 | 0.35 | 2.13 | 0.36 | 2.2 |
| | | BAS | −0.09 | 0.74 | −0.04 | 0.86 | 0 | 1 | −0.09 | −0.32 | 0 | 0 |
| | | BIS | −0.3 | 0.29 | −0.41 | 0.14 | −0.28 | 0.32 | −0.3 | −1.09 | −0.28 | −1.01 |
| | F8/F7 (FTA) | Positive affect | 0.0003 | 0.99 | −0.01 | 0.91 | −0.01 | 0.92 | 0.0003 | 0.0018 | −0.01 | −0.09 |
| | | Negative affect | 0.42 | 0.01 | 0.42 | 0.01 | 0.38 | 0.02 | 0.42 | 2.64 | 0.38 | 2.34 |
| | | BAS | −0.17 | 0.54 | −0.18 | 0.52 | −0.18 | 0.53 | −0.17 | −0.62 | −0.18 | −0.64 |
| | | BIS | −0.32 | 0.25 | −0.45 | −1.7 | −0.33 | −1.22 | −0.32 | −1.19 | −0.33 | −1.22 |

**Table 1.** Robust correlation (Pearson, bend, spearman and skipped) of standard and proposed microstate based frontal hemispheric asymmetry measures with psychological scores.

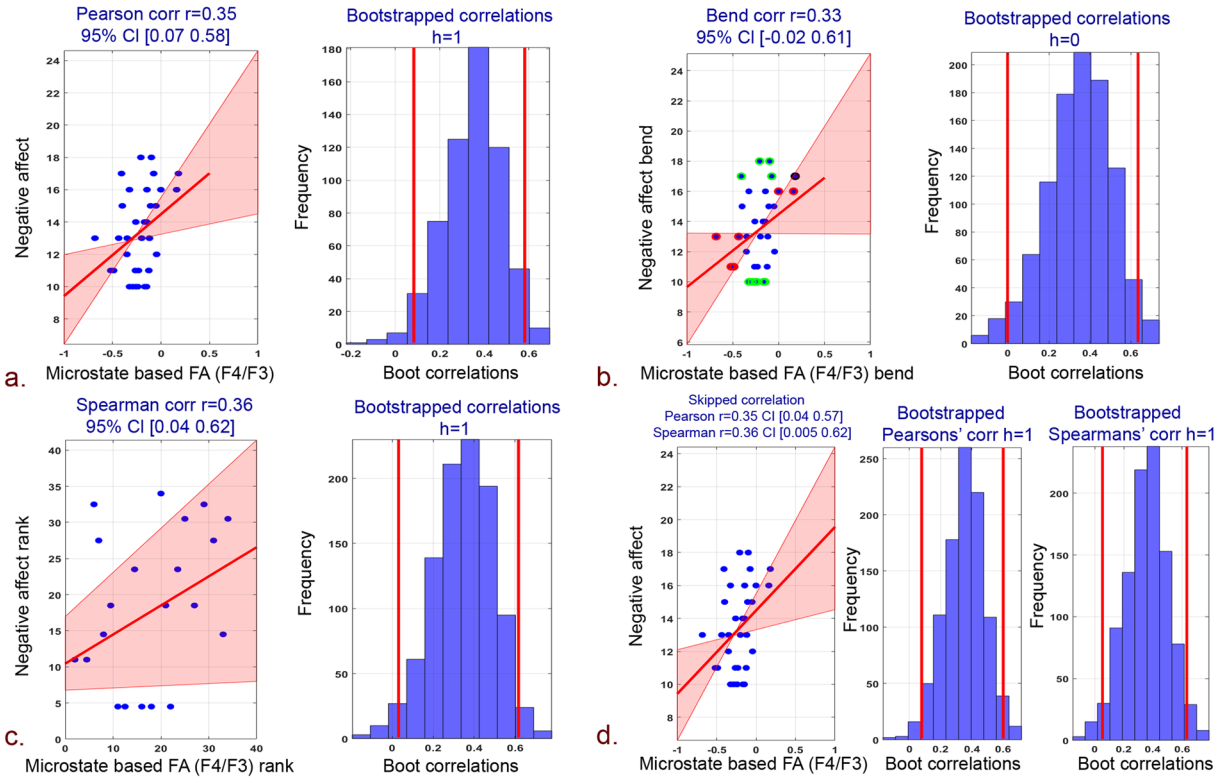


**Figure 2.** Correlation plots between negative affect scores and microstate based FA (F4/F3) and associated histograms of correlations for bootstrapped data. (**a**) Pearson correlation. (**b**) 20% Bend correlation. (**c**) Spearman correlation. (**d**) Skipped (Pearson and Spearman) correlations.

0.70], pcorr = 0.01; Fig. 3c: spearman r = 0.38, 95% CI = [0.02; 0.68], pcorr = 0.02). Skipped (pearson and spearman) correlations among microstates-derived FTA and negative affect scores has also yielded stronger correlations (Fig. 3d: Pearson skipped = 0.42, 95% CI = [0.14; 0.67]; Spearman skipped = 0.38, 95% CI = [0.04; 0.68]).

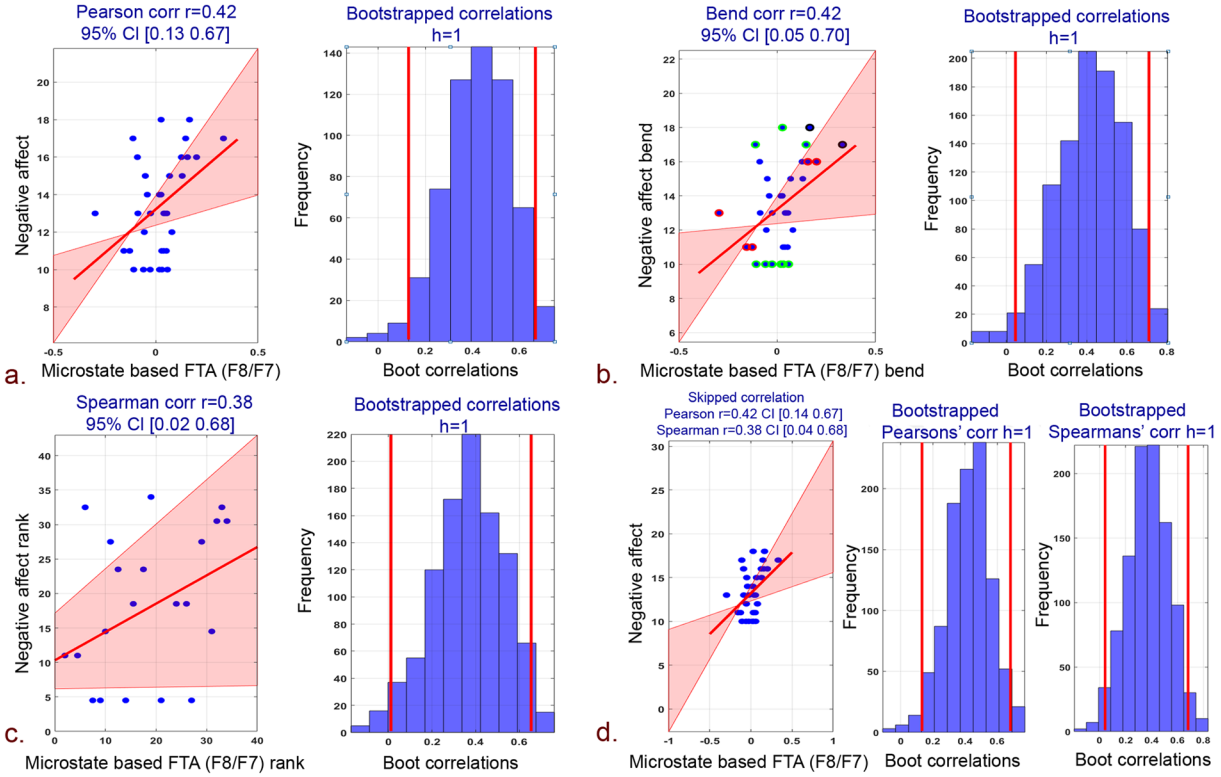


**Figure 3.** Correlation plots between negative affect scores and microstate based FTA (F8/F7) and associated histograms of correlations for bootstrapped data. (**a**) Pearson correlation. (**b**) 20% Bend correlation. (**c**) Spearman correlation. (**d**) Skipped (Pearson and Spearman) correlations.

However, BAS measures yielded a statistically insignificant low correlation with proposed microstate asymmetry. The analysis with BIS measures for both FA and FTA revealed high correlation, but the p-values remained insignificant.

**EEG informed fMRI analysis.** The proposed microstate and standard hemispherical asymmetry measures were subjected to the EEG informed fMRI analysis to assess their neural underpinnings, respectively. The observed neural underpinnings were inferred with FDR corrected p-values less than 0.05, and a cluster size of more than 20 voxels were considered for analysis.

**Neural underpinnings of standard hemispheric asymmetry.** Neural underpinnings of standard FA encompassed right as well as left-hemispheric regions (Fig. 4a). Table 2 comprises of these areas, their peak coordinates, and cluster size. Specifically, in the right hemisphere, EEG frontal asymmetry negatively correlated with BOLD activity in occipital cortex with major clusters in lateral occipital cortex and occipital pole. Additionally, BOLD activity in temporal cortex also correlated negatively with standard FA. However, BOLD of parietal cortex regions, particularly postcentral gyrus, correlated positively with standard FA. Withal, in the left hemisphere, standard FA correlated positively with BOLD activity in the postcentral gyrus. However, activity in the occipital fusiform gyrus and temporal lobe regions correlated negatively with this alpha asymmetry measure. Majority of frontal lobe regions correlated negatively. However, superior frontal gyrus correlated positively (high t-value as compared to the right hemisphere) with standard FA.

Figure 4b shows the neural underpinnings of standard FTA. Both right and left hemispheres revealed positive as well as negative correlations between BOLD activity and standard FTA (Table 3). In the right hemisphere, BOLD activity in occipital lobe regions (cuneal cortex, lingual gyrus, and superior division of lateral occipital cortex) correlated negatively with standard FTA. Major clusters in the frontal lobe, specifically frontal pole, and activity in precuneus cortex also found a negative correlation with this frontal asymmetry index. In the left hemisphere, standard FTA correlated negatively with BOLD activity in Inferior frontal gyrus. Few clusters in parietal, occipital and temporal pole also correlated negatively with standard FTA. The neural underpinnings of standard FA showed left-hemispheric dominance whilst FTA revealed right-hemispheric dominance.

**Neural underpinnings of microstate based EEG asymmetry.** Right and left-lateralized neural underpinnings of microstate based FA are shown in Fig. 5a. A complete list of activation clusters is provided in Table 4. In the right hemisphere, microstate based FA correlated negatively with BOLD activity in the frontal medial cortex and frontal pole regions of the frontal lobe. Similarly, BOLD activity in the posterior division of cingulate gyrus has also correlated negatively. However, few clusters in the frontal lobe, occipital lobe, and temporal

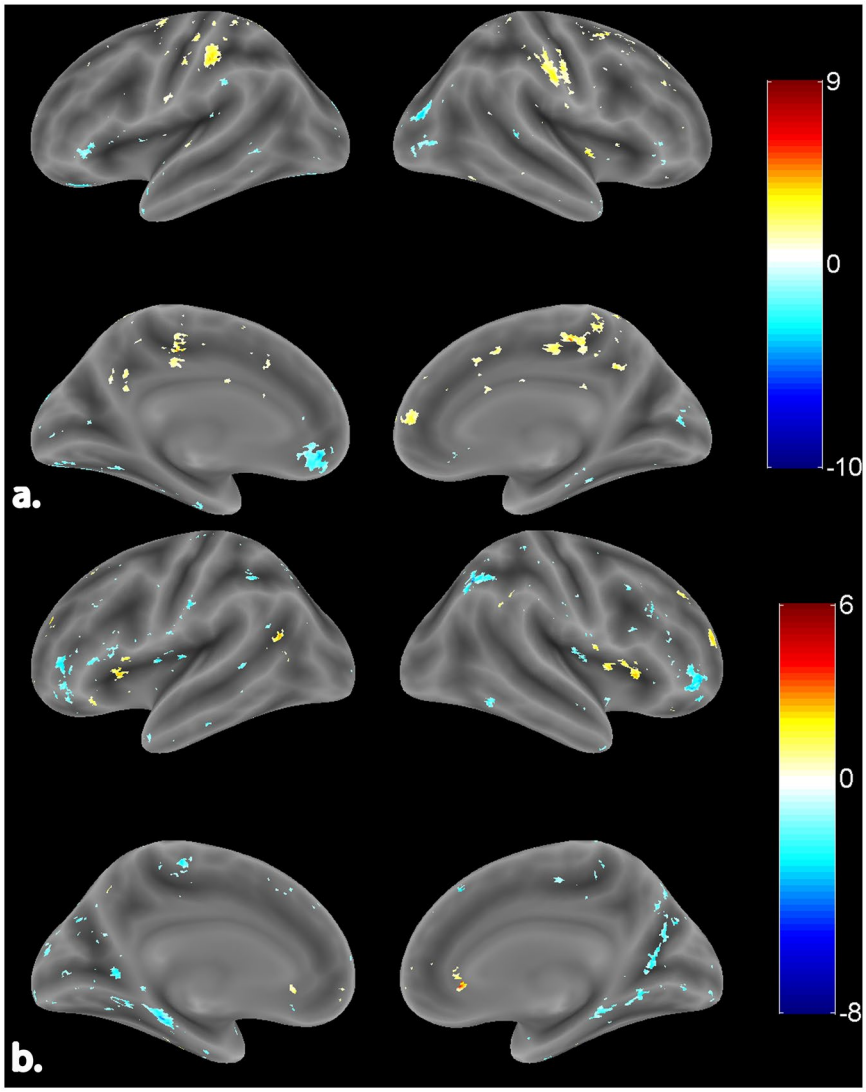


**Figure 4.** Surface rendered view of neural underpinnings of standard. (**a**) FA (channel pair F4/F3). (**b**) FTA (channel pair F8/F7). The color bar indicates the t-values with blue being the least and red being the highest. The activations are represented at FDR corrected $p < 0.05$.

pole revealed a positive correlation with microstate FA. In the left hemisphere, resting-state microstate based FA correlated positively with major clusters in all lobes with frontal lobe having the maximum cluster extent. This is evident as microstates are known to represent the global brain activity.

Figure 5b shows the neural underpinnings in both right and left hemispheres for resting-state microstate based FTA. Table 5 comprises of these areas, their peak coordinates, and cluster size. In the right hemisphere, activity in the frontal lobe and limbic lobe regions correlated negatively with this EEG alpha asymmetry. BOLD of specific regions of the parietal lobe (Angular gyrus) and temporal lobe (Planum temporale) correlated negatively with microstate based FTA. Pertaining to the left hemisphere, activations in the frontal lobe and limbic lobe (a posterior division of cingulate gyrus) correlated negatively with microstate based FTA. Negative correlation also emanated from BOLD activity in specific regions of the parietal lobe (Angular gyrus, Superior parietal lobule) and lateral occipital cortex of occipital lobe. The neural underpinnings for microstate based FA and FTA showed left-hemispheric dominance.

**Robust correlation of HLI with PANAS, BIS/BAS measures.** The correlation and p-values for all the significant results obtained for this analysis are tabulated in Table 6. The robust correlation between negative affect measure and HLI of neural underpinnings of microstate frontal alpha asymmetry yielded a significantly strong negative correlation in the anterior division of the middle temporal gyrus. Further, superior frontal gyrus emerged as the positive correlate for correlation among positive affect scores and HLI pertaining to neural underpinnings of microstate alpha asymmetry. Moreover, the correlation of BIS measure with HLI pertaining to neural underpinnings of microstate frontal alpha asymmetry yielded a significantly strong positive correlation in inferior frontal gyrus (pars triangularis) and frontal medial cortex. Further, the HLI of occipital fusiform gyrus correlated negatively with BAS measure.

| Cluster Center Region | Cluster No. | Voxels | MNI Coordinates | | | T-Stats |
|---|---|---|---|---|---|---|
| **Right Hemispheric Activations** | | | | | | |
| **Frontal Lobe** | | | | | | |
| Superior frontal gyrus | 1 | 43 | 22 | 4 | 48 | 4.271 |
| **Parietal Lobe** | | | | | | |
| Postcentral gyrus | 1 | 246 | 50 | −20 | 38 | 6.414 |
| | 2 | 97 | 16 | −28 | 44 | 8.087 |
| | 3 | 33 | 14 | −44 | 60 | 3.886 |
| | 4 | 23 | 48 | −26 | 64 | −3.349 |
| Superior parietal lobule | 1 | 48 | 18 | −46 | 64 | 4.345 |
| **Occipital Lobe** | | | | | | |
| Lateral occipital cortex, superior division | 1 | 96 | 38 | −86 | 14 | −4.214 |
| Lateral occipital cortex, inferior division | 1 | 31 | 36 | −72 | −30 | −2.84 |
| | 2 | 20 | 46 | −80 | 2 | −3.317 |
| Occipital pole | 1 | 96 | 22 | −90 | 26 | −4.04 |
| Intracalcarine cortex | 1 | 27 | 10 | −80 | 10 | −2.747 |
| **Temporal Lobe** | | | | | | |
| Temporal pole | 1 | 20 | 42 | 14 | −32 | −2.74 |
| **Limbic Lobe** | | | | | | |
| Paracingulate gyrus | 1 | 34 | 12 | 50 | 10 | 3.121 |
| Insular cortex | 1 | 38 | 34 | −6 | −2 | 9.396 |
| **Left Hemispheric Activations** | | | | | | |
| **Frontal Lobe** | | | | | | |
| Superior frontal gyrus | 1 | 118 | −24 | −4 | 62 | 7.828 |
| | 2 | 26 | −6 | 56 | 30 | −3.36 |
| Frontal medial cortex | 1 | 117 | −12 | 42 | −10 | −5.587 |
| Frontal orbital cortex | 1 | 60 | −22 | 26 | −18 | −6.658 |
| Precentral gyrus | 1 | 60 | −16 | −26 | 40 | 6.636 |
| Inferior frontal gyrus | 1 | 27 | −46 | 30 | −2 | −3.36 |
| **Parietal Lobe** | | | | | | |
| Postcentral gyrus | 1 | 147 | −46 | −26 | 38 | 5.015 |
| | 2 | 36 | −36 | −28 | 70 | 3.992 |
| | 3 | 21 | −62 | −8 | 22 | 2.715 |
| Superior parietal lobule | 1 | 132 | −30 | −46 | 64 | 7.511 |
| **Occipital Lobe** | | | | | | |
| Occipital fusiform gyrus | 1 | 159 | −22 | −84 | −10 | −3.179 |
| Occipital pole | 1 | 29 | −16 | −90 | 30 | −3.58 |
| | 2 | 20 | −2 | −98 | 0 | −2.736 |
| **Temporal Lobe** | | | | | | |
| Temporal Occipital Fusiform Cortex | 1 | 159 | −28 | −66 | −22 | −2.946 |
| Temporal Fusiform cortex, posterior division | 1 | 39 | −36 | −14 | −26 | −3.441 |
| **Limbic Lobe** | | | | | | |
| Cingulate gyrus, posterior division | 1 | 34 | −8 | −54 | 28 | 4.73 |

**Table 2.** Neural underpinnings of standard FA (channel pair F4/F3). The activations after correction for multiple comparisons are represented at $p < 0.05$ (FDR corrected). The coordinates reported are in Montreal Neurological Institute (MNI) space.

However, the robust correlation between negative affect measure and HLI of neural underpinnings of standard frontal alpha asymmetry yielded low and insignificant correlation with all cortical regions. Whilst correlation of positive affect scores with HLI pertaining to standard alpha asymmetry revealed a significant positive correlation with the insular cortex. Further, the correlation of BAS and BIS measures with HLI revealed a low and insignificant correlation with all cortical regions pertaining to standard alpha asymmetry.

**Robust correlation among frontal hemispherical asymmetry measures.** Figure 6 shows the Pearson robust correlation of proposed microstate frontal hemispheric asymmetry with standard frontal hemispheric asymmetry measures. Proposed microstate based FA and FTA yielded insignificant low correlation with

| Cluster Center Region | Cluster No. | Voxels | MNI Coordinates | | | T-Stats |
|---|---|---|---|---|---|---|
| **Right Hemispheric Activations** | | | | | | |
| **Frontal Lobe** | | | | | | |
| Frontal pole | 1 | 67 | 26 | 54 | 22 | 3.822 |
| | 2 | 385 | 46 | 38 | 10 | −5.757 |
| | 3 | 385 | 30 | 48 | −12 | −5.113 |
| | 4 | 385 | 50 | 44 | −10 | −2.962 |
| Subcallosal cortex | 1 | 25 | 6 | 30 | −4 | 6.522 |
| | 2 | 20 | 6 | 14 | −4 | −3.574 |
| Middle frontal gyrus | 1 | 94 | 50 | 14 | 36 | −8.063 |
| Precentral gyrus | 1 | 27 | 50 | 6 | 40 | −3.411 |
| **Parietal Lobe** | | | | | | |
| Precuneous cortex | 1 | 392 | 28 | −52 | 10 | −4.401 |
| | 2 | 392 | 22 | −66 | 26 | −2.890 |
| Supramarginal gyrus, posterior gyrus | 1 | 36 | 64 | −46 | 32 | 3.054 |
| **Occipital Lobe** | | | | | | |
| Cuneal cortex | 1 | 392 | 8 | −78 | 38 | −5.546 |
| Lateral occipital cortex, superior division | 1 | 174 | 34 | −62 | 46 | −6.328 |
| Occipital fusiform cortex | 1 | 149 | 26 | −68 | −26 | −4.764 |
| Lingual gyrus | 1 | 210 | 14 | −58 | −4 | −2.931 |
| | 2 | 48 | 2 | −76 | 0 | −2.582 |
| Occipital pole | 1 | 20 | 8 | −96 | 2 | −2.553 |
| **Temporal Lobe** | | | | | | |
| Inferior temporal gyrus, temporooccipital part | | 39 | 56 | −54 | −14 | −3.061 |
| Central operculum cortex | | 28 | 36 | −12 | 22 | −2.751 |
| **Limbic Lobe** | | | | | | |
| Insular cortex | | 56 | 30 | 20 | 8 | 3.558 |
| **Left Hemispheric Activations** | | | | | | |
| **Frontal Lobe** | | | | | | |
| Inferior frontal gyrus | 1 | 305 | −50 | 32 | 16 | −3.912 |
| | 2 | 20 | −46 | 16 | 26 | −2.703 |
| Middle frontal gyrus | 1 | 42 | −52 | 22 | 30 | −3.196 |
| | 2 | 21 | −50 | 14 | 36 | −3.502 |
| Frontal operculum cortex | 1 | 46 | −34 | 18 | 12 | 3.808 |
| Precentral gyrus | 1 | 36 | −6 | −26 | 52 | −2.984 |
| | 2 | 22 | −32 | −20 | 72 | −3.16 |
| **Parietal Lobe** | | | | | | |
| Supramarginal gyrus, posterior division | 1 | 32 | −36 | −44 | 36 | −2.772 |
| Postcentral gyrus | 1 | 24 | −62 | −14 | 36 | −2.86 |
| **Occipital Lobe** | | | | | | |
| Occipital pole | 1 | 60 | −4 | −94 | 22 | −2.882 |
| Lateral occipital cortex, superior division | 1 | 26 | −8 | −86 | 38 | −2.893 |
| Lingual gyrus | 1 | 42 | −24 | −54 | 2 | −2.896 |
| **Temporal Lobe** | | | | | | |
| Temporal pole | 1 | 40 | −50 | 10 | −28 | −3.633 |
| **Limbic Lobe** | | | | | | |
| Parahippocampal gyrus, posterior division | 1 | 175 | −10 | −38 | −22 | −5.375 |
| Parahippocampal gyrus, anterior division | 1 | 23 | −30 | −10 | −30 | −3.412 |
| Cingulate gyrus, posterior division | 1 | 22 | −10 | −40 | 2 | −2.716 |

**Table 3.** Neural underpinnings of standard FTA (channel pair F8/F7). The activations after correction for multiple comparisons are represented at $p < 0.05$ (FDR corrected). The coordinates reported are in Montreal Neurological Institute (MNI) space.

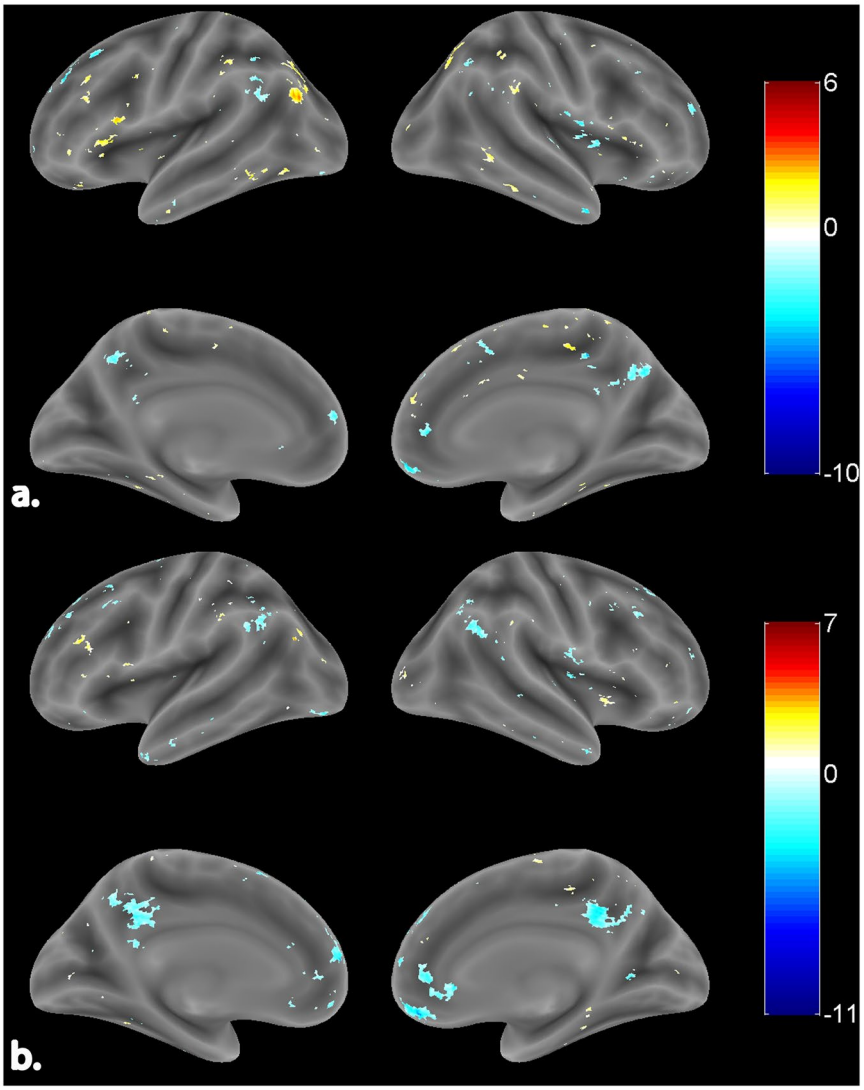


**Figure 5.** Surface rendered view of neural underpinnings of proposed microstate based. (**a**) FA (channel pair F4/F3). (**b**) FTA (channel pair F8/F7). The color bar indicates the t-values with blue being the least and red being the highest. The activations are represented at FDR corrected $p < 0.05$.

standard FA and FTA. Pearson correlation among standard and microstate based FA and FTA revealed correlation coefficients and p-values as Pearson $r = -0.14, 0.013$; $pcorr = 0.37, 0.93$ respectively.

## Discussion

Valence[56–59] and motivation hypothesis[60] propose that higher values of positive affect/approach behavior and negative affect/withdrawal behavior are associated with the greater relative left and right cortical activation, respectively. These hypotheses are established in task-based EEG alpha asymmetry studies where the implications are based on alpha inhibition (desynchronization w.r.t BOLD) in event-specific regions[45,47]. Thus, following this abstraction, the above-mentioned hypothesis holds when standard frontal hemispheric asymmetry ($\ln(\alpha^{Right}) - \ln(\alpha^{Left})$) correlates positively with positive affect/ approach behavior and negatively with negative affect/withdrawal behavior. Howbeit, the validity of these hypotheses in resting-state recordings which involves sole perception and not induction of valence/ behavior still remains vacillating. The inconsistent results of the relationship between the standard resting frontal asymmetry and affect and approach/withdrawal behavior are tabulated in Table 7. The line of studies by Tomarken *et al.*[29,30] and Jacob and Snyder[31] supported the above hypothesis. Similarly, for approach/withdrawal dichotomy, Harmon-Jones and Allen[33], Shackman *et al.*[61], and De Pascalis *et al.*[34] supported the above-mentioned hypotheses. Nonetheless, Sutton and Davidson[35] and Schneider *et al.*[36] observed no association of affect, approach/withdrawal dichotomy with frontal asymmetry, respectively. Conversely, the study by Hagemann *et al.*[38] proposed that subjects with high negative affect exhibited high left cortical activation. Further, Hewig *et al.*[62] propounded a higher approach measure to be associated with the bilateral frontal cortical activity. Hence, in order to bring more clarity, the present study aims to assess the capability of quasi-stable microstates based frontal hemispheric asymmetry in explaining the affect and approach/withdrawal dichotomy as against standard frontal hemispheric asymmetry.

| Cluster Center Region | Cluster No. | Voxels | MNI Coordinates | | | T-Stats |
|---|---|---|---|---|---|---|
| **Right Hemispheric Activations** | | | | | | |
| **Frontal Lobe** | | | | | | |
| Middle frontal gyrus | 1 | 32 | 42 | 34 | 40 | 5.93 |
| | 2 | 26 | 44 | 4 | 58 | 3.035 |
| Superior frontal gyrus | 1 | 24 | 4 | 14 | 60 | 3.421 |
| Frontal operculum cortex | 1 | 20 | 40 | 22 | 4 | 3.036 |
| Frontal medial cortex | 1 | 59 | 4 | 44 | −14 | −6.743 |
| Frontal pole | 1 | 20 | 22 | 48 | 18 | −3.366 |
| **Parietal Lobe** | | | | | | |
| Precuneous cortex | 1 | 23 | 6 | −50 | 66 | 4.279 |
| **Occipital Lobe** | | | | | | |
| Lateral occipital cortex, superior division | 1 | 64 | 22 | −58 | 48 | 4.138 |
| **Temporal Lobe** | | | | | | |
| Temporal occipital fusiform cortex | 1 | 60 | 32 | −40 | −28 | 3.691 |
| Middle temporal gyrus, temporoccipital part | 1 | 42 | 62 | −50 | −8 | 4.211 |
| Inferior temporal gyrus,temporoccipital part | 1 | 22 | 54 | −38 | −18 | 3.538 |
| Central operculum cortex | 1 | 22 | 50 | −8 | 10 | −4.769 |
| Middle temporal gyrus, anterior division | 1 | 23 | 52 | 0 | −36 | −5.849 |
| **Limbic Lobe** | | | | | | |
| Insular cortex | 1 | 48 | 40 | 14 | −4 | 6.748 |
| | 2 | 29 | 36 | 2 | 4 | −3.17 |
| Parahippocampal gyrus, posterior division | 1 | 27 | 36 | −28 | −10 | 5.738 |
| Cingulate gyrus, posterior division | 1 | 106 | 8 | −52 | 28 | −3.381 |
| **Left Hemispheric Activations** | | | | | | |
| **Frontal Lobe** | | | | | | |
| Inferior frontal gyrus | 1 | 82 | −54 | 10 | 14 | 5.142 |
| Frontal operculum cortex | 1 | 37 | −40 | 24 | 6 | 3.055 |
| Middle frontal gyrus | 1 | 29 | −42 | 30 | 42 | 2.89 |
| | 2 | 42 | −24 | 24 | 36 | −7.953 |
| Frontal pole | 1 | 42 | −22 | 40 | 32 | −4.002 |
| Precentral gyrus | 1 | 41 | −36 | −10 | 66 | −3.66 |
| **Parietal Lobe** | | | | | | |
| Supramarginal gyrus, anterior division | 1 | 57 | −60 | −30 | 46 | 3.13 |
| Supramarginal gyrus, anterior division | 2 | 23 | −44 | −36 | 44 | 3.112 |
| Postcentral gyrus | 1 | 23 | −14 | −38 | 76 | 3.168 |
| Supramarginal gyrus, posterior division | 1 | 22 | −54 | −42 | 54 | 3.485 |
| | 2 | 35 | −38 | −48 | 36 | −3.261 |
| Precuneous cortex | 1 | 144 | −4 | −58 | 42 | −4.005 |
| **Occipital Lobe** | | | | | | |
| Lateral occipital cortex, superior division | 1 | 74 | −42 | −74 | 28 | 4.041 |
| | 2 | 50 | −28 | −62 | 30 | 2.992 |
| | 3 | 41 | −30 | −78 | 36 | 3.427 |
| Lateral occipital cortex, inferior division | 1 | 24 | −30 | −82 | −28 | −3.625 |
| Occipital fusiform gyrus | 1 | 21 | −34 | −86 | −20 | −3.382 |
| **Temporal Lobe** | | | | | | |
| Temporal fusiform cortex, posterior division | 1 | 66 | −38 | −48 | −32 | 3.132 |
| Inferior temporal gyrus, temporoocipital part | 1 | 23 | −58 | −54 | −14 | 2.967 |
| **Limbic Lobe** | | | | | | |
| Parahippocampal Gyrus, posterior division | 1 | 66 | −22 | −36 | −20 | 3.035 |

**Table 4.** Neural underpinnings of proposed microstate based FA (channel pair F4/F3). The activations after correction for multiple comparisons are represented at $p < 0.05$ (FDR corrected). The coordinates reported are in Montreal Neurological Institute (MNI) space.

**Prelude to the present research study.** This study primarily focuses on exploring the ability of EEG microstates based frontal hemispherical asymmetry measure against standard Davidson's approach in explaining mechanisms of the resting state affect and approach/ withdrawal behavior. The rationale for examining EEG microstates-derived frontal asymmetry was based on the specific observation that affect and approach/

| Cluster Center Region | Cluster No. | Voxels | MNI Coordinates | | | T-Stats |
|---|---|---|---|---|---|---|
| **Right Hemispheric Activations** | | | | | | |
| **Frontal Lobe** | | | | | | |
| Frontal medial cortex | 1 | 192 | 2 | 42 | −12 | −11.711 |
| Frontal pole | 1 | 81 | 8 | 50 | 42 | −3.819 |
| | 2 | 25 | 8 | 58 | 14 | −2.958 |
| Subcallosal cortex | 1 | 68 | 6 | 28 | −4 | −4.043 |
| Superior frontal gyrus | 1 | 23 | 16 | 32 | 56 | −3.107 |
| **Parietal Lobe** | | | | | | |
| Angular gyrus | 1 | 104 | 50 | −56 | 28 | −3.685 |
| **Occipital Lobe** | | | | | | |
| Lingual gyrus | 1 | 20 | 26 | −56 | 2 | −3.676 |
| **Temporal Lobe** | | | | | | |
| Planum Temporale | 1 | 124 | 62 | −12 | 6 | −3.416 |
| **Limbic Lobe** | | | | | | |
| Cingulate gyrus, posterior division | 1 | 203 | 4 | −44 | 38 | −5.841 |
| Insular cortex | 1 | 124 | 36 | −12 | 14 | −5.241 |
| **Left Hemispheric Activations** | | | | | | |
| **Frontal Lobe** | | | | | | |
| Middle frontal gyrus | 1 | 25 | −42 | 34 | 24 | 3.014 |
| | 2 | 51 | −26 | 20 | 38 | −3.049 |
| | 3 | 25 | −42 | 18 | 48 | −3.022 |
| Superior Frontal Gyrus | 1 | 138 | −4 | 52 | 36 | −3.021 |
| | 2 | 30 | −6 | 40 | 50 | −4.585 |
| | 3 | 21 | −2 | 14 | 66 | −3.298 |
| Frontal pole | 1 | 138 | −8 | 58 | 14 | −6.323 |
| | 2 | 75 | −20 | 52 | 30 | −3.548 |
| | 3 | 21 | −20 | 44 | 38 | −2.748 |
| Precentral gyrus | 1 | 21 | −36 | −12 | 68 | −2.877 |
| **Parietal Lobe** | | | | | | |
| Supramarginal gyrus, anterior division | 1 | 87 | −62 | −28 | 40 | 7.244 |
| | 2 | 41 | −44 | −36 | 46 | 2.927 |
| Angular gyrus | 1 | 181 | −46 | −56 | 54 | −3.641 |
| | 2 | 181 | −58 | −54 | 36 | −3.615 |
| Superior Parietal Lobule | 1 | 181 | −34 | −52 | 38 | −2.478 |
| **Occipital Lobe** | | | | | | |
| Lateral occipital cortex, inferior division | 1 | 91 | −30 | −88 | −18 | −3.47 |
| **Temporal Lobe** | | | | | | |
| Temporal pole | 1 | 47 | −44 | 10 | −36 | −4.092 |
| **Limbic Lobe** | | | | | | |
| Cingulate gyrus, posterior division | 1 | 386 | −6 | −48 | 36 | −5.096 |
| | 2 | 386 | −4 | −44 | 14 | −2.506 |

**Table 5.** Neural underpinnings of proposed microstate based FTA (channel pair F8/F7). The activations after correction for multiple comparisons are represented at $p < 0.05$ (FDR corrected). The coordinates reported are in Montreal Neurological Institute (MNI) space.

withdrawal measures associated significantly with stable EEG signatures. Microstate analysis estimates the global pattern of coherence across entire EEG channels from temporal EEG data and thus assesses patterns of quasi-stable activities. The interaction within a large scale brain network involves a rapid change in the dynamics of these quasi-stable activity patterns. Further, the neural mechanism associated with any cognitive process generally involves the coordinated activity of many neural assemblies located at different cortexes. Correspondingly, the neural mechanisms of resting-state affect and approach/ withdrawal behavior are also the result of one such coordinated activity of the large scale brain networks.

Thus, in this study, a novel approach is explored, which assesses the frontal hemispherical asymmetry of quasi-stable activity patterns (microstates) from large scale brain interactions of the resting state affect and approach/ withdrawal behavior. These EEG microstates based frontal hemispherical asymmetry measures are further subjected to the EEG informed fMRI analysis to estimate their neural underpinnings. Subsequently, the lateralization index, which measures the hemispherical asymmetry of these large scale brain networks based on their hemodynamic information, is measured and correlated with affect and approach/ withdrawal psychological

| Hemodynamic Lateralization Index (HLI) | Behavioral measure | Cortical regions | Pearson Correlation | | Bend correlation | | Spearman correlation | | Skipped correlation | | | |
|---|---|---|---|---|---|---|---|---|---|---|---|---|
| | | | | | | | | | Pearson | | Spearman | |
| | | | r | p | r | p | r | p | r | t | r | t |
| Standard neural underpinnings | Negative affect | No region survived | — | — | — | — | — | — | — | — | — | — |
| | BIS | No region survived | — | — | — | — | — | — | — | — | — | — |
| | Positive affect | Insular cortex | 0.44 | 0.004 | 0.44 | 0.005 | 0.4 | 0.01 | 0.53 | 3.82 | 0.41 | 2.75 |
| | BAS | No region survived | — | — | — | — | — | — | — | — | — | — |
| Microstates Neural underpinnings | Negative affect | Middle temporal gyrus, anterior division | −0.4 | 0.01 | −0.38 | 0.01 | −0.43 | 0.006 | −0.4 | −2.67 | −0.43 | −2.91 |
| | BIS | Inferior frontal gyrus | 0.69 | 0.005 | 0.63 | 0.01 | 0.69 | 0.005 | 0.69 | 3.36 | 0.69 | 3.39 |
| | | Frontal medial cortex | 0.71 | 0.004 | 0.76 | 0.001 | 0.75 | 0.001 | 0.71 | 3.53 | 0.75 | 4.04 |
| | Positive affect | Superior frontal gyrus | 0.36 | 0.02 | 0.3 | 0.05 | 0.31 | 0.05 | 0.36 | 2.37 | 0.31 | 2.01 |
| | BAS | Occipital fusiform gyrus | −0.58 | 0.02 | −0.57 | 0.03 | −0.55 | 0.03 | −0.58 | −2.51 | −0.55 | −2.32 |

**Table 6.** Robust correlation (Pearson, bend, spearman and skipped) of HLI based on standard and proposed microstate based frontal hemispheric asymmetry measures with psychological scores.

measures. Lastly, the insights brought by the proposed EEG microstates based approach is compared with the standard EEG asymmetry measures to understand the effectiveness of microstate derived asymmetry measures in explaining resting-state affect and approach/ withdrawal behavior. The insights of the present study are summarized in the following subsections.

**Standard alpha asymmetry and its HLI reveal no correlation with PANAS and BIS/BAS measures.** The current study is in line with the observation of Davidson and colleagues[35] and other earlier studies[4,36,63], where no correlation was observed for affect and BIS/BAS measures with standard hemispheric asymmetry. However, these previous studies never explored the neurovascular underpinnings and associated hemodynamic asymmetry of these underpinnings. In the present study, the absence of linkage of standard hemispheric asymmetry with affect and BIS/BAS measures is further strengthened by the lack of correlation of HLI of neural underpinnings of standard alpha asymmetry with PANAS, BIS, and BAS measures. This supports the understanding that neural mechanisms that are measured as standard EEG frontal alpha asymmetry may not be the marker to explain the affect and/or approach-withdrawal measures during resting state. It might possibly are influenced by the neural activity associated with other ongoing resting-state neural mechanisms, which limit its sensitivity towards the neural mechanisms associated with affect and approach-withdrawal measures during resting state. Thus, our finding strengthens the understanding that the standard EEG alpha asymmetry model, especially in the male population, is effectual in explaining affect or approach-withdrawal measures only when arousing situations such as those relying on mood induction procedures are present.

**Microstates based asymmetry correlates with and delineates the neural mechanisms of Negative affect.** In contradistinction to the standard hemispheric asymmetry, the proposed microstates based measure brings better insights into the global coordinated activity of large scale brain networks pertaining to negative affect. In this study, the robust correlational analysis revealed a positive correlation of negative affect with microstates based frontal hemispheric asymmetry. This implies that negative affect increases with an increase in right hemispheric alpha activity or a decrease in left-hemispheric alpha activity. Further, the most common neurovascular hypotheses state that when engaged in the task, the brain region exhibits suppression in alpha power with an increase in BOLD signal[47]. This causes a negative correlation between alpha power and BOLD signal and is termed as alpha-BOLD desynchronization. Figure 7 depicts these underlying dynamics for the association between alpha asymmetry measures and the BOLD signal during alpha-BOLD synchronization/ desynchronization. Following this, the positive correlation of negative affect with microstates based frontal hemispheric asymmetry implies left-hemispheric interaction with negative affect. These observations do not support the valence hypothesis explained in the earlier section but goes in line with the observations by Hagemann *et al.*[38], wherein negative affect has been linked to the left-hemisphere. Our results were also in line with a mood induction study by Gale *et al.*[64], where negative mood increased with an increase in left frontal activation. Further, recently Farahi *et al.*[65] showed the associativity of fear positively with the left hemisphere.

Additionally, neural underpinnings of microstate derived asymmetry revealed the involvement of temporal lobe regions. In this study, HLI ($HRF\_Amp_n^R - HRF\_Amp_n^L$), which was estimated by utilizing the amplitude of the HRF of each neural underpinning of microstate based frontal asymmetry linked negatively the HLI of the anterior division of middle temporal gyrus neural underpinning to negative affect. This implies that relatively

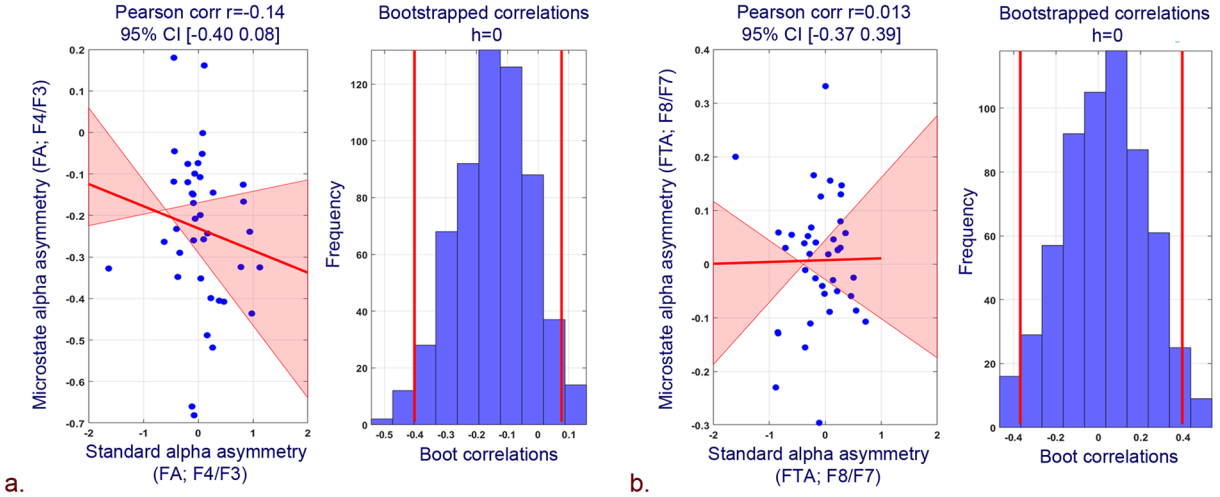


**Figure 6.** Pearson correlation plots and associated histograms for bootstrapped data for correlation between. (**a**) Standard and microstate based FA (F4/F3). (**b**) Standard and microstate based FTA (F8/F7).

left-lateralized HRF amplitude of temporal underpinning pertaining to microstate based frontal asymmetry is associated with negative affect. Studies in the past have connected left anterior temporal cortical activation as well as temporal lobe per se to the negative affect;[66–69] this proves the efficacy of microstate based frontal asymmetry in explaining the neurovascular mechanism of negative affect which remains absent in the previous literature. Batut *et al.*[70] signaled the involvement of mesial temporal regions in emotional processes; further, Yun *et al.*[71] showed that the angst for social communication in social anxiety disorder could be resultant of the imbalanced functional connectivity of left middle temporal gyrus. The association of anterior division of middle temporal gyrus with negative affect is plausible as studies[72–74] have indicated the interaction between middle temporal gyrus and amygdala for better prediction of memory for emotional events. Hence, the middle temporal gyrus may be more tightly functionally coupled with affect specific regions for the memory of negative events. The significant correlation of negative affect with temporal region's HLI, which is independently measured from resting fMRI data for neural underpinnings of microstate frontal asymmetry and its relative left lateralization, also strengthens the finding of positive correlation of negative affect with microstate based frontal asymmetry measures (FA and FTA).

**Microstate based asymmetry reveals no correlation with BIS, Positive affect, and BAS.** Microstate based asymmetry showed a high but insignificant correlation with BIS measure. It also showed no correlation with positive affect and BAS measure. One possible explanation for these findings is the fact that the positive affect scale is a diverse measure with components of joy, interest, and activation. Each one of these components might involve distinct and sometimes even opposite whole-brain activations[75]. Similarly, BAS is also composed of varied components (reward, drive, and fun)[76]. These varied brain activation patterns might not be producing definite patterns at cortical levels to be picked by the alpha power.

**HLI of microstates neural underpinnings reveals significant association with BIS, positive affect, and BAS measures.** The hemodynamic lateralization measure of neural underpinnings of the proposed technique revealed a high and positive correlation of BIS in frontal cortical regions. Frontal cortical regions play a very important role in inhibition systems, and it has been one of the cornerstones of neuroscience research[13,77,78]. Further, Fuentes *et al.*[79] also emphasized the association of individual differences in the behavioral inhibition system with the orbitofrontal cortex. Hence, our results suggest that the HLI, which constitutes the voxel-level hemispheric differences in HRF amplitude of neural underpinnings of microstates based asymmetry better manifests BIS measure. Further, though microstate based alpha asymmetry found no significant correlation with positive affect and BAS measure, the HLI of occipital fusiform gyrus was found to strongly correlate with BAS measure. This is consonant with the hypothesis where the BAS system is proposed to be modulated by occipital cortices[80]. The nature of correlation was strong but negative and thus was inverse of the BIS system. Moreover, positive affect was correlated positively with hemodynamic lateralization measures in superior frontal gyrus. The link of the prefrontal cortex with positive affect is consistent with recent studies. Wager *et al.*[81] showed the association of the prefrontal cortex with positive affect as compared to negative affect. Similarly, Roy *et al.*[82] observed more frequent activity was found in the prefrontal cortex during positive as compared with negative feelings. Hence, hemodynamic lateralization measures of microstates neural underpinnings bring better insight into the positive affect and BAS as compared to the standard EEG based hemispherical asymmetry measures.

Interestingly, the neural underpinnings (middle temporal gyrus (anterior division), inferior frontal gyrus, frontal medial cortex) whose HLI revealed significant correlation (r-value) with negative affect and BIS scores have been observed to be undergoing only alpha-BOLD desynchronization process. They were found to be either correlating positively in the left hemisphere or negatively in the right hemisphere. On the other hand, the neural underpinnings whose HLI correlated with positive affect and BAS scores have

| Study | Alpha EEG Asymmetry (R-L) | Mood Measures | Subjects | Main Results |
|---|---|---|---|---|
| Tomarken *et al.*[136] | FA (F4/F3); | Acquisition of resting EEG followed by the presentation of affective clips to obtain subjective ratings for emotional reactions | 32 females,<br>Cohort A: 17 to 41 years<br>Cohort B: 20 to 54 years | Resting FA significantly predicted self-reported global NA |
| Tomarken *et al.*[29] | FA (F4/F3);<br>ATA (T4/T3) | Resting EEG on two occasions; 3 weeks apart; PANAS | 90 females,<br>17–21 years | FA:↓NA<br>ATA:↑PA |
| Tomarken *et al.*[30] | Same as in Tokarman *et al.*, 1992a | Same as in Tomarken *et al.*, 1992a | 85 females,<br>17–21 years | Same as in Tomarken *et al.*, 1992a |
| Jacobs and Snyder,1996[31] | FA (F4/F3);<br>FTA (F8/F7) | Resting EEG on<br>1-time measurement; PANAS | 40 males,<br>18–53 years | FTA:↓NA |
| Sutton and Davidson,1997[35] | FA (F4/F3) | Resting EEG on two occasions 6 weeks apart<br>PANAS first session; BIS/BAS scales the second session | 46 (23 females)<br>18–22 years | No correlation between FA and PA, NA, BAS, BIS |
| Hagemann *et al.*[37] | FA (F4/F3);<br>ATA (T4/T3) | Acquisition of resting EEG followed by the presentation of affective slides to obtain subjective ratings for emotional reactions | 37 (22 females: 15 males:<br>Mean age 24.5) | Subjects with greater relative left-sided anterior temporal cortical activation reported more intense NA in response to negative stimuli |
| Hagemann *et al.*[38] | FA (F4/F3);<br>ATA (T4/T3) | Resting EEG; PANAS | 36 (24 females)<br>Mean age 24.7 | Subjects with high NA exhibited high left cortical activation at the anterior temporal site |
| Hall and Petruzzello, 1999[32] | FA (F4/F3) | Resting EEG and measures of physical activity; PANAS | 41 (26 females)<br>Mean age 68.7 | FA positively predicted PA |
| Harmon-Jones and Allen, 1997[33] | FA (F4/F3); | Resting EEG from females who scored in the upper or lower third of the distribution of social anxiety scores; BAS,BIS | 37 females | FA:↑BAS |
| Hewig *et al.*[62] | FA (F4/F3);<br>FTA (F8/F7);<br>ATA (T4/T3) | Resting EEG on four occasions; four weeks apart; BAS, BIS | 59 (30 females: Mean age 23;<br>29 males: Mean age 25) | Higher BAS associated with bilateral frontal cortical activity |
| Shackman *et al.*[61] | FA (F4/F3);<br>FTA (F8/F7) | Resting EEG on two occasions; several weeks apart; BAS, BIS | 51 females<br>Mean age 19.5 | A significant relationship between BIS and FA. Higher BIS associated with right posterior DLPFC |
| De Pascalis *et al.*[34] | FA (F4/F3);<br>FTA (F8/F7) | Resting EEG; BAS,BIS | 51 females<br>Mean age 24.1 | FA:↑BAS,<br>Higher BAS associated with left-sided activation in MFG |
| Schneider *et al.*[36] | FA (F4/F3); | Two assessments of resting EEG; BAS, BIS | 99 (50 females; 49 males aged 10–12 years) | No correlation of BAS, BIS measures with FA |

**Table 7.** List of studies for positive/negative affect and approach/withdrawal dichotomy. EEG, Electroencephelography;↑Positive correlation;↓Negative correlation; FA, Frontal Asymmetry (F4/F3); FTA, Frontal Temporal Asymmetry (F8/F7); ATA, Anterior Temporal Asymmetry (T4/T3); BAS, Behavioral Activation System; BIS, Behavioral Inhibition System; PA, Positive Affect; NA, Negative Affect; DLPFC, Dorsolateral Prefrontal Cortex; MFG, Middle Frontal Gyrus.

revealed both alpha-BOLD synchronization and desynchronization. Particularly, superior frontal gyrus, which correlated with positive affect, underwent both alpha-BOLD synchronization and desynchronization. However, the occipital fusiform gyrus correlated negatively in the left hemisphere, which thus undergoes alpha-BOLD synchronization. Thus, the neural mechanisms involved in negative affect/withdrawal in the resting state exhibited only alpha-BOLD desynchronization. On the contrary, the positive affect and an approach relevant region involved both alpha-BOLD synchronization and desynchronization. However, the underlying innate cause of these mechanisms remains elusive and needs to be explored in the future. Thus, our finding implicates that microstates based frontal alpha asymmetry may provide newer insights into the association of alpha asymmetry with mood and personality measures in both healthy and clinical populations. The plausible explanation is that different cognitive states, including affect and approach/withdrawal behavior, generally involve coordinated activity of many neural assemblies located at the different cortex, and the microstate prototypes could represent these cognitive states.

**Absence of correlation among proposed microstate and standard frontal hemispheric asymmetry measures.** The proposed microstate based FA and FTA yielded an insignificant low correlation with standard FA and FTA. The proposed microstate based FA and FTA measure the quasi-stable coordinated brain activity and, in the present study, brings better insights into the large scale brain networks of negative affect. Previous works of literature[29,39] have also emphasized the prominence of stability in the standard EEG patterns in bringing forth the linkage among standard frontal alpha asymmetry and affect and approach/withdrawal measures. Hence, the lack of correlation among proposed microstate and standard frontal hemispheric asymmetry measures might be caused by the unstable nature of standard EEG and its frontal alpha asymmetry indices, which

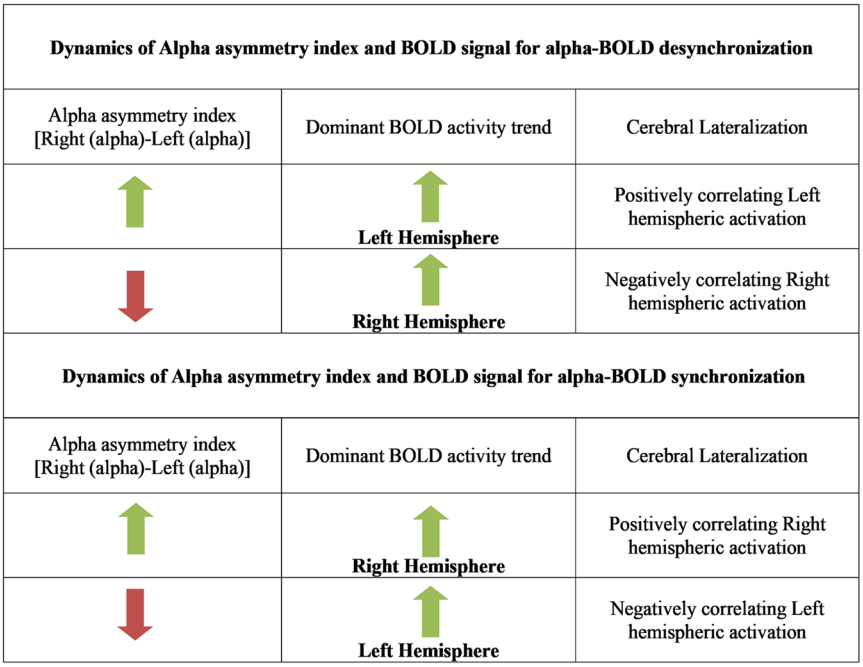


**Figure 7.** Underlying dynamics associated with alpha asymmetry index and BOLD signal.

is caused by a substantial interference from many other cognitive factors. As this interference is different at different time points across volunteers, the standard EEG and its frontal alpha asymmetry are likely to correlate less with the quasi-stable patterns assessed by the proposed microstate frontal alpha asymmetry indices.

**Limitation of the study.** The present study utilizes 39 volunteers' data to validate the role of microstate based resting frontal alpha asymmetry in understanding the neural mechanisms of affect and approach/withdrawal behavior. However, affect and approach/withdrawal behavior is known to be elicited by mood induction tasks. Hence, it is necessary to carry out future studies to validate the proposed microstate based frontal alpha asymmetry during such task engagements. Further, the current research involves healthy volunteers from the Indian urban population. Many studies[83–85] in the past have revealed the association of affect and approach/withdrawal behavior with the cultural, ethnic, and social background of the individuals. Thus, it is required to examine the proposed microstate based frontal alpha asymmetry approach in a larger population dataset, which includes individuals from various cultural, ethnic, and social backgrounds.

Also, the topographies of average-referenced, preprocessed standard EEG are known to represent the posterior alpha than frontal alpha, and these topographies have also been studied in comparison with other referencing schemes[54,86]. However, the microstate analysis employed in the current study uses an average referencing scheme for frontal alpha asymmetry estimation. The present study follows average referencing for microstate analysis as various studies[40,87] adequately understand the cognitive phenomena through average-referenced microstate estimations. Further, the effect of different EEG referencing schemes on microstate estimations is still not clearly understood. Extensive, systematic work needs to be undertaken to properly understand the role of varying EEG reference montages based microstate analysis in explaining frontal, posterior, and temporal EEG frequency signatures and topographies.

## Conclusion

The above study validates the effectiveness of resting quasi-stable microstate based asymmetry in explaining the neural mechanisms of affect and approach/withdrawal behavior for healthy young male volunteers during 1-time measurement. The novelty of our work emanates from the fact that we estimated the frontal asymmetry of the alpha power from the average GFP amplitude of the quasi-stable microstates topographies, which might reflect the degree of coordination of the neurons underlying alpha-neural underpinnings. Microstate frontal alpha asymmetry correlated positively with negative affect scores, which are defended by the negative correlation of HLI based on microstates' temporal neural underpinning with negative affect. Further, a significant association of HLI based on microstate neural underpinnings with positive affect, BAS and BIS measures concludes that the neural mechanisms of affect and approach/withdrawal dichotomy are better explained by the synchronized global firing of neurons and on-going activity of entire brain networks as assessed by quasi-stable microstates frontal alpha asymmetry. This study also stands unique in exploring the underlying neurovascular synchronization/desynchronization mechanisms of microstate based frontal asymmetry measures. The analysis revealed that neural underpinnings involved both positively and negatively correlating brain regions, thus satisfying alpha-BOLD desynchronization and synchronization criteria. However, specifically the microstates neural underpinnings

whose HLI correlated with negative affect and inhibition involved alpha-BOLD desynchronization, however the positive affect and approach relevant regions involved alpha-BOLD synchronization as well as desynchronization.

## Methods

Figure 8 depicts the schema of the methodology adopted in this study.

**Sample and procedure.** Thirty-nine healthy participants (all males; age range 18–24 M = 19.57; SD = 1.28) took part in this study after providing a written and informed consent to the protocol. The experiment has been carried out in accordance with The Code of Ethics of the World Medical Association (Declaration of Helsinki), and all measurements were also approved by the Institute of Nuclear Medicine and Allied Sciences (INMAS) institutional ethical committee (Number: ECR/824/Inst/DL/2016). All subjects were volunteers recruited among university students and were right-handed. Subjects completed a personality questionnaire for positive affect and negative affect and Behavioral inhibition system (BIS)/Behavioral approach system (BAS). The questionnaires were in the English language, and all the volunteers were fluent in the English language. The resting-state fMRI and EEG data analyzed in this paper were collected after the subject completed the psychological questionnaires. The simultaneous EEG-fMRI resting-state recording lasted for 6 minutes with eyes closed condition.

**Behavioral measures.** To assess the dispositional affect and approach/withdrawal parameters in resting state, PANAS scores, and BIS/BAS measures were evaluated for each individual. We also estimated the Profile of mood states using POMS scores for prior exclusion criteria. Table 8 presents descriptive characteristics for the study participants with the mean and standard deviation values.

**Positive and negative affect.** Positive and negative affect scores were evaluated for each volunteer. Positive and Negative Affect Schedule (PANAS) consists of mood scales designed to assess affect at the present moment[88]. These scales are highly uncorrelated, stable over time, and consistent, and both scales demonstrate good convergent and discriminant validity[89,90]. Positive and negative affect scores showed good internal consistency in our study (Cronbach's alphas = 0.89; 0.91).

**Behavioral approach system (BAS)/behavioral inhibition system (BIS).** BIS and BAS scores were calculated for each subject[91] and evaluation included 24 items (20 score-items and four fillers, each measured on four-point Likert scale), and two total scores for BIS (range = 7–28; 7 items) and BAS (range = 13–52; 13 items). In our study, BIS and BAS scales showed good internal consistency (Cronbach's alphas = 0.93; 0.92).

**POMS (Profile of mood states).** Volunteers were also asked to fill in forms for the POMS[92]. It measures six different dimensions of mood swings, namely Tension or Anxiety, Anger or Hostility, Vigor or Activity, Fatigue or Inertia, Depression or Dejection, Confusion, or Bewilderment. These scores formed the basis for exclusion criteria. All selected volunteer returned self-report scores for all the modes within a relatively normal range.

**Simultaneous EEG-fMRI data acquisition and preprocessing.** MRI data was acquired in a Siemens 3 T scanner. After acquiring a high-resolution T1-weighted anatomic rapid gradient-echo image (T1 MPRAGE sequence TR 1900ms, TE 2.49 ms, FA 9°, 160 slices with slice thickness 0.9 mm and distance factor of 50%, FoV 240 mm with voxel size 0.9 × 0.9 × 0.9 mm), we acquired 205 T2*-weighted EPI images for resting-state eyes-closed condition (T2* EPI sequence: TR 2000ms, TE 30 ms, FA 90°, 30 slices with thickness 5 mm and distance factor 0%, FoV 240 mm with voxel size 3.8 × 3.8 × 5.0 mm). Continuous EEG data were acquired simultaneously during resting state T2* acquisition using a 32-channel MR-compatible brain vision cap. The electrodes were placed according to the international 10–20 system with a separate electrode called the Reference electrode, placed between Fz and Cz electrodes, that provided the reference for recording the data. Electrocardiogram (ECG) was also recorded. The impedance level for each electrode was kept less than 5 KΩ. The recorded EEG signal was digitized and transmitted with a sampling frequency of 5000 Hz. The acquisition of EEG signals was accomplished using Brain vision analyzer software.

The fMRI data preprocessing for 205 resting-state volumes was done using the default preprocessing pipeline for volume-based analysis in CONN software. The pre-processing procedure included the realignment and unwarping of T2*-weighted image with the mean functional image for motion correction followed by the translation of center to (0, 0, 0) coordinates and slice time correction of functional data. Functional outlier detection (ART- based identification of outlier scans for scrubbing) was performed, followed by segmentation and direct normalization to MNI space. Next, functional smoothening with a Gaussian Kernel with FWHM of 6 mm was carried out. Further, translation of structural center to (0, 0, 0) and simultaneous structural segmentation and normalization were performed.

EEG data were corrected for gradient artifact using the Brain vision analyzer's[93,94] average artifact subtraction algorithm (AAS)[95,96]. A template from MR scanner artifacts was created by averaging the MR scanner artifacts over fixed intervals which were accurately specified by utilizing the fMRI volume markers (labeled as 'TR'). Subsequently, this average was subtracted from the EEG data. Further, the gradient artifact removed data accommodated six seconds of data prior to the start of the first fMRI block acquisition (identified by the first TR marker). These six seconds is the time the fMRI pulse sequence prepares itself before acquiring the first fMRI block. This prior time interval accommodated gradient-contaminated ECG; hence we truncated these 6 seconds prior data and subjected only the data pertaining to the fMRI volumes to the subsequent cardio ballistic (CB) artifact removal. The CB artifact removal was performed in the FMRIB plugin. The method detects the QRS peaks in the ECG data using combined adaptive thresholding[97] and Teager energy operator[98], followed by a correction algorithm. Further, the removal of the CB artifact is performed based on the Optimal Basis Set (OBS) method[99].

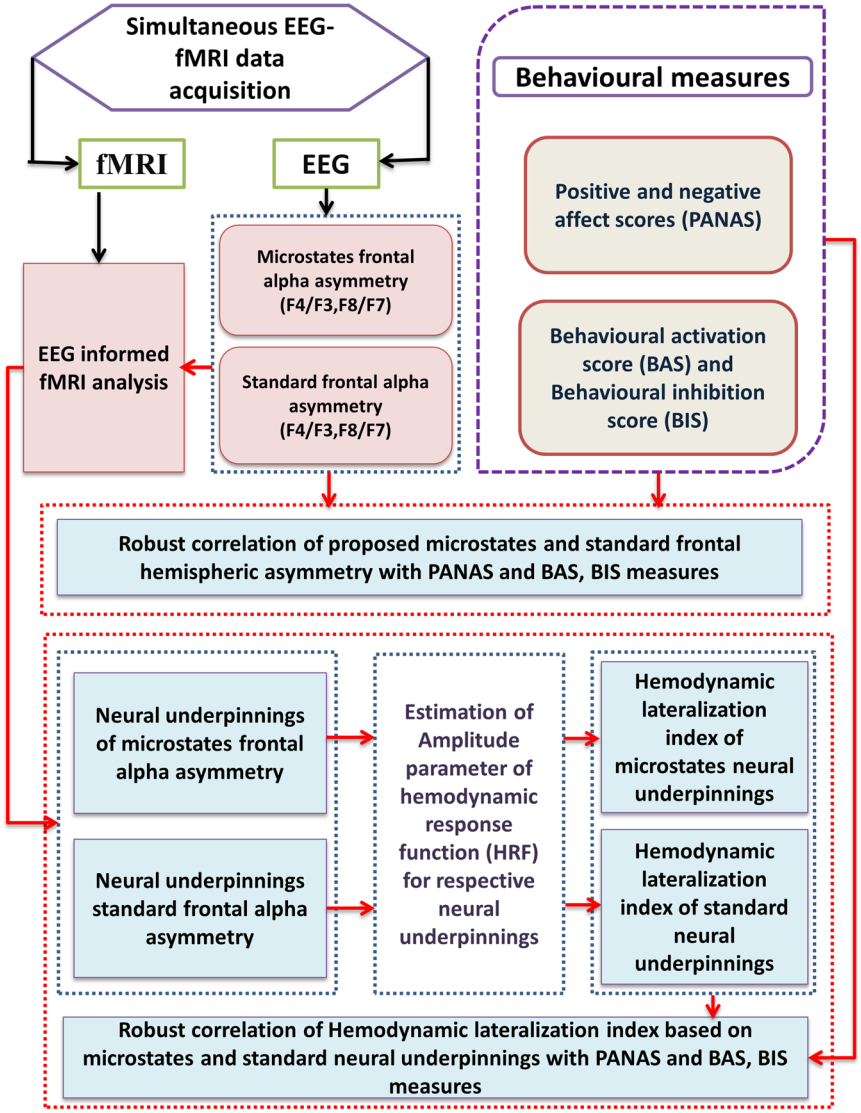


**Figure 8.** Schema of the methodology adopted in this study.

| Variable | Mean (M) | Std. Dev (SD) |
|---|---|---|
| Age | 19.57 | 1.28 |
| Positive Affect scores | 39.66 | 5.66 |
| Negative Affect scores | 14.64 | 4.29 |
| BAS scores | 23.42 | 3.5 |
| BIS scores | 15.28 | 2.7 |

**Table 8.** Demographic and behavioral characteristics of study participants (N = 39).

In addition, we also employed the HAPPE toolbox[100] for further ensuring the quality of conventional EEG artifact removal from the scanner and CB artifact corrected datasets. The following steps utilizing the HAPPE toolbox were adopted. First, the scanner and CB artifact removed data were subjected to the filtering process with 0.1 Hz high pass and 70 Hz low pass filtering, and all the EEG channels were selected for further analysis. This was followed by removal of the electrical (line) noise using the Cleanline plugin[101] of EEGLAB. The functionality of HAPPE was utilized next to identify and remove the contaminated channels. HAPPE identifies the contaminated channels by evaluating the normed joint probability of average log power across all the channels and rejecting the channels whose joint probability is more than three standard deviations. Wavelet enhanced ICA (W-ICA) approach was implemented subsequently to correct for EEG artifact while retaining the entire length of the data file. The W-ICA approach removes ocular and muscle-related artifacts and also improves the decomposition of later performed ICA, which eventually rejects artifact components. Next, independent components (ICs) with

the extended infomax independent component analysis (ICA) were computed, and the MARA plugin[102,103] of EEGLAB was employed for automatic component rejection. MARA evaluates each component on six features and eventually assigns a probability of artifact contamination to that component. Further, HAPPE's pipeline automatically rejected any components with artifact probabilities higher than 0.5. Subsequently, segmentation of data based on the markers, rejection of segments, and interpolation of removed channels were carried out. Finally, the processing report about the quality of data was generated. The EEG preprocessing procedures in this study have been explained in detail in Supplementary methods and discussion section. Further the processing report about the quality of data for all volunteers has been tabulated in Supplementary Table 1.

To ensure the quality of preprocessing, we also subjected both raw and final artifact removed EEG data (CSD referenced) to the estimation of the power spectrum between 0.2 Hz to 50 Hz frequency range. The median power spectrum plots of both raw and final artifact removed EEG data (CSD referenced) for channels F3, F4, F7, F8, Pz, Oz, and POz are shown in Supplementary Figs. 1 and 2 respectively. The median spectral power of artifact removed EEG data clearly reveals parietal and occipital alpha and beta bands. Data was down-sampled to 250 Hz for further analysis.

**Assessment of frontal hemispherical asymmetry measures.** The main objective of the study was to understand the neural mechanisms associated with the affect, approach/withdrawal behavior, as explained by the hemispherical asymmetry measures. For this purpose, the present study proposes an EEG microstate based frontal hemispheric assessment approach and aims to compare its advantage over the standard EEG frontal asymmetry approach. The following subsections explain the methods for estimating the proposed EEG microstate based frontal hemispheric asymmetry as well as the standard frontal EEG asymmetry.

**EEG microstates based estimation of hemispheric asymmetry.** Many recent studies[40,104,105] have clearly indicated that individual brain functions involve massive parallel processing in distributed brain networks. These distributed brain networks are observed as the scalp field potential in EEG, and the state of global neural activity is measured as a topographical map at that moment of time. The changes in this topography reflect changes in the global coordination of neural activity over time. EEG microstates were proposed to represent changes in behavior, thoughts, and emotions and can be classified into few topographies, which have explained 90% of the variance of continuous EEG. Microstate analysis considers millisecond time range signal from all electrodes to create a global picture of a functional state during that interval.

The schema of the methodology adopted for microstate estimation is explained in Fig. 9. The aim of a microstate analysis is first to segment EEG maps into microstate prototypes and second to re-express the spatial-temporal characteristics of the time series of EEG through these microstate prototypes.

In this study, let X be the time series EEG information that was acquired from the volunteers. At first, the EEG data X has been pre-processed for removing the artifacts and was referenced to the average referencing. Then, it was subjected to the estimation of Global field power (GFP). GFP is the measure of global brain response to an event and is represented as:

$$\mathrm{GFP} = \sqrt{\left(\sum_{i=1}^{C}(X_i(t) - X_{mean}(t))^2\right)/C} \tag{1}$$

where $X_i$ is the measured potential at the i$^{th}$ electrode at a given time-point t, $X_{mean}$ is the mean value of all $X_i$'s and C represents the total number of channels. GFP, therefore, represents the standard deviation of the electrode values and indicates, on average, how strong potential is being recorded across the electrode montage[106]. For each volunteer, a selection of data points for the further processing has been carried out by filtering estimated GFPs based on minimum peak distance of 20 milliseconds, and the threshold amplitude of one standard deviation of estimated GFP. Then, the filtered EEG data points of every individual are concatenated to form the GFP datasets for further clustering process as follows:

$$\chi = \{x_{GFP}{}^{1}, x_{GFP}{}^{2}, \ldots\ldots\ldots x_{GFP}{}^{S}\} \tag{2}$$

where $\chi$ is of the concatenated GFP dataset and $x_{GFP}{}^{i}$ are selected data points based on the GFP criteria of the i$^{th}$ volunteer, and S is the total number of volunteers. In this study, thirty-nine volunteers dataset has been subjected to analysis.

Further, concatenated GFP dataset $\chi$ was subjected to the clustering process through the modified K-means clustering algorithm[107]. Modified K-means clustering algorithm requires the initialization of both number (K) of microstate prototype vectors and their components values[108]. Thus, the clustering algorithm was randomly initialized with a set of microstate prototype vectors as the center of initial clusters as follows:

$$Z = \{z_i | i = 1 \; to \; K\} \tag{3}$$

where K is the total number of microstate prototype vectors (cluster center). In this study, the K is initialized with 8. The clustering algorithm was allowed to iterate and minimize the orthogonal euclidean distance between the data points in $\chi$ as given below.

$$\tau_n = arg\min_k\{D_{kn}^2\} \tag{4}$$

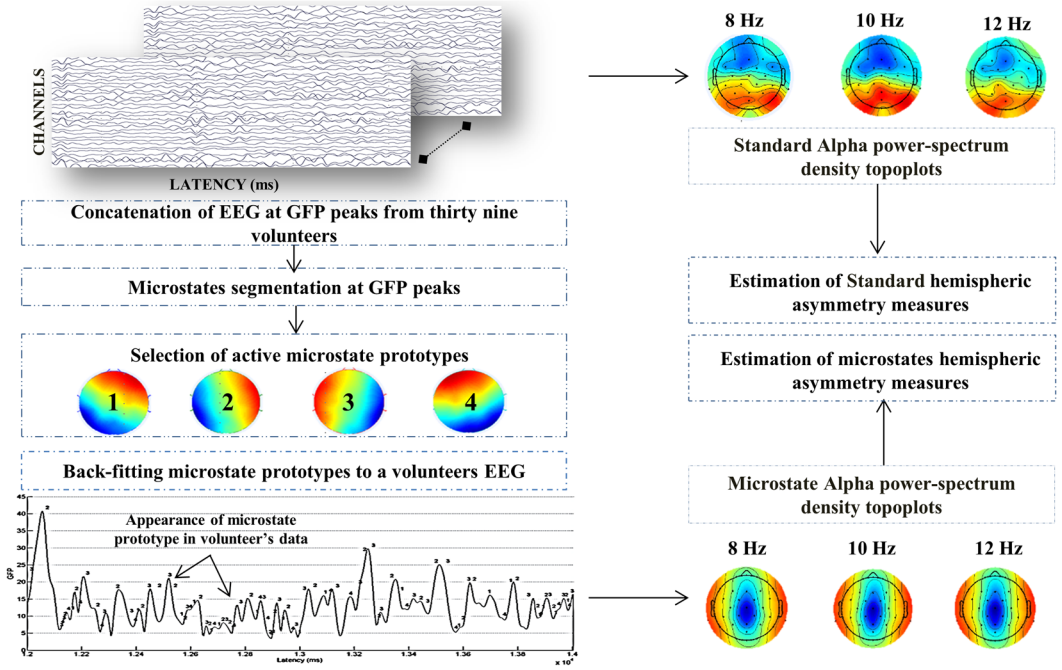


**Figure 9.** Schema of the methodology adopted for proposed microstate estimation and assessment of standard and microstates based frontal alpha hemispheric asymmetry measures.

$$D_{kn}^2 = \chi_n^T . \chi_n - (\chi_n^T . z_k)^2 \tag{5}$$

where $\tau_n$ represents the microstate label for n$^{th}$ sample, $\chi_n$ represents the n$^{th}$ time sample of the concatenated dataset, $z_k$ represents the prototypical map for the k$^{th}$ microstate cluster and $D_{kn}$ represents the distance between $\chi_n$ and microstate $k$ for the n$^{th}$ time sample. Thus, this clustering algorithm allocates each EEG sample to the cluster whose prototype it is most similar to and then re-estimates microstate prototypes by averaging newly assigned samples[107]. The maximum number of iterations was set to 1000, and the threshold for convergence was set at $1e^{-6}$ for analysis in this study.

Subsequently, a review of goodness of fit and selection of active microstates is carried out based on global explained variance (GEV) and cross-validation (CV) criterion. It basically evaluates how well microstate segmentation explains the EEG data, which has been used to estimate the prototypes. Therefore, GEV measures how similar the EEG sample and the microstate prototype are; and is calculated as follows.

$$GEV_n = \frac{(Corr(\chi_n, z_{\tau_n}) . x_{GFP_n})^2}{\sum_{n'}^{N} x_{GFP_{n'}}^2} \tag{6}$$

where $\chi_n$ represents the n$^{th}$ time sample of the concatenated dataset, $z_{\tau_n}$ $(\tau_n = k)$ is the prototypical map for the k$^{th}$ microstate cluster and $x_{GFP_n}$ represents the n$^{th}$ time sample of the GFP data, and N represents the total number of time samples in concatenated dataset $\chi$. GEV is thus the correlation between the EEG dataset and associated microstate prototype weighted by the EEG dataset's fraction of the total squared GFP[107]. Thereafter to calculate the GEV for a given cluster, the GEV of its members is summed. Subsequently, CV which is a measure related to the residual noise $\in$ is estimated as,

$$CV = \sigma^2 . \left(\frac{C-1}{C-K-1}\right) \tag{7}$$

$$\sigma^2 = \frac{\sum_n^N \chi_n^T . \chi_n - (\chi_n^T . z_k)^2}{N(C-1)} \tag{8}$$

where $\sigma^2$ is the variance of the residual noise, C is the number of EEG channels, N represents the total number of time samples in concatenated dataset $\chi$, and K is the number of clusters. The aim is to obtain a low value of CV. The active microstate prototypes obtained in this study are consistent with the normative EEG microstate classes identified by many studies[40,41,87,109–111].

Following the selection of an active number of microstate prototypes, the EEG of each volunteer is re-expressed as a sequence of microstate classes by back-fitting these active microstate prototypes on each volunteer's EEG

data. Back fitting implies assigning microstate labels to the EEG dataset based on the dataset's topographic similarity with the microstate prototype. The estimated re-expressed back fitted dataset is represented as follows

$$X_{re-expressed} = \{\mu_n | where\ \mu_n \in Z_{k'}\} \tag{9}$$

$$\text{where } \mu_n = arg\ \min(GMD_n)$$

The global map dissimilarity (GMD) index measures the topographical similarity between each microstate prototype vector with the EEG sample vector. The GMD is calculated as,

$$GMD_n = \frac{\left\| \frac{X_n}{X_{GFP_n}} - \frac{z_{k'}}{z_{GFP_{k'}}} \right\|}{\sqrt{C}} \tag{10}$$

where $X_n$ represents the n$^{th}$ time sample of the preprocessed dataset, $z_{k'}$ represents the prototypical map for the k$^{th}$ microstate cluster. In an ideal condition, if the microstate prototype vector and the EEG sample vector of interest are having the same topographic distribution, then the GMD index will be zero. In case, if both the vectors are topographically opposite, then GMD index would be positively higher. Hence, in this study, instead of the thresholding the GMD index, the microstate prototype vector, which yields a very less GMD index, is chosen as the label for that particular EEG sample vector. Finally, microstates statistics using labels obtained from back-fitted prototypes were calculated.

Subsequently, the amplitude of the microstate prototype vector associated with each label in microstate re-expressed EEG data of every individual is subjected to the alpha band power (8–12 Hz) estimation. The estimated alpha power map of the microstate re-expressed EEG data was used to estimate EEG microstate based frontal hemispheric asymmetry as follows:

$$Asymmetry_{MS} = \ln(\alpha(X_{re-expressed}{}^{Right})) - \ln(\alpha(X_{re-expressed}{}^{Left})) \tag{11}$$

$\alpha(X_{re-expressed}{}^{Right})$ and $\alpha(X_{re-expressed}{}^{Left})$ are the alpha powers measured at the right and left hemispheric channel of microstate re-expressed EEG data, respectively.

**Standard EEG estimation of hemispheric asymmetry.** In order to estimate standard frontal asymmetry, the preprocessed EEG data is first re-referenced to CSD reference using the CSD toolbox[112,113]. Recent work suggests that the CSD transformation reduces the influence of non-frontal sources to frontal asymmetry and may provide a better index of individual differences in frontal asymmetry[114]. Subsequently, the power spectral density (PSD) of alpha frequency (8–12 Hz) was extracted. The estimated alpha power map EEG data was used to calculate standard EEG frontal hemispheric asymmetry as follows:

$$Asymmetry_{Standard} = \ln(\alpha(X)^{Right}) - \ln(\alpha(X)^{Left}) \tag{12}$$

$\alpha(X)^{Right}$ and $\alpha(X)^{Left}$ are the standard alpha powers measured at the right and left hemispheric channels of individual EEG data, respectively.

Table 9 presents the median and median absolute deviation values for EEG asymmetries for mid-frontal and lateral-frontal sites.

**Robust correlation of frontal hemispherical asymmetry measures with psychological measures.** Further, estimated EEG microstate and standard frontal hemispherical asymmetries are correlated with PANAS and BAS, BIS measures. These robust correlations were carried out for hemispherical measures that are estimated for both channel pairs F4/F3 i.e. Frontal Asymmetry (FA) and F8/F7 i.e. Frontal Temporal Asymmetry (FTA) independently. The rationale for choosing these channels was based on the linkage of hemispheric asymmetry to mid-frontal (F3, F4) and lateral frontal (F7, F8) sites[39,60,115]. Robust correlations were implemented in Robust correlation Matlab toolbox[116]. This method detects and protects against any bivariate or univariate outliers. Pearson, Bend, and Spearman correlation coefficients, as well as bootstrapped confidence intervals, were computed to evaluate each correlation. Both p-values and confidence intervals were Bonferroni corrected for multiple comparisons.

**Assessment of neural mechanisms associated with functional hemispheric asymmetry measures.** One of the focuses of the present study is to understand the neural mechanisms associated with proposed and standard functional hemispheric asymmetry measures in explaining the affect and approach/ withdrawal behavior during resting state. For this purpose, both proposed and standard hemispheric asymmetry measures were subjected to the EEG informed fMRI, and their neural underpinnings were estimated. Subsequently, the lateralization index based on differences in the amplitude of hemodynamic response of neural underpinnings of both hemispheric asymmetry measures was assessed. Finally, the estimated lateralization index was correlated with PANAS and BAS, BIS psychological measures to understand the ability of both hemispheric asymmetry measures in explaining affect and approach/ withdrawal behavior during resting state. The following sub-sections explain these operations in detail.

**EEG informed fMRI analysis.** Estimation of neural underpinnings of proposed microstate based EEG asymmetry and standard asymmetry was carried out as follows. At first, the estimated alpha powers for frontal

| Variable | Channel pair F4/F3 (FA) | | Channel pair F8/F7 (FTA) | |
|---|---|---|---|---|
| | Median | Median Absolute Deviation | Median | Median Absolute Deviation |
| Standard hemispheric asymmetry[a] | 0.0347 | 0.3509 | −0.052 | 0.3655 |
| Microstates based hemispheric asymmetry[a] | −0.2324 | 0.1427 | 0.0256 | 0.0896 |

**Table 9.** Median and median absolute deviation of the standard and proposed microstates based frontal hemispheric asymmetry measures. [a]The difference between log-transformed alpha values from one right-hemispheric electrode to the corresponding electrodes on the left.

channels F3, F4 F7, and F8 were down sampled to match the acquisition blocks of fMRI (TR: 2 seconds). This was carried out by taking the median of the alpha powers for these specific channels corresponding to each fMRI scan time, which is 2 seconds. The onset time of EEG and fMRI acquisition were also matched. This yielded one EEG alpha power corresponding to each fMRI scan, respectively. Thereafter, microstate based and standard FA and FTA were estimated. The first-level analysis in the present study was performed in SPM12. Different design matrices were obtained each for microstate based and standard asymmetry respectively for each subject wherein microstate based and standard FA and FTA parametrically modulated the fMRI regressors in EEG informed fMRI analysis[117–121].

The first-level analysis in our study was performed in SPM12, and the time series of fMRI regressors and parametric modulators were convolved with canonical HRF and with its time and dispersion derivatives. Further, at first-level, an F-contrast was defined for parametric modulators subsuming both non-derivative (canonical HRF) and derivative terms (time and dispersion derivatives) for microstate based FA, standard FA, microstate based FTA and standard FTA models.

Subsequently, for the second level of analysis, the first-level contrast images, along with the dispersion and temporal derivatives, were subjected to extraction of amplitude measures from the basis sets[122–126]. The robust regression toolbox[127] was used to conduct group-level random-effects analysis. The robust regression toolbox uses iteratively re-weighted least squares (IRLS), which detects influential extreme outliers. Thus, the IRLS analysis reduces the likelihood of false-positive and negative findings with no reduction in power and minimizes the effect of extreme outliers[128]. The IRLS has proved beneficial with small samples ($n = 10$), and the benefits tend to increase with larger sample sizes ($n = 40$). Further, IRLS controls false-positive rates at an appropriate level when no true effects are present. The contrast image for amplitude summary measure was then subjected for the whole brain analysis corrected with voxel-wise False Discovery Rate (FDR) thresholded at $q < 0.05$. This yielded the underpinning of both microstate based FA and FTA and standard FA and FTA.

**Estimation of Hemodynamic lateralization index and its robust correlation with psychological measures.** The lateralization index measures the hemispherical dominance within the large scale brain network that integrates the neural underpinnings associated with resting affect and approach/withdrawal behavior. The neural activity associated with the neural underpinnings of each hemisphere causes differential electrical potential on the cortical surface of the respective hemisphere. This is measured as the EEG asymmetry index, as explained in the earlier sections. In the mean-time, these differential neural activities of each hemisphere generate a feed-forward signal, which results in differential hemodynamic response at the location of neural activity. Measurement of these hemodynamic hemispherical differences facilitates a better understanding of hemispherical dominance within the large scale brain interactions. Diverse methods have been proposed to calculate the hemodynamic lateralization index on the basis of fMRI BOLD information. As most of these studies involved task engagement, the hemispherical difference of cluster size and BOLD signal strength[129–133] were normally used to estimate the HLI.

The main motivation behind this estimation is to understand whether hemodynamic asymmetry reveals more insight into understanding the neurovascular mechanisms of the affect and approach /withdrawal behavior. For this purpose, initially, we estimated the hemodynamic response function metric that is hemodynamic response function amplitude (HRF_Amp) at every voxel by independently subjecting the preprocessed resting fMRI data to blind deconvolution method as proposed by Wu *et al.*[134,135]. The estimation of HRF was carried out independently by assuming acquired fMRI BOLD signal $y(t)$ as the convolution of neural states $n(t)$ with $HRF(t)$. This is represented as,

$$y(t) = conv(n(t), HRF(t)) + \in (t) \tag{13}$$

where $\in(t)$ is the noise in the measurement. Further, $n(t)$ is substituted by a hypothetical neural activation model:

$$\hat{n}(t) = \sum_{\tau=0}^{\infty} \delta(t - \tau) \tag{14}$$

where $\delta(t - \tau)$ is the delta function. This allows fitting $HRF(t)$ according to $\hat{n}(t)$ using a canonical HRF and two derivatives (temporal and dispersion derivatives). This model is subjected to blind deconvolution approach for retrieving the hemodynamic response function ($HRF(t)$) of every voxel. Once $HRF(t)$ is obtained, an approximation of $\tilde{n}(t)$ can be calculated using the inverse Fourier transform (deconvolution). Then, $HRF(t)$ was utilized to estimate the HLI for the neural underpinnings of both microstate based FA and FTA and standard FA and FTA,

all considered together. Hence, the cluster results of EEG informed fMRI were used only for the selection of regions for estimating HLI as follows,

$$HLI(n) = HRF\_Amp_n^R - HRF\_Amp_n^L \quad (15)$$

where $HRF\_Amp_n^R$ and $HRF\_Amp_n^L$ are the median amplitude of hemodynamic response function of the $n^{th}$ neural underpinnings in the right and left hemispheres, respectively. The median of estimated HLI of neural underpinnings of proposed microstate based EEG asymmetry and the standard EEG asymmetry measures were finally subjected to the robust correlations with PANAS and BIS/BAS measures.

## Data availability

The data for this study is available from the corresponding author on a reasonable request.

Received: 4 July 2019; Accepted: 12 February 2020;
Published online: 06 March 2020

## References

1. Killgore, W. D. S. & Yurgelun-Todd, D. A. The right-hemisphere and valence hypotheses: Could they both be right (and sometimes left)? *Soc. Cogn. Affect. Neurosci.* **2**, 240–250 (2007).
2. Nijboer, T. C. W. & Jellema, T. Unequal impairment in the recognition of positive and negative emotions after right hemisphere lesions: A left hemisphere bias for happy faces. *J. Neuropsychol.* **6**, 79–93 (2012).
3. Aben, H. P. *et al*. Impaired Emotion Recognition after Left Hemispheric. *Stroke: A Case Report and Brief Review of the Literature. Case Rep. Neurol. Med.* **2017**, 1–6 (2017).
4. Palmiero, M. & Piccardi, L. Frontal EEG Asymmetry of Mood: A Mini-Review. *Front. Behav. Neurosci.* **11**, 1–8 (2017).
5. Allen, J. J. B., Keune, P. M., Sch, M. & Nusslock, R. Frontal EEG alpha asymmetry and emotion: From neural underpinnings and methodological considerations to psychopathology and social cognition. 1–6, https://doi.org/10.1111/psyp.13028 (2018).
6. Hewig, J. Intentionality in frontal asymmetry research. *Psychophysiology* **55**, 1–18 (2018).
7. Davidson, R. J., Saron, C. D., Senulis, J. A., Ekman, P. & Friesen, W. V. Approach/withdrawal and cerebral asymmetry: Emotional\ rexpression and brain physiology: I. *J. Pers. Soc. Psychol.* **58**, 330–341 (1990).
8. Davidson, R. J., Kalin, N. H. & Shelton, S. E. Lateralized response to diazepam predicts temperamental style in rhesus monkeys. *Behav. Neurosci.* **107**, 1106–1110 (1993).
9. Davidson, R. J. What does the prefrontal cortex 'do' in affect: Perspectives on frontal EEG asymmetry research. *Biol. Psychol.* **67**, 219–234 (2004).
10. Carver, C. S. & Harmon-Jones, E. Anger Is an Approach-Related Affect: Evidence and Implications. *Psychol. Bull.* **135**, 183–204 (2009).
11. Jacob, T. J. C. *et al*. Light and smell stimulus protocol reduced negative frontal EEG asymmetry and improved mood. *Open Life Sci.* **12**, 51–61 (2017).
12. Rey, B., Clemente, M., Wrzesien, M., Rodríguez, A. & Alcañiz, M. Assessing brain activations associated with emotional regulation during virtual reality mood induction procedures. *Expert Syst. Appl.* **42**, 1699–1709 (2014).
13. Andreas, M. & Hewig, J. Mind the movement: Frontal asymmetry stands for behavioral motivation, bilateral frontal activation for behavior. 1–19, https://doi.org/10.1111/psyp.12908 (2017).
14. Balconi, M., Vanutelli, M. E. & Grippa, E. Resting state and personality component (BIS/BAS) predict the brain activity (EEG and fNIRS measure) in response to emotional cues. *Brain Behav.* **7**, 1–15 (2017).
15. Studer, B., Pedroni, A. & Rieskamp, J. Predicting Risk-Taking Behavior from Prefrontal Resting-State Activity and Personality. *Plos One* **8**, 1–8 (2013).
16. Eftekhari, E., Tran, A. & McGregor, I. Decentering increases approach motivation among distressed individuals. *Pers. Individ. Dif.* **119**, 236–241 (2017).
17. Gollan, J. K. *et al*. Frontal alpha EEG asymmetry before and after behavioral activation treatment for depression. *Biol. Psychol.* **99**, 198–208 (2014).
18. Fedorowicz, G. The Effects of Mindfulness Meditation on Mental Health. (2012).
19. Kelley, N. J. & Schmeichel, B. J. The effects of negative emotions on sensory perception: fear but not anger decreases tactile sensitivity. *Front. Psychol.* **5**, 1–8 (2014).
20. Brzezicka, A., Kamiński, J., Kamińska, O. K., Wołyńczyk-Gmaj, D. & Sedek, G. Frontal EEG alpha band asymmetry as a predictor of reasoning deficiency in depressed people. *Cogn. Emot.* **31**, 868–878 (2017).
21. Greimel, E. *et al*. Resting frontal EEG asymmetry patterns in adolescents with and without major depression. *Biol. Psychol.* **132**, 212–216 (2018).
22. Quaedflieg, C. W. E. M. *et al*. The role of frontal EEG asymmetry in post-traumatic stress disorder. *Biol. Psychol.* **108**, 62–77 (2015).
23. Frenkel, T. I. *et al*. ADHD Symptoms in Post-Institutionalized Children Are Partially Mediated by Altered Frontal EEG Asymmetry. *J. Abnorm. Child Psychol.* **45**, 857–869 (2017).
24. Stewart, J. L. & Allen, J. J. B. Resting frontal brain asymmetry is linked to future depressive symptoms in women. *Biol. Psychol.* **136**, 161–167 (2018).
25. van der Vinne, N., Vollebregt, M. A., van Putten, M. J. A. M. & Arns, M. Frontal alpha asymmetry as a diagnostic marker in depression: Fact or fiction? A meta-analysis. *NeuroImage Clin.* **16**, 79–87 (2017).
26. Lachman, M. E. *et al*. Frontal brain asymmetry, childhood maltreatment, and low-grade inflammation at midlife. *Psychoneuroendocrinology* **75**, 152–163 (2016).
27. Flasbeck, V., Popkirov, S. & Brüne, M. Frontal EEG asymmetry in borderline personality disorder is associated with alexithymia. *Borderline Personal. Disord. Emot. Dysregulation* **4**, 4–9 (2017).
28. Adolph, D. & Margraf, J. The differential relationship between trait anxiety, depression, and resting frontal α-asymmetry. *J. Neural Transm.* **124**, 379–386 (2017).
29. Tomarken, A. J., Davidson, R. J., Wheeler, R. E. & Doss, R. C. Individual-Differences in Anterior Brain Asymmetry and Fundamental Dimensions of Emotion. *J. Pers. Soc. Psychol.* **62**, 676–687 (1992).
30. Tomarken, A. J., Davidson, R. J., Wheeler, R. E. & Kinney, L. Psychometric Properties of Resting Anterior EEG Asymmetry: Temporal Stability and Internal Consistency. *Psychophysiology* **29**, 576–592 (1992).
31. Jacobs, G. D. & Snyder, D. Frontal brain asymmetry predicts affective style in men. *Behav. Neurosci.* **110**, 3–6 (1996).
32. Hall, E. E. & Petruzello, S. J. Frontal Asymmetry, Dispositional Affect and Physical Activity in Older Adults. *J. Aging Phys. Act.* **7**, 76–90 (1999).
33. Harmon-Jones, E. & Allen, J. J. B. Behavioral activation sensitivity and resting frontal EEG asymmetry: Covariation of putative indicators related to risk for mood disorders. *J. Abnorm. Psychol.* **106**, 159–163 (1997).

34. De Pascalis, V., Cozzuto, G., Caprara, G. V. & Alessandri, G. Relations among EEG-alpha asymmetry, BIS/BAS, and dispositional optimism. *Biol. Psychol.* **94**, 198–209 (2013).
35. Sutton, S. K. & Davidson, R. J. Prefrontal brain asymmetry: A Biological Substrate of the Behavioral Approach and Inhibition Systems. *Psychol. Sci.* **8**, 204–210 (1997).
36. Schneider, M. *et al*. EEG asymmetry and BIS/BAS among healthy adolescents. *Biol. Psychol.* **120**, 142–148 (2016).
37. Hagemann, D., Naumann, E., Becker, G., Maier, S. & Bartussek, D. Frontal brain asymmetry and affective style: A conceptual replication. *Psychophysiology* **35**, 372–388 (1998).
38. Hagemann, D. *et al*. EEG asymmetry, dispositional mood and personality. *Pers. Individ. Dif.* **27**, 541–568 (1999).
39. Wheeler, R. E., Davidson, R. J. & Tomarken, A. J. Frontal brain asymmetry and emotional reactivity: A biological substrate of affective style. *Psychophysiology* **30**, 82–89 (1993).
40. Michel, C. M. & Koenig, T. EEG microstates as a tool for studying the temporal dynamics of whole-brain neuronal networks: A review. *Neuroimage* **180**, 577–593 (2018).
41. Khanna, A. Microstates in Resting-State EEG: Current Status and Future Directions. 105–113, https://doi.org/10.1016/j.neubiorev.2014.12.010.Microstates (2016).
42. Lehmann, D., Strik, W. K., Henggeler, B., Koenig, T. & Koukkou, M. Brain electric microstates and momentary conscious mind states as building blocks of spontaneous thinking: I. Visual imagery and abstract thoughts. *Int. J. Psychophysiol.* **29**, 1–11 (1998).
43. Milz, P., Pascual-Marqui, R. D., Achermann, P., Kochi, K. & Faber, P. L. The EEG microstate topography is predominantly determined by intracortical sources in the alpha band. *Neuroimage* **162**, 353–361 (2017).
44. Shafi, M. M. *et al*. EEG Microstate Correlates of Fluid Intelligence and Response to Cognitive Training. *Brain Topogr.* **30**, 502–520 (2017).
45. Wright, D., Makin, A. D. J. & Bertamini, M. Right-lateralized alpha desynchronization during regularity discrimination: Hemispheric specialization or directed spatial attention? *Psychophysiology* **52**, 638–647 (2015).
46. Lenartowicz, A. *et al*. Alpha desynchronization and fronto-parietal connectivity during spatial working memory encoding deficits in ADHD: A simultaneous EEG-fMRI study. *NeuroImage Clin.* **11**, 210–223 (2016).
47. Fink, A., Grabner, R. H., Neuper, C. & Neubauer, A. C. EEG alpha band dissociation with increasing task demands. *Cogn. Brain Res.* **24**, 252–259 (2005).
48. Klimesch, W., Doppelmayr, M., Schwaiger, J., Auinger, P. & Winkler, T. 'Paradoxical' alpha synchronization in a memory task. *Cogn. Brain Res.* **7**, 493–501 (1999).
49. Arakaki, X. *et al*. Alpha desynchronization/synchronization during working memory testing is compromised in acute mild traumatic brain injury (mTBI). *Plos One* **13**, 1–19 (2018).
50. Palva, S. & Palva, J. M. Functional roles of alpha-band phase synchronization in local and large-scale cortical networks. *Front. Psychol.* **2**, 1–15 (2011).
51. Benedek, M., Bergner, S., Könen, T., Fink, A. & Neubauer, A. C. EEG alpha synchronization is related to top-down processing in convergent and divergent thinking. *Neuropsychologia* **49**, 3505–3511 (2011).
52. Rohr, C. S., Okon-Singer, H., Craddock, R. C., Villringer, A. & Margulies, D. S. Affect and the Brain's Functional Organization: A Resting-State Connectivity Approach. *Plos One* **8** (2013).
53. Lindquist, K. A., Satpute, A. B., Wager, T. D., Weber, J. & Barrett, L. F. The Brain Basis of Positive and Negative Affect: Evidence from a Meta-Analysis of the Human Neuroimaging Literature. *Cereb. Cortex* **26**, 1910–1922 (2016).
54. Tenke, C. E., Kayser, J., Abraham, K., Alvarenga, J. E. & Bruder, G. E. Posterior EEG alpha at rest and during task performance: Comparison of current source density and field potential measures. *Int. J. Psychophysiol.* **97**, 299–309 (2015).
55. Rashed-Al-Mahfuz, M., Islam, M. R., Hirose, K. & Molla, M. K. I. Artifact suppression and analysis of brain activities with electroencephalography signals. *Neural Regen. Res.* **8**, 1500–1513 (2013).
56. Davidson, R. J., Mednick, D., Moss, E., Saron, C. & Schaffer, C. E. Ratings of emotion in faces are influenced by the visual field to which stimuli are presented. *Brain Cogn.* **6**, 403–411 (1987).
57. Davidson, J. Anterior cerebral asymmetry and the nature of emotion. **151**, 125–151 (1992).
58. Baijal, S. & Srinivasan, N. Emotional and hemispheric asymmetries in shifts of attention: An ERP study. *Cogn. Emot.* **25**, 280–294 (2011).
59. Wyczesany, M., Capotosto, P., Zappasodi, F. & Prete, G. Hemispheric asymmetries and emotions: Evidence from effective connectivity. *Neuropsychologia* **121**, 98–105 (2018).
60. Harmon-Jones, E., Gable, P. A. & Peterson, C. K. The role of asymmetric frontal cortical activity in emotion-related phenomena: A review and update. *Biol. Psychol.* **84**, 451–462 (2010).
61. Shackman, A. J., McMenamin, B. W., Maxwell, J. S., Greischar, L. L. & Davidson, R. J. Right dorsolateral prefrontal cortical activity and behavioral inhibition. *Psychol. Sci.* **20**, 1500–1506 (2009).
62. Hewig, J., Hagemann, D., Seifert, J., Naumann, E. & Bartussek, D. The relation of cortical activity and BIS/BAS on the trait level. *Biol. Psychol.* **71**, 42–53 (2006).
63. Quaedflieg, C. W. E. M., Meyer, T., Smulders, F. T. Y. & Smeets, T. The functional role of individual-alpha based frontal asymmetry in stress responding. *Biol. Psychol.* **104**, 75–81 (2015).
64. Gale, A., Edwards, J., Morris, P., Moore, R. & Forrester, D. Extraversion-introversion, neuroticism-stability, and EEG indicators of positive and negative empathic mood. *Pers. Individ. Dif.* **30**, 449–461 (2001).
65. Farahi, S. M. M., Ebrahimabad, M. J. A., Gorji, A., Bigdeli, I. & Farahi, S. M. M. M. Neuroticism and frontal EEG asymmetry correlated with dynamic facial emotional processing in adolescents. *Front. Psychol.* **10**, 1–9 (2019).
66. Meador, K. J., Kapur, R., Loring, D. W., Kanner, A. M. & Morrell, M. J. Quality of life and mood in patients with medically intractable epilepsy treated with targeted responsive neurostimulation. *Epilepsy Behav.* **45**, 242–247 (2015).
67. Hennion, S. *et al*. Experiences of self-conscious emotions in temporal lobe epilepsy. *Epilepsy Behav.* **90**, 1–6 (2019).
68. Ritchey, M., Wang, S. F., Yonelinas, A. P. & Ranganath, C. Dissociable medial temporal pathways for encoding emotional item and context information. *Neuropsychologia* **124**, 66–78 (2019).
69. Ives-Deliperi, V. L. & Jokeit, H. Impaired Social Cognition in Epilepsy: A Review of What We Have Learnt From Neuroimaging Studies. *Front. Neurol.* **10**, (2019).
70. Batut, A. C. *et al*. Neural responses associated with positive and negative emotion processing in patients with left versus right temporal lobe epilepsy. *Epilepsy Behav.* **9**, 415–423 (2006).
71. Yun, J. Y. *et al*. The left middle temporal gyrus in the middle of an impaired social-affective communication network in social anxiety disorder. *J. Affect. Disord.* **214**, 53–59 (2017).
72. Dolcos, F., Iordan, A. D. & Dolcos, S. Neural correlates of emotion Á cognition interactions: A review of evidence from brain imaging investigations. **23**, 669–694 (2011).
73. Dolcos, F., Labar, K. S. & Cabeza, R. Remembering one year later: Role of the amygdala and the medial temporal lobe memory system in retrieving emotional memories. *Proc. Natl. Acad. Sci. USA* **102**, 2626–2631 (2005).
74. Buchanan, T. W., Tranel, D. & Adolphs, R. Memories for emotional autobiographical events following unilateral damage to medial temporal lobe. *Brain* **129**, 115–127 (2006).
75. Egloff, B., Schmukle, S. C., Burns, L. R., Kohlmann, C. W. & Hock, M. Facets of Dynamic Positive Affect: Differentiating Joy, Interest, and Activation in the Positive and Negative Affect Schedule (PANAS). *J. Pers. Soc. Psychol.* **85**, 528–540 (2003).

76. Taubitz, L. E., Pedersen, W. S. & Larson, C. L. BAS Reward Responsiveness: A unique predictor of positive psychological functioning. *Pers. Individ. Dif.* **80**, 107–112 (2015).
77. Coan, J. A. & Allen, J. J. B. Frontal EEG asymmetry as a moderator and mediator of emotion. *Biol. Psychol.* **67**, 7–49 (2004).
78. Harmon-Jones, E. & Gable, P. A. On the role of asymmetric frontal cortical activity in approach and withdrawal motivation: An updated review of the evidence. *Psychophysiology* **55** (2018).
79. Fuentes, P. *et al*. Individual differences in the Behavioral Inhibition System are associated with orbitofrontal cortex and precuneus gray matter volume. *Cogn. Affect. Behav. Neurosci.* **12**, 491–498 (2012).
80. Barrós-Loscertales, A. *et al*. Behavioral activation system modulation on brain activation during appetitive and aversive stimulus processing. *Soc. Cogn. Affect. Neurosci.* **5**, 18–28 (2010).
81. Wager, T. D., Barrett, L. F., Weber, J., Lindquist, K. A. & Satpute, A. B. The Brain Basis of Positive and Negative Affect: Evidence from a Meta-Analysis of the Human Neuroimaging Literature. *Cereb. Cortex* **26**, 1910–1922 (2015).
82. Roy, M., Shohamy, D. & Wager, T. D. Ventromedial prefrontal-subcortical systems and the generation of affective meaning. *Trends Cogn. Sci.* **16**, 147–156 (2012).
83. Thayer, J. F. & Koenig, J. Resting Cerebral Blood Flow and Ethnic Differences in Heart Rate Variability: Links to Self-Reports of Affect and Affect Regulation. *Neuroimage* **202**, 116154 (2019).
84. Consedine, N. S., Magai, C., Cohen, C. I. & Gillespie, M. Ethnic variation in the impact of negative affect and emotion inhibition on the health of older adults. *Journals Gerontol. - Ser. B Psychol. Sci. Soc. Sci.* **57**, P396–P408 (2002).
85. Deer, L. K., Shields, G. S., Ivory, S. L., Hostinar, C. E. & Telzer, E. H. Racial/ethnic disparities in cortisol diurnal patterns and affect in adolescence. *Dev. Psychopathol.* **30**, 1977–1993 (2018).
86. Barzegaran, E., Vildavski, V. Y. & Knyazeva, M. G. Fine Structure of Posterior Alpha Rhythm in Human EEG: Frequency Components, Their Cortical Sources, and Temporal Behavior. *Sci. Rep.* **7**, 1–12 (2017).
87. Al Zoubi, O. *et al*. EEG Microstates Temporal Dynamics Differentiate Individuals with Mood and Anxiety Disorders From Healthy Subjects. *Front. Hum. Neurosci.* **13**, 1–10 (2019).
88. Watson, D. & Clark, L. A. Development and Validation of Brief Measures of Positive and Negative Affect: The PANAS Scales. **54**, 1063–1070 (1988).
89. John, R. & Julie, D. The Positive and Negative Affect Schedule (PANAS): Construct validity, measurement properties and normative data in a large non-clinical sample. *Br. J. Clin. Psychol.* **43**, 245–65 (2004).
90. Tuccitto, D. E., Giacobbi, P. R. & Leite, W. L. The Internal Structure of Positive and Negative Affect: A Confirmatory Factor Analysis of the PANAS. *Educ. Psychol. Meas.* **70**, 125–141 (2010).
91. Cooper, A., Gomez, R. & Aucote, H. The Behavioural Inhibition System and Behavioural Approach System (BIS/BAS) Scales: Measurement and structural invariance across adults and adolescents. *Pers. Individ. Dif.* **43**, 295–305 (2007).
92. Renger, R. A review of the profile of mood states (POMS) in the prediction of athletic success. *J. Appl. Sport Psychol.* **5**, 78–84 (1993).
93. Ritter, P., Becker, R., Freyer, F. & Villringer, A. EEG quality: The image acquisition artefact. *EEG - fMRI Physiol. Basis, Tech. Appl.* 153–171, https://doi.org/10.1007/978-3-540-87919-0_9 (2010).
94. Ritter, P., Becker, R., Graefe, C. & Villringer, A. Evaluating gradient artifact correction of EEG data acquired simultaneously with fMRI. *Magn. Reson. Imaging* **25**, 923–932 (2007).
95. Allen, P. J., Polizzi, G., Krakow, K., Fish, D. R. & Lemieux, L. Identification of EEG events in the MR scanner: The problem of pulse artifact and a method for its subtraction. *Neuroimage* **8**, 229–239 (1998).
96. Allen, P. J., Josephs, O. & Turner, R. A method for removing imaging artifact from continuous EEG recorded during functional MRI. *NeuroImage* **12**, 230–239 (2000).
97. Niazy, R. K., Beckmann, C. F., Iannetti, G. D., Brady, J. M. & Smith, S. M. Removal of FMRI environment artifacts from EEG data using optimal basis sets. *Neuroimage* **28**, 720–737 (2005).
98. Christov, I. I. Real time electrocardiogram QRS detection using combined adaptive threshold. *Biomed. Eng. Online* **3**, 1–9 (2004).
99. Kim, K. H., Yoon, H. W. & Park, H. W. Improved ballistocardiac artifact removal from the electroencephalogram recorded in fMRI. *J. Neurosci. Methods* **135**, 193–203 (2004).
100. Gabard-Durnam, L. J., Leal, A. S. M., Wilkinson, C. L. & Levin, A. R. The harvard automated processing pipeline for electroencephalography (HAPPE): Standardized processing software for developmental and high-artifact data. *Front. Neurosci.* **12**, 1–24 (2018).
101. Mullen, T. CleanLine EEGLAB Plugin. San Diego, CA: Neuroimaging Informatics Toolsand Resources Clearinghouse (NITRC). (2012).
102. Winkler, I., Haufe, S. & Tangermann, M. Automatic Classification of Artifactual ICA-Components for Artifact Removal in EEG Signals. *Behav. Brain Funct.* **7**, 1–15 (2011).
103. Winkler, I. *et al*. Robust artifactual independent component classification for BCI practitioners. *J. Neural Eng.* **11** (2014).
104. Pessoa, L. Understanding brain networks and brain organization. *Phys. Life Rev.* **11**, 400–435 (2014).
105. Sigman, M. & Dehaene, S. Brain Mechanisms of Serial and Parallel Processing during Dual-Task Performance. *J. Neurosci.* **28**, 7585–7598 (2008).
106. Murray, M. M., Brunet, D. & Michel, C. M. Topographic ERP analyses: A step-by-step tutorial review. *Brain Topogr.* **20**, 249–264 (2008).
107. Poulsen, A. T., Pedroni, A., Langer, N. & Hansen, L. K. Microstate EEGlab toolbox: An introductory guide. *bioRxiv* 289850, https://doi.org/10.1101/289850 (2018).
108. Rokach, L. & Maimon, O. *Data Mining with Decision Trees*. (2008).
109. Musso, F., Brinkmeyer, J., Mobascher, A., Warbrick, T. & Winterer, G. Spontaneous brain activity and EEG microstates. A novel EEG/fMRI analysis approach to explore resting-state networks. *Neuroimage* **52**, 1149–1161 (2010).
110. Van De Ville, D., Britz, J. & Michel, C. M. EEG microstate sequences in healthy humans at rest reveal scale-free dynamics. *Proc. Natl. Acad. Sci. USA* **107**, 18179–18184 (2010).
111. Brodbeck, V. *et al*. EEG microstates of wakefulness and NREM sleep. *Neuroimage* **62**, 2129–2139 (2012).
112. Kayser, J. & Tenke, C. E. Principal components analysis of Laplacian waveforms as a generic method for identifying ERP generator patterns: I. Evaluation with auditory oddball tasks. *Clin. Neurophysiol.* **117**, 348–368 (2006).
113. Kayser, J. & Tenke, C. E. Principal components analysis of Laplacian waveforms as a generic method for identifying ERP generator patterns: II. Adequacy of low-density estimates. *Clin. Neurophysiol.* **117**, 369–380 (2006).
114. Smith, E. E., Reznik, S. J., Stewart, J. L. & Allen, J. J. B. Assessing and conceptualizing frontal EEG asymmetry: An updated primer on recording, processing, analyzing, and interpreting frontal alpha asymmetry. *Int. J. Psychophysiol.* **111**, 98–114 (2017).
115. Coan, J., Coan, J. A. & Allen, J. J. B. Frontal EEG asymmetry and behavioral activation and inhibition systems. *Frontal EEG asymmetry and the behavioral activation and inhibition systems.* **40**, 106–114 (2003).
116. Pernet, C. R., Wilcox, R. & Rousselet, G. A. Robust correlation analyses: false positive and power validation using a new open source Matlab toolbox. **3**, 1–18 (2013).
117. Abreu, R., Leal, A. & Figueiredo, P. EEG-Informed fMRI: A Review of Data Analysis. *Methods.* **12**, 1–23 (2018).
118. Pisauro, M. A., Fouragnan, E., Retzler, C. & Philiastides, M. G. Neural correlates of evidence accumulation during value-based decisions revealed via simultaneous EEG-fMRI. *Nat. Commun.* **8**, 15808 (2017).
119. Murta, T., Leite, M. & Carmichael, D. W. Electrophysiological Correlates of the BOLD Signal for EEG-Informed fMRI. **00** (2014).

120. Sclocco, R. *et al*. EEG-informed fMRI analysis during a hand grip task: Estimating the relationship between EEG rhythms and the BOLD signal. *Front. Hum. Neurosci.* **8**, 1–13 (2014).
121. Laufs, H. *et al*. EEG-correlated fMRI of human alpha activity. *Neuroimage* **19**, 1463–1476 (2003).
122. Calhoun, V. D., Stevens, M. C., Pearlson, G. D. & Kiehl, K. A. fMRI analysis with the general linear model: Removal of latency-induced amplitude bias by incorporation of hemodynamic derivative terms. *Neuroimage* **22**, 252–257 (2004).
123. Lindquist, M. A. & Wager, T. D. Validity and power in hemodynamic response modeling: A comparison study and a new approach. *Hum. Brain Mapp.* **28**, 764–784 (2007).
124. Gawlowska, M., Domagalik, A., Beldzik, E., Marek, T. & Mojsa-Kaja, J. Dynamics of error-related activity in deterministic learning - an EEG and fMRI study. *Sci. Rep.* **8**, 2–11 (2018).
125. Kok, P., Van Lieshout, L. L. F. & De Lange, F. P. Local expectation violations result in global activity gain in primary visual cortex. *Sci. Rep.* **6**, 1–10 (2016).
126. Wymbs, N. F., Bassett, D. S., Mucha, P. J., Porter, M. A. & Grafton, S. T. Differential Recruitment of the Sensorimotor Putamen and Frontoparietal Cortex during Motor Chunking in Humans. *Neuron* **74**, 936–946 (2012).
127. Wager, T. D., Keller, M. C., Lacey, S. C. & Jonides, J. Increased sensitivity in neuroimaging analyses using robust regression. *Neuroimage* **26**, 99–113 (2005).
128. Fritsch, V. *et al*. Robust regression for large-scale neuroimaging studies. *Neuroimage* **111**, 431–441 (2015).
129. Seghier, M. L. Laterality index in functional MRI: methodological issues. *Magn. Reson. Imaging* **26**, 594–601 (2008).
130. Bradshaw, A. R., Bishop, D. V. M. & Woodhead, Z. V. J. Methodological considerations in assessment of language lateralisation with fMRI: a systematic review. *PeerJ* **5**, e3557 (2017).
131. Jansen, A. *et al*. The assessment of hemispheric lateralization in functional MRI-Robustness and reproducibility. *Neuroimage* **33**, 204–217 (2006).
132. Branco, D. M. *et al*. Functional MRI of memory in the hippocampus: Laterality indices may be more meaningful if calculated from whole voxel distributions. *Neuroimage* **32**, 592–602 (2006).
133. Jones, S. E., Mahmoud, S. Y. & Phillips, M. D. A practical clinical method to quantify language lateralization in fMRI using whole-brain analysis. *Neuroimage* **54**, 2937–2949 (2011).
134. Wu, G. R., Deshpande, G., Laureys, S. & Marinazzo, D. Retrieving the Hemodynamic Response Function in resting state fMRI: Methodology and application. *Proc. Annu. Int. Conf. IEEE Eng. Med. Biol. Soc. EMBS* **2015-Novem**, 6050–6053 (2015).
135. Ding, J.-R. *et al*. A blind deconvolution approach to recover effective connectivity brain networks from resting state fMRI data. *Med. Image Anal.* **17**, 365–374 (2013).
136. Tomarken, A. J., Davidson, R. J. & Henriques, J. B. Resting frontal brain asymmetry predicts affective responses to films. *J. Pers. Soc. Psychol.* **59**, 791–801 (1990).


## Acknowledgements

This research did not receive any specific grant from funding agencies in the public, commercial, or not-for-profit sectors.

## Author contributions

The study was designed by Ardaman Kaur and Dr. Vijayakumar Chinnadurai. Data was acquired and processed by Ardaman Kaur. Data was interpreted and analyzed by Dr. Vijayakumar Chinnadurai, Ardaman Kaur and Dr. Rishu Chaujar. The manuscript was written by Ardaman Kaur with the help of Dr. Vijayakumar Chinnadurai. All authors reviewed the manuscript.

## Competing interests

The authors declare no competing interests.

## Additional information

**Supplementary information** is available for this paper at https://doi.org/10.1038/s41598-020-61119-7.

**Correspondence** and requests for materials should be addressed to V.C.

**Reprints and permissions information** is available at www.nature.com/reprints.

**Publisher's note** Springer Nature remains neutral with regard to jurisdictional claims in published maps and institutional affiliations.